Positron Interactions at low-dimensional Condensed Surfaces

K. Umar Rao

B.Sc. Lond., MSc. Lond.

A thesis Submitted for the Degree of Ph.D.

September 1987

Royal Holloway & Bedford New College

University of London

ABSTRACT

A microprocessor control system for automatic data acquisition in a photon spectroscopy system was developed. The control process performed Doppler broadening measurements over the temperature range 4.2-600K with simultaneous recording when necessary of pressure. After work on the chalcogenide semiconductor (Pb,Ge)Te, Doppler broadening studies concentrated on the phenomenon of gas condensation on cooled graphite substrates. This class of adsorbent, of proven homogeneity was found ideal to explore the interaction of positrons at surfaces. By measurement of positronium, adlayer formation of methane, krypton, argon, nitrogen and oxygen was followed. All gases produced peaks in positronium emission with an investigation of the substrate further revealing an underlying thermal variation. Sound evidence in the form of accurate simultaneous pressure measurements and isotherms was found for a coverage of one half at the maximum in positronium. These studies of gas physisorption were conducted under a variety of temperatures and with pressures embracing atmospheric to under one Torr. Although results for the gases were of the same form each produced different maximum levels of positronium which appeared to relate to substrate-adsorbate binding energy. Maximum emission in the case of argon showed a temperature dependence however this requires verification. Oxygen was a special case as it yielded 12% para-positronium at half-coverage. The coupling of this to a low 1.5% ortho-positronium emission was attributed to chemical quenching. A convolution procedure based on the superposition of an additional para-positronium derived narrow gaussian to the usual gaussian and inverted parabola components was employed for an estimate of the positronium energy. This was used to attack the question of whether positronium is bound at the surface or is created flying.

Acknowledgements

I express sincere and deepest gratitude to Dr. P. Rice-Evans for his masterful supervision and commitment to research.

To Drs. B. P. Cowan, P. Fozooni I express a special thanks for general know how and assistance. It is a pleasure to acknowledge the advice of and discussions with former group member Dr. M. Moussavi-Madani and present, for a short duration, members Mr. S. Creamer and Mr. D. Britton and also Mr. M. Fardis, Mr. C. Erin and Mr. D. Smith. Humble gratitude is due to Mr. A. K. Betts without whose professionalism and technical ability the automated system would still only be a fantasy. Thanks are due for software advice from Mr. G. Rock and from Mr. P. Taylor and Mr. L. Nodes of the computer centre. I should also like to thank the operations staff of the computer centre especially Miss S. Marshall and also Drs. P. Pal and L. Morgan and Mr. J. Anderson. For technical assistance may I thank Messrs. J Henley, J. Sales, F. Greenough, R. Elton, M. Thyer, D. Smith, A. Alway, D. Young and G. Cakebread and also staff of the electronics section Mr. L. Ellison, Mr. T. Brooks and Mr. R. Jordan. Thanks are due also to Mrs. S. Pearson, Mr. G. Wells and Mrs. V. Leach. Gratitude is due to Dr. M. Green for taking into consideration the groups needs when setting up departmental computing facilities. I am grateful to the Imperial College reactor centre and especially Dr. G. Burholt for the provision of radioactive sources. Also to the college radiation officer Mr. M. Stephens. I am indebted to the SERC for the provision of finanicial assistance and to the college disruption fund and Prof. R. Dobbs and especially to Dr. P. Banham.

Finally I should like to thank my family and foremost my brothers Nusrat A. Rao and Anis A. Rao, without their infinite patience, care and moral support this work could not have been completed.

TABLE OF CONTENTS

Abstract i

Acknowledgements ii

Table of contents iii

Chapter I Positron Annihilation

1.1 Introduction 1

1.2 The Annihilation Process 1

1.3 Positronium Formation 2

1.4 Annihilation in the Free State 3

1.5 Effect of Defects 4

1.6 The Two State Trapping Model 5

1.7 The Experimental Techniques 7

1.7.1 Lifetime 7

1.7.2 Angular Correlation 8

1.7.3 Doppler Broadening 10

1.7.4 The Low Energy Positron Beam 11

1.8 The Two State Trapping Model Applied to Lineshape Analysis 12

1.9 Prevacancy Effects 13

1.10 Slow Positron Interaction with Matter 14

Chapter II Introduction to Physisorption

2.1 Introduction 25

2.1.1 Van der Waal Forces 26

2.2 Experimental Techniques 26

2.3 The Langmuir Model 29

2.4 Boltzmann Approximation 29

2.4.1 Weak Interactions 31

2.5 BET Formula 32

Chapter III Experimental Equipment

3.1 Low Temperature Measurements 37

3.1.1 Cryostat and Sample Chamber Construction 37

3.1.2 Automatic Feeder Arrangement 38

3.2 The Furnace 39

3.3 Detector and Electronics 40

3.3.1 The Detector 40

3.3.2 The Analogue to Digital Converter 41

3.3.3 Link MultiChannel Analyser 41

3.4 The Cage 42

3.5 Pressure Instruments 42

3.5.1 Pressure Gauges 42

3.5.2 The Druck Pressure Instruments 43

3.6 Gas Handling 44

Chapter IV Microprocessor Control System

4.1 Introduction 50

4.2 Control Electronics 50

4.2.1 The Digital Temperature Controller 50

4.2.2 The Master Temperature Controller 51

4.2.3 The MAster Control Unit 51

4.3 The 380Z Microcomputer and Control Aspects 52

4.3.1 The Microcomputer 52

4.3.2 MCU Interface 52

4.3.3 MTC Interface 53

4.3.4 DTC, Link Analyser Interface 54

4.3.5 VAX Minicomputer Link 54

4.3.6 Druck Pressure Indicator Link 54

4.3.7 Slave 380Z Interface 55

4.3.8 Perex Perifile Interface 56

Chapter V Microprocessor Control Software

5.1 Introduction 60

5.2 Monitor and Control of Sample Temperature 60

5.3 Command of MultiChannel Analyser 61

5.4 Collection and Recording of Data 62

5.5 User Interface to College Minicomputer 63

5.6 Run Cycle Automation 64

5.7 Development of Menu 66

Chapter VI Data Analysis

6.1 Traditional Lineshape Parameters 69

6.2 Positronium Parameters 70

6.3 Background Subtraction 70

6.4 Convolution Analysis 72

Chapter VII A Positron Annihilation Study of (Pb,Ge)Te

7.1 Introduction 80

7.2 The Structural Phase Transition 80

7.3 Sample Preparation 81

7.4 Experimental Method 81

7.5 Results 82

7.5.1 Lineshape Parameters 82

7.5.2 Lineshape Analysis 83

Chapter VIII Substrate Preparation and Grafoil in Vacuum

8.1 Substrate Preparation 93

8.2 Positron Annihilation in Grafoil 94

8.3 Sample Preparation and Method 95

8.4 Results 96

8.4.1 Lineshape and Positronium Parameters 96

8.4.2 Lineshape Analysis 96

Chapter IX Methane on Grafoil

9.1 Introduction 106

9.2 Method 107

9.3 Results 107

9.3.1 Lineshape and Positronium Parameters 107

9.3.2 Pressure Results 110

9.3.3 Convolution Analysis 111

9.4 Conclusion 111

Chapter X Krypton on Grafoil

10.1 Introduction 129

10.2 Experimental 130

10.3 Results 131

10.3.1 Positronium and Lineshape Parameters 131

10.3.2 Pressure Results 132

10.3.3 Convolution Analysis 133

10.4 Summary 134

Chapter XI Argon Adsorption on Grafoil

11.1 Introduction 148

11.2 Method 149

11.3 Results 150

11.3.1 Positronium and Lineshape Parameters 150

11.4 Conclusion and Discussion 151

Chapter XII Nitrogen on Grafoil

12.1 Introduction 161

12.2 Method 162

12.3 Results 162

12.3.1 Positronium and Lineshape Parameters 162

12.4 Conclusion 163

Chapter XIII Observation of Para-Positronium in Oxygen on Grafoil

13.1 Introduction 169

13.2 Experimental Method 169

13.3 Results and Discussion 170

13.3.1 Lineshape Parameter Analysis 170

13.3.2 Pressure Variation 172

13.3.3 Convolution Analysis 173

Appendices 198

Bibliography 209

Chapter I Positron Annihilation

§1.1 Introduction

Since the discovery of positrons in the 1930's their interactions with electrons in matter have formed an important area of physics. With increasing knowledge, especially since the 1950's, measurements on positron annihilation have proved to be a valuable tool for probing matter. Early applications were to condensed matter in the bulk state but recently following the development of low energy beams, positrons have been employed in the study of surfaces. They form essentially a non-destructive method, information simply emerging in the form of annihilation radiation. A particularly successful area of application has been in the study of lattice defects where the trapping of positrons is sensitive to very low concentrations.

§1.2 The Annihilation Process

When energetic positrons enter condensed matter they rapidly lose energy by collisions with electrons and ions and are quickly brought to thermal energies. A positron emitted by a radioactive source with an energy of several 100 keV is slowed to thermal energies (of the order of 0.01eV varying as $\frac{3}{2}$kT) in a time $\sim 10^{-12}$ seconds. This is around two orders of magnitude less than the average positron lifetime in matter. At first energy loss is through ionization, plasmon and atom excitations then later electron-positron pair and phonon creation. In some instances for example when the positron experiences high electron densities thermalization may be incomplete before annihilation which acts to complicate analysis. Once thermalized positrons live for an order of 10^{-10} seconds in which time they may interact in various ways, characteristic of the medium, with defects and the initial electronic system. The eventual annihilation with an electron is announced by emergence of energetic photons. The utility of the positron method relies on the fact that observed characteristics of annihilation (for example energy, momenta and time of emission of the photons) depend almost entirely on the initial state of

the positron-many-electron system. Traditionally two distinct forms of study are possible *viz.* electronic structure and defect studies. The first requires annihilation from a common, well-defined and delocalised state. In defect studies interaction of the charged positron with the surrounding medium plays the important role in examining localized states which result from positron coupling to structural defects. In this case then it is interpretation of the change in annihilation parameters between a well annealed sample and a defect ridden situation which provides information on the concentration, nature and origin of defects. The basic annihilation process can be hindered by two mechanisms *viz.* positronium formation and positron trapping by defects.

§1.3 Positronium Formation

In the final stages of thermalization it is possible for the positron to capture an electron from the surrounding medium and form a positronium atom (Ps atom). Positronium formation is more likely to occur in molecular media owing to the relatively large size of positronium ($\sim$ twice the diameter of a hydrogen atom). Once formed positronium will moderate more slowly than a free positron as a result of its weaker interactions. The energetics of positronium formation in solids can be written in terms of the 'Ore gap' (Ore and Powell 1949). The Ore gap model states that positronium formation is most probable when the positron energy is within a certain range where no other electronic energy transfer process is possible. If the ionization potential of a molecule of the medium is V_i, positronium formation is probable when the positron energy (E) is greater than: $V_i - V_{ps}$, where V_{ps} is the positronium binding energy (6.8eV in free space but possibly less in molecular media). Although if E is greater than V_i ionization through inelastic scattering is possible it has to be less than the lowest excitation potential of the electron V_{ex}. If $E > V_{ex}$ excitation will compete with positronium formation. The Ore gap can thus be written

$$V_i - V_{ps} < E < V_{ex}$$

However even when the positron energy is within the Ore gap other processes such as excitation of vibrational modes and formation of positron and molecular complexes may diminish the positronium yield. The ground states of the positronium atom are the singlet 1^1S_0 (parapositronium, where orbital angular momentum (l) and spin are both zero) and the triplet 1^3S_1 (orthopositronium, l=0 and total spin unity). A system of two photons cannot have states of angular momentum equal to unity and as this bars ortho→para conversion, $\frac{1}{4}$ of the positronium is formed in the singlet and $\frac{3}{4}$ in the triplet state. The lifetime of the para state (p-Ps) is of the same order as that of free positrons. However that of ortho-Ps (o-Ps) is about three orders of magnitude greater. This is due to selection rules. In general positronium acts to complicate analysis and interpretation of positron measurements. The longer positronium lifetime for example shows as a tail in lifetime spectra. These complications may be exacerbated by 'quenching' or spin exchange processes. Here the normal mean lifetime of positronium is reduced. Pickoff annihilation is an example of quenching, it occurs when o-Ps suffers 2γ annihilation by collision with a second electron of opposite spin. Chemical reactions and magnetic quenching are further examples.

§1.4 Annihilation in the Free State

The annihilation process supplies an energy $2m_0c^2$, where m_0 is the positron (or electron) rest mass, and c the velocity of light. For slowly moving pairs two other bodies must be involved in the annihilation. Thus the normal mode for annihilation is creation of two photons each with an energy $\sim m_oc^2$. Single photon annihilation is only possible in the presence of a third body to absorb recoil momentum. Figure(1.4.1) shows Feynman diagrams for one, two and three photon emissions. It is seen that the diagrams for three and single photon annihilations have three vertices, one more than for two photon annihilation. The additional vertex reduces the cross-section of the event by a factor of the order of the fine structure constant, $\alpha = \frac{1}{137}$. The cross-section for single photon annihilation is reduced further by an additional factor $\lambda_c^3\rho$, where λ_c is the Compton wavelength of the

electron and ρ the density of additional bodies able to absorb recoil momentum. The largest value of ρ likely makes this factor of the order α^3. Ratios for the three processes (single, two and three photon annihilation respectively) are thus

$$\sigma(1) : \sigma(2) : \sigma(3) = \alpha^4 : 1 : \alpha$$

At low energies the cross-section is inversely proportional to positron velocity v (Dirac 1930)

$$\sigma(2) = \frac{\pi r_o^2 c}{v}$$

giving the annihilation probability ($\sigma(2)vn_e$) or rate (λ),

$$\lambda = \pi r_o^2 c n_e \tag{1.1}$$

where r_o is the classical electron radius and n_e the electron density experienced by the positron. Hence by measuring annihilation rates one can obtain the electron density at the site of annihilation.

§1.5 Effect of Defects

After or just prior to thermalization it is possible for a positron to exist in various stable or metastable localized states as a result of becomimg 'trapped' at lattice defects. The positron during its thermalized passage experiences strong repulsive coulomb forces. It is thus natural for it to 'shelter' at sites where this is minimal. Sites such as lattice vacancies, dislocation cores and other voids. At a defect the electron density is reduced and is mapped by an increase in positron lifetime. Electrons with which a positron can annihilate are generally of two types *viz.* core and conduction. Core electrons are those that are tightly bound about the nucleus (for example the K shell electrons), conduction electrons are those of the electron gas responsible for conduction in metals (essentially the outer less tightly bound electrons in the conduction band). Annihilation with these different electron

states results in two contributions to the final energy distribution of annihilation photons. The greater reduction in density of core electrons at defects alters the ratio of core to conduction electron annihilations and can be followed in for example Doppler broadening measurements by changes in the photopeak.

§1.6 The Two State Trapping Model

The annihilation rate for a positron in a stationary state is time independent (1.1) and depends only on the electron density seen by the positron in that state. As a result of the diversity of lattice defects trapped positrons may exist in a spectrum of quasi-stationary states S, each with an annihilation rate $\lambda(S)$. In the simplest case a lifetime spectrum consists of separate components for each state but this is complicated by the fact that each state can have time-independent transition rates K_{ij} ($K_{ij} \neq K_{ji}$, $K_{ii} = 0$) for transition between traps. Furthermore each state has a persistence, $\tau(S)$ relative to the corresponding annihilation lifetime $\lambda(S)^{-1}$. If $\tau(S) << 1/\lambda(S)$ for all S, each experiences many states before annihilating and the measured spectrum may be approximated by a single component

$$\overline{\lambda} = \int \lambda(S)P(S)dS \tag{1.2}$$

where P(S) is a normalised distribution function for relative probabilities of occurence of the states S. If $\tau(S) >> 1/\lambda(S)$ the spectrum has the form

$$I(t) = \int P(S)e^{-\lambda(S)t}dS \tag{1.3}$$

where I(t) is the intensity of the lifetime component t. If the range of $\lambda(S)$ is restricted (1.3) becomes

$$I(t) = \sum_i I_i e^{-\lambda_i t} \tag{1.4}$$

So that the I_i provide relative positron populations and each λ_i respective electron densities. From the transition rate between traps, K_{ij}, the initial positron population decays as

$$n(t) = \sum_i n_i(t) \tag{1.5}$$

where the $n_i(t)$ are the solutions of

$$\frac{dn_i(t)}{dt} + \left(\lambda_i + \sum_{j \neq i} K_{ij} \right) n_i(t) = \sum_{j \neq i} K_{ji} n_j(t) \tag{1.6}$$

The lifetime spectrum is then

$$I(t) = \sum_v I_v e^{-r_v t} \tag{1.7}$$

where I_v and r_v are functions of λ_i and K_{ij}. In the model the following simplifications are made: $K_{ij} >> \lambda_i$, $N = 2$ and that at some time, $t = 0$, all positrons exist in a common delocalized state ($t << \lambda_i^{-1}$). Putting i= 1 to represent the initial state and assuming that escape from traps is negligible (i.e. a positron goes initially from 1 to j but then stays at this particular j) one can write (1.6) as

$$\begin{aligned} &\frac{dn_1(t)}{dt} + \left(\lambda_1 + \sum_{j \neq 1} K_{1j} \right) n_1(t) = 0 \\ &\frac{dn_j(t)}{dt} + \lambda_j n_j(t) = K_{1j} n_1(t) \end{aligned} \tag{1.8}$$

for all $j \neq 1$.

The mean lifetime (t) will be given by

$$t = \frac{1 + \sum_j K_{1j}/\lambda_j}{\lambda_1 + \sum_j K_{1j}} \tag{1.9}$$

If the transition rate K_{ij} is of the same order as the decay rate in that state and the λ_j are sufficiently different from λ_1 it will be possible to deconvolute the resulting lifetime spectra into respective components.

§1.7 The Experimental Techniques

§1.7.1 Lifetime

Positrons are emitted from a number of sources by the process of β-decay. Table(1) lists some sources with their properties.

Isotope	Half-life	End-Point energy (keV)	β^+ Fraction (%)
^{19}Ne	17.5s	2220	100
^{22}Na	2.58yr	545	90
^{44}Ti	47yr	1470	94
^{58}Co	71.3d	480	15
^{64}Cu	12.9h	650	19
^{68}Ge	275d	1880	86

Table(1) Primary Positron Sources

In lifetime work the isotope ^{22}Na is most common, the sample is arranged in a sample-source-sample sandwich after deposition of a few microcuries, by evaporation, of an aqueous ^{22}NaCl source. ^{22}Na is used because the positron emission is followed almost immediately ($<$ 10 psec) by a 1.28MeV gamma ray which is emitted in the de-excitation of the resulting ^{22}Ne* nucleus

$$^{22}\mathrm{Na} \longrightarrow ^{22}\mathrm{Ne}^* + \mathrm{e}^+ + \nu$$

$$^{22}\mathrm{Ne}^* \longrightarrow ^{22}\mathrm{Ne} + \gamma$$

The 1.28MeV acts as the zero of time signal for the entry of the positron into the sample. The time interval between detection of the 1.28MeV photon and the 0.511MeV annihilation photon is measured by a fast-slow coincidence circuit, figure(1.7.1.1). Considering the fast arm circuit, one of the constant fraction discriminators (for example that connected to detector 1) indicates an annihilation and the other time of entry. A constant fraction discriminator (CFD) has an output for only those incoming signals that are above a preset amplitude. Thus CFD1 would be set to just below 1.28MeV and CFD2 to a little under 0.511MeV. The

output from CFD1 is fed to the 'start input' on a Time to Pulse Height Converter (TPHC) and that from CFD2 fed via a variable delay to the 'stop input'. A TPHC has an output pulse whose magnitude is proportional to the time delay between start and stop signals. Now as there is an output from a CFD for every input above the threshold, TPHC output has to be gated such that only true pairs of events are passed onto the MultiChannel Analyser (MCA). The slow arm acts as the gate. The Single Channel Analyser's (SCA's) have windows set such that SCA2 outputs a logic pulse only if the input is 0.511MeV, and SCA1 if its input is 1.28MeV. If differential constant fraction discriminators are available the slow arm may be omitted. The MCA builds up a spectrum of count versus signal amplitude or lifetime. Ideally the random or systematic errors in the measuring process are negligible compared to the measured delays but in practice the stored spectrum is corrupted by such errors and can be regarded as a convolution of the real spectrum with instrumental resolution. The system responce can be measured by replacing the sample with a ^{60}Co source which emits two almost simultaneous photons. The ^{60}Co spectrum can then be deconvoluted from the sample spectrum. A resolution of 300ps at Full Width at Half Maximum (FWHM) is typically obtained. Scintillator decay time sets an upper resolution limit. In a perfect well annealed sample all positrons annihilate from a delocalized free state and produce a spectrum with a single annihilation rate λ and of form $e^{-\lambda t}$. However in the presence of defects or positronium mutiexponential curves result which require sophisticated computer fitting procedures (see for example Kirkegaard and Eldrup 1972,1974).

§1.7.2 Angular Correlation

In the centre-of-mass frame the two photons of annihilation each have an energy equal to 511keV and are moving in strictly opposite collinear directions. However due to the residual momentum of the annihilating pair the photons deviate from collinearity in the laboratory frame. Departure from collinearity (θ), figure(1.7.2.1) is (by conservation of momentum)

$$\theta \approx \frac{P_t}{m_o c} \tag{1.10}$$

where P_t is the transverse momentum component of the electron-positron pair. As mentioned earlier, annihilating positrons have been reduced to thermal energies so that their contribution to this divergence is negligible. Hence measurement of angular correlation yields information on the momentum distribution of annihilating electrons. The situation however is different in deformed samples where positrons do not necessarily annihilate in a free (thermalized) state. Figure(1.7.2.2) shows a 'long slit geometry' for measurement of the angular correlation of annihilation photons. Typical sources for positrons are ^{22}Na, ^{58}Co and ^{64}Cu and source strengths range from 10mCi to 1Ci. The source is placed as close to the sample as feasible; if this is impractical the positrons may be focussed onto the sample by a suitable magnetic field. Lead collimators shield two NaI scintillation counters from direct view of the source. Greater collimation effects higher instrumental resolution (normally $\sim$ 1mrad). Thus it is normal to have the detectors several metres away on either side of the sample (hence the need for very high source strengths). Additionally to collect the largest number of photons the detectors and slits are made as long as possible in the x-direction, figure(1.7.2.2). A coincidence gate syphons annihilation pairs (of coincidence less than 10 nsec), after SCA's have filtered the 511keV photons and the scaler then counts these as a function of angle θ_z (performed by moving one of the detectors around the sample) to yield a $N(\theta)$ versus θ distribution. Good statistics normally require counting over many days. Figure(1.7.2.3) shows the form of typical angular correlation curves. If the thermalized positron annihilates with a gas of free electrons $N(\theta)$ may be calculated from

$$N(\theta) = N(0)\left[1 - \left(\frac{\theta_z}{\theta_f}\right)^2\right] \qquad (1.11)$$

for $\theta_z < \theta_f$

where θ_f is the Fermi cutoff.The curves are interpreted on the basis of two components *viz.* an inverted parabola representing annihilations with free electrons and a broader gaussian arising from core electron annihilations.

§1.7.3 Doppler Broadening

It has been mentioned that the motion of annihilating pairs causes a deviation from collinearity in the resulting photons; in addition a Doppler shift in the energy of the annihilating photons (as measured in the laboratory frame) is created. The frequency shift ($\Delta\nu$) is

$$\frac{\Delta\nu}{\nu} = \frac{v}{c} \tag{1.12}$$

where $v = p/2m_o$, p is momentum and c the velocity of light. Photon energy is given by $h\nu$ (where h is Planck's constant) so that

$$\frac{\Delta E}{E} = \frac{v}{c} \quad \rightarrow \quad \Delta E = \frac{pc}{2} \tag{1.13}$$

where $E = m_o c^2$. This shift broadens the observed photopeak. The effect is illustrated in figure(1.7.3.1) where a Doppler broadened peak and an ^{85}Sr gamma line are shown normalized to equal height. The ^{85}Sr peak with a FWHM of $\sim$1.15keV represents the detector resolution. Annihilation of positrons at rest with a gas of free electrons with Fermi velocity v_f yields an energy spectrum of an inverted parabola centred at $m_o c^2$ and extending to $m_o c^2(1 \pm v_f/2c)$. In similarity with angular correlation a broad gaussian function usually represents the contribution of core electron annihilations. A possible configuration for Doppler broadening is shown in figure(1.7.3.2). The resolution required necessitates use of a high resolution solid state detector. The biased amplifier expands the energy scale so that only regions of interest are sampled by the Analogue to Digital Converter (ADC). A digital stabilizer is ideally available to minimise electronic drift. The MCA builds up a spectrum of energy versus counts. Annihilation lineshapes yield essentially the same information as angular correlation of annihilation radiation (ACAR) but with a much reduced resolution (about an order of magnitude worse). However the method has merits some of which are listed:

(i) Efficiency or count rate is two orders of magnitude higher than that given by ACAR.

(ii) Only a single detector is required.

(iii) Samples may be investigated in enviromental conditions unsuitable for ACAR.

(iv) Instrumental stability can be measured in coincidence with Doppler broadening. This is acheived by placing a reference gamma source such as ^{103}Ru alongside the sample.

§1.7.4 The Low Energy Positron Beam

The concept of a low energy positron beam (LEPB) was introduced by Madanski and Rosetti (1950). They used a ^{64}Cu source to subject various solid surfaces to a flux of positrons in the hope that some, which slowed close to the surface, would diffuse through and out of the surface. The fraction of positrons emitted in this manner was expected to be equal to the ratio of the positron diffusion length ($\sim 10^3$Å) and the positron implantation depth (10^{-2} cm). This early work however did not prove successful; its failure is now attributed to low sensitivity and surface contamination. It was Cherry (1958) who first succeeded in producing slow positrons when he irradiated chromium plated mica surfaces. A slow positron yield expressed as a ratio to total positron flux of $\epsilon = 3 \times 10^{-8}$ was obtained. Initial application of slow positrons was in the measurement of secondary positron emission yields of surfaces under positron and electron bombardment (Cherry 1958) and the total scattering cross-section of positrons in Helium (Groce *et al* 1968, Costella *et al* 1972). The discovery of the MgO smoked positron moderator (Canter *et al* 1972) with an efficiency $\epsilon = 3 \times 10^{-5}$ provided the basis for the observation of surface positronium and its excited state (Canter *et al* 1974, 1975). Figure(1.7.4.1) shows the MgO moderator slow positron source developed by Canter *et al* (1972). A disadvantage of MgO is the relatively large energy spread (ΔE) of the positron beam. This spread, of the order of eV's, compares with 0.25eV reported for a boron

target (Stein *et al* 1974). Dale *et al* (1980) obtained best results with a tungsten vane moderator prepared by heating to 2500K in vacuum. Figure(1.7.4.2) shows the energy spectrum of the positron beam where ΔE is seen to be $\sim$ 1.5eV.

§1.8 The Two State Trapping Model Applied to Lineshape Analysis

The relative number of annihilations in each localized positron state (N_j) dictates the Doppler or ACAR spectrum obtained. One has

$$N_j = \int_0^\infty \lambda_j n_j(t) dt \tag{1.14}$$

and for the trapping model

$$N_1 = \frac{\lambda_1 n_0}{\lambda_1 + \epsilon}, \quad N_j = \frac{K_{ij} n_0}{\lambda_1 + \epsilon}, \quad \text{where} \quad \epsilon = \sum_j K_{ij} \tag{1.15}$$

To obtain quantitive information on trapping rates, defect concentrations and sites a parameter which is some linear function of positron state is introduced. This characteristic of annihilation (see also chapter 6), F, is linear in the sense that

$$F = \frac{\sum_j F_j N_j}{\sum_j N_j} \quad = \sum_j F_j P_j \tag{1.16}$$

where P_j are the normalized distributions of the N_j states. For ACAR one can define an H-parameter

$$H = \frac{\int_{-1}^{+1} N(P_z) dP_z}{\int_{-\infty}^{+\infty} N(P_z) dP_z} \tag{1.17}$$

Typical curves for the variation of lineshape parameter against temperature for annealed samples are shown in figure(1.8.1). Initially the temperature dependence is weak but after a 'threshold' temperature a strong dependence is shown prior to a plateau or saturation region. At low temperatures thermalized positrons annihilate freely from a delocalized state with a rate $\lambda_1 = \lambda_f$ where λ_f is essentially temperature independent. At the high temperature extreme let the positrons annihilate from a localized state with a rate λ_{1v} (1v for 'monovacancy') which

can be written K_{1v}. If the lineshape parameter F has been defined correctly there shall be two distinct values, F_f and F_{1v} for the free and the monovacancy trapped positron respectively. Equation (1.16) can thus be written

$$F = \frac{\lambda_f F_f + K_{1v} F_{1v}}{\lambda_f + K_{1v}} \tag{1.18}$$

K_{1v} can be replaced by its dependence on monovacancy concentration (C_{1v}). Let $K_{1v} = v_{1v} C_{1v}$, where v_{1v} is a constant. Now C_{1v} will depend on the entropy (S^F_{1v}) and enthalpy (H^F_{1v}) of monovacancy formation. C_{1v} will increase with S^F_{1v} (temperature independently) and decrease with H^F_{1v}. In particular

$$C_{1v} = \frac{\exp(S^F_{1v}/k)}{\exp(H^F_{1v}/kT)} \tag{1.19}$$

where k is the Boltzmann constant and T temperature.

So that

$$F = \frac{\lambda_f F_v + F_{1v} v_{1v} \exp(S^F_{1v}/k) \exp(-H^F_{1v}/kT)}{\lambda_f + v_{1v} \exp(S^F_{1v}/k) \exp(-H^F_{1v}/kT)} \tag{1.20}$$

from (1.18) and (1.19). As temperature is raised K_{1v} increases and from (1.18) the limit when $K_{1v} >> \lambda_f$ is $F \rightarrow F_{1v}$ so that there will be a saturation limit for the lineshape parameter.

§1.9 Prevacancy Effects

At extremely low temperatures the lineshape parameter may exhibit a slight negative slope with rising temperature. The difference induced in H^F_{1v} by lineshape variation between temperature independent and low temperature ranges is greater than expected from volume expansion (see for example the work on Cadmium by Lichtenberger *et al* 1975). As mentioned a thermalized positron experiences repulsive coulomb forces and drifts into regions of lower than average ion density where it is said to be trapped. There may however be a perturbation of the lattice by the positron sufficient to trap it in a self-created hole or defect. The idea of positron self-trapping was first suggested for ionic crystals by Goldanskii and

Prokop'ev (1965). For metals it was suggested by Stott (1973) and followed up by Lichtenberger et al (1975). It is most often used to explain anomalous temperature behaviour. Another phenomenon 'detrapping' which can be likened as opposite to self-trapping is believed to be the cause of the negative gradient. The relatively shallow potential holding the self-trapped positron at lower temperatures (<50K) is not sufficiently deep (holding energies 10^{-2} - 10^{-1}eV) so that as temperature is raised the positron escapes into the free state. At the other end of the scale, positron trapping at divacancies may start to play a role rendering the two state 'no escape' trapping model inaccurate. There is then a three state problem and the spectrum is built up from monovacancy and divacancy contributions. Detrapping from monovacancies will again be possible but because of the higher binding energy of the positron in divacancies a 'no escape' model can be assumed for these.

§1.10 Slow Positron Interaction with Matter

When a low energy positron impinges on a sample it rapidly thermalizes and may annihilate with electrons of the bulk. However dependent upon the initial penetration the thermalized positron may diffuse back to the surface. At the surface the following phenomena are possible:

(i) The positron may become trapped at a vacancy, interface or other crystalline imperfection, or by its 'image' potential well (Lynn 1979, Mills 1979b).

(ii) The positron may escape through formation of positronium (Lynn 1979, Mills 1979b, Mills and Pfeiffer 1979)

(iii) A trapped surface positron may be thermally desorbed and again produce positronium on escape (Lynn 1979, Mills 1979b)

(iv) In rare-gas solids the positron may reach the surface at energies sufficiently high to overcome the positron work function ($\phi^+ > 0$) and in other materials where the positron has a negative work function it may be spontaneously emitted (Gullikson and Mill 1986, Cherry 1958, Costello *et al* 1972, Mills *et al* 1978)

(v) Reflection of the positron from the surface potential back into the metal (Lynn and Lutz 1980, Nieminen and Oliva 1980)

These possibilities and the Bragg reflection of incident positrons are illustrated in figure(1.10.1). Observation of positronium formation in metals (Lynn and Welch 1980, Canter *et al* 1974, Mills 1978, Lynn 1979) leads to speculation of production at or near the surface since it is believed the high electron density within a metal precludes positronium formation (Held and Kahana 1964, Lowy and Jackson 1975) and because positronium formation has not been observed in the presence of vacancies or voids (Mogensen *et al* 1972, Cotterill *et al* 1972). Positronium formation is quite acceptable as a means for the positron to escape from the surface as its binding energy (6.8eV) more than compensates for typical electron work functions. The presence of positronium may be ascertained by a variety of properties for example through the long lifetime of the *o*-Ps state, the 0-511keV energy spread of the three photon decays of *o*-Ps (Lynn and Welch 1980, Mills 1978, Ore and Powell 1949) and through magnetic quenching of *o*-Ps. Positronium formation not only enables detection of the positron leaving the sample but can be studied under a variety of experimental conditions and as a function of sample temperature, incident positron energy (Mills 1978, Lynn 1979), sample angle, surface conditions (Lynn and Lutz 1980) and defect concentration. A study by Lynn and Welch (1980) on Ps formation at metal single crystal surfaces found strong temperature dependence. Figure(1.10.2) shows their Ps fraction results for Ag(100) as a function of temperature and at different incident positron energies. A three phase effect for the higher incident energies and temperatures is apparent. The temperature dependent formation starting at $\sim$ 600K is attributed to detrapping of the positron from a surface state with electron pick up on emission. Prior to this the escape as positronium of free surface positrons is seen. The negative curvature at higher temperatures is associated with creation of thermal vacancies. From these curves Lynn and Welch obtained an activation energy for each incident positron energy. The Born-Haber cycle may be used to estimate the binding energy (E_b) of surface traps (Mills 1979, who identified this with the activation energy for thermal emission of Ps). This E_b is the energy required to remove a positron from a surface trap to

rest at infinity, similarly the electron work function (ϕ_e) is the energy that must be given to remove an electron to rest at infinity. Thus the energy required (E_a) to form Ps at rest, away from the surface is

$$E_a = E_b + \phi_e - 6.8eV \tag{1.21}$$

where 6.8eV is the energy released when Ps is created. In fact it is more likely that $E_a \geq E_b + \phi_e - 6.8eV$ since it may be necessary to excite the trapped positron to a distance sufficient from the surface electron density to enable Ps to form (Held and Kahana 1964, Lowy and Jackson 1975). Figure(1.10.3) illustrates this schematically for the case of a positive positron work function (ϕ_p) and where E_a^{min} is the minimum energy required for thermal activation.

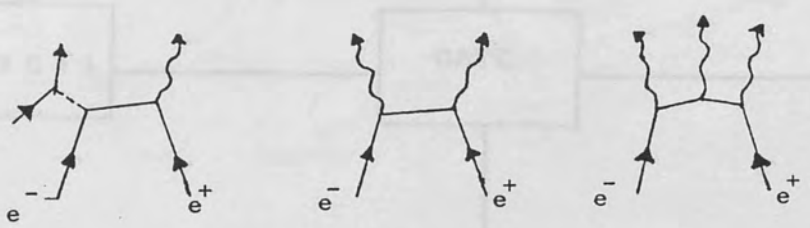

Figure(1.4.1) Feynmann diagrams for one, two and three photon annihilations.

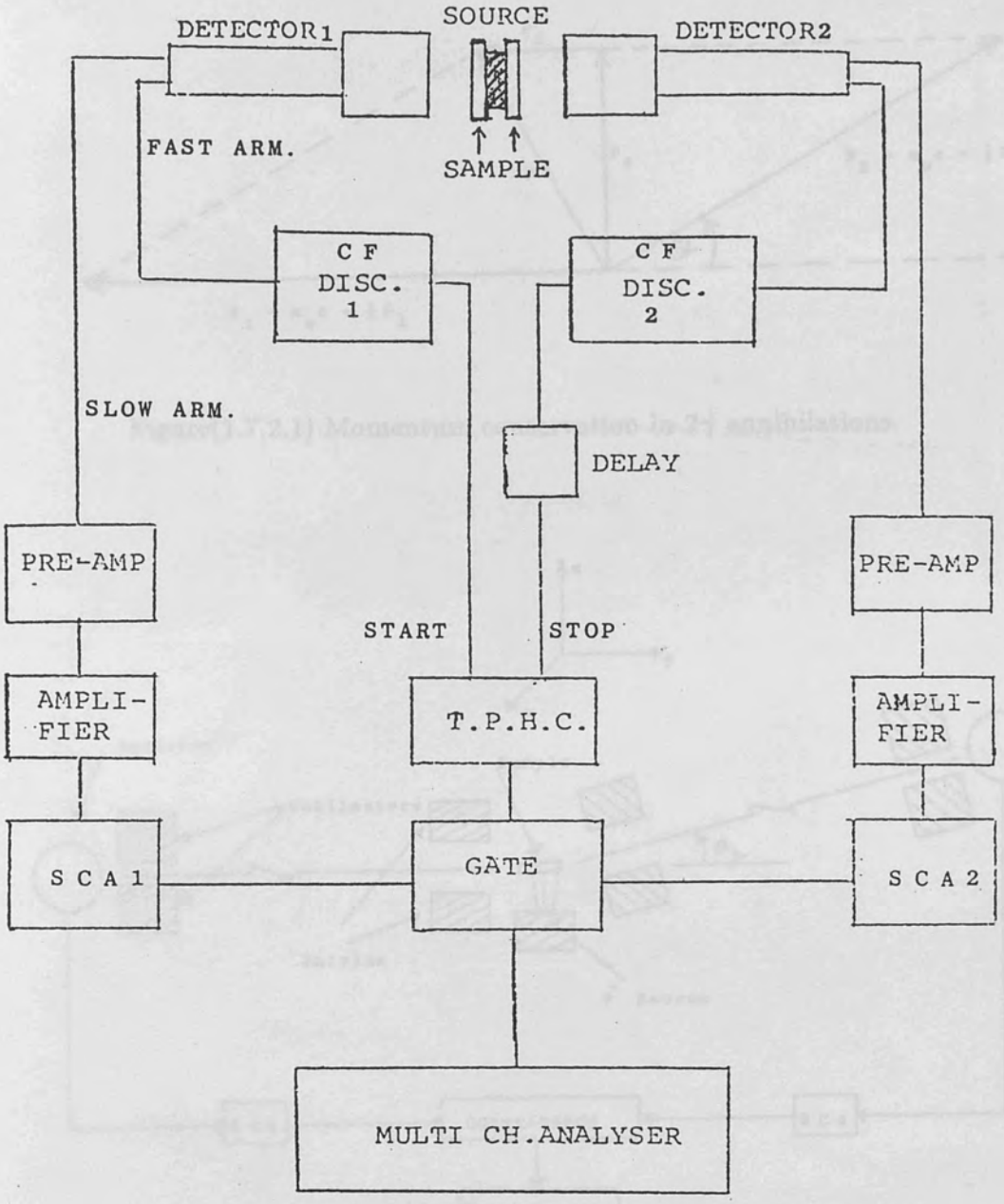

Figure(1.7.1.1) Fast-slow coincidence lifetime system.

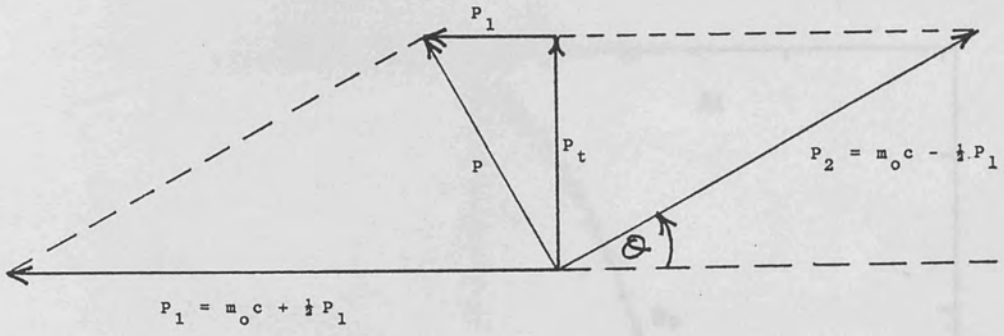

Figure(1.7.2.1) Momentum conservation in 2γ annihilations.

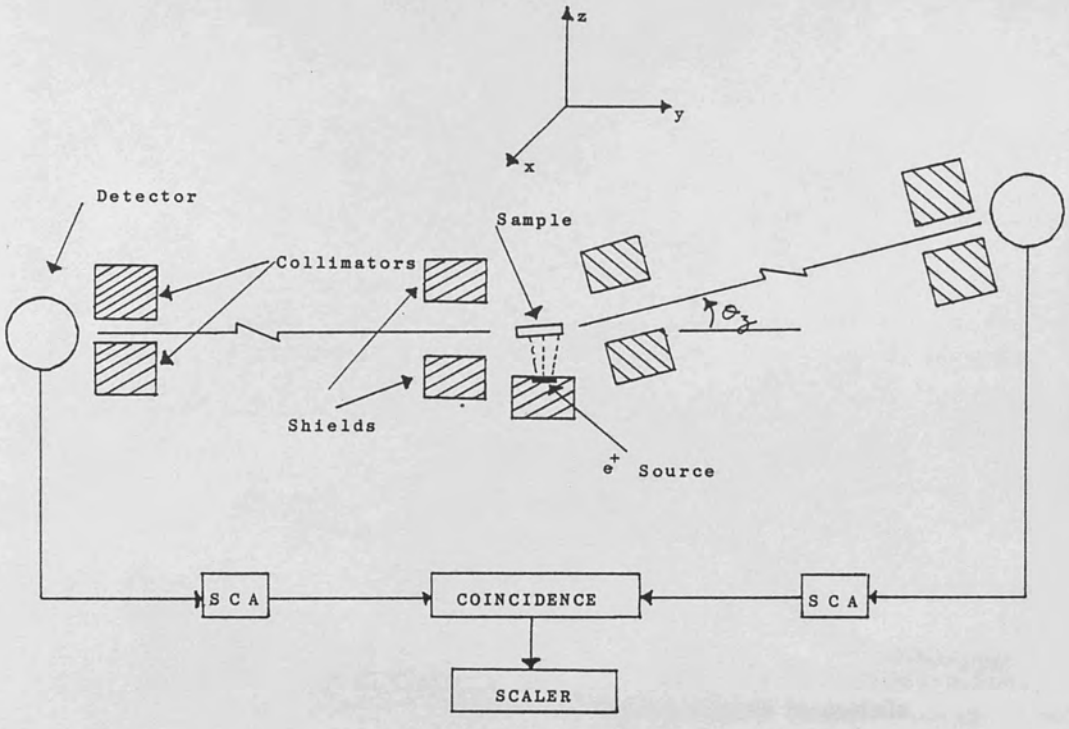

Figure(1.7.2.2) Long-slit geometry in angular correlation.

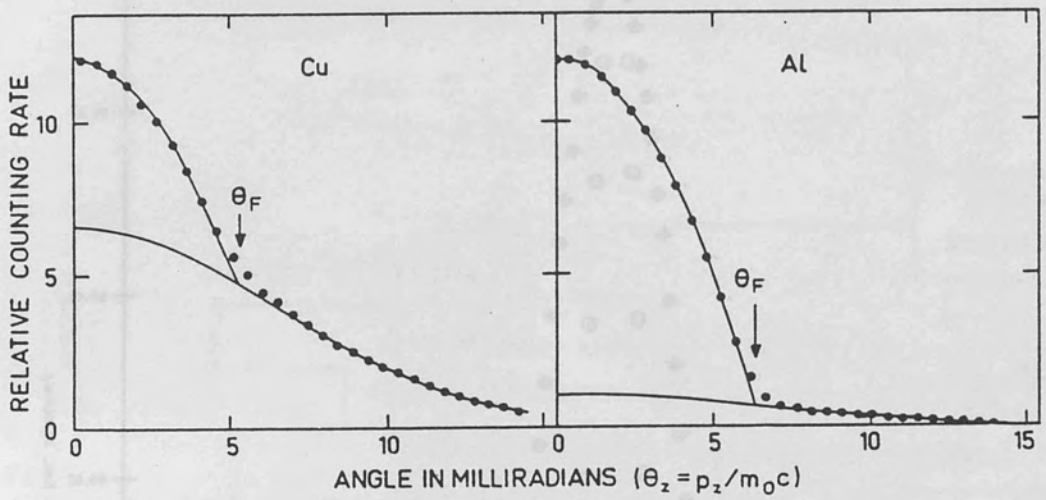

Figure(1.7.2.3) Form of angular correlation curves in metals. θ_F is the Fermi cutoff for the inverted parabola due to annihilation with valence electrons (Hautojärvi 1979).

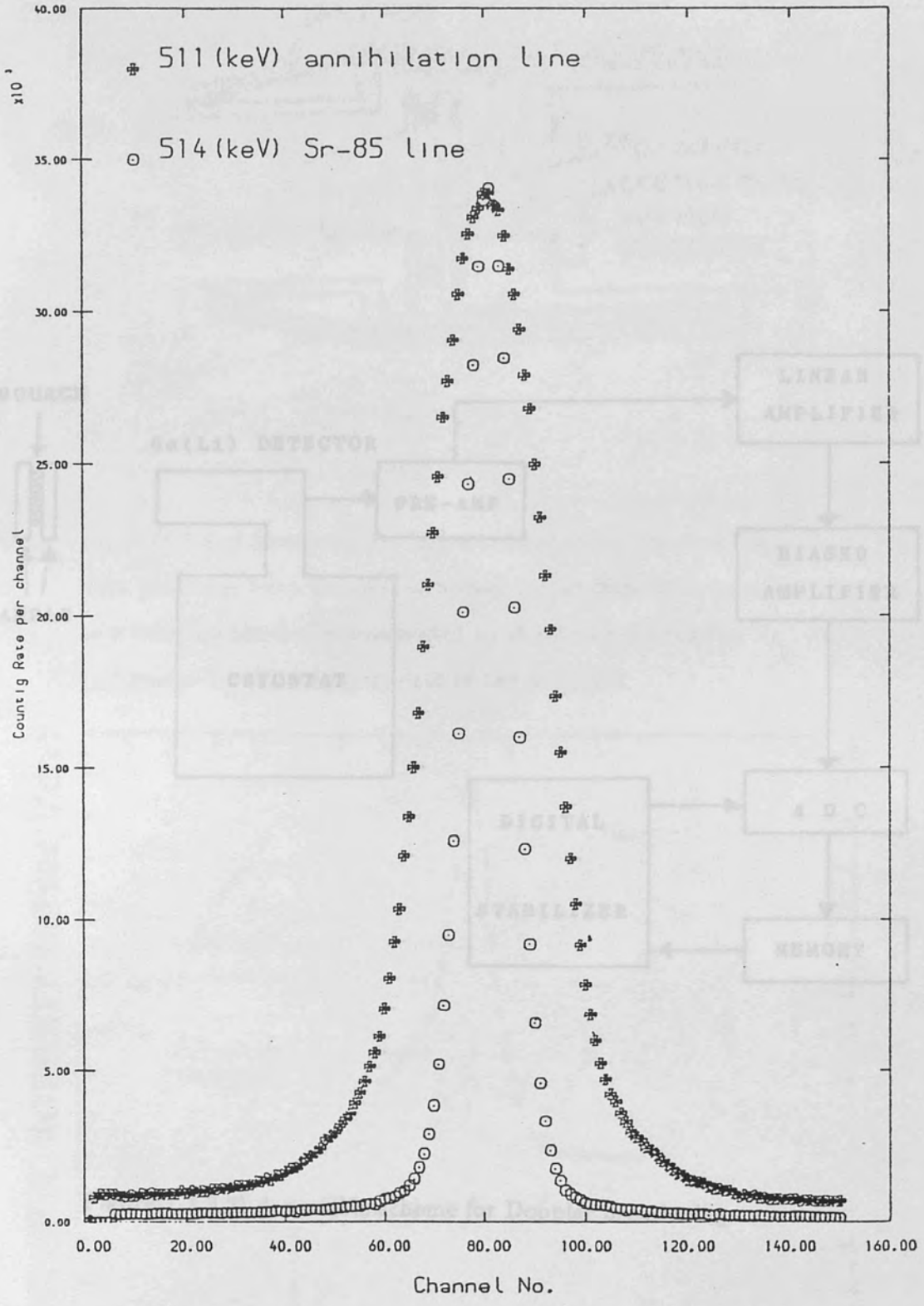

Figure(1.7.3.1) Annihilation line and 514keV ^{85}Sr system responce normalised to equal height.

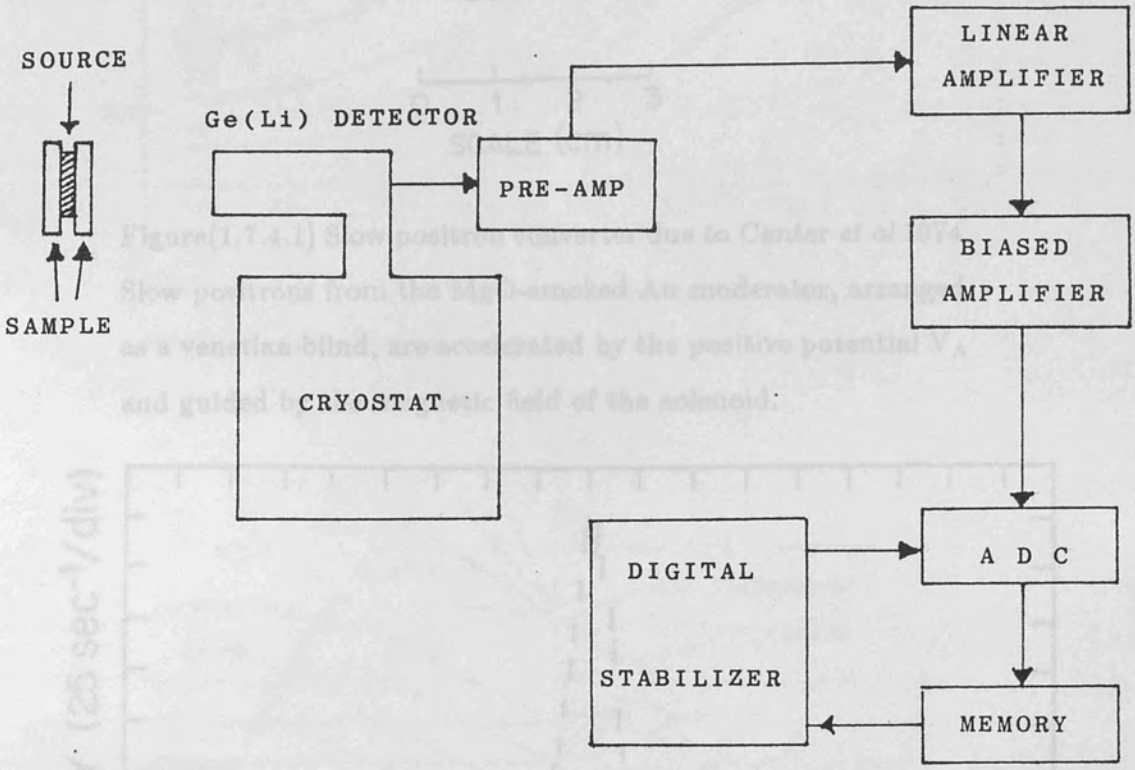

Figure(1.7.3.2) A possible scheme for Doppler broadening.

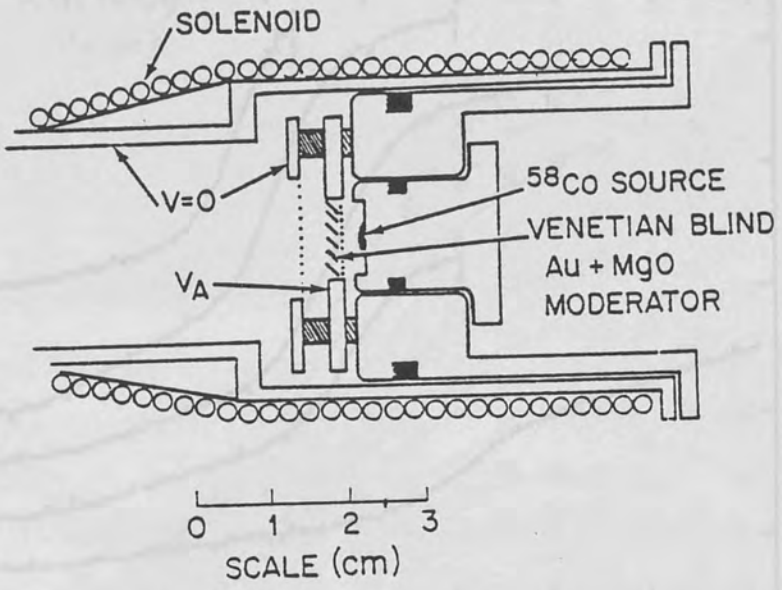

Figure(1.7.4.1) Slow positron converter due to Canter *et al* 1974. Slow positrons from the MgO-smoked Au moderator, arranged as a venetian blind, are accelerated by the positive potential V_A and guided by the magnetic field of the solenoid.

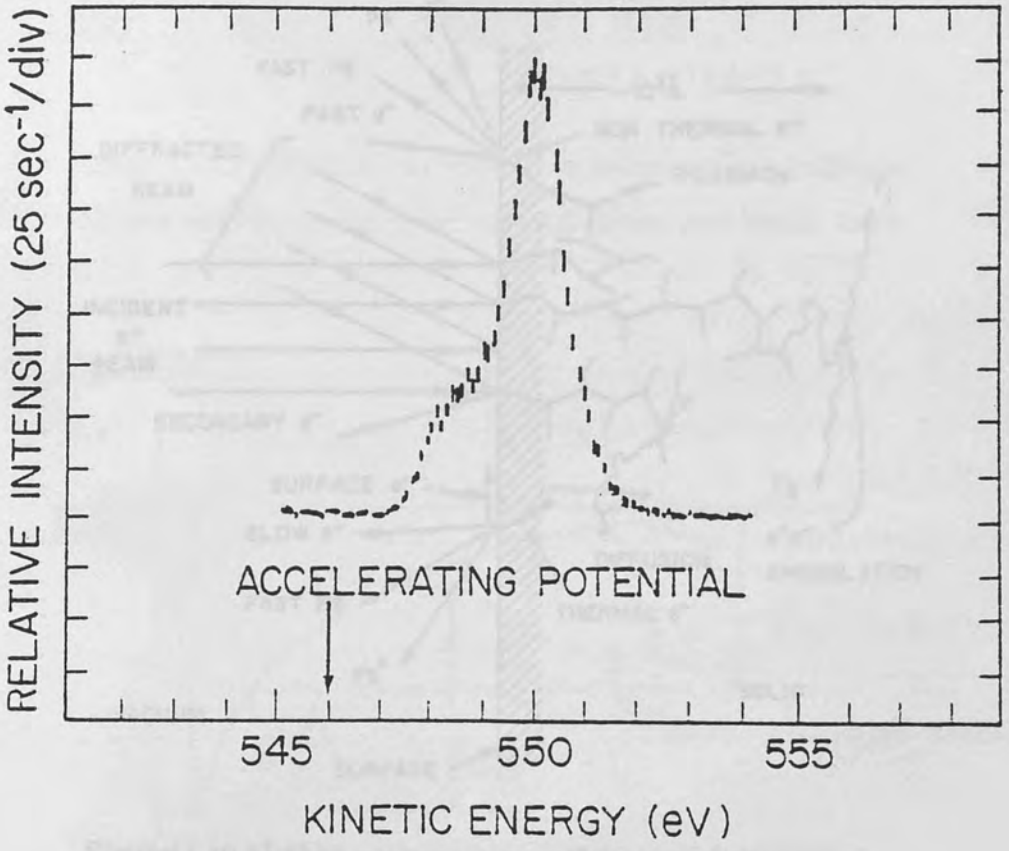

Figure(1.7.4.2) Example energy dispersion of a positron beam Dale *et al* 1980.

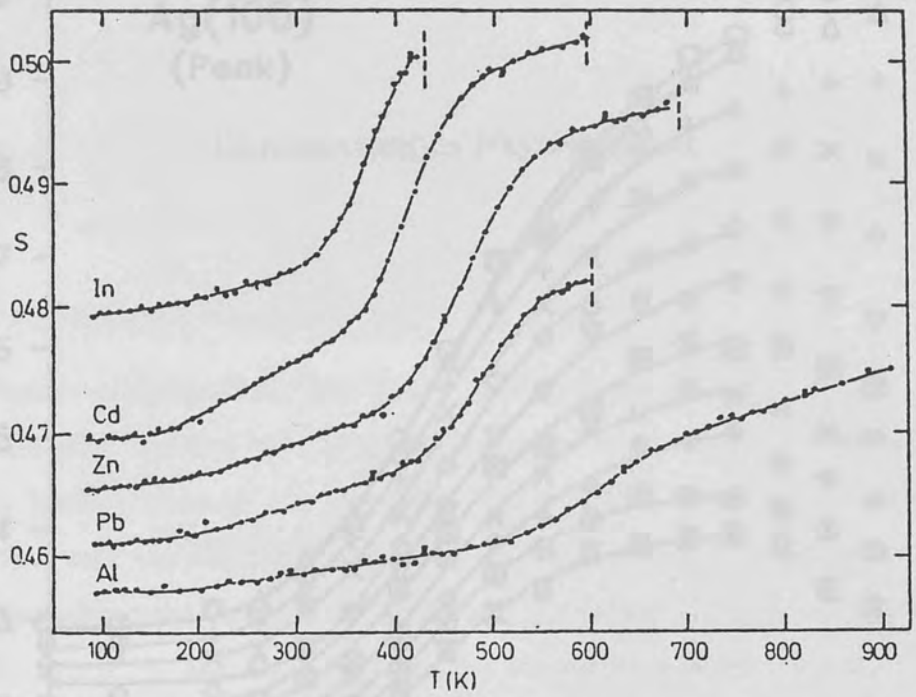

Figure(1.8.1) Lineshape parameter against temperature for several metals (Hautojärvi 1979).

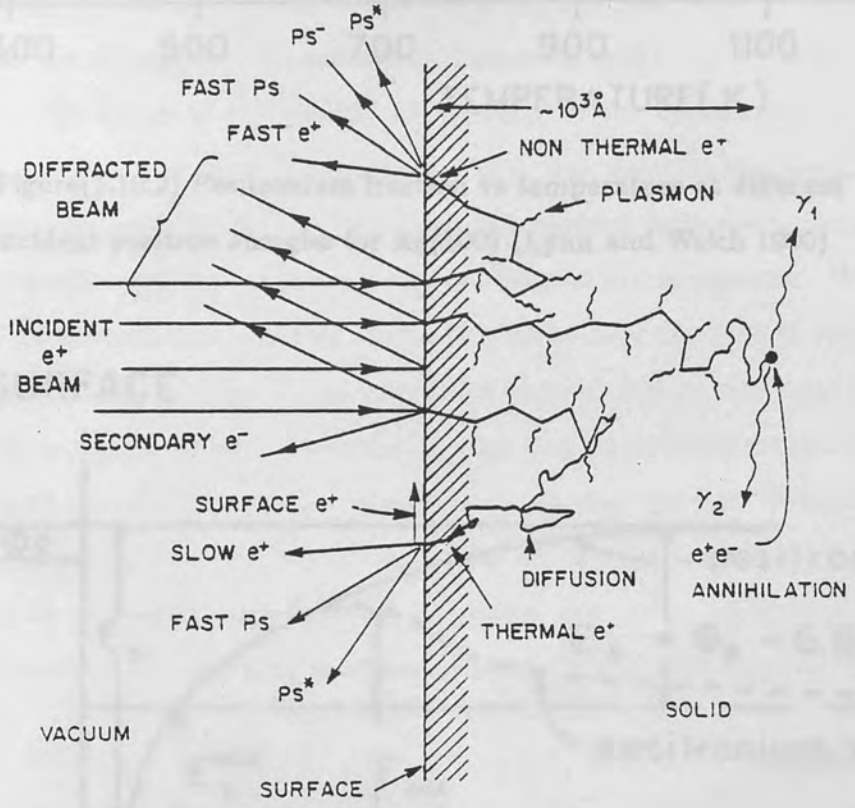

Figure(1.10.1) Slow positron interactions at a surface.

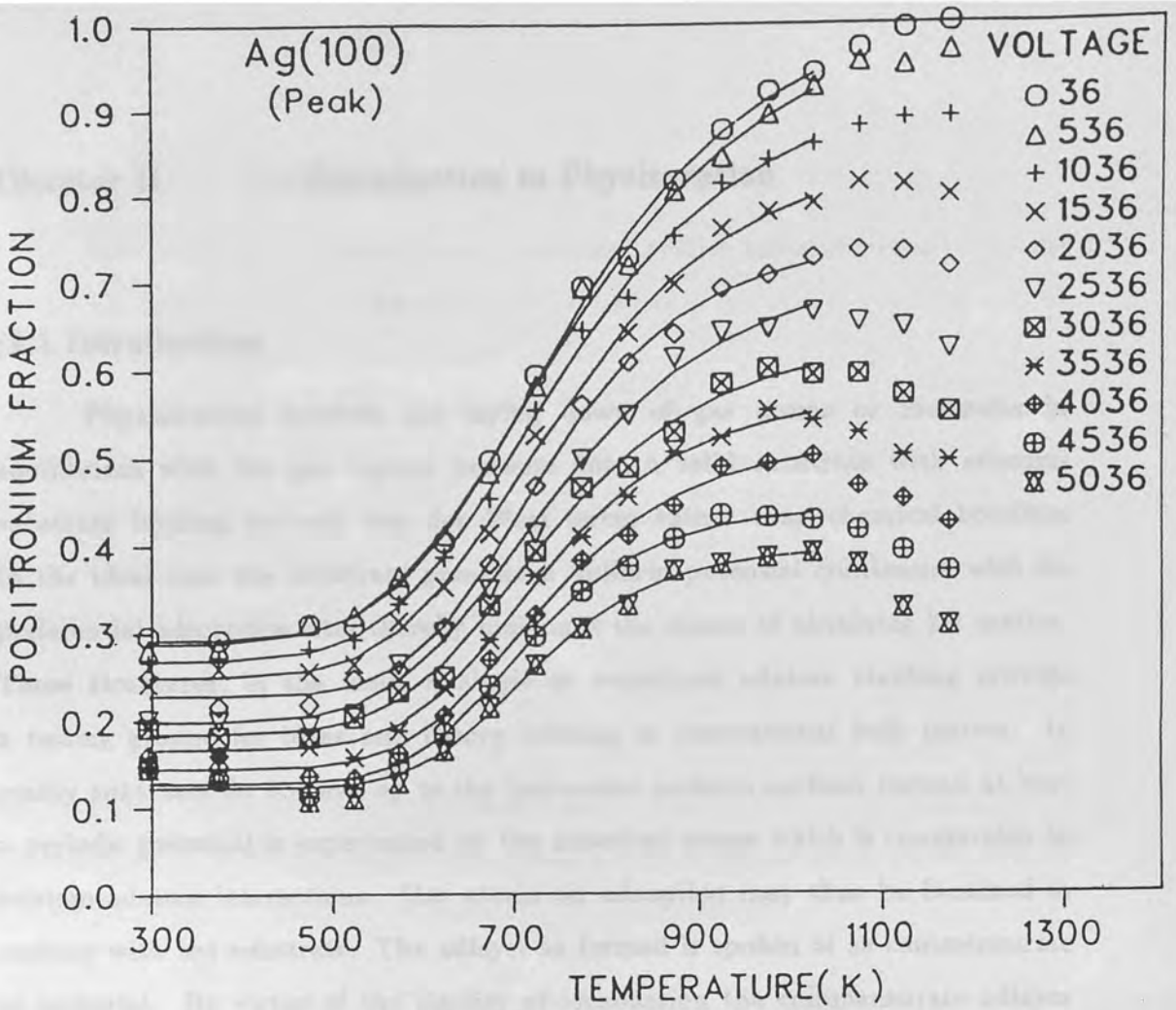

Figure(1.10.2) Positronium fraction vs temperature at different incident positron energies for Ag(100) (Lynn and Welch 1980)

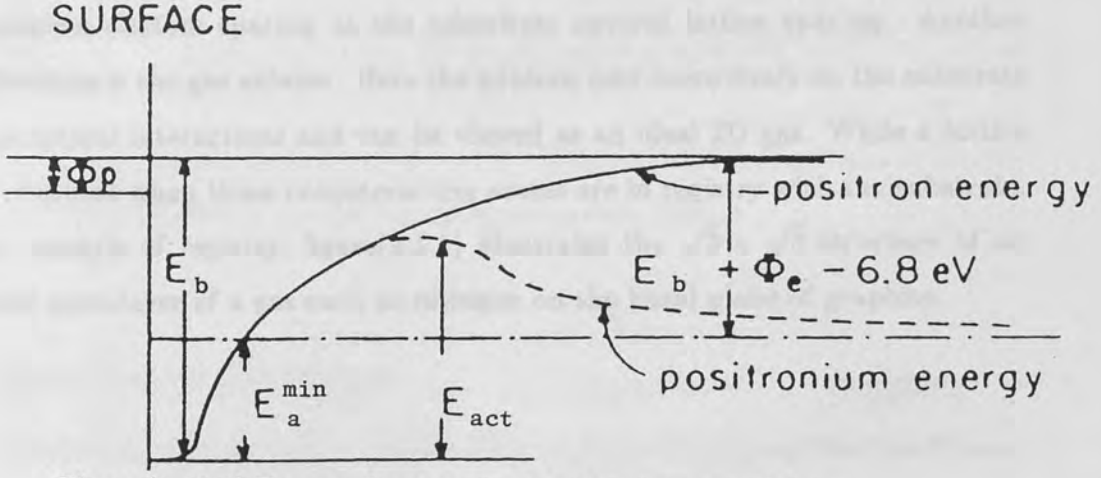

Figure(1.10.3) Energy diagram for positronium emmision.
The activation energy for positronium emission E_a^{min} is exceeded by the actual activation energy E_{act}.

Chapter II Introduction to Physisorption

§2.1 Introduction

Physisorption involves the laying down of gas atoms or molecules in equilibrium with the gas vapour pressure onto a solid substrate with adatom-substrate binding through van der Waal forces rather than chemical bonding. In the ideal case the substrate presents a uniform potential continuum with no preferential adsorption sites thereby making it the means of obtaining 2D matter. These structures, in the main of single or monolayer adatom stacking provide a testing ground for ideas and theory relating to conventional bulk matter. In reality subtrates do not live up to the featureless uniform surface; instead at best a periodic potential is experienced by the adsorbed atoms which is comparable to adatom-adatom interactions. Gas atoms on adsoption may thus be localized in registry with the substrate. The adlayer so formed is spoken of as commensurate or epitaxial. By virtue of the rigidity of localization the commensurate adlayer is classified as solid. An incommensurate solid is also possible the result usually of commensurate compression. In this case the natural lattice structure of the adsorbate prevails and the substrate potential periodicity is ignored. When the adatoms of an incommensurate film are free to move laterally a fluid state exists with adatom-adatom spacing at the adsorbate natural lattice spacing. Another possible state is the gas adlayer. Here the adatom may move freely on the substrate with no lateral interactions and can be viewed as an ideal 2D gas. While a lattice gas is obtained when these noninteracting atoms are in registry with the substrate. As an example of registry, figure(2.1.1) illustrates the $\sqrt{3} \times \sqrt{3}$ structure of an epitaxial monolayer of a gas such as nitrogen on the basal plane of graphite.

§2.1.1 Van der Waal Forces

Low energy interactions between nonpolar neutral molecules result from the attraction between electric dipoles induced mutually by the fluctuating charge distribution of atoms. This London dispersion or van der Waal's type force (Dalgarno and Davison 1966, Hirschfelder 1954, 1967, Torrens 1972) is attractive at distances an order of magnitude greater than molecular diameters (σ). At near distances overlap of the electron clouds begins to play a role so that the potential has a minimum at a separation of the order of 1Å. A traditional form for the interaction is the Lennard-Jones potential

$$u(r) = 4\epsilon \left[\left(\frac{\sigma}{r}\right)^{12} - \left(\frac{\sigma}{r}\right)^{6} \right] \tag{2.1}$$

where u(r) is the potential at a distance r and ϵ a constant. In physisorption the potential felt by a neutral nonpolar gas atom at the surface of a van der Waal solid can be found from a simple summation of pair interactions

$$u(r) = \sum_i u_i(|r - r_i|) \tag{2.2}$$

where the r_i are the locations of the atoms of the solid. Using the approximation of a uniform continuum valid for distances of above several angstroms from the surface one obtains from (2.1)

$$u(d) = 4\pi\epsilon n_s \left[\left(\frac{\sigma^{12}}{45d^9}\right) - \left(\frac{\sigma^6}{6d^3}\right) \right] \tag{2.3}$$

where n_s is the atomic density of the solid. This expression implies a cube law decline in the attractive potential for distances greater than σ.

§2.2 Experimental Techniques

Modern surface science includes a host of methods ranging from traditional thermal and vapour pressure measurements to low energy electron diffraction (LEED), Auger electron spectroscopy (AES), field emission and ionization

microscopy not omitting the low energy positron. Each has a limitation and only a combination can provide the total picture. The most widely used is LEED (Haas 1971) in which the surface is bombarded by monoenergetic electrons (Lander 1965). The electrons, of a few hundred volts energy, penetrate only topmost layers of a surface so that a high proportion of the information relayed is purely of the adlayer. The symmetries and sharpness of a diffraction pattern provide detail of surface structure. A most useful application is to surface preparation where it is used to verify surface purity from contaminants prior to adsorption studies by other methods. LEED requires a vacuum better than 10^{-5}Torr and is limited to systems having these low vapour pressures. Other disadvantages include the desorption of film weakly bound (physisorbed) (Farell *et al* 1972) and the uncertainties often experienced in interpretation. A varient of the basic technique; reflection high energy electron diffraction (RHEED) can examine deeper substrate or film structure and measure longer range order. Another electronic method is AES. The technique is based on recording the electron emission spectra of atoms returning to their ground state after inner shell excitation. Ellipsometry originating from the end of the last century (Drude 1889, 1890) has gained popularity in recent years. It involves changes in the state of polarization of light on reflection from a surface. The techniques of nuclear magnetic resonance (NMR) and electron paramagnetic resonance (Aston 1966) which have origins in the study of bulk properties have found application to adatom mobility (Rollefson 1972, 1973). A method complementing LEED is neutron diffraction which may be used in cases of high vapour pressure and which is free from the desorption effect of LEED.

These modern techniques have advantages over traditional measurements of vapour pressure, heats of adsorption and heat capacity. Advantages include the fact that information is yielded on microscopic states of the adsorbate and that much smaller adsorption areas are required. Nevertheless a thermodynamic study, by either vapour pressure or calorimetric measurements is often essential to completely characterize an adsorption system. Heat capacity measurements can be used to follow melting transitions. Figure(2.2.1), as an example, shows heat capacity scans for neon at various coverages on exfoliated graphite. In isotherm

measurements substrate areas ranging from a metre to several hundred metres squared are exposed to known amounts of gas at constant temperature. Shots of gas are applied and vapour pressure measured. A step function form, figure(2.2.2), is seen where each knee corresponds to layer completion. This form originates in the following manner: as gas is introduced vapour pressure rises in accordance with the ideal gas law but at a point dependent on binding energy of a gas molecule to the substrate, layer growth begins and further shots serve only to feed this growth. Upon completion of a layer further adsorption is precluded until the gas vapour pressure is sufficient for next layer adsorption. A measurement of the amount of gas adsorbed for monolayer coverage enables estimation of substrate surface area given knowledge of the adlayer structure and can act as a calibration. The higher the substrate homogeneity and adatom-substrate binding energy the sharper the observed steps. On heterogeneous surfaces there will be patches of varying binding energy which physisorb at different pressures and produce blurring of the steps of layer formation. With increasing heterogeneity there is a progressive loss of detail through layer superposition resulting eventually in a smooth sigmoid shape, figure(2.2.3), which can be described by the BET formula. Thermal promotion between layers is a further feature tending to obscure steps and appears when kT becomes comparable or larger than the difference in layer-substrate binding energies. Detailed isotherm measurements can reveal regions of phase coexistence and transitions. Figure(2.2.4) from the work of Thomy and Duval (1970) shows definite features during the formation of the first layer. These features are identified with a succession of gas, liquid and solid phases with vertical sections indicating regions of two-phase coexistence. They arise from, for example, different packing densities of different phases. For example a change from commensurate ordering to incommensurate for a solid adlayer usually implies an increase in adsorbate density so that further adsorption would be required for layer coverages equivalent to those of commensurate.

§2.3 The Langmuir Model

This model is applicable to registered noninteracting adlayers. It assumes the adatom to have a binding energy (ϵ_0) fixing it to an adsorption site but no other internal energy (Langmuir 1918, Fowler and Guggenheim 1939). The binding energy acts only in a direction normal to the surface and there is no interaction between adatoms but for short-range repulsive forces which limit site occupation to a single adatom. By equating chemical potentials of film and vapour, a vapour pressure relation may derived (Dash 1975)

$$P = \left(\frac{2\pi m}{h^2}\right)^{\frac{3}{2}} (kT)^{\frac{5}{2}} \frac{x}{1-x} \exp\left(-\frac{\epsilon_0}{kT}\right) \tag{2.4}$$

Where P is the vapour pressure, m the adatom mass, h Planck's constant, k Boltzmann's constant, T absolute temperature and x fractional coverage. The $x/(1-x)$ relationship between vapour pressure and coverage is linear at small x but diverges as monolayer completion nears. The isosteric heat of adsorption q_{st} may be obtained from (2.4)

$$q_{st} = kT^2 \left(\frac{\partial \ln P}{\partial T}\right)_x = \epsilon_0 + \frac{5}{2}kT \tag{2.5}$$

A heat of adsorption describes the energetics of adsorption. It equals the adatom-substrate binding energy in the limit of zero temperature and coverage. At finite temperature and coverage the heat of adsorption can serve as a probe of the state of the adsorbed film. A variety of heats of adsorption may be defined and these then refer to specific processes. The isosteric heat of adsorption is an often used derivative of temperature under constant coverage and volume.

§2.4 Boltzmann Approximation

The substrate is assumed uniform of area A on which N_f particles are adsorbed. A binding energy ϵ_0 holding the adatom with respect to surface-normal motion is assumed however there is freedom for the particle to move in surface-parallel directions. At sufficiently high temperatures and low densities the

Boltzmann approximation can be used (Fowler and Guggenheim 1939, Band 1955), provided the condition of validity

$$n\lambda^2 \ll 1 \tag{2.6}$$

is satisfied, where $n = N_f/A$, $\lambda = h(2\pi mkT)^{-\frac{1}{2}}$. By combining the film energy function with the quasi-classical partition function and using Stirling's approximation, principle thermodynamic properties may be obtained (Dash 1975). Furthermore equating film and vapour chemical potentials yields

$$P = \frac{n}{\beta\lambda}\exp(-\beta\epsilon_0), \quad \text{where} \quad \beta = \frac{1}{kT}$$

or

$$P = \left(\frac{2\pi mk^3}{h^2}\right)^{\frac{1}{2}} nT^{\frac{3}{2}} \exp\left(-\frac{\epsilon_0}{kT}\right) \tag{2.7}$$

where P is the adsorbate vapour pressure, m the adatom mass, k Boltzmann's constant, h Planck's constant and T film temperature.

Also

$$q_{st} = \epsilon_0 + \frac{3}{2}kT \tag{2.8}$$

where q_{st} is the isosteric heat of adsorption. In this model, applicable to noninteracting fluid adlayers, the region of linear coverage dependence for pressure, known as the 'Henry law', extends to coverages of monolayer and beyond. This extension is strictly dependent on noninteraction. For typical gases and substrates Henry's law holds for coverages below only about 0.1 monolayer and is affected by substrate heterogeneity, which can cause substrate-mediated interactions. At higher densities and/or lower temperatures quantum statistical interactions become important. An equation valid at all temperatures and coverages for noninteractive adsorption may be derived based on these statistical interactions (Dash 1975)

$$P\pm = (\pm)\left[e^{\pm n\lambda^2} - 1\right]\left[\frac{e^{-\beta\epsilon_0}}{\beta\lambda^3}\right] \tag{2.9}$$

In the classical limit, $n\lambda^2 \ll 1$, expansion of the $n\lambda^2$ exponential yields the Boltzmann isotherm (2.7).

§2.4.1 Weak Interactions

When adatom-adatom interactions are taken into account an expression may be presented valid for relatively high temperatures (Volmer 1925, Fowler and Guggenheim 1939, Cassel 1944)

$$P = \left(\frac{nkT}{\lambda}\right) e^{-\beta\epsilon_0} e^{2nB} \tag{2.10}$$

where B (= $B_f(T)$) is the second virial coefficient due to pairs of adatoms. $B_f(T)$ can be written as the sum of two terms when the pair interaction is formulated to be strongly repulsive at close approach and weakly attractive at greater distances. Then in a high temperature approximation

$$B_f(T) = b - a\beta \tag{2.11}$$

where b is a constant for the repulsive force the 'effective collision' area and a that for the attractive. When $b > a\beta$ (at high temperature) the vapour pressure rises as n exp(const n) and resembles the behaviour of the Langmuir isotherm at moderate coverage. At B = 0 ($b = a\beta$) the ideal Boltzmann isotherm is obeyed. At lower temperatures the vapour pressure falls below this ideal curve, the rate of change of pressure with coverage decreases due to tendency of adatoms to attract vapour atoms to the surface. This is reflected by an increase of q_{st} with increasing coverage. The critical parameters of the 2D van der Waal equation (identified with those of the 3D case) can be written in terms of the repulsive and attractive components of the virial coefficient

$$n_c = \frac{b}{3}, \quad kT_c = \frac{8a}{27b}, \quad \phi_c = \frac{a}{27b^2} \tag{2.12}$$

where the subscript c for n, T, and ϕ denotes critical values for density, temperature and spreading pressure respectively. The critical and triple-point temperatures of

a monolayer are expected to be lower than those of the bulk, as a result of the reduction in coordination number. For simple gases on uniform substrates,

$$\frac{T_c(2D)}{T_c(3D)} \sim 0.5$$

and

$$\frac{T_t(2D)}{T_t(3D)} \sim 0.6$$

is expected.

§2.5 BET Formula

The Brunauer-Emmett-Teller (BET) law (Brunauer *et al* 1938, Young and Crowell 1962) may be used to describe adsorption to monolayer and higher coverages on relatively heterogeneous substrates. The law is a two parameter equation between vapour pressure (P) and volume (v) of adsorbed gas

$$\frac{x}{v(1-x)} = \frac{1}{v_m c} + \frac{(c-1)}{v_m c}x \qquad (2.13)$$

where $x = P/P_o$, P_o being the bulk adsorbate vapour pressure at the temperature of the isotherm, v_m is the volume of the monolayer, c is related to the free energy difference between the first and succeeding layers. Although the equation is useful in extracting gross features for example estimation of surface area, from isotherms on as mentioned heterogeneous surfaces because of the unrealistic and internally inconsistent model from which it is derived the formula cannot be considered to be of fundamental significance. For example the model assumes a Langmuir monolayer but that additional layers are fluid. This presumes incorrectly that the substrate field is felt only by the first layer. Furthermore higher layers are assumed to be formed without lateral interactions which conflicts with the supposition of a liquid state. The BET isotherm is sigmoid in form and correctly follows isotherms obtained from the average adsorbent, figure(2.2.3), however the lack of distinct steps is accounted for in the BET theory by statistical variations in film thickness which again is not the true cause (section 2.2).

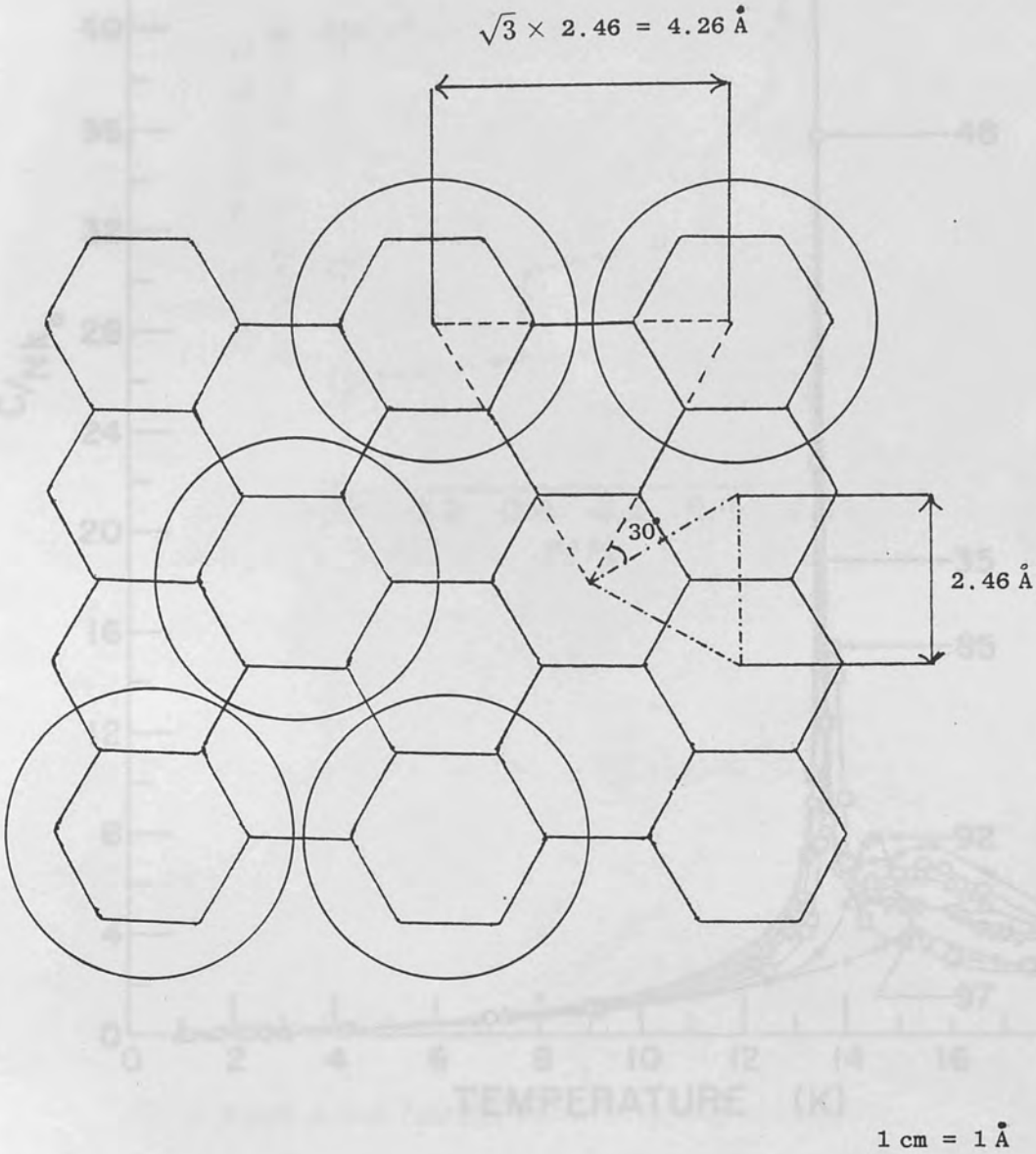

Figure(2.1.1) Second-neighbour adsorption of a gas such as nitrogen on the basal plane of graphite. Illustrated are the unit cells of graphite and the $\sqrt{3} \times \sqrt{3}$ configuration whose surface spacing is $\sqrt{3}$ larger and which is rotated 30° with respect to the graphite. In the case of nitrogen this structure forces a 4% expansion from a 4.1Å natural spacing.

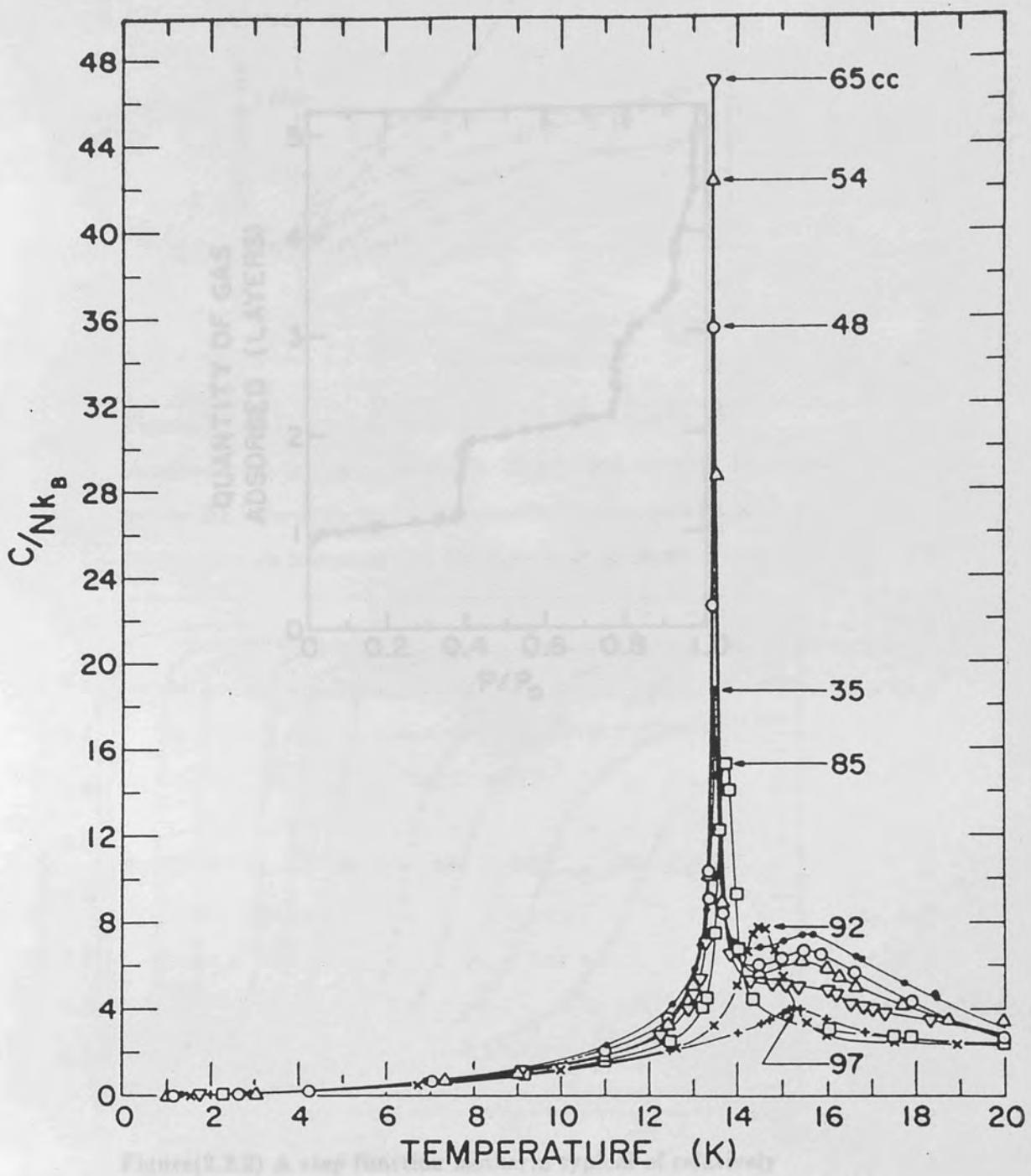

Figure(2.2.1) Heat capacity scans at constant coverage of neon on exfoliated graphite (Huff and Dash 1974, Huff 1973) indicating triple point at $\sim$ half-coverage. Monolayer capacity is 115cc at STP

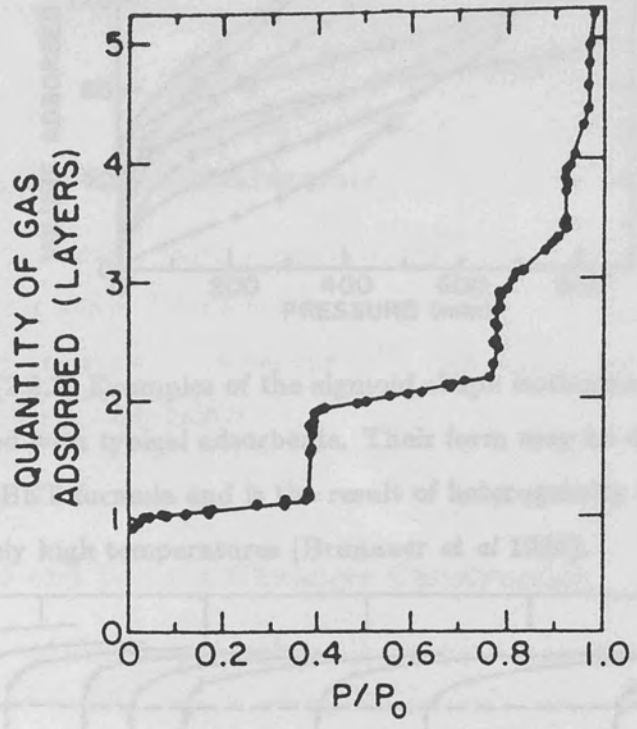

Figure(2.2.2) A step function isotherm typical of relatively uniform surfaces at low temperature. The isotherm is of Kr on exfoliated graphite at 77.3°K (Thomy and Duval 1969). P_0 is the bulk vapour pressure at the temperature of the isotherm.

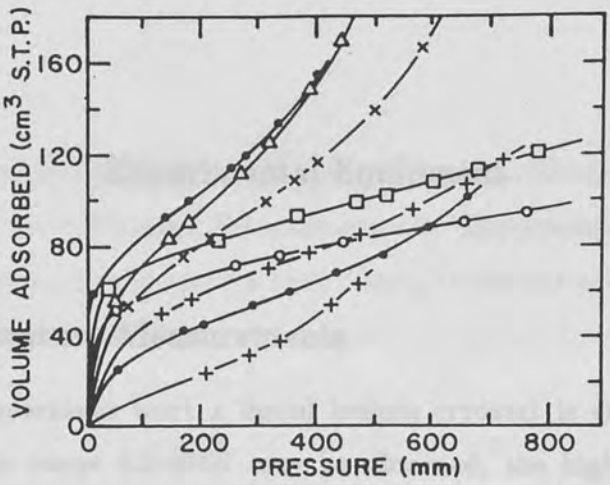

Figure(2.2.3) Examples of the sigmoid shape isotherms obtained with typical adsorbents. Their form may be described by the BET formula and is the result of heterogeneity and relatively high temperatures (Brunauer *et al* 1938).

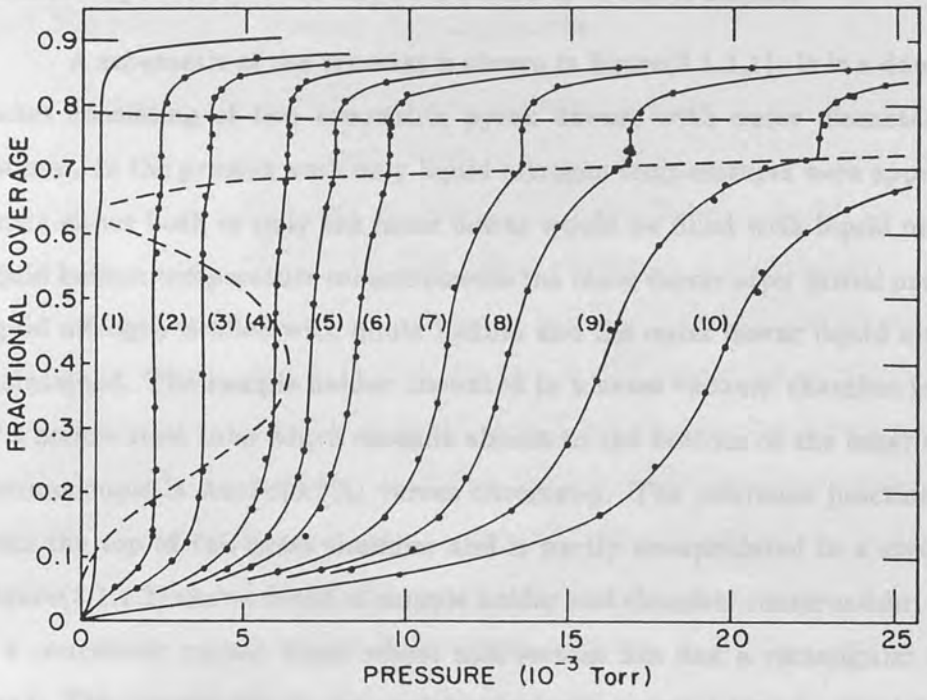

Figure(2.2.4) Vapour pressure isotherms of Kr on exfoliated graphite to monolayer coverages (Thomy and Duval 1970). The loci map phase boundaries. The triple point temperature is seen to be a little above 85K. Isotherm temperatures (°K) are: (1) 77.3, (2) 82.4, (3) 84.1, (4) 85.7, (5) 86.5, (6) 87.1, (7) 88.3, (8) 89.0, (9) 90.1, (10) 90.9.

Chapter III Experimental Equipment

§3.1 Low Temperature Measurements

For low temperature work a liquid helium cryostat is employed. Sample temperatures in the range 4.2-490K may be obtained, the highest temperatures requiring vacuum conditions. In vacuum the high temperature limit is set by materials used in the sample holder.

§3.1.1 Cryostat and Sample Chamber Construction

A schematic of the cryostat is shown in figure(3.1.1.1). It is a double vacuum jacket consisting of two concentric pyrex dewars with outer diameters of 90and 150mm. In the present work only liquid nitrogen temperatures were approached and hence either both or only the inner dewar would be filled with liquid nitrogen. For liquid helium temperature measurements the inner dewar after initial pre-cooling by liquid nitrogen is filled with liquid helium and the outer dewar liquid nitrogen level maintained. The sample holder, mounted in a brass vacuum chamber is at the end of a hollow steel tube which extends almost to the bottom of the inner dewar. The thermocouple is Au-Fe(0.3%) versus chromel-p. The reference junction protrudes from the top of the brass chamber and is partly encapsulated in a stycast mould. Figure(3.1.1.2) shows detail of sample holder and chamber construction. The holder is a concentric copper block whose mid-section has had a rectangular section cut away. The sample sits in this rectangular area, secured by an overplate. At both ends adjacent to the sample area, concentric areas have been cut and these take the heater wire. A nylon screw attaches this copper block to a thermal platform which itself is fixed to the covering brass plate of the vacuum chamber. Thermocouple and heater wires pass from the head of the cryostat assembly along the hollow steel tube and into the vacuum chamber. These wires are wrapped around the thermal platform, for thermal anchoring, before being drawn on to the copper sample holder. The Au-Fe thermocouple is soldered to the chromel-p at the body of the holder and

the junction held tightly against the holder by a top plate. The point of securement is no more than a few millimetres from the sample. The heater wire, of nichrome covered by PTFE (supplied by Vactite Ltd) , has a resistance of $\sim 70\Omega$ and can be heated to ~480K. An indium ring resting in a shallow groove is used for the vacuum seal when the brass chamber is screwed to its cover plate. A chamber vacuum better than 10^{-6}Torr is usually obtained for vacuum measurements. With liquid nitrogen in the inner dewar the lowest attainable temperature in vacuum is around 79K and is limited by heat leakeage through the thermocouple and heater wires. The sample has to be normally left overnight before it cools to this value.

§3.1.2 Automatic Feeder Arrangement

The promise of unmanned continuous equipment operation offered by a microcomputer control system (described in chapters 4 and 5) could only be fully realized with the addition of an automatic liquid nitrogen feeder for the cryostat. An earlier attempt (Berry 82) had found success in a pressure feed arrangement using timer operated electrical valves but this had been deinstated and it was only after the final move to the Egham site that a fresh commitment was pursued. The pressure feed arrangement was based upon a self-pressurising (by means of an heat exchanger) 200 litre dewar. Operation problems had been encountered with this method. The valves were liable to icing and before operation the system would be flushed with nitrogen or helium gas. On an occasion the contents of the 200l dewar were lost when the valve iced in the open position. A solution was to employ two valves in series. The heart of the present system is a nitrogen dispensor supplied by Cryoproducts. The empaler type dispensor has a 12V motor which turns a propeller at the end of a metre long steel tube. Close to, almost touching, the propeller is a slightly conical mild steel plate. The action of this plate upon the propeller turning is to direct liquid nitrogen up through a feed tube. Behind the propeller head is a hard rubber stalk that fits tightly within an outer steel tube. The arrangement is most precise in that the propeller only turns freely at liquid nitrogen temperatures. The dispensor sits in the 200l dewar with its top, containing the motor, resting on

the dewar neck. The nitrogen dispensor maintains only the inner cryostat dewar, the outer dewar being left dry. Lagged copper pipework connects the dispensor outlet to the inner dewar. Coupled with the dispensor is the output of a single sensor level controller. A level controller normally consists of two sensors, one for a low level limit the other for a fill level. The single thermal sensor of the available controller is placed at the dewar full position. An RS mains timer relay allows the nitrogen level to fall before activating the dispensor. The operation of the relay is to channel input power to one of two outputs. On energising output is to channel 1 but after a time preset on a 0-3 minute timer the relay is triggered and output is switched to channel 2. For the present application the 3 minute delay was extended to 50 minutes by insertion of a 2MΩ resistor. Two other mains relays are incorporated. These act to make the dispensing system failsafe. The dispensor is ordinarily switched off by the level controller, but if a break develops in the feed line the second relay would trigger after 10 minutes and cut power from the dispensor. The third relay on the second triggering switches power to the Digital Temperature Controller (DTC) off and sounds an alarm. The DTC controls sample temperature and in the event of dispensor failure and inner dewar drying could cause sample holder burn out. Figures(3.1.2.1 - 3) show the dispensing system and provide timing diagrams. A mains trip between the third relay and DTC ensures that the DTC can only be powered up again manually after a power cutoff.

§3.2 The Furnace

For measurements between 300-600K a furnace is used. The upper temperature limit of 600K is not set by the furnace but is the highest temperature considered safe before vaporization of the ^{22}Na source (see for example McGetrick 1981). Temperature measurement is with a Chromel-Alumel (T_1-T_2) thermocouple with the reference junction held at melting ice temperature and sample junction secured to a steel sample holder. The sample holder is mounted at the end of a 30cm Alumina twin bore tube along which the thermocouple wires pass. The body of the furnace is an aluminous porcelain tube of 2.3cm bore around the central region of

which is wound a nichrome heater wire and which is insulated by an asbestos layer. Two brass ends with 'O' rings seal the sample chamber. All heating is performed under vacuum conditions and the furnace at its hot spot can safely reach 2000K. Furnace temperature is regulated by an Oxford Instruments temperature controller with an appropiate furnace range card. The temperature controller is coupled with an external power supply unit to provide the necessary power output.

§3.3 Detector and Electronics

§3.3.1 The Detector

Almost all Doppler measurements undertaken in this work employed the original Bedford college intrinsic germanium planar detector. The detector supplied by Princeton Gamma-Tech has an active volume of $\sim$ 2cm^3, 16mm diameter and 10mm thickness. The detector has required two overhauls, the last was to replace a matched FET housed in the cooled region. The measured resolution (Full Width at Half Maximum) is 1.15-1.20keV for the 514keV ^{85}Sr gamma line. The crystal and associated electronics are kept at 77K by a cold finger and the encased assembly protrudes from a 20l liquid nitrogen dewar. An optical feedback preamplifier is attached to the detector assembly. The feedback pulses of frequency normally $<$ 10Hz compensate for the crystal leakage current and are fed to the anticoincidence input of an Analogue to Digital Converter (ADC). The necessary bias of between -1600 and -2000V for charge collection in the germanium crystal is supplied by a Tennelac TC941 stabilized high voltage power supply. The positive output pulses of the preamplifier are amplified to $\sim$6V by a Tennelac TC205 amplifier using a shaping time constant of 0.5μsec. A Laben 8192 ADC is next in the chain, with its output connected to a Link systems MultiChannel Analyser memory unit.

§3.3.2 The Analogue to Digital Converter

A Laben 8192 ADC with a conversion time of 4.5μsec plus pulse rise time is employed. The 8K ADC is operated in a 4K mode, the restricton being imposed by the external memory unit. The ADC has a user settable rise time protection. This is the time the ADC allows the input pulse to attain its maximum amplitude before starting conversion. There is a zero threshold potentiometer pot which can be set to blank out noise on the input, and also pots for lower and upper signal limits to define a conversion window. The input voltage may range from 0-6V and this after a digital back bias of 2048 channels is scaled to span 4096 channels. Channel dispersion with this 2K digital back bias is ~90eV. A parallel connector with 13 data, 3 handshaking plus ADC control and dead time lines is used for the interface to the memory unit. The ADC has the capability to start a fresh conversion whilst still transferring previous data. In this way, up to a limit, the ADC dead time is not contributed to by a slow memory unit. Further units are linkable to a modified Laben for peak stablization.

§3.3.3 The Link MultiChannel Analyser

The memory unit interfaced to the ADC is a Link Systems 4K MultiChannel Analyser (MCA). The MCA builds up a spectrum of count versus channel (energy) by recording according to magnitude each conversion output by the ADC. The input binary signal can range from 0 to 4095. The MCA incorporates a Nova-2 computer, based upon an Intel 8080 microprocessor, with 8K read/write memory. A source program held on paper tape is read for initialization and provides the user with a real time VDU display and the MCA facilities. The MCA has an external control keypad. With the keypad the user can start/stop, erase, set counting time etc. The spectrum can additionally be displayed in a logarithmic scale. A virtue of the MCA is its magnetic core memory which is non-volatile so that after a power failure the Link can be reset and resume counting. On a spectrum regions (windows) may be selected which are later output to an external recording device. The MCA provides the centre channel and the integral of counts for each window. During a run the

analyser maintains a real counting time which indicates the system dead time. The sytem dead time is the sum of ADC dead time and detector reset pulses. The software was specifically modified by Link Systems to allow a maximum channel count of 99,999. The Link has two hardware ports for interfacing to outside units. A 20mA current loop operating at 110baud for output to a teletype and RS232 operating at 1200baud.

§3.4 The Cage

All sensitive electronics are housed in a constant temperature cage. The equipment in the cage takes power through mains filters and regulators. Additionally to avoid glitches in data transfers and equipment control it was found necessary at the Egham site to incorporate ferrite cores either at mains inputs or on data lines. The cage has a wooden framework, thermal isolation is provided by fire retardent painted polysterene slabs sitting within the frame. Temperature control is through an Air Conditioner, two heaters and air fans. A mercury contact thermometer regulates cage temperature to within .25°C at 19.5°C. An external chart recorder monitors cage temperature during experiments. A T_1-T_2 thermocouple is used for this while a Zeroff zero reference source provides the thermocouple ice junction. Of the two heaters one is constant and one intermittent, controlled by the contact thermometer.

§3.5 Pressure Instruments

§3.5.1 Pressure Gauges

At the start of the grafoil work two types of pressure gauges were at hand. A Budenberg relative gauge measuring pressure up to atmospheric calibrated to 1Bar and scaled to 5mBar. The Budenberg indicates the pressure difference between its two inlets. Hence for accurate pressure determination a knowledge of the ambient

pressure is required. Aside from another relative gauge with a high limit of two atmospheres an absolute Genevac for low pressure work was employed. The Genevac reads up to 20Torr and is scaled to 0.5Torr. The gauge has an evacuated capsule and pressure measurement is against this.

§3.5.2 The Druck Pressure Instruments

For automatic recording of pressure a Druck Ltd pressure transmitter was installed. The transmitter measures pressure by a silicon diaphram, the perturbations of which are converted to voltage fluctuations. The particular transmitter measures relative pressures. It has positive and negative pressure inlets. The negative inlet is kept evacuated and the positive inlet exposed to the gas under study. A constant current output is generated with a variable, to a large tolerance, voltage input. The maximum output, corresponding to a 1Bar pressure differential, is 20mA. Across a 100Ω resistence this gives a measure voltage between 0 and 20mV. Before use the transmitter would be calibrated by taking measurements at atmospheric and zero pressure. Further a gas under study would have a known or calculable vapour pressure at liquid nitrogen temperature and this would serve as an additional calibration point. A spare furnace DTC measured the transmitter voltage and the output of this was fed to the experiment microcomputer.

The transmitter is located within the cage for temperature stability. In practice the transmitter sensitivity was no better than ±0.5Torr and was used with some difficulty for the lowest pressure experiments. The zero was also found to drift and a careful note of this was kept. Late in the grafoil work a Druck DPI101 pressure indicator with two transducers was incorporated. A transducer unlike a transmitter does not have the necessary electronics to make it stand alone, the indicator provides an excitation voltage and is calibrated on separate channels for each transducer. One transducer is scaled to measure 0-760Torr the other, for low pressure work, measures to 52Torr. Both are differential. The indicator presents the pressure in Torr or Millibar, and for the 52Torr range to two places of decimal. The indicator was ordered with a four decade BCD output interface and this is read

directly by the controlling 380Z microcomputer. With the new equipment, pressure can confidently be measured to an accuracy better than ± 0.05Torr.

§3.6 Gas Handling

By means of controlled volumes gas is introduced into the sample chamber to either its vapour pressure at 77.4K or a lower pressure. A gas feed line connecting a gas cylinder to the cryostat assembly would normally, after evacuation and flushing, be used as the source. Figure(3.6.1) details the final arrangement. A single transducer positioned in the cage measures pressure. A gas store is available for isotherm measurements. Ahead of the store are two shot volumes, the smaller being the dead volume between two 5mm vacuum valves.

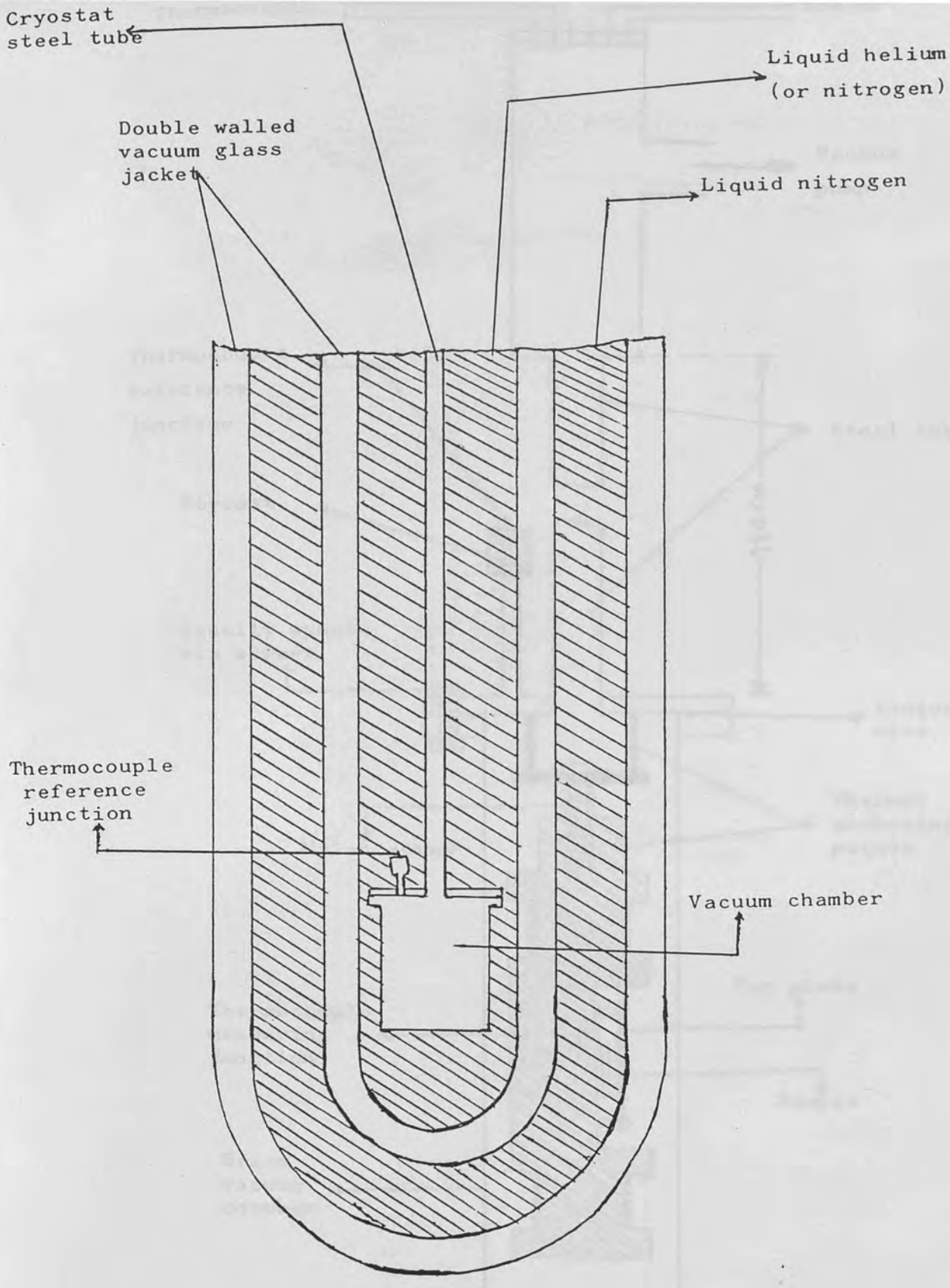

Figure(3.1.1.1) Cross-section of liquid helium cryostat.

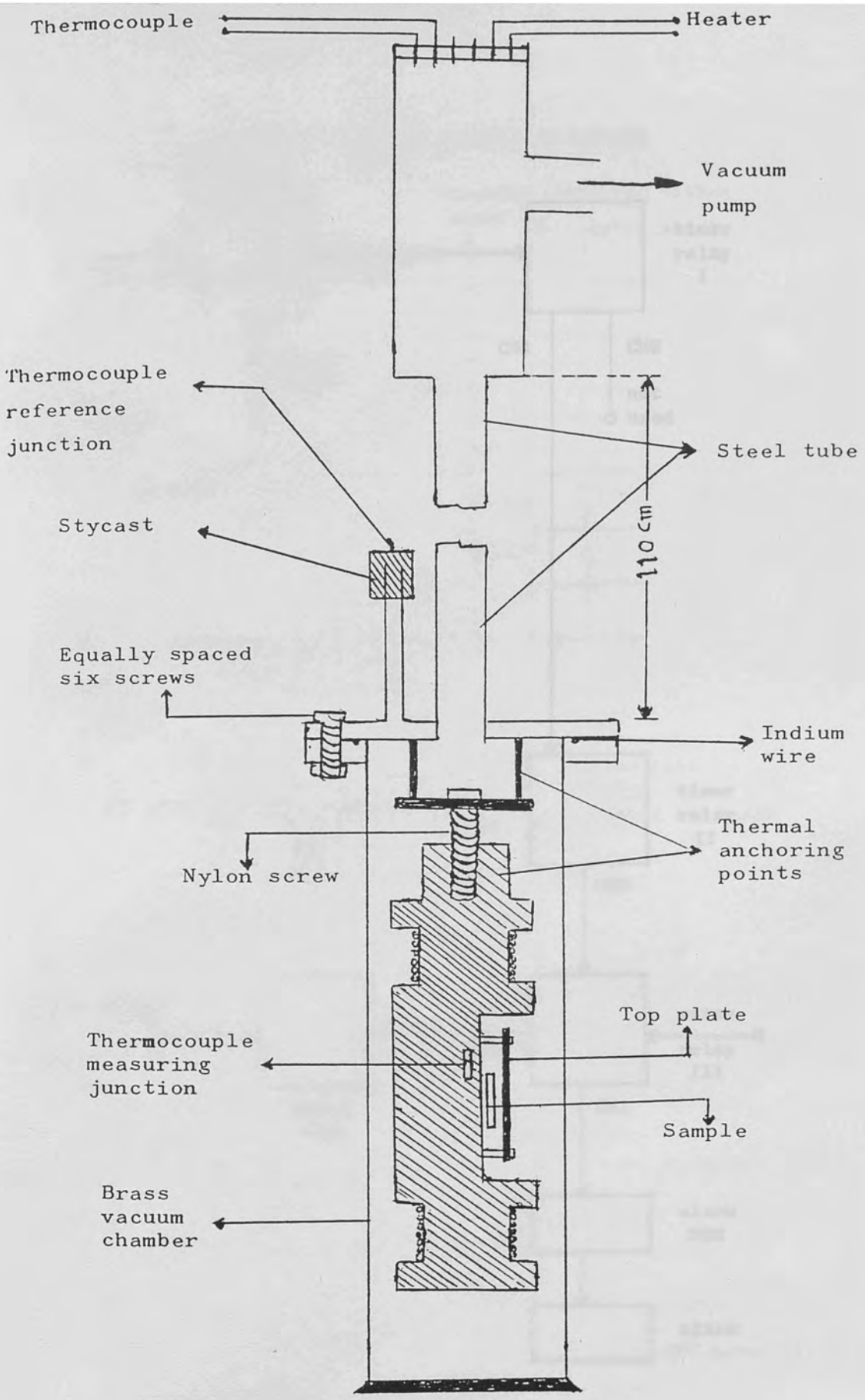

Figure(3.1.1.2) Cryostat sample holder and chamber.

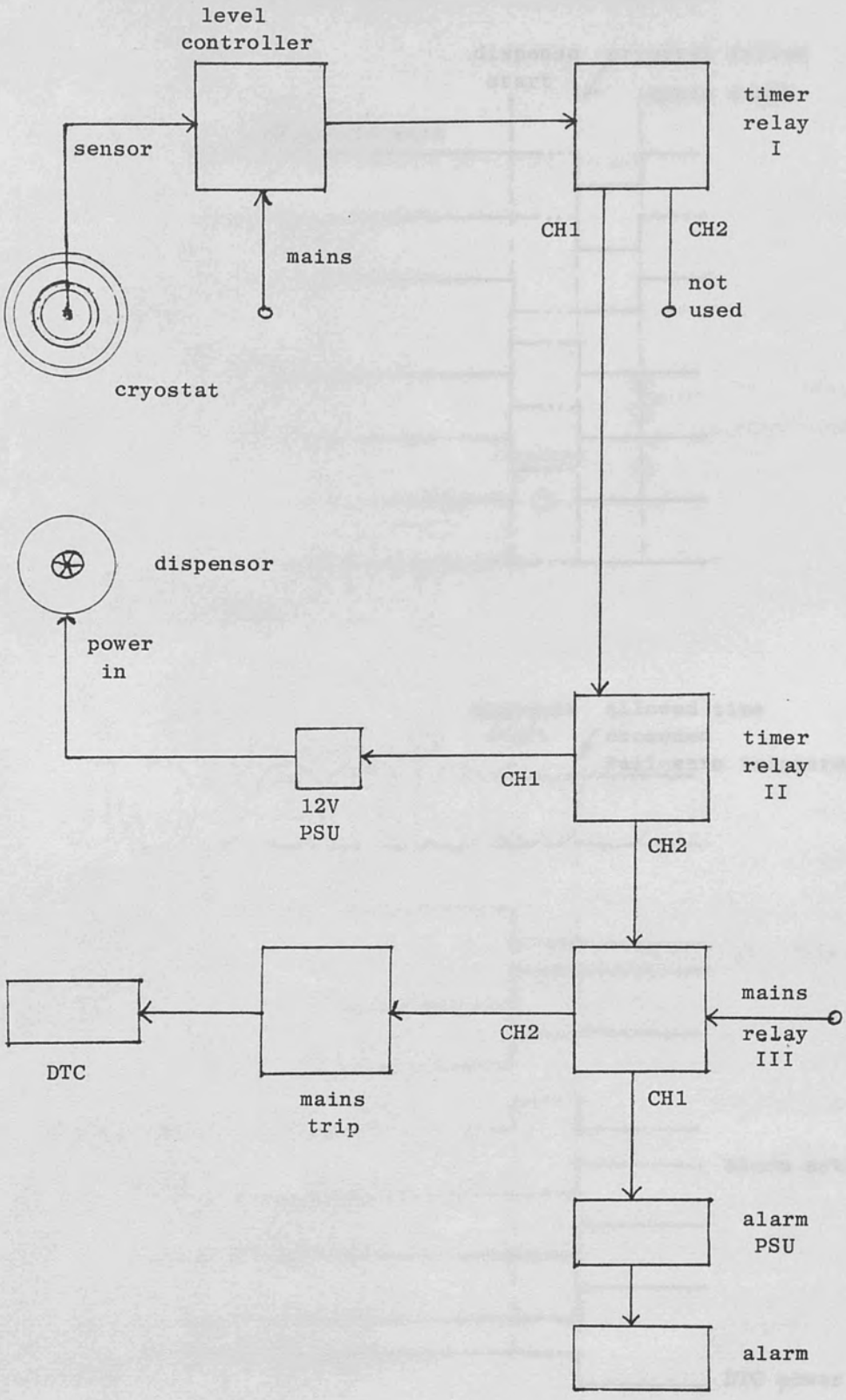

Figure(3.1.2.1) Liquid nitrogen dispensor system.

Liquid Nitrogen dispensor timing diagrams

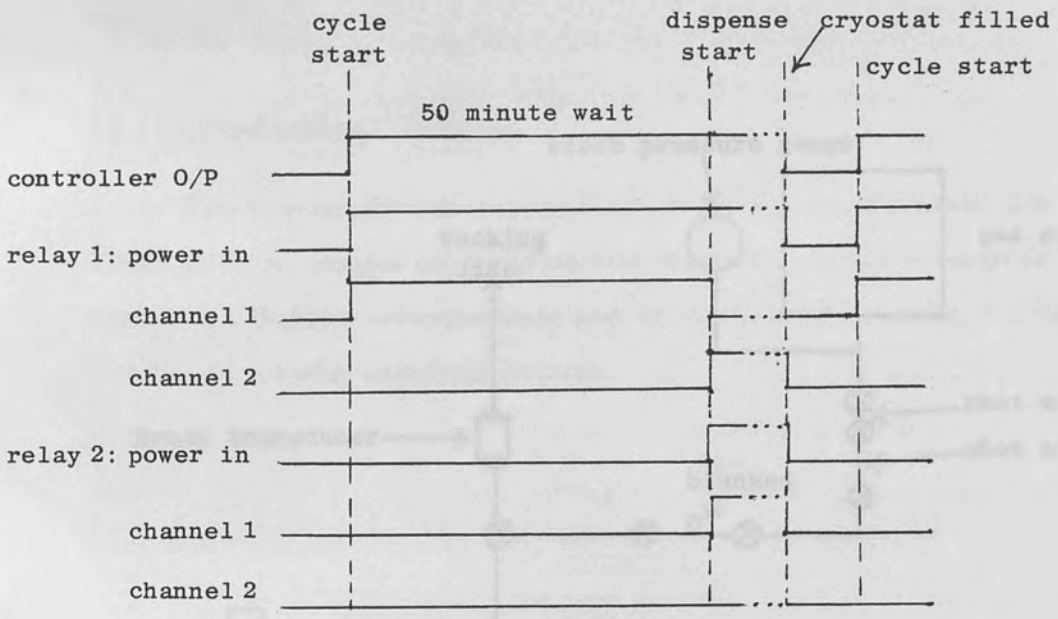

Fig(3.1.2.2) Normal operation.

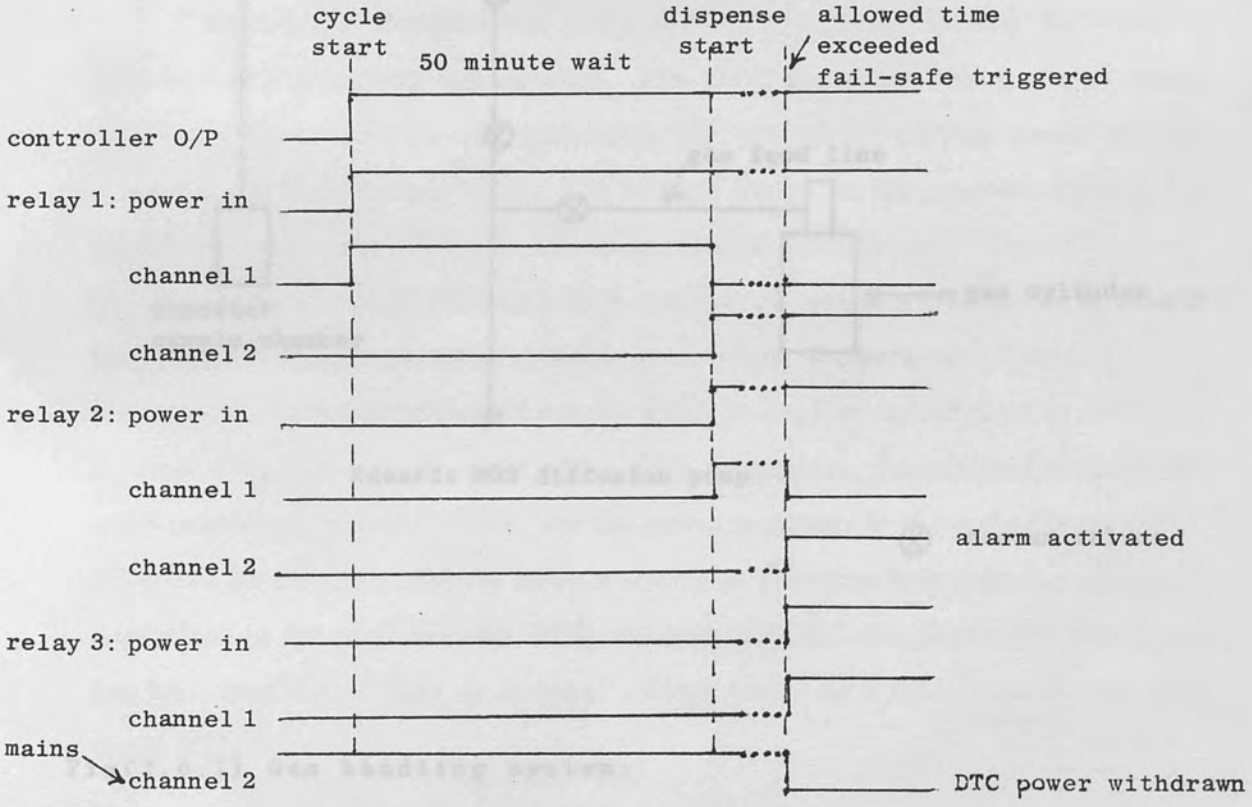

Fig(3.1.2.3) Fail-Safe operation.

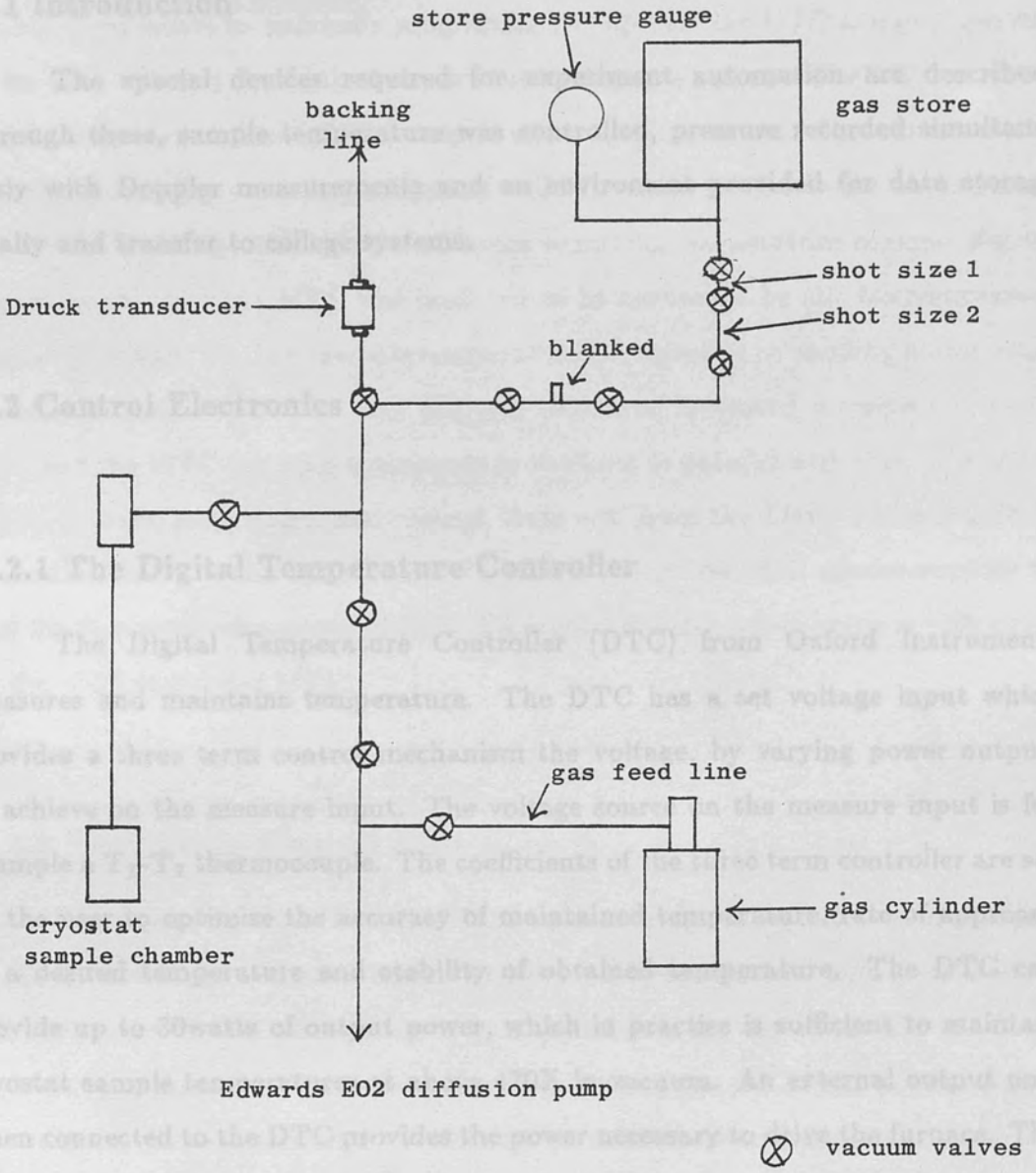

Fig(3.6.1) Gas handling system.

Chapter IV Microprocessor Control System

§4.1 Introduction

The special devices required for experiment automation are described. Through these, sample temperature was controlled, pressure recorded simultaneously with Doppler measurements and an enviroment provided for data storage locally and transfer to college systems.

§4.2 Control Electronics

§4.2.1 The Digital Temperature Controller

The Digital Temperature Controller (DTC) from Oxford Instruments measures and maintains temperature. The DTC has a set voltage input which provides a three term control mechanism the voltage, by varying power output, to achieve on the measure input. The voltage source on the measure input is for example a T_1-T_2 thermocouple. The coefficients of the three term controller are set by the user to optimise the accuracy of maintained temperature, rate of approach to a desired temperature and stability of obtained temperature. The DTC can provide up to 30watts of output power, which in practise is sufficient to maintain cryostat sample temperatures at above 470K in vacuum. An external output unit when connected to the DTC provides the power necessary to drive the furnace. The DTC can be used in a manual mode whereby its power output is user set and not dependent on the error between DTC measure and DTC set. Each DTC under use has been modified to take an external voltage source as a substitute for the front panel DTC set.

§4.2.2 The Master Temperature Controller

The Master Temperature Controller (MTC) was developed by A. K. Betts. The device can be controlled from front panel thumbwheel switches and in its original form would be manually programmed to operate the DTC and perform run cycles with this and the Link Systems MultiChannel Analyser. The MTC controls sample temperature through the output of an integral motor. The output of the motor is fed to the set voltage input of a DTC. Winding the motor up increases this set DTC voltage and vice-versa, hence achieving temperature control. For its present application the MTC was modified to be controlled by the Microprocessor Control Unit (MCU). Thus sample temperature is controlled by sending motor pulse commands to the MCU. The Link analyser command keyboard is connected to the MTC and the MTC can send commands to the Link in parallel with this. The MTC is able to start, stop, erase, and request 'data out' from the Link. There is a BCD connection between the MTC and DTC which allows the 380Z microcomputer to read the displayed voltage on the DTC. Figure(4.2.2.1) gives the timing specification for the 380Z controlled MTC.

§4.2.3 The Master Control Unit

The Master Control Unit (MCU) is another purpose built device, developed by A. K. Betts. It acts as a buffer between hardware devices and a controlling microprocessor. In its present use it is a go-between for the 380Z and MTC. In addition to communication and command interfaces the MCU has several relays that may be software activated. These may be used to control motorised dispensor valves. As an example of use it, provides the 380Z in serial ASCII form the display reading of the DTC. Almost all control the microcomputer has over the electronics is achieved through this versatile interface.

§4.3 The 380Z Microcomputer and Control Aspects

§4.3.1 The Microcomputer

The 380Z is a Z80 based 8 bit microcomputer manufactured by Research Machines Ltd. Its specification after a number of upgrades is:

Two 360K double density double sided $5\frac{1}{4}$" disk drives.

56K RAM available to user. Although the machine has the full 64K addressable by an 8 bit microprocessor, 4K is in the form of ROM and contains the monitor program and 4K is taken by CP/M when the micro is booted. Further the programming language used, BASIC, itself takes ~13K leaving at most ~43K free for user applications.

Block mode graphics capability.

16 bit memory mapped user parallel port. (8 bits configured for input, 8 for output.)

20mA active current loop port. Note this can only be used as an alternative to the user port as both go to the same driver.

2 serial RS232 ports, operable at speeds from 300-9600baud.

3 Z80 PIO parallel ports.

1 Z80 programmable CTC.

Figure(4.3.1) shows these ports with their external connections.

§4.3.2 MCU Interface

This is via two Z80 Parallel Input/Output (PIO) interfaces. A PIO has two 8 bit input/output (i/o) ports (ports A and B) which under software control may be configured in a number of ways. By means of a data direction register each of the 16 PIO i/o lines is separately programmable for input or output. The software

programmability of a PIO is usually governed by its hardware enviroment. For example to match the bidirectional software control, bidirectional data buffers and extra decoding is required. The PIO is able to generate a Z80 mode 2 interrupt, after suitable programming the arrival of a handshake and data to port A or B initiates an interrupt and only when the PIO has been serviced by the microprocessor is the handshake to the external device completed. In the MCU interface the PIO's, labeled A, B both have port A hardwired for output and port B for input. In PIO A port A is used to supply instructions to the MCU, port B to receive peripheral status information. In PIO B port A can be used for 'data out' (if for example a printer is attached to the MCU, with the correct control word the 380Z could dump output to the printer). Data the MCU wishes to supply to the 380Z travels along port B of this PIO.

§4.3.3 MTC Interface

The 380Z controls this device by sending appropiate control words to the MCU. Whenever the 380Z for example wishes to read the DTC display a read peripheral command is sent, activating a data transfer chain which results in the four digits of the display being received as four sequential ASCII bytes. Another control example is the 'pulsing' of the MTC motor. Dependent on the state of the motor up/down latch each 'turn motor' command pulses the motor on the MTC up or down, a single step (each step corresponds to $\sim 0.5\mu$V, for a Au-Fe thermocouple). The MTC was substantially modified to run in the microcomputer control mode and timing conflicts between the hardware run cycles of the MTC and 380Z software cycles were encountered. As it stands these conflicts have been subdued by various software precautions.

§4.3.4 DTC, Link Analyser Interface

Both these devices have attachments to the MTC and hence all control and access is realized by appropiate commands to the MTC. The set voltage on the DTC can be adjusted by the 380Z, and its display read. As mentioned earlier, essential Link analyser functions are under the control, in parallel with the Link keyboard, of the 380Z. Figure(4.3.4.1) illustrates the connections between the mentioned devices.

§4.3.5 VAX Minicomputer Link

The 380Z has a permanent departmental PAD line. Through a PAD concentrator it has access to both the computer centre VAX 11/780's and the departmental VAX 8200. A serial port on the 380Z is devoted to the link and through developed software data transfers are accomplished.

§4.3.6 Druck Pressure Indicator Link

The 380Z performs pressure measurements by a BCD (Binary Coded Decimal) connection to its third PIO. On acquiring a Druck pressure transmitter a DTC acted as a DVM with the ability to output the voltage reading through a BCD interface. The voltage once read would be converted to pressure (Torr) and displayed by the 380Z. To read the four digit BCD code all 16 lines of the PIO are configured for input, four lines for each digit or decade. The handshake control lines of both PIO ports are soldered together and those of port A connected to appropiate control pins on the DTC. Later the pressure transmitter was superceded by a pressure transducer/indicator system. The pressure indicator has a BCD interface and this is now connected, by a different cable, to the third PIO. The indicator gives a reading in Torr or mbar directly, freeing the 380Z from conversion. If desired, in future the remote capability of the pressure indicator could be utilised to change ranges and transducer channels automatically.

§4.3.7 Slave 380Z Interface

Due to the grossly limited data storage capability of the single 380Z means were sought of incorporating a data buffer. Data transfer and storage problems between the Link and the 380Z arose because the Link does not entertain any form of hardware or software handshake. In fact initially when the transfer routine was written in BASIC and was relatively slow, data losses were abound. The 380Z has a little over 40K of user available memory and with the control program loaded and running a compromise between the number of channels collected from the Link and 380Z 'out of memory' crashes had to be made. In practise 500 channels could be recorded. This number of channels is quite adequate for traditional Doppler lineshape parameter analysis but for the $2\gamma/3\gamma$ ratio, collection of all 4K channels was the ideal situation. Software was written initially to make use of a magnetic tape storage device (the Perex Perifile) but this was superceded when another 56K 380Z was acquired. The slave 380Z, as it is termed, was without the three PIO ports of the master 380Z (original 380Z) but in other respects was identical, having in fact the additional feature of High Resolution Graphics (HRG). A serial port is used for the connection to the Link analyser and master 380Z. Communication with either device is via the MCU. The master 380Z is able to control, by appropiate commands to the MCU, which device (itself or the Link) is at any one time in communication with the slave. The slave 380Z after software loading has ~30K available for data storage. This is sufficient to collect ~half of a 4K channel spectrum. Originally an IEEE standard interface board was purchased for the single 380Z but it proved impractical to mount because of a lack of slots, this board is now fitted in the slave 380Z and gives it apart from the IEEE interface a free Zilog Counter Timer Circuit (CTC) and two PIO's. The IEEE interface could in future be used to read and control the 95A Keithley DMM. The CTC and one PIO together with the HRG board were later used to implement an 8K MCA.

§4.3.8 Perex Perifile Interface

The Perifile is a magnetic tape storage device. It takes a standard 3M data cassette (cartridge). Four storage channels are available, each holding up to 99 separate files. The capacity of each channel is 0.5Mb giving a total of 2Mb per cartridge (over five times the capacity of a 380Z disk). The Perifile can operate in two modes viz. local, where the user has control of front panel functions, and automatic where an external computer has full control and the front panel is inoperative. The connection to the external controller is via an RS232 serial interface operable at speeds up to 9600baud. In mode A (the automatic mode) there is a software, xon/xoff, handshake for data transfers. This ensures the integrity of downloaded data. However in the local mode this handshake is not available for data transfers. The Perifile was the first device to be tried as a data buffer between the Link MCA and 380Z. It was later abandoned owing to intermittent error conditions arising on creating or finding files.

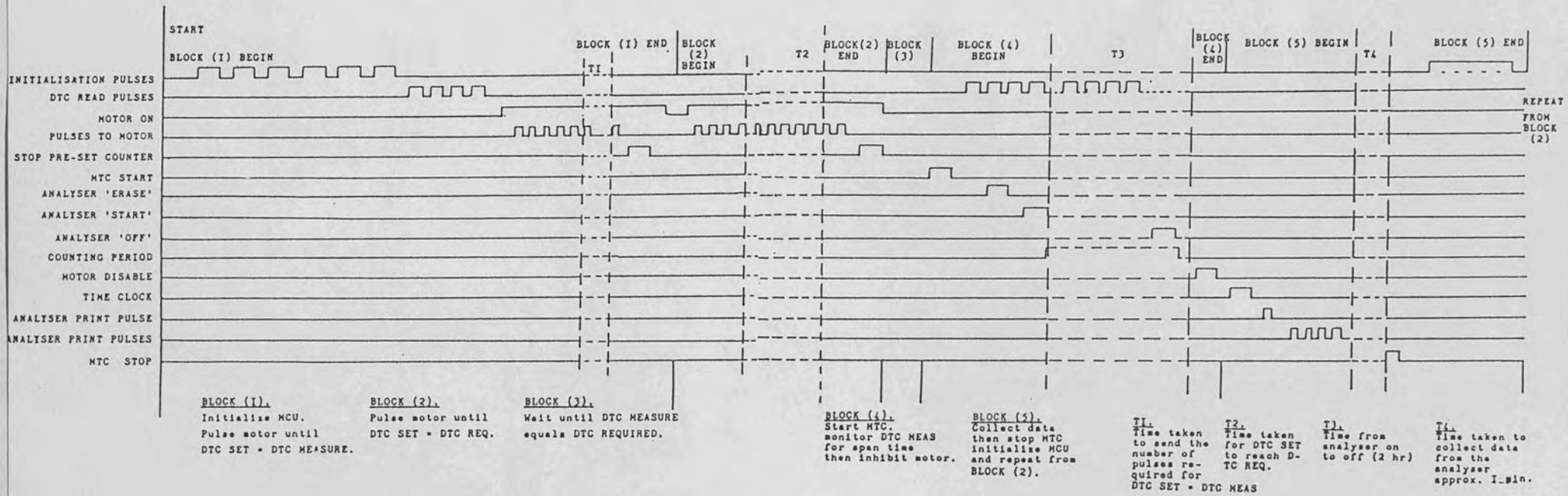

Figure(4.2.2.1) MTC-380Z time diagram.

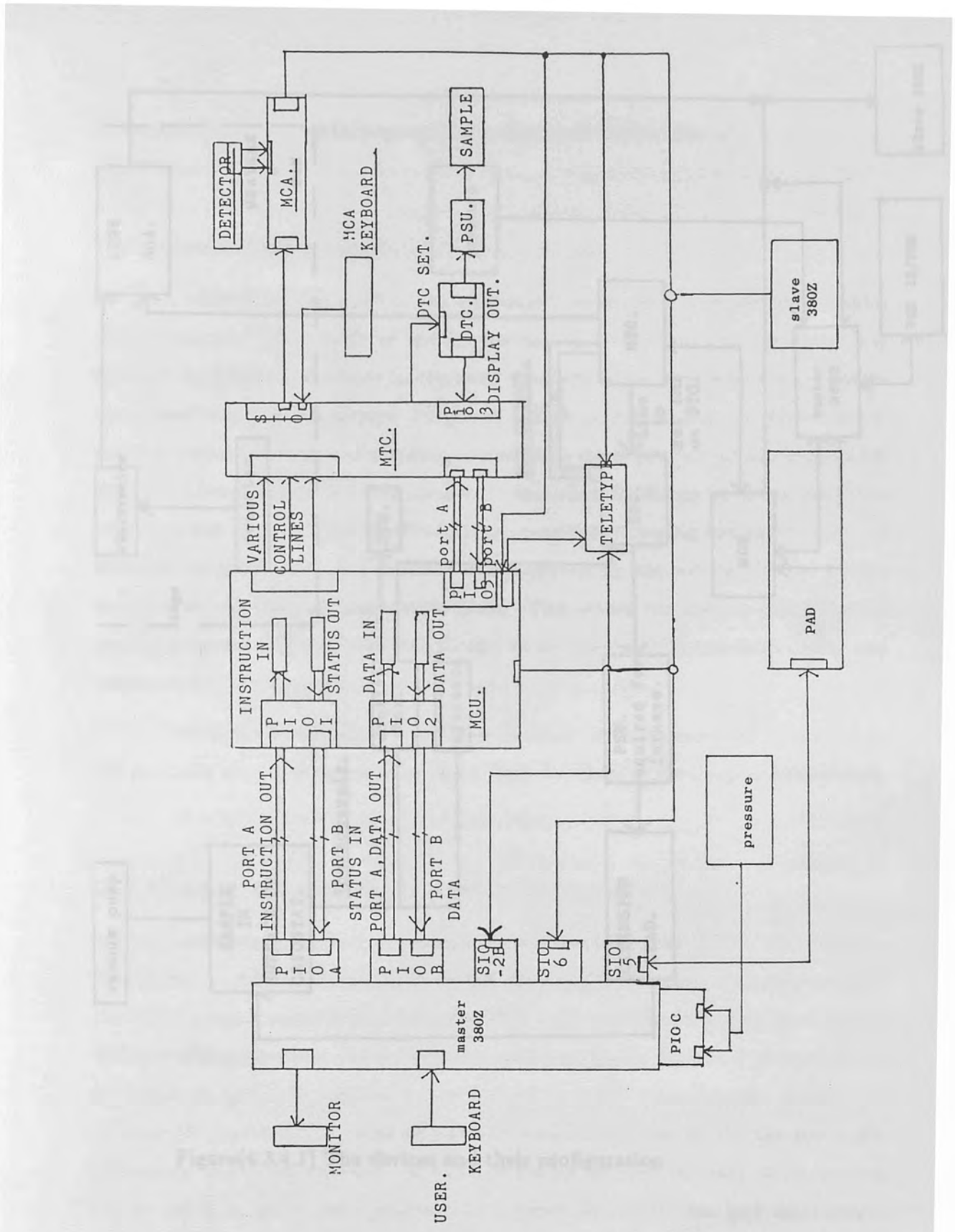

Figure(4.3.1) System ports

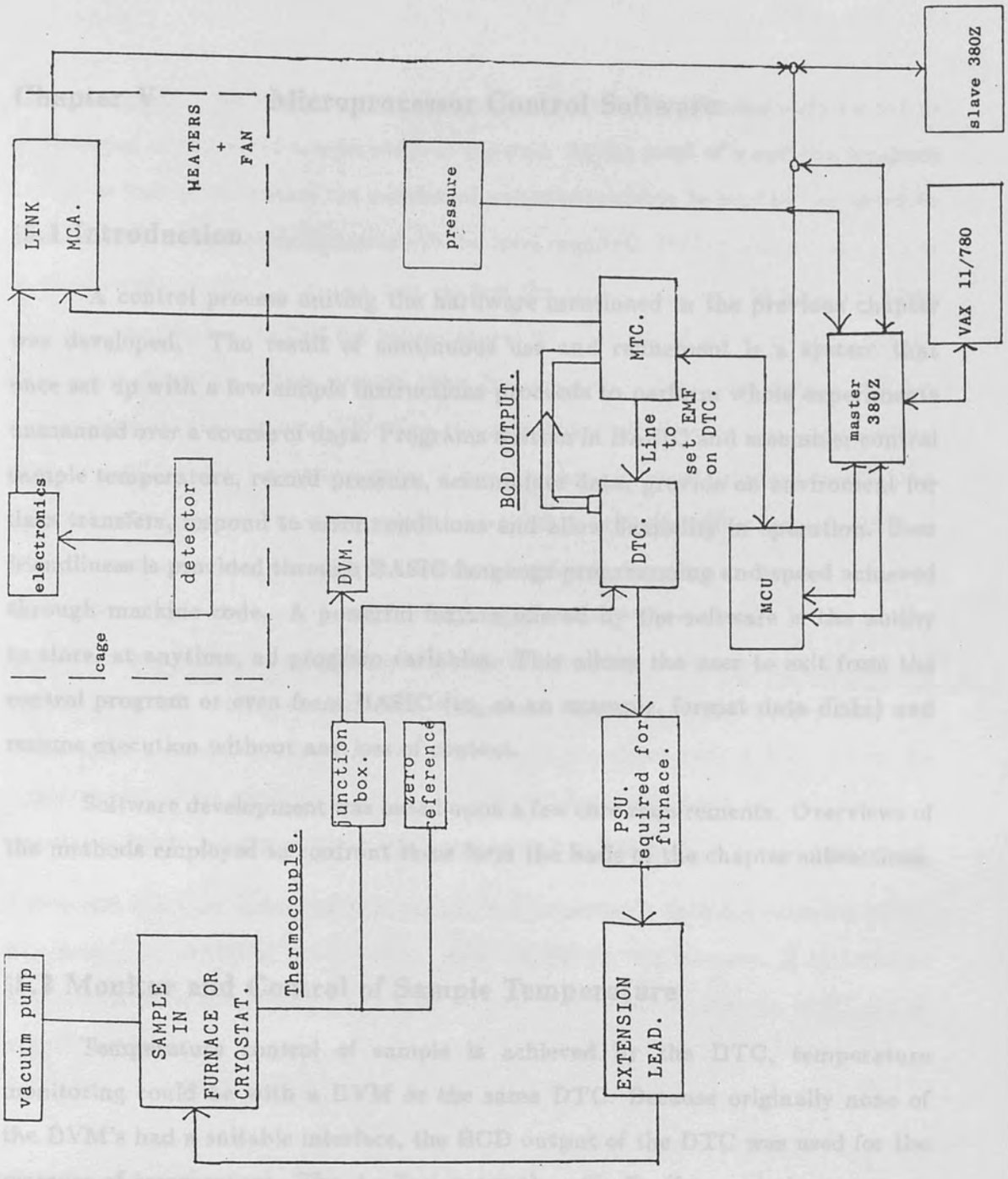

Figure(4.3.4.1) The devices and their configuration

Chapter V Microprocessor Control Software

§5.1 Introduction

A control process uniting the hardware mentioned in the previous chapter was developed. The result of continuous use and refinement is a system that once set up with a few simple instructions proceeds to perform whole experiments unmanned over a course of days. Programs written in BASIC and assembler control sample temperature, record pressure, accumulate data, provide an enviroment for data transfers, respond to error conditions and allow flexibility in operation. User friendliness is provided through BASIC language programming and speed achieved through machine code. A powerful feature offered by the software is the ability to store, at anytime, all program variables. This allows the user to exit from the control program or even from BASIC (to, as an example, format data disks) and resume execution without any loss of context.

Software development was based upon a few core requirements. Overviews of the methods employed to confront these form the basis of the chapter subsections.

§5.2 Monitor and Control of Sample Temperature

Temperature control of sample is achieved by the DTC, temperature monitoring could be with a DVM or the same DTC. Because originally none of the DVM's had a suitable interface, the BCD output of the DTC was used for the measure of temperature. The Au-Fe (cryostat) or T_1-T_2 (furnace) thermocouple generates an e.m.f proportional to the temperature difference between a reference and sample junction. Hence to display and record temperature the thermocouple calibration has to be on hand. It was decided for greater accuracy in conversion not to use a fit generated equation but to store the calibration and use straight line interpolation between adjacent points. Temperature control is acheived by pulsing up or down the motor on the MTC. This changes the DTC set voltage and, when in the automatic mode, the DTC adjusts power output accordingly. During

a measurement a running mean temperature is calculated and eventually stored to be recorded as the mean temperature of the run. At the start of a run the program computes from a calibration the number of pulses required to be sent to the motor to increase or decrease the temperature to the level required. It then sends these pulses at an interval controllable by the user. In fact the rate of approach to a temperature was later modified to be fast for temperatures for example of error greater than 10 deg. then slower for those greater than for example 5 deg. and slower still for smaller temperature errors. This had the advantage of allowing fast temperature changes whilst maintaining accuracy of final setting. In practise there would be a residual error between the temperature set and that achieved. This error ($\sim$ 10% of the temperature change) could be tolerated for single direction measuremants but when work began on grafoil and repeat measurements were performed as a rule, greater accuracy was sought. It was decided to employ a temperature correction algorithm which would be activated whenever the temperature discrepancy was larger than a preset allowed amount. To avoid overshoot only a fraction of the correction would be applied at a time. Safeguards had to be built against relentless corrections when for example the DTC was unable to maintain a high temperature.

A constant check on temperature is maintained to ensure it does not exceed a preset maximum, usually 500K for the cryostat and 600K for the furnace. If at anytime this maximum is exceeded an alarm on the MCU is sounded and the MTC motor wound to zero.

§5.3 Command of MultiChannel Analyser

Before the microcomputer control system the governing device was the MTC and as such it has control of all accessed MCA functions. A typical run entails the following sequence of Link related events:

(1) Erase memory

(2) Send start/stop instruction

(3) Allow Link to accumulate counts for preset time

(4) Instruct Link to perform 'data out'

(5) Repeat from (1)

Each available Link function has a separate command code on the MCU. For example to perform a Link 'data out' the microcomputer sends the byte 9D (hex) to the MCU. On receiving this code the MCU triggers the MTC to send the required print pulses to the Link. A deficiency encountered with the Link was the single start/stop command. Ideally separate instructions to start and stop would have been available, but as it is care has to be taken to start both devices (the Link and microcomputer) synchronously. When sending a sequence of commands to the Link a delay between successive instructions was found to be necessary, to allow MTC and MCU circuit relays to activate. The 'data out' instruction imitates the pressing of the print spectrum key on the Link keyboard. The MTC sends four of these pulses to the Link. Dependent on the number of print pulses received in any single sequence the Link prints out the full spectrum, or just the windowed channels, or only the integral of counts in the windowed areas.

§5.4 Collection and Recording of Data

After the print spectrum command has been sent, the microcomputer must be ready to collect and store the Link analyser output. The 1200baud RS232 output of the Link is used. The spectrum is output as a string of ASCII bytes. This means for example that an internal channel count of say 23909 is not output as the binary number equivalent to 23909 but as five separate bytes which correspond to the ASCII codes of the digits. As a consequence of this protocol each output line of 72 bytes contains just 5 channels so that a 4K spectrum would consume ~60K of external memory. On completion of a run the control program writes run particulars on a disk file, stores filename and access details in a File Control Block

(FCB) area and calls a machine code data collection routine. The data collection routine on the master 380Z has a counterpart on the slave and both work together to first store incoming data on the slave and then transfer this under a handshake to disk on the master. Figures(5.4.1) and (5.4.2) give software flowcharts for the three devices involved. Particular care is given to handling a disk full error. Each spectrum consists of three windows, one containing 655 channels, the other two, 300 channels each. The three windows together with header information make up a 28K spectrum data file. The number of files per disk side is user programmable and is set at 10 for the 28K files. The program automatically after storing 10 files on a disk side selects the next logical side (disk). If however a disk full error occurs before this preset limit is passed, the disk side is incremented and the data transfer repeated to a new file on the fresh disk (side). The total time taken to complete the transfer of 955 channels is in the region of 10 minutes.

§5.5 User Interface to College Minicomputer

The development of this software was essential to the feasibility of automation. In the past data from the Link was held on paper tape and this after being cut and spliced taken to the computer centre to be read. It was required to collect spectra onto disk, then to transfer these to the college VAX 11/780 as and when convenient. Originally it was thought to upgrade the 380Z to 8" disk drives, which would be IBM compatable and hence possibly be able to be read by the computer centre. However the upgrade was to the cheaper $5\frac{1}{4}$" drives option, essentially on the premise that transfer software could be developed.

The developed user interface is menu driven and its overskin written in BASIC with machine code subroutines forming the working skeleton. It consists of a dumb terminal emulator and receive and transfer (output) routines. A teletype read utility is also provided (this was based upon an example program described in a Research Machines publication). The emulator and transfer routines work at up to 9600baud. The VAX does not entertain hardware handshaking and all communication is under the xon/xoff protocol. The VAX interface is an option in the control program menu and is accessed as a subroutine. A typical data transfer session would consist of the following steps:

(1) Select VAX interface

(2) Select terminal emulator option and logon to the VAX

(3) Exit terminal emulator (by pressing cntrl R) and select data transfer option

(4) Give file to be transferred and name of VAX file to receive data

(5) File (files) are transmitted to VAX

(6) Select emulator again and logoff

(7) Select return to control program option

At 9600baud and a low user load on the VAX a 28K file is transferred in about 30seconds. Files can also be downloaded onto 380Z disks. This two way flow between the 380Z and VAX proved of great value, for example the more powerful editing facilities of the VAX were used for 380Z program creation and development.

§5.6 Run Cycle Automation

Once the earlier core requirements had been developed a software envelope was required which would house these and facilitate autocycling. In principle after the framework to link the basic functions was developed it was thought autocycling would be easy to achieve, by simply building an outer control loop. However the 380Z does not have an inbuilt system clock (apart from the 4MHz Z80 oscillator) and the task of incorporating and programming the available CTC chip was not straightforward. The CTC has four programmable time channels connected in a chain, each able to be loaded with a count. A channel has an input and an output. The input acts as a trigger. On each trigger the channel count is decremented. When the channel count reaches zero an output pulse is sent and the channel reloaded with the preset count. This channel output pulse acts as the trigger input for the next channel in the chain. A channel may be interrogated for its current count. In this fashion the feed input of 4MHz (or 4MHz/256) may supply seconds, minutes etc time constants. In practise with only four channels it did not prove possible to generate a time constant for hours. Measurement of time in hours is through

software. Time measurement and display software was developed independently and then incorporated as a subroutine in the main control process. Completion of the time routine paved the way for complete autocycling.

Given now are the main steps in the control cycle:

(1) Read thermocouple and MTC motor calibration from disk, read machine code 'read Link' routine, initialize program variables, set up graphics display.

(2) Prompt user for start temperature and other details, such as date and time.

(3) Move DTC set to start temperature.

(4) Begin run cycle:

  (4a) Wait for preset temperature stablization time, correcting temperature as necessary

  (4b) Erase and start Link analyser

  (4c) Monitor and display, keeping a running mean, temperature and pressure. Keep this up for the run time (typically 2 hours), correcting temperature, if necessary, at preset intervals

  (4d) Store graphics screen and perform data transfer, this completes the run cycle.

(5) Store run variables, such as mean temperature and pressure.

(6) If experiment completed, output to printer résumé of experiment and go into monitoring state. Otherwise on to (7)

(7) Recall and update graphics screen.

(8) Repeat from (3).

The user can select the behaviour of the control process at the end of an experiment. The process can be requested to maintain the last temperature or to take it to some value (the default value being 77K).

§5.7 Development of Menu

It was decided at an early stage to make the control program menu driven. Although the control process itself is not open to alteration a user interface is provided by the inclusion of a menu. A major obstacle limiting the facilities offered by the menu was found to be the memory of the microcomputer. A method was developed of allowing, by a process of program merging, two or more options to occupy the same area of memory. The 380Z provides a powerful merging command, the action of which is to overwrite present program lines if they clash with those of the new program. Three major routines were written with the same line numbers so that all three on loading would occupy the same memory. A consequence of this approach which proved of value was the necessary storing of all program variables each time a merger took place.

The original method of accessing the menu was for the user to preset the interval, in terms of runs, before each automatic call. The shortest interval between menu requests being single runs. This approach was superceded by a method of continuous keyboard monitoring. The keyboard is monitored for a menu request control code (cntrl R) allowing the user to make a request at anytime within a run cycle. This was a most convenient development. As a precaution against user forgetfulness the menu is exited after a certain time of inactivity. A list of the top menu options is given below:

(1) Link to Vax
(2) Repeat Run
(3) Enter New Temperatures
(4) Perform Rapid Heating or Cooling
(5) Edit Program
(6) Change Key Constants
(7) Continue Program
(8) Disable Menu

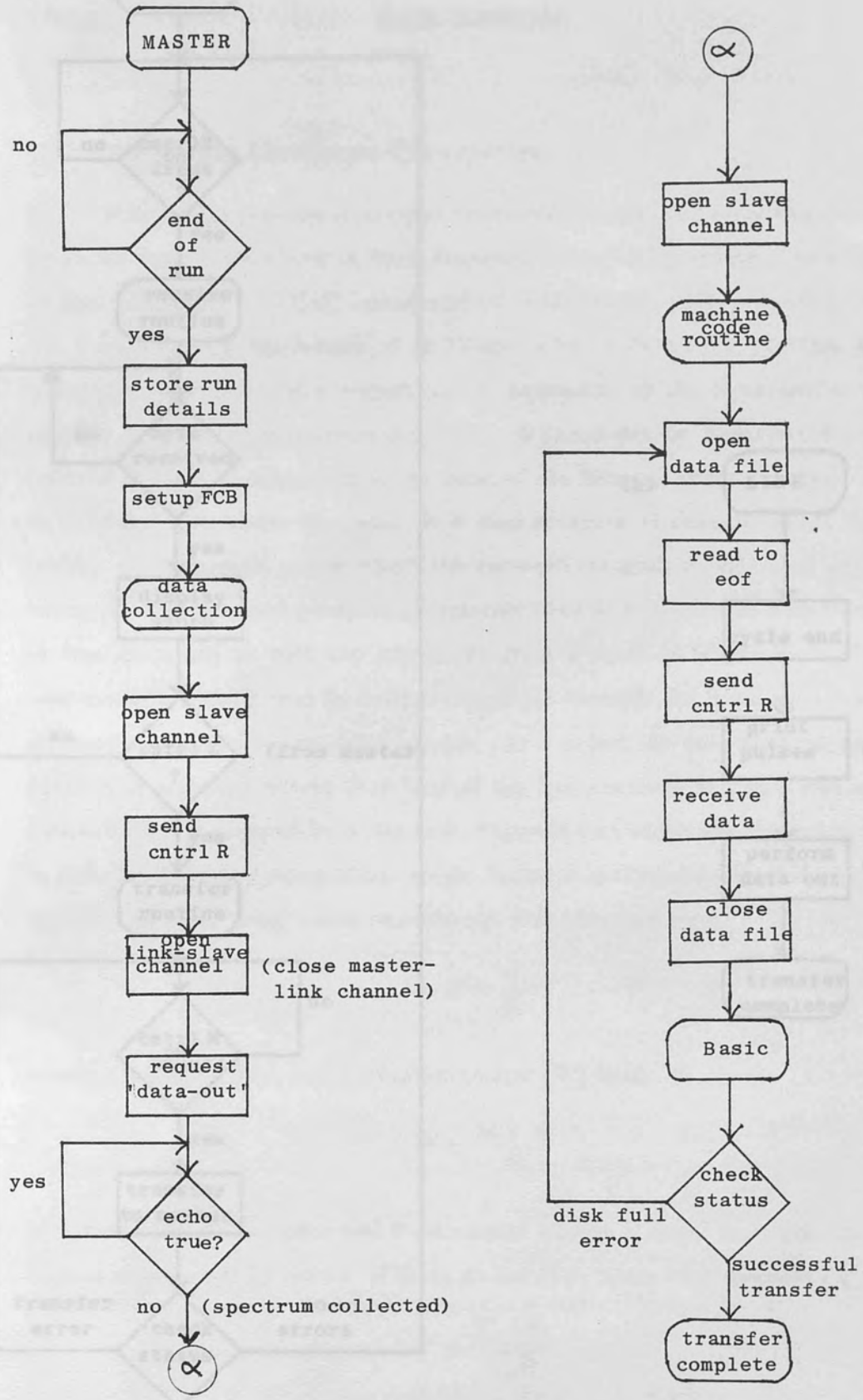

Fig(5.4.1) 'Data collect' flowchart for master 380Z.

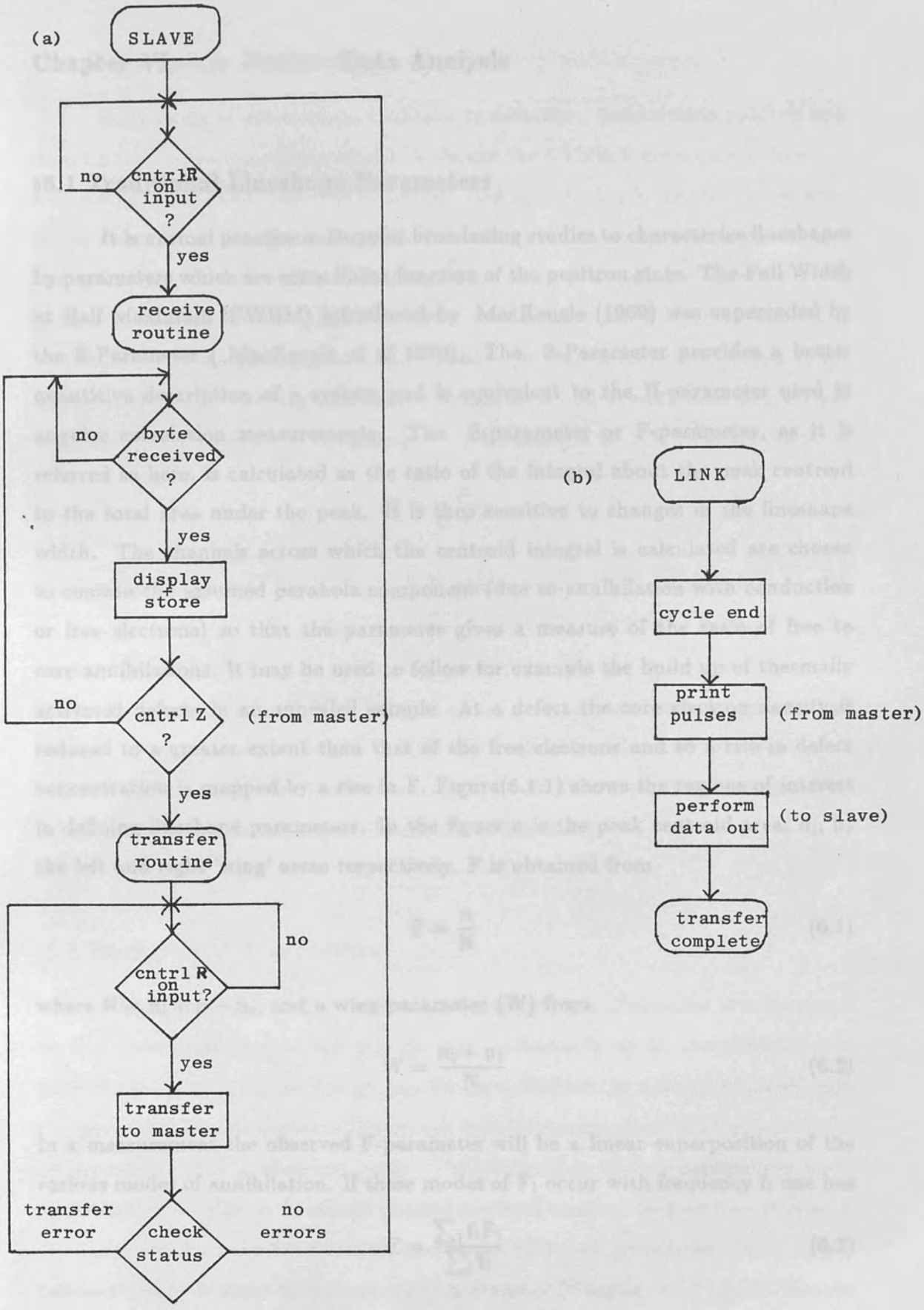

Fig(5.4.2) Data transfer flowcharts: (a) Slave 380Z data receive,
(b) Link MCA data transmit.

Chapter VI Data Analysis

§6.1 Traditional Lineshape Parameters

It is normal practise in Doppler broadening studies to characterize lineshapes by parameters which are some linear function of the positron state. The Full Width at Half Maximum (FWHM) introduced by MacKenzie (1969) was superceded by the S-Parameter (MacKenzie *et al* 1970). The S-Parameter provides a better quantitive description of a system and is equivalent to the H-parameter used in angular correlation measurements. The S-parameter or F-parameter, as it is referred to here, is calculated as the ratio of the integral about the peak centroid to the total area under the peak. It is thus sensitive to changes in the lineshape width. The channels across which the centroid integral is calculated are chosen to contain the assumed parabola component (due to annihilation with conduction or free electrons) so that the parameter gives a measure of the ratio of free to core annihilations. It may be used to follow for example the build up of thermally activated defects in an annealed sample. At a defect the core electron density is reduced to a greater extent than that of the free electrons and so a rise in defect concentration is mapped by a rise in F. Figure(6.1.1) shows the regions of interest in defining lineshape parameters. In the figure n is the peak centroid area, n_l, n_r the left and right 'wing' areas respectively. F is obtained from

$$F = \frac{n}{N} \tag{6.1}$$

where $N = n_l + n + n_r$, and a wing parameter (W) from

$$W = \frac{n_l + n_r}{N} \tag{6.2}$$

In a measurement the observed F-parameter will be a linear superposition of the various modes of annihilation. If these modes of F_i occur with frequency f_i one has

$$F = \frac{\sum_i f_i F_i}{\sum_i f_i} \tag{6.3}$$

§6.2 Positronium Parameters

Both forms of positronium facilitate its detection. Convolution analysis may detect a narrow component ascribed to p-Ps and the 0-511keV energy distribution of o-Ps decays (Ore 1949, Mills 1978) are reflected in a decline in Doppler peak area. Extra channels at energies of $\sim 2m_oc^2/3$, where m_o is the positron or electron rest mass, may be sampled and Ps parameters defined as ratios of these to peak. Figure(6.2.1) illustrates regions of interest in defining these Ps parameters. The optimum energy for detection of o-Ps (~340keV) is seen to lie unfortunately at the Compton edge. By and large the ratio of windows A and C was found to give best sensitivity. The adopted Ps-parameter R (to be changed to $Y = 1/R$) is defined as

$$R = \frac{A}{B + C} \tag{6.4}$$

while other parameters for example A/C are written in full. R does not provide an absolute value of o-Ps presence instead it is judged to be the increase, in the present work at least, from an underlying (graphite) emission. In work with positron beams the zero positronium level is taken as the ratio at high beam energies (found perhaps by extrapolation) which sample the bulk only, where no positronium is believed to form. Likewise 100% positronium levels are obtained by extrapolation to low-incident positron energies (Lynn and Welch 1980).

§6.3 Background Subtraction

All photon peaks have an underlying background. Primarily this is caused by Compton scattering of the gamma ray, additionally as in the case of ^{22}Na from the Compton of other energy gamma rays. Further, in a detector incomplete charge collection and photoelectric escape from the crystal active volume induces an asymmetry in the observed peak. The elimination of this background leads to greater sensitivity in lineshape parameters and enables, to a certain degree, a normalization between spectra obtained under different geometries, for example between those obtained in a furnace and a cryostat (Chaglar *et al* 1981). Various

types of background subtractions have been attempted. The simplest approach is of a polynomial (Jorch *et al* 1977), where channels on either side of the peak are fitted by a cubic which is subtracted from the measured peak. The disadvantage of a polynomial is that its form does not follow a predefined pattern and each subtraction would require careful selection of the wing bands to avoid inaccurate or ill behaved backgrounds. The background form is a smooth step function and Jackman *et al* (1974) used straight line segments to represent each of the three background regions viz. left wing, peak, right wing. A drawback of straight line segment backgrounds is the sharp changes of slope. In the present work a complementary error function was found to be the simplest and most dependable. It was attempted to improve on this step function by a refined straight line segments approach and by a background composed of gaussian and error function terms. In the refined straight line segments approach instead of simply joining by a line the extrapolated wing fits it was thought to use a parabola at each vertex, to smoothen the overall shape. This proved difficult to implement as the underlying quadratic depended strongly on the channels chosen and it was impractical to change these for each peak. The composite function approach was more successful, with trial and error very reasonable subtractions could be performed but in this method also the same fit channels would not produce the same ideal backgrounds from one peak to another.

The error function subtraction is given by

$$S(i) = \frac{H}{2}\mathrm{erfc}\left(\frac{i - i_o}{c}\right) \tag{6.5}$$

where erfc is the complementary error function, i channel, i_o peak centroid, H the height difference between left and right wings and c a broadening constant set at the FWHM for optimal smoothness. Figure(6.3.1) is a blown up view of a Doppler lineshape and the error function generated background. The step functon is used essentially to eliminate peak asymmetry and is usually preceded by a constant background subtraction which accounts for the 1.28MeV line Compton. In practice smoother F-parameter variations are obtained when no form of background is subtracted but as mentioned earlier, background stripping has to be performed if results obtained in different enviroments are to be compared.

§6.4 Convolution Analysis

It is required to extract from Doppler lineshapes information about electron-positron momentum and contributions from core and conduction electron annihilations. In some cases evidence for positronium (Ps) formation. The inherent resolution of Doppler broadening is an order of magnitude poorer than obtainable from angular correlation. Although this is countered by the very high source strengths and long counting times required in the latter, Doppler broadening can only seriously compete in the quality of information available if the system resolution is adequately deconvoluted from the experimental spectrum. The system resolution or response function can be illustrated by the finite width observed for monoenergetic gamma rays. This width is only a ~factor of two less than the Doppler width (Figure 1.7.3.1). The observed distribution A(E) is the result of the convolution of the true spectrum (T) with the instrumental resolution (R) and can be written

$$A(E) = \int_0^\infty T(E')R(E - E')\,dE' \tag{6.6}$$

where E is the energy or channel number. An early attempt to remove the resolution function R(E−E′) by Hotz *et al* (1968) concentrated on solving iteratively the matrix equation

$$S = X \cdot R \tag{6.7}$$

where S is the observed or synthetic spectrum and X the true spectrum and. For an initial guess of X the chi-squared (χ) would be calculated [from $\chi^2 = \sum_i (S_i - A_i)^2/A_i$] and the components of X altered to obtain a new lower χ^2. This would be repeated to minimise χ^2 and hence obtain X. An analytical model approach was adopted by Rama *et al* (1970) in which they represented the resolution function by the sum of two gaussians (obtained by least-squares fitting) and then convoluted this with the arbitrary function X and repeated the iterative procedure. An extension of the model dependent convolution is to present an analytical function to describe the distribution X. It is customary to describe Doppler spectra from metals as a sum of an inverted parabola (to account for annihilations with free

electrons) and gaussian (core electron annihilations), both with a common centroid. This leads to, Rice-Evans *et al* (1978)

$$Y(i) = A \int_{-\infty}^{+\infty} \exp\left[-\frac{(i' - i_0)^2}{2\sigma_g^2}\right] R(i - i')\, di' + B \int_{-\sigma_p\sqrt{2}}^{+\sigma_p\sqrt{2}} \left[1 - \frac{(i' - i_0)^2}{2\sigma_p^2}\right] R(i - i')\, di' \qquad (6.8)$$

where i is channel (energy), i_o centroid, $\sigma_g\sqrt{2}$,$\sigma_p\sqrt{2}$ gaussian and parabola widths respectively, A and B constants, Y(i) the observed distribution and $R(i - i')$ the resolution function. In practise the 514keV ^{85}Sr gamma line is used for the response and the integrals replaced by discrete summations and the inverted parabola included only for $|i' - i_o| < \sigma_p\sqrt{2}$. A NAG library routine (E04FCF) is employed to perform a least squares fit for the gaussian and parabola widths and heights, based on

$$Y(i) = \sum_{i'=1}^{m} A(i')R(i - i') \qquad (6.9)$$

where $A(i') = H_g \exp\left[-(i' - i_0)^2/2\sigma_g^2\right] + H_p\left[1 - (i' - i_0)^2/2\sigma_p^2\right]$; again the parabola component is included only for $|i' - i_o| < \sigma_p\sqrt{2}$ and where H_g and H_p are the respective gaussian and parabola heights. Before being used the resolution function is normalized to unit area. Also for efficiency in the minimisation, components and sum of residuals squared are scaled so as to lie between ~ 0 and 1. Traditionally background terms are included in (6.9) either as part of $A(i')$ i.e. prior to convolution or added as a separate sum (El Khangi 1980, Berry 1982, Moussavi-Madani 1986). However in the present work it was found that stripping error function backgrounds from both Doppler and resolution lineshapes before the least squares fitting gave not only faster convergence but results with better χ^2 and less scatter. Including background terms in (6.9) allows the minimisation routine greater freedom and it would often be found, especially with a polynomial inclusion, that the fit generated background was ill behaved. The fit gives the component widths, component intensities are found by calculating the component contributions to the

total fitted peak area. Figure(6.4.1) shows an example fit. The goodness of fit is given by the reduced chi-squared (χ^2/ν)

$$\frac{\chi^2}{\nu} = \frac{1}{m-n} \frac{\sum_{i=1}^{m} (y(i) - c(i))^2}{y(i)} \tag{6.10}$$

where ν is the number of degrees of freedom (m − n), m the number of channels (usually 100 or 150), n the number of components and the c(i) computed values. For detection of p-Ps a second gaussian term, identical in form to the first, is added to the A(i′) in (6.9). Para-Ps because of the possesion of a low pair momentum is expected to yield a narrow ~3 channels component (at 90eV/channel). In the grafoil work there were signs of this third narrow component; these were most striking with oxygen and figure(6.4.2) shows an oxygen analysis where the additional component appears as a spike.

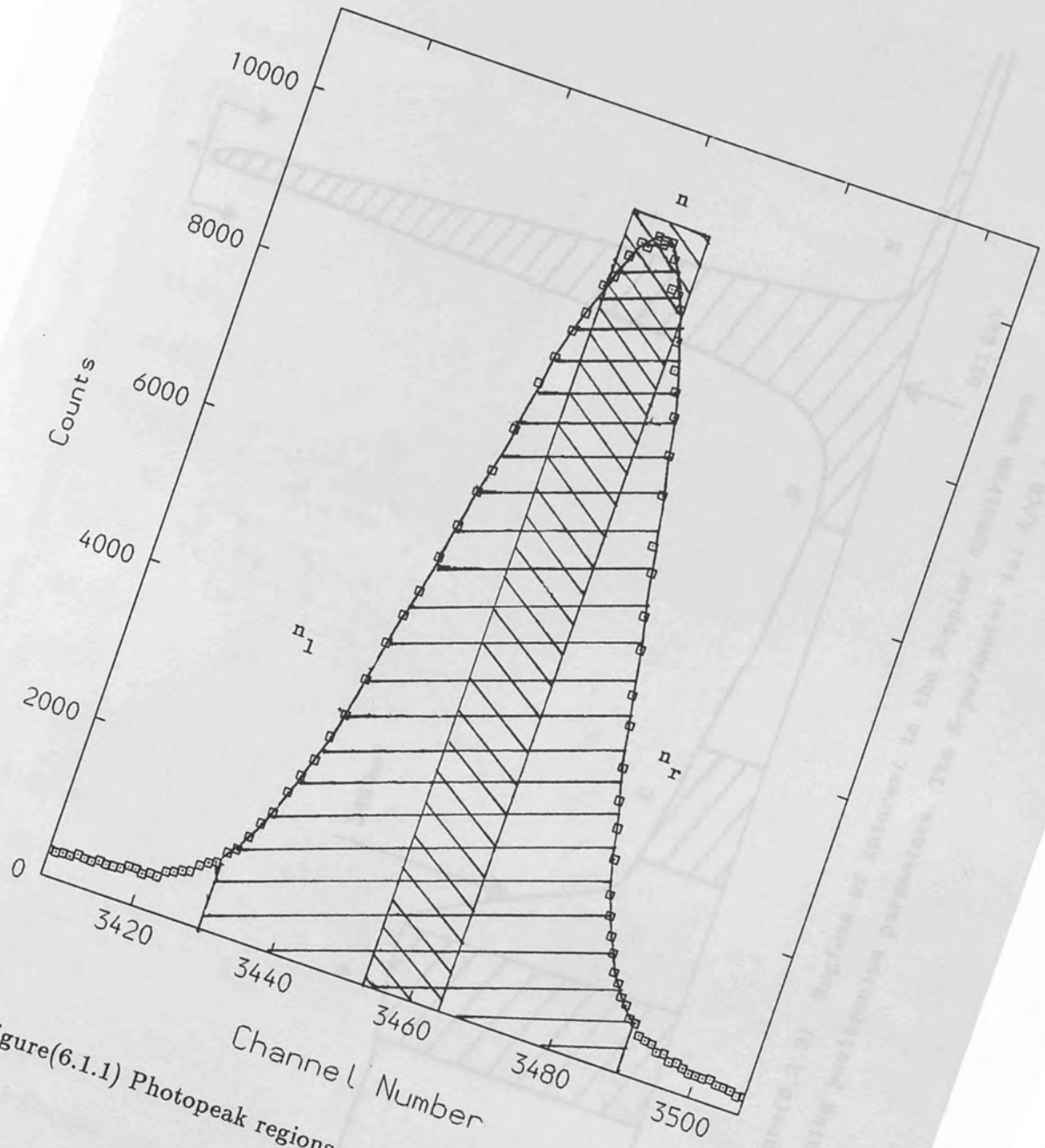

Figure(6.1.1) Photopeak regions used to calculate F and W.

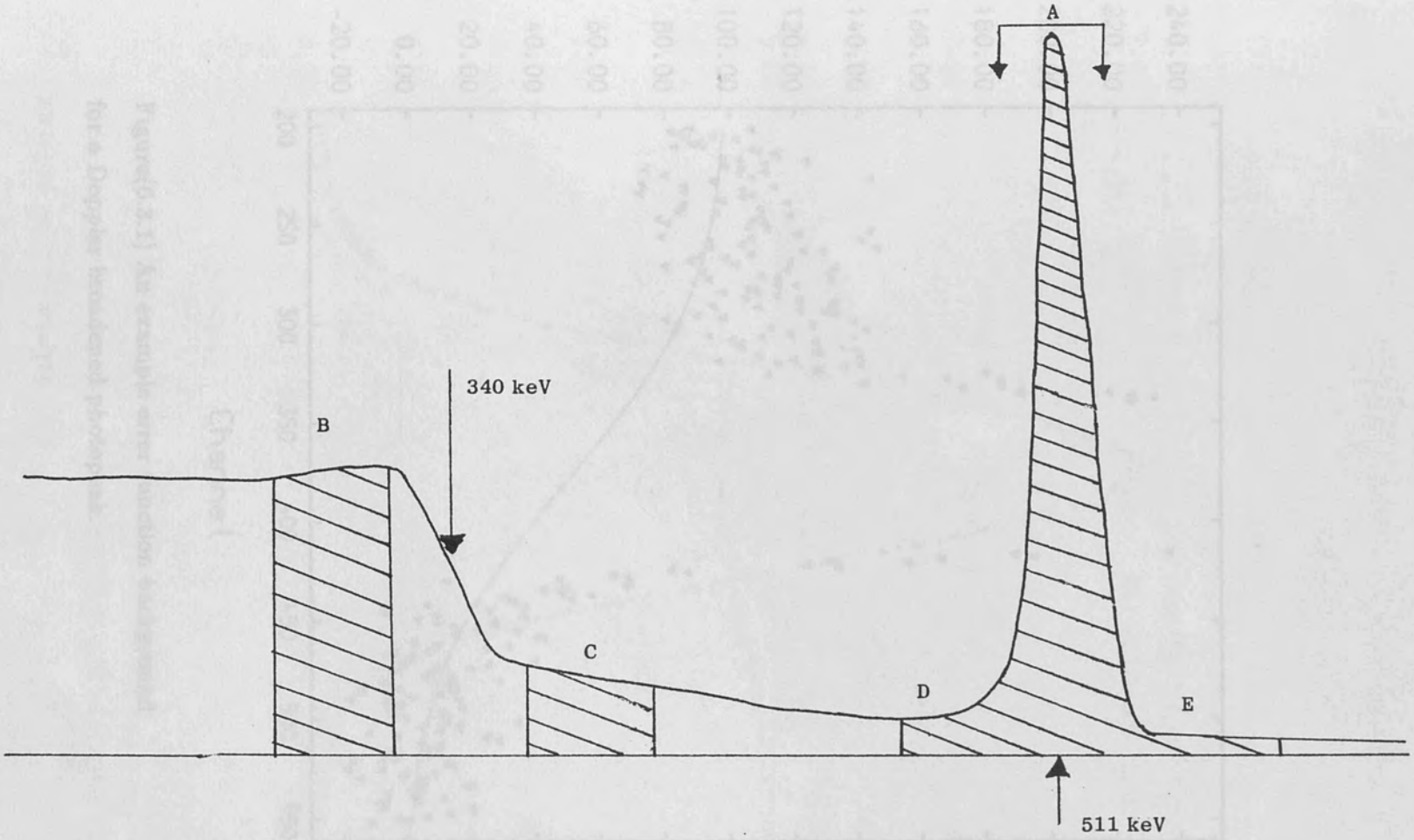

Figure(6.1.2) Regions of interest in the Doppler spectrum when defining positronium parameters. The R-parameter is: A/(B + C).

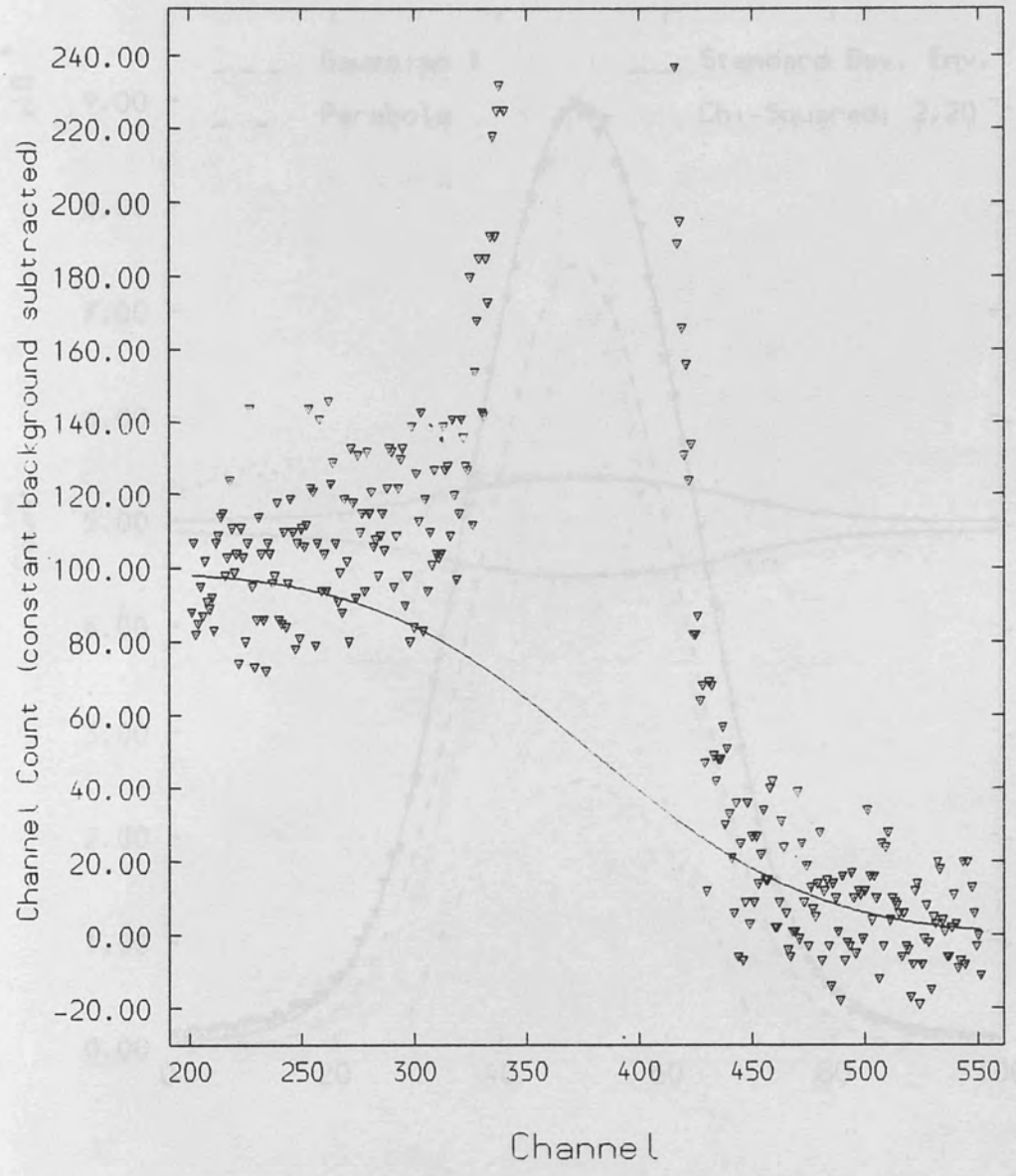

Figure(6.3.1) An example error function background for a Doppler broadened photopeak.

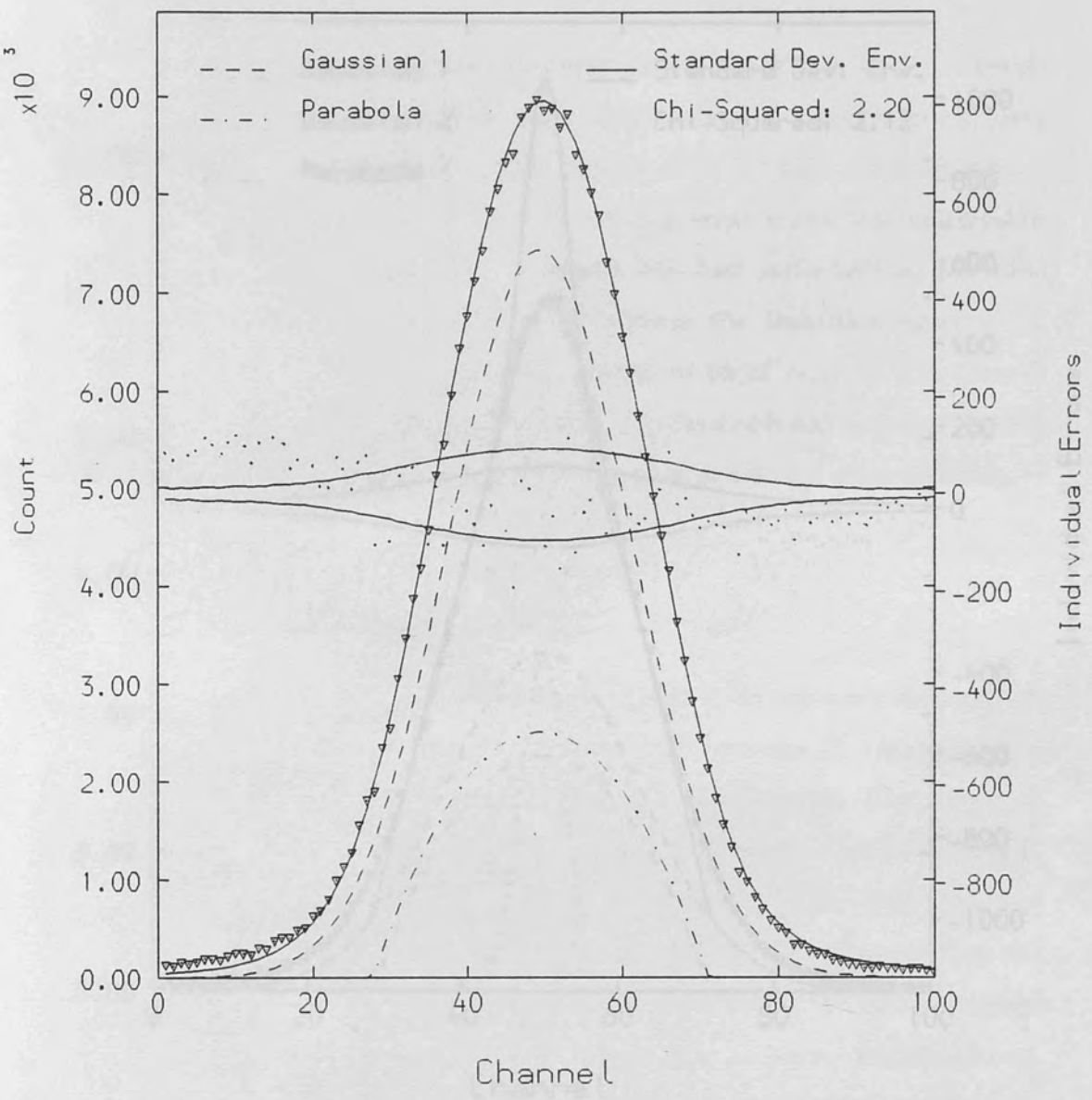

Figure(6.4.1) Two component convolution analysis.
Shown is a grafoil + oxygen fit where background has been stripped prior to analysis.

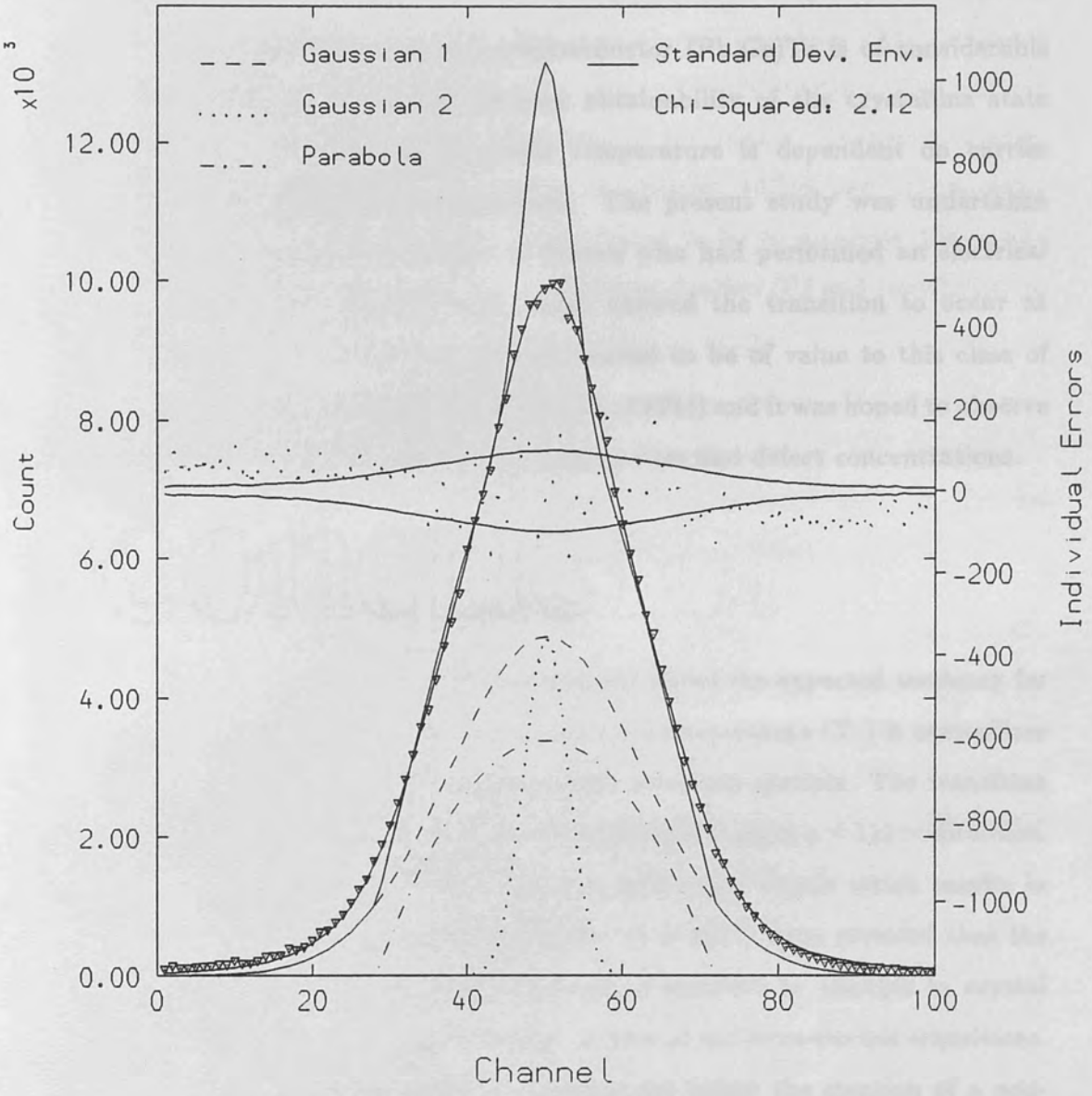

Figure(6.4.2) Three component convolution analysis.

Grafoil + oxygen free fit with weighting for peak.

Presence of narrow component is indicative of para-Ps.

Chapter VII A Positron Annihilation Study of (Pb,Ge)Te

§7.1 Introduction

The chalcogenide narrow gap semiconductor (Pb,Ge)Te is of considerable interest technologically as a result of easy obtainability of the crystalline state and a structural phase transition whose temperature is dependent on carrier concentration and germanium composition. The present study was undertaken in collaboration with He and Grassie of Sussex who had performed an electrical resistivity measurement, figure(7.1.1), which showed the transition to occur at $\sim$ 150K. Positron annihilation has already proved to be of value to this class of semiconductor (Mokrushin et al 1980, Kobrin et al 1984) and it was hoped to observe this transition and gain information on trapping sites and defect concentrations.

§7.2 The Structural Phase Transition

(Pb,Ge)Te is a group IV-VI compound and shows the expected tendency for a ferroelectric phase transition. Above a transition temperature (T_c) it crystallizes to a NaCl structure. Below T_c a rhombohedral structure persists. The transition consists of a relative displacement of the two sublattices along a $<111>$ direction. The rhomohedral structure will give rise to a permanent dipole which results in ferroelectricity. Positron lifetime studies (Davé *et al* 1977) have revealed that the lifetime and intensity of annihilating positrons is sensitive to changes in crystal structure and symmetry during para-electric to ferro or antiferro-electric transitions. Schulte (1980) showed that Doppler broadening can follow the creation of a non-equilibrium defect population during hcp $\leftrightarrow$ fcc phase changes in Cobalt samples.

§7.3 Sample Preparation

The first part of the preparation was performed by He at Sussex. The source elements (99.9999% pure, from Mining and Chemical Products Ltd) were cut and etched. Amounts for the composition $Pb_{0.93}Ge_{0.07}Te$ were weighed into a reaction tube which was evacuated and sealed. The charge was melted in a radio-frequency furnace at a temperature above the melting point of PbTe (1210K). This ensured good mixing. The charge was then quenched in iced water, crushed into small crystallites and placed in a growth tube set at between 1070K and 1120K. After three weeks the crystals were extracted and found to be of diameter 10mm and weigh 6-10g. The inhomogeneity as to carrier concentration (P) and resisitivity (ρ) was found to be less than 10% in both P and ρ.

At the positron laboratory the usual sample-source-sample sandwich was constructed. The source was deposited onto the surfaces of two samples by repeatedly allowing carrier free aqueous $^{22}NaCl$ drops to evaporate. The process was continued until the sample source strength was some $100\mu Ci$.

§7.4 Experimental Method

The sample source arrangement was wrapped in aluminium foil and mounted and secured onto the cryostat sample holder. Care was taken not to induce any deformity. The sample holder assembly was placed inside the cryostat and its position noted. After sample chamber evacuation both cryostat dewars were filled with liquid nitrogen and the chamber given shots of helium to aid cooling to 80K. A ^{103}Ru source placed beside the cryostat acted as a check for instrumental drift. The experiment was begun and 2 hour runs at 10 deg. intervals taken, at a rate of 5-6 per day from 80-440K. It was hoped to take the sample to 460K however the DTC was only able to attain a maximum of 438K followed by 434K and 422K. The sample was next placed in the furnace and two sets of 31 runs taken. Both sets spanned 290-600K. Continuous 24 hour operation was possible with the furnace. Lastly the sample was again placed in the cryostat and runs from 88-300K taken. It was intended to continue to 420K but the microprocessor control system failed

and the sample thermocouple junction melted. The experiment was concluded after taking two runs at liquid nitrogen temperatures.

§7.5 Results

§7.5.1 Lineshape Parameters

From the spectra three lineshape parameters were calculated *viz.* G, F and W. The G-parameter is the F-parameter equivalent for the reference peak. Figure(7.5.1.1) shows the G-parameter and FWHM calculated under both constant and error function background subtractions. Figure(7.5.1.2) shows the same but this time without prior background subtraction. The set of points labeled C1 are the first cryostat set, points F1 the first furnace runs. Similarly C2 and F2 are the respective second set of measurements. The distinct regions shown by G in figure(7.5.1.2) reflect the different sample geometries between sets of runs. The slight negative slopes are a consequence of the relatively short half-life of the ^{103}Ru. As the ^{103}Ru peak diminishes the underlying Compton from the ^{22}Na 1.28MeV gamma line increases in proportion resulting in the decline. For the F-parameter the results without prior background stripping compared to those with, are less scattered, Figure(7.5.1.3). The breaks are again due to changes in geometry. Figure(7.5.1.4) shows the F-parameter after a normalisation attempt which involved bringing together, by means of a fit calculated subtraction, the two sets of cryostat measurements and by a percentile offset the two furnace sets. The following observations may be made:

(a) No evidence for a phase change at 150K or thereabouts (region A $\rightarrow$ B)

(b) A negative slope, up to 350K (A $\rightarrow$ B $\rightarrow$ C)

(c) A sharp rise between 350-440K (D $\rightarrow$ E)

(d) The position of the repeat run (F)

(e) A rise then fall in F (G $\rightarrow$ I and I $\rightarrow$ K)

(f) The matching of the second cryostat and furnace runs (Q → M → P)

The lack of a positron annihilation signal for the phase change indicates perhaps only a small participation in the transition on part of the electrons. For set C1 the high initial values can be attributed to the ice quenching that was performed in the sample preparation freezing the defect population. The negative slope thus to thermal detrapping from these shallow traps (Smedsjaer *et al* 1980). The rise between 350-440K is taken to indicate the clustering of shallow defects to create deeper traps, possibly vacancies (Petersen 1983). The position of the repeat run (F) can be explained as a freezing of the defect concentration present at the cluster of points marked E and implies that the positron trapping rate for these deep traps is independent of temperature. The rise in the F1 set between 300-430K is rather suprising and suggests the clustering at the highest C1 (E) temperatures was not complete but continued at a slow rate over the same temperature range. The I → J → K decline is presumed to represent the annealing of defects. Sets C2 and F2 (Q → M → P), after being brought together, produce the characteristic behaviour of an annealed crystal.

§7.5.2 Lineshape Analysis

The model dependent convolution analysis outlined in the previous chapter was performed. Backgrounds were stripped from both the system resolution function and Doppler peaks (see later chapters for detail) and common peak centroid introduced as a free component. The results are presented in figures(7.5.2.1 - 3). The gaussian intensity, figure(7.5.2.2a), remains ~constant (with perhaps a hint of a negative slope) for set C1 and the first part of F1, at ~55% and 300K. At 500K, a little above the preannealing maximum in the F-parameter, it declines to meet the annealed variation at 45%. The gaussian width remains at ~ 17 channels (at 94eV/channel), figure(7.5.2.2b), with the C1 and F1 points coinciding until 500K. At 500K the width rapidly climbs to meet the annealed trend at 20 channels. The parabola width, figure(7.5.2.3b) shows a better defined variation, starting off at ~ 15.2 there appears to be a gentle up then down trend until the sharp rise at 500K

to 17 channels where it meets the annealed line. The average parabola width of 15.5 channels may be used to obtain a Fermi energy for the free electrons. From equation(1.13)

$$\frac{2\Delta E}{E} = \frac{v_f}{c} \tag{7.1}$$

where $2\Delta E$ is the energy spread (2×15.5 channels), $E = m_0c^2 = 511keV$, m_0 being the positron rest mass, v_f is the Fermi velocity, and c the velocity of light, one has

$$v_f = \frac{2c\Delta E}{m_0c^2} \tag{7.2}$$

so that

$$E_f = \frac{1}{2}m_0v_f^2 = \frac{2(\Delta E)^2}{m_oc^2}$$

or

$$E_f = \frac{2(\Delta E)^2}{511} \tag{7.3}$$

giving a Fermi energy of 8.3eV.

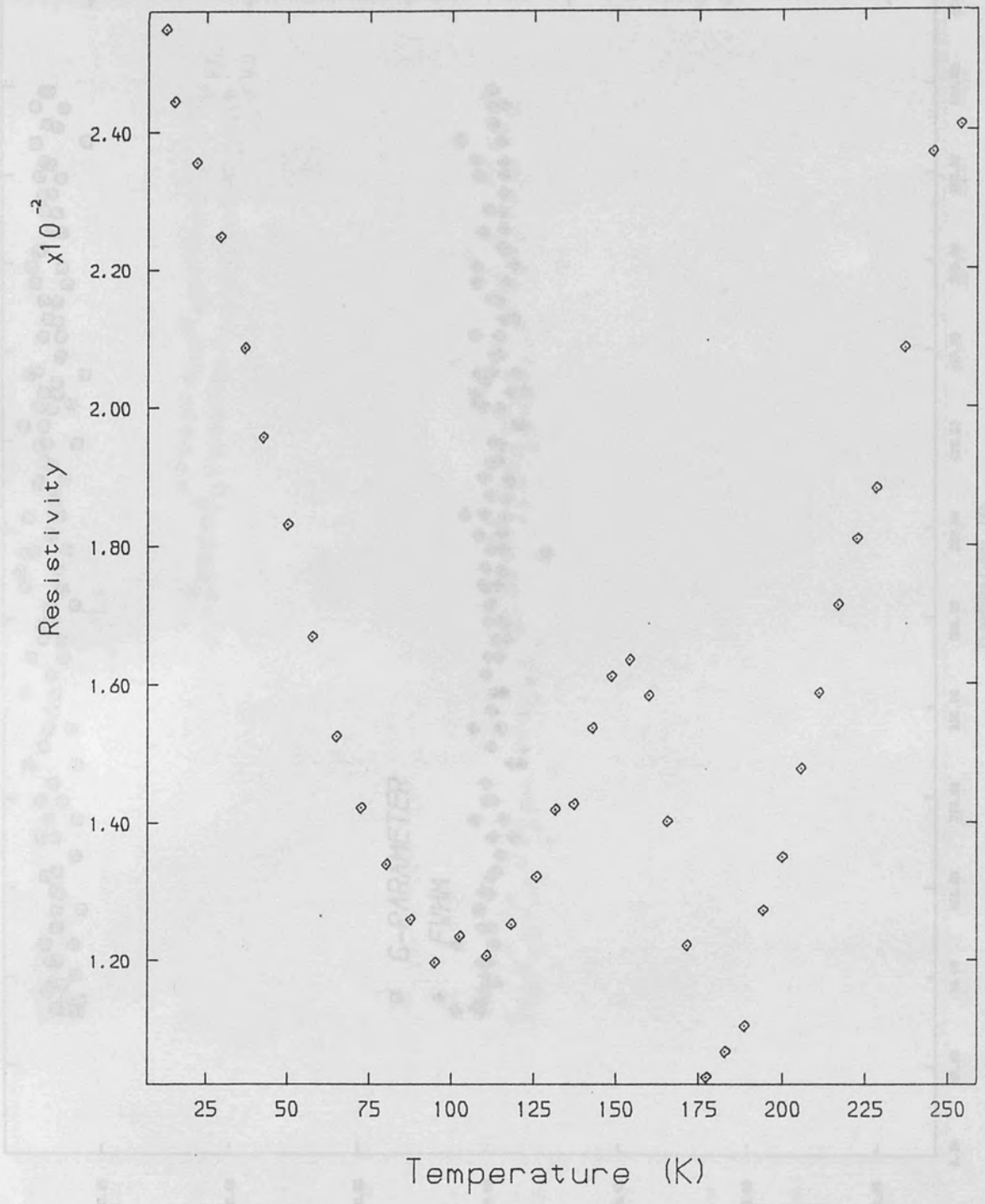

Figure(7.1.1) (Pb,Ge)Te resistivity vs temperature.

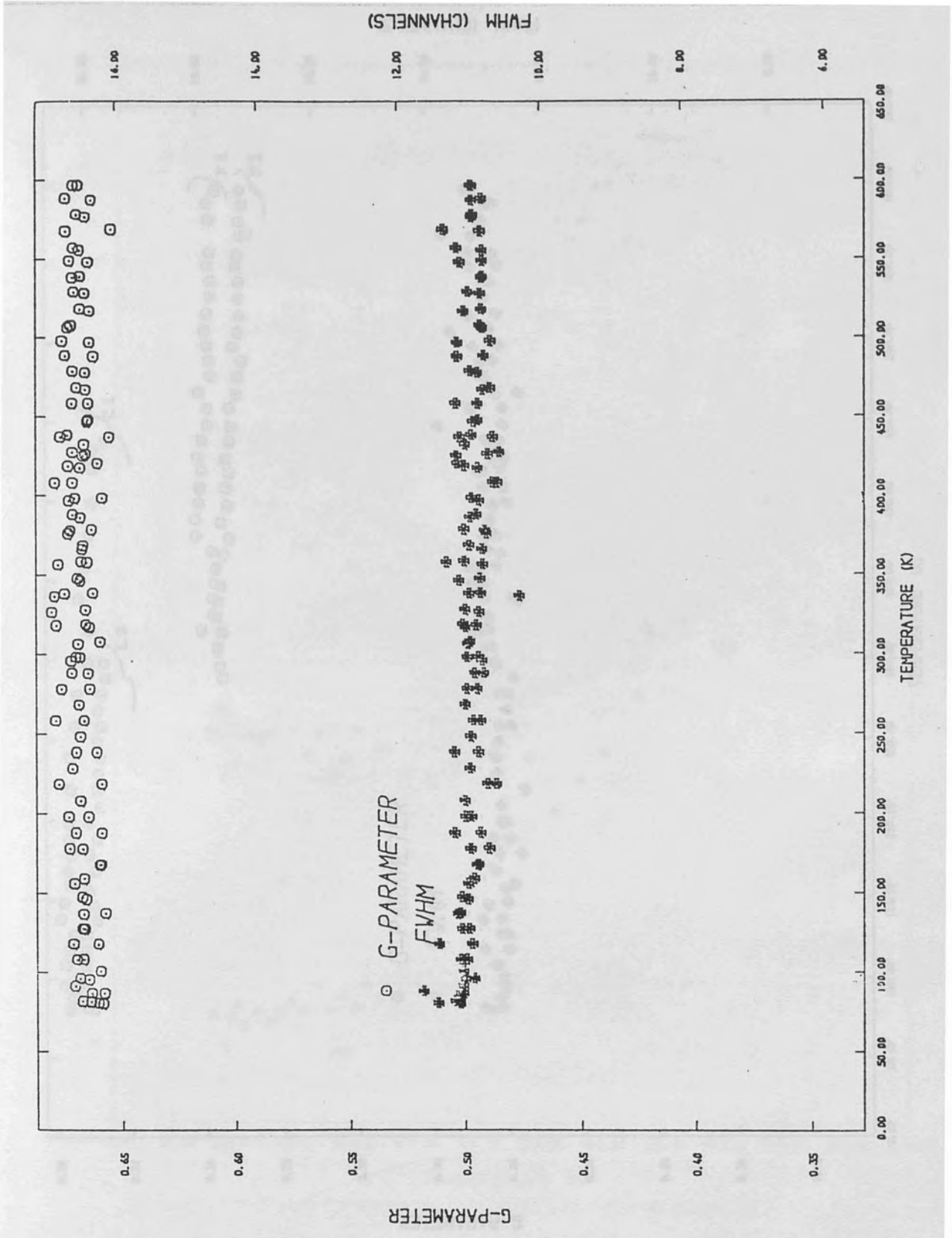

Figure(7.5.1.1) Lineshape parameter and FWHM of reference peak (background subtracted).

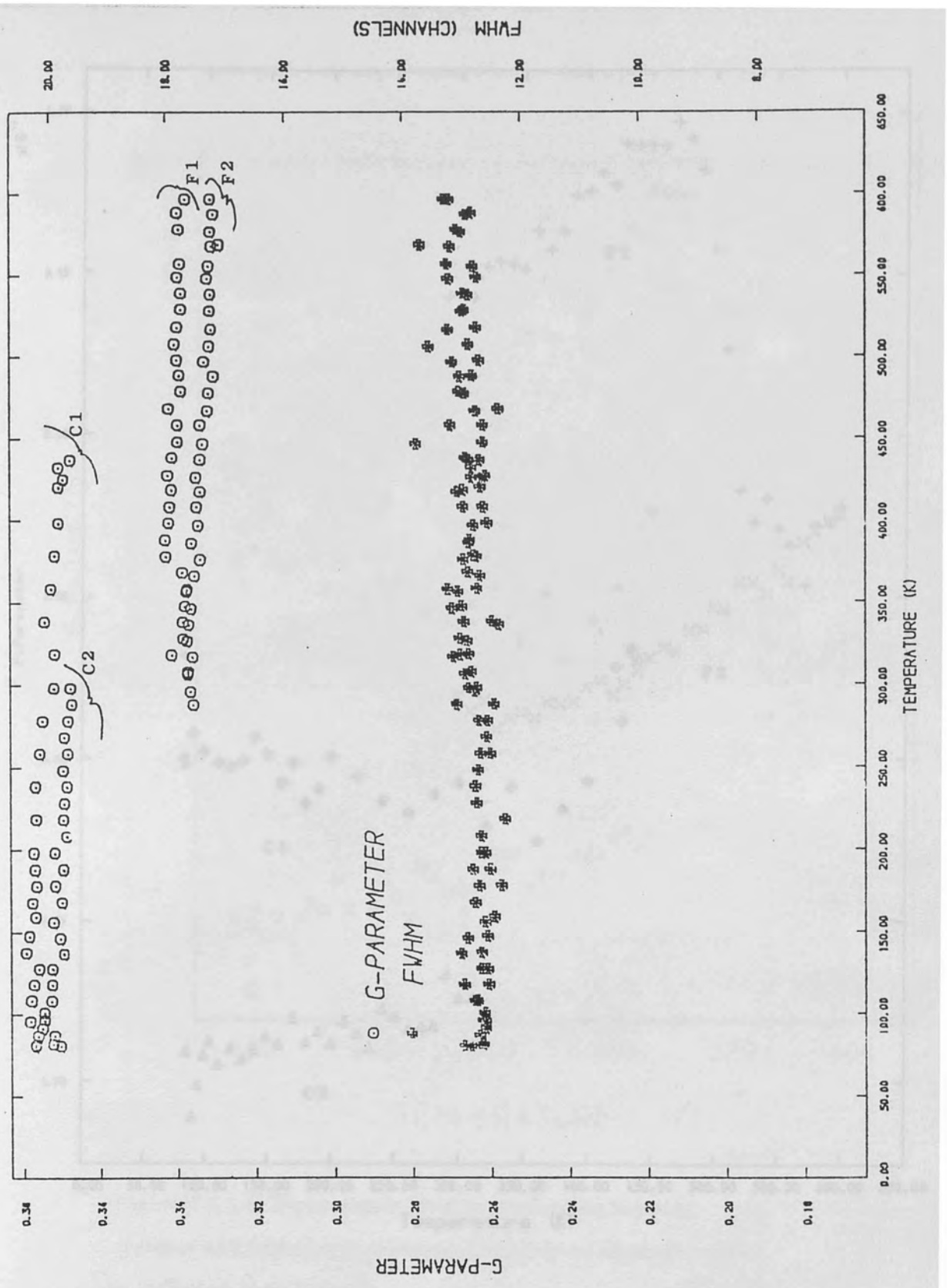

Figure(7.5.1.2) Peak parameters of reference line
(no prior background stripping).

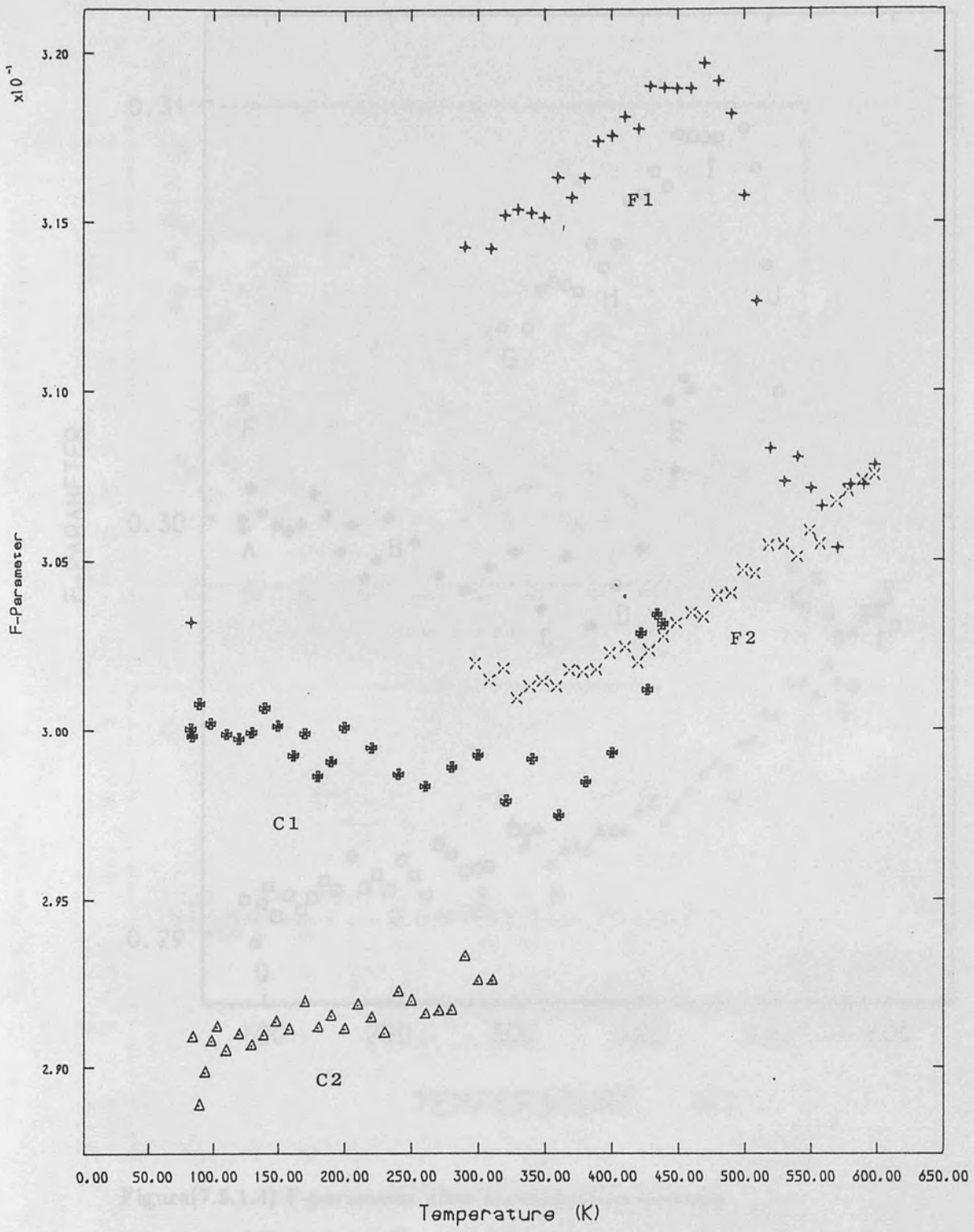

Figure(7.5.1.3) Line-height parameter F vs temperature without background subtraction.

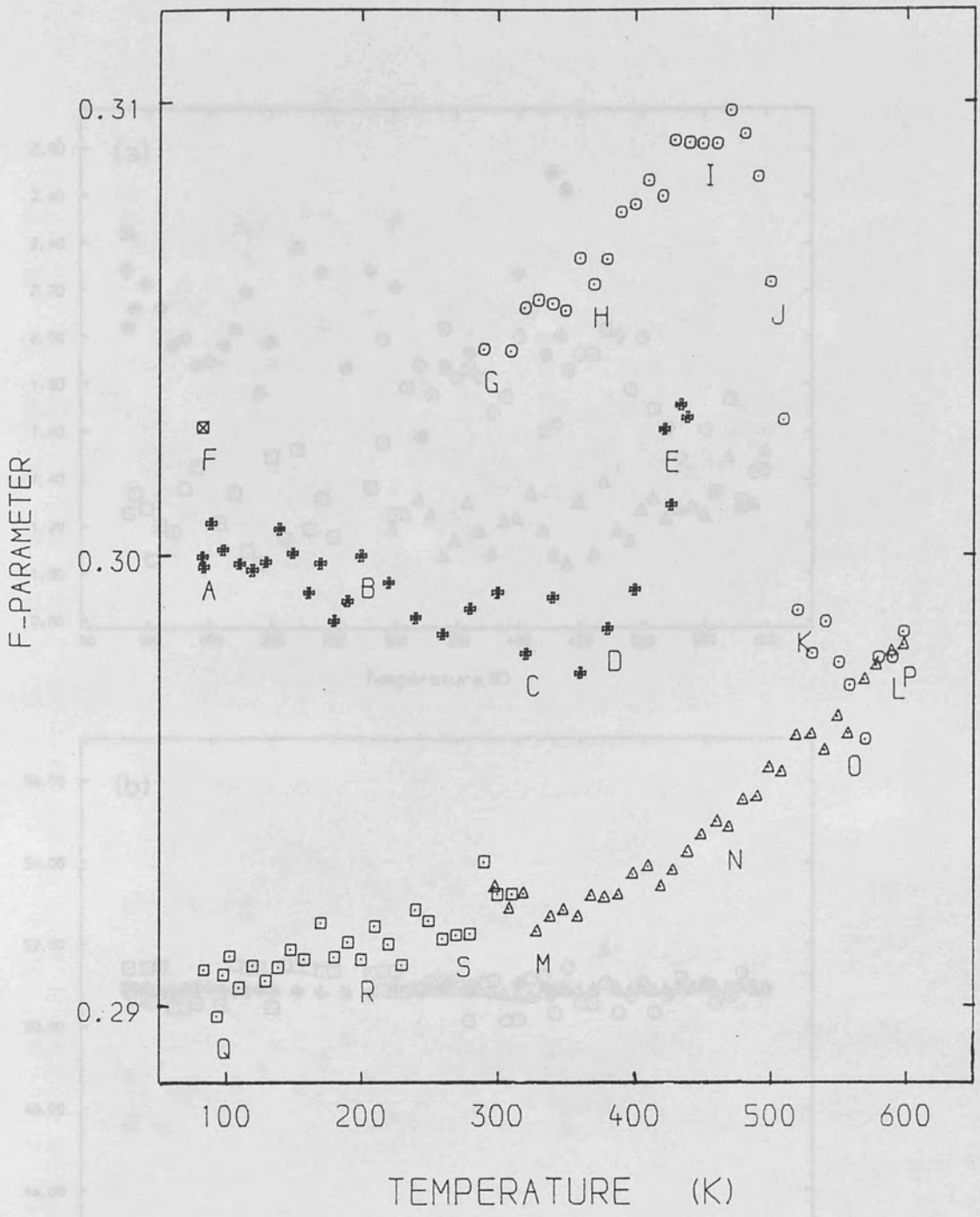

Figure(7.5.1.4) F-parameter after normalisation between cryostat and furnace experiments. Sequence of measurements is indicated alphabetically.

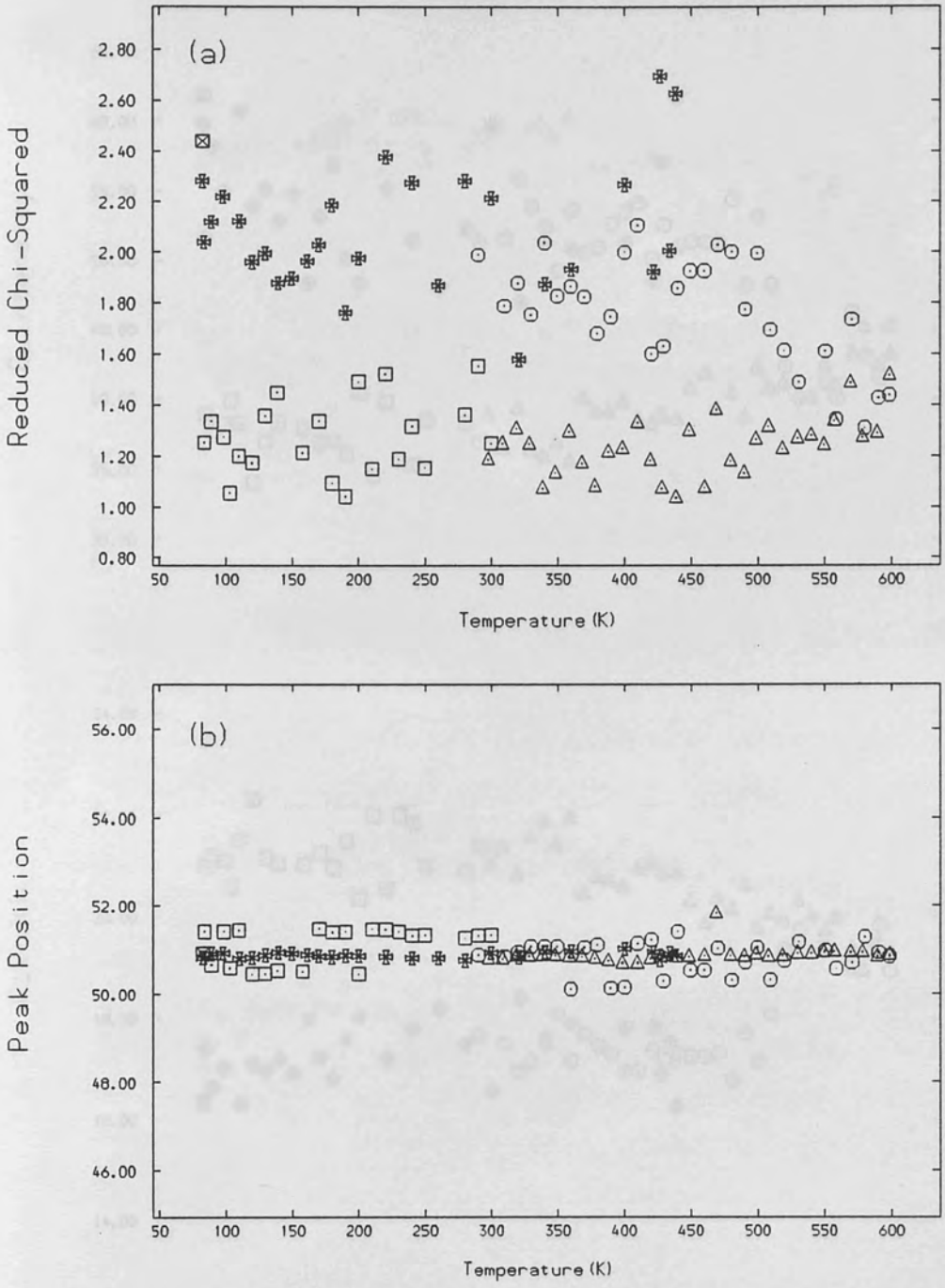

Figure(7.5.2.1) Two component lineshape analysis on (Pb,Ge)Te

(a) χ^2/ν.

(b) Common peak centroid.

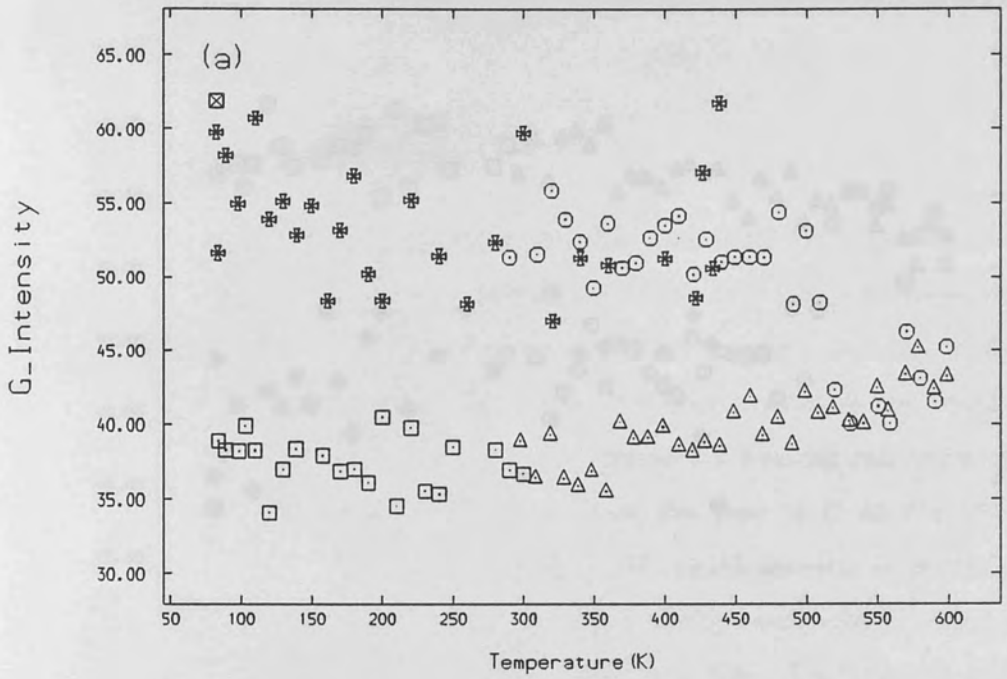

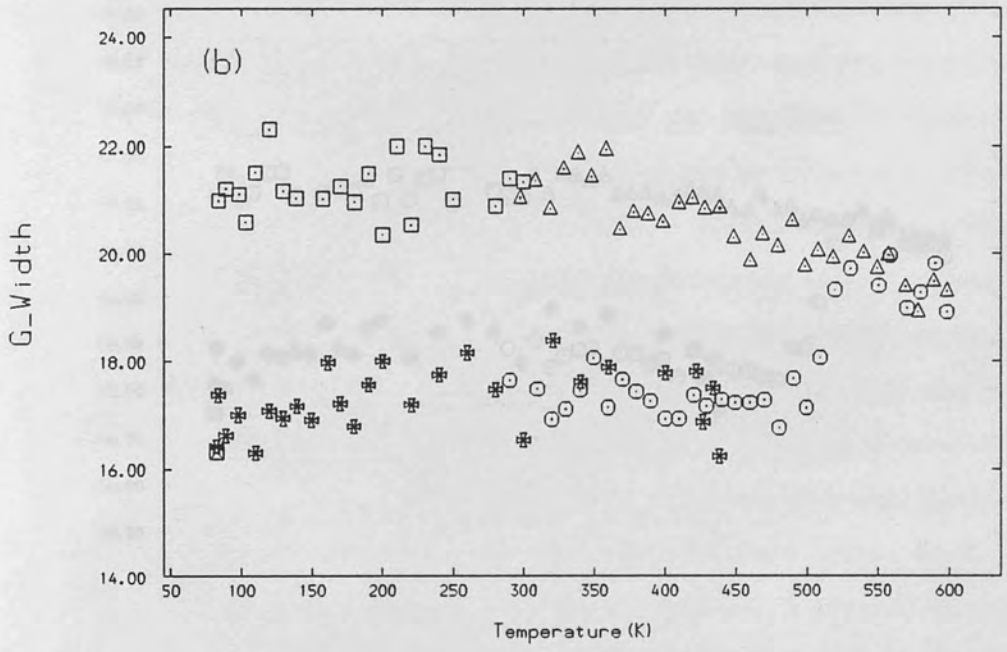

Figure(7.5.2.2) Two component lineshape analysis on (Pb,Ge)Te

(a) Gaussian Intensity.

(b) Gaussian Width.

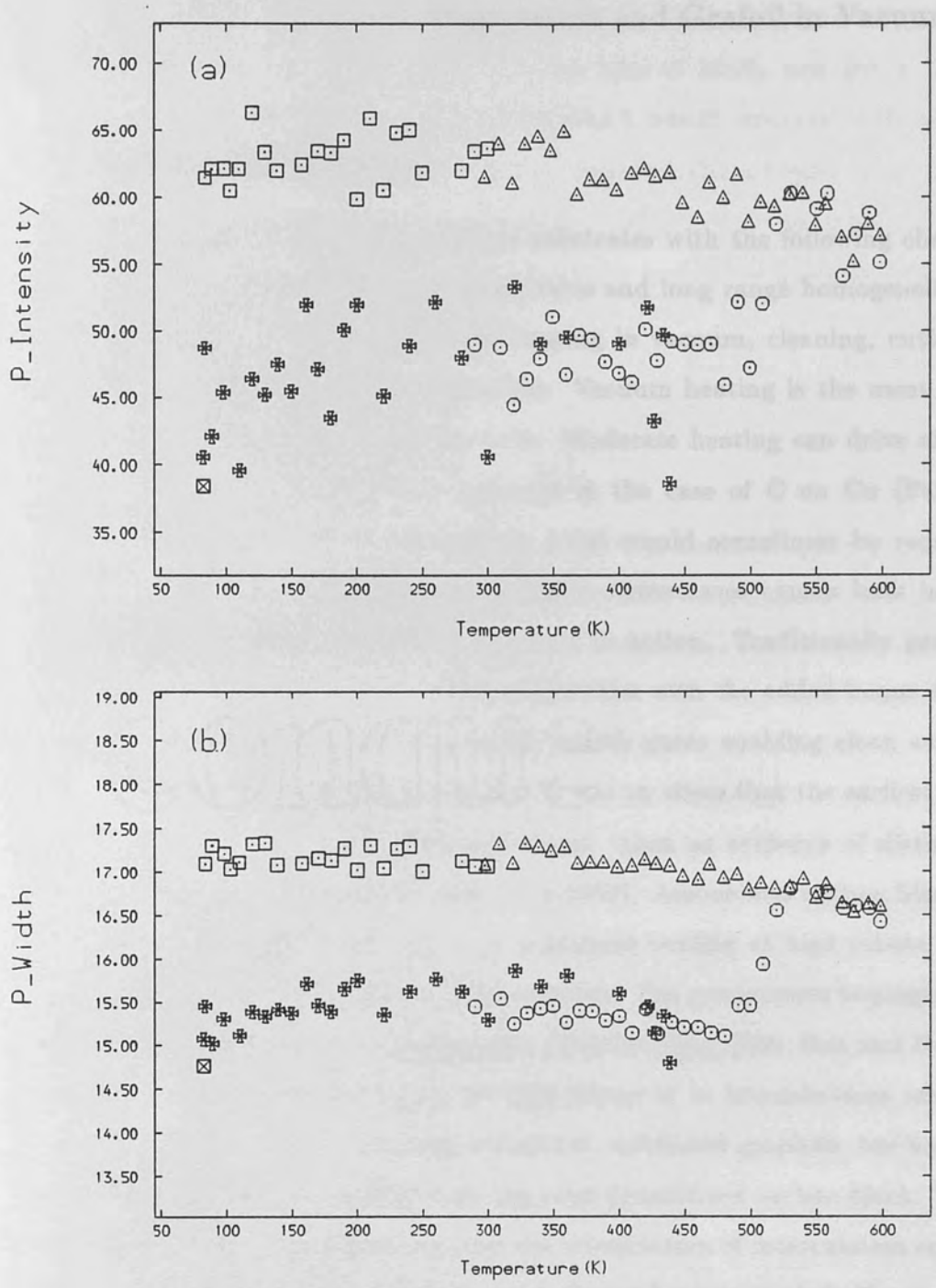

Figure(7.5.2.3) Two component lineshape analysis on (Pb,Ge)Te

(a) Parabola Intensity.

(b) Parabola Width.

Chapter VIII Substrate Preparation and Grafoil in Vacuum

§8.1 Substrate Preparation

The study of adsorption requires substrates with the following characteristics: high purity, high surface to volume ratio and long range homogeneity. Techniques for surface preparation include heating in vacuum, cleaning, cutting, polishing and etching and vapour deposition. Vacuum heating is the most common method of obtaining high purity surfaces. Moderate heating can drive off weakly bound impurities however, as for example in the case of C on Cu (Farnsworth 1966) a temperature above the melting point would sometimes be required for chemisorbed species. Furthermore heating in some cases causes bulk impurities to diffuse to the surface and so be negatory in action. Traditionally graphitized carbon blacks have given best surface uniformities with the added bonus of carbon oxidation products (CO and CO_2) being volatile gases enabling clean surfaces to be maintained by only moderate heating. It was on these that the earliest stepwise vapour pressure isotherms were observed and taken as evidence of distinct layer formation (Polley *et al* 1953, Schaeffer *et al* 1953). Amorphous carbon black develops graphite structure on heating with prolonged heating at high (above 1000 °C) temperatures producing complete graphitization. The pronounced homogeneity is a result of the exposure of basal planes only (Hess and Ban 1966, Ban and Hess 1969) so that adsorption does not occur on edge planes or in imperfections which have different binding energies. Recently a material, exfoliated graphite, has been found which has superior homogeneity than the most graphitized carbon black. The process of production -exfoliation- involves the introduction of intercalation complexes within the graphite crystals which through abrupt heating explode the crystal layers apart. The expanded particles are pressed together and rolled into binderless flexible sheets which have a density some one-half that of crystalline graphite. The basal plane surfaces are strongly oriented parallel to the plane of the sheet in the c-axis and have a specific adsorption area of around $20 m^2/g$. The better homogeneity is evidenced by sharper step isotherms with some revealing novel substep forms.

Stepwise adsorption is also displayed by other adsorbents such as MoS_2, BN, NaCl, KCl, RbCl and NaBr (Dash 1975). In the case of MoS_2 and BN a possibility of applying the exfoliation process exists which would enhance their adsorption homogeneity. The adsorbate used in the reported (Rice-Evans *et al* 1986) and present work is a commercially available form of exfoliated graphite known as grafoil, from Union Carbide Corporation. This particular grafoil has a density of $0.94 g/cm^3$ and specific adsorption area of $10 m^2/g$.

§8.2 Positron Annihilation in Grafoil

It required the development of a high flux monoenergetic source of slow positrons (Mills 1979a, Howell *et al* 1982) to firmly foot the positron as a new surface probe. With samples however of high surface area such as powders the conventional positron method of fast positrons from radioactive decay may also be applied in the study of surface phenomena. Recent applications of slow positrons to condensed matter physics have primarily focussed on surface electronic structure and interfacial phenomena (Rosenberg *et al* 1980, Fischer *et al* 1983). The methods of positron annihilation *viz.* lifetime, angular correlation and Doppler broadening can be used as accurate tools in the determination of surface states, as photons from surface annihilations can readily be distinguished from those pertaining to annihilations in the bulk. This is primarily as a result of the reduced electron density experienced by positrons at the surface but also to formation of positronium through electron capture by emerging positrons. Positronium formation in the bulk is unlikely due to high electron densities. Surface lifetime studies thus require inclusion of at least three components and this is exemplified by the work of Jean *et al* (1984) who performed lifetime measurements on graphite derived samples of varying surface area. They reported lifetimes of 0.2, 0.45 and 2ns attributed to annihilations in the bulk, on the surface and of *o*-Ps respectively. In Doppler broadening surface annihilations are recognised through the presence of positronium. It is detectable in both forms; the *o*-Ps (triplet state) because of the wide energy distribution from

the decay to three photons and the *p*-Ps (singlet state) as a spike component in the Doppler peak (chapter 6).

The Doppler broadening work on grafoil presented here in addition to providing a backbone to the gas adsorption studies gives results of a three component convolution analysis.

An investigation, over the wider temperature range 80-600K, is described by Moussavi-Madani (1986).

§8.3 Sample Preparation and Method

A traditional sample-source-sample sandwich was constructed. Drops of carrier-free ^{22}NaCl solution were allowed to evaporate on the central portions of two grafoil sheets. The thickness of the two activated sheets, of dimension 12x10x0.4mm^3, was found to be less than the stopping range of the positron in graphite (1.9mm, Moussavi-Madani 1986) and five extra sheets were added to each side of the sandwich. The final arrangement was wrapped in thin aluminium foil. In the furnace under a vacuum of better than 10^{-6}Torr, the 100μCi grafoil produced 600,000 counts over the Doppler peak in a two hour accumulation period. This preparation was performed by Moussavi-Madani. The results presented here are from one set of grafoil in vacuum runs performed by way of course prior to gas adsorption studies. The sample mounted in the cryostat was heated to 470K and the temperature maintained for 15hr, under a vacuum of better than 10^{-6}Torr. This constituted a heat treatment additional to earlier treatments in the furnace at 600K. Spectra were collected between 440 and 90K. 90K proving to be the lowest temperature attainable in vacuum.

§8.4 Results

§8.4.1 Lineshape and Positronium Parameters

The lineshape F-parameter calculated without background subtractions is shown in figure(8.4.1.1). For metals variations in F represent changes in electron density and or momenta. In the grafoil the large surface area ensures that annihilations are predominantly from the surface state. As such they are sensitive to contributions from positronium. In fact the rising trend for increasing temperature is most likely positronium production. The traditional explanations *viz.* thermal expansion and positron trapping are not applicable. Positron trapping in graphite occurs at temperatures above 1575K (Shinotomai *et al* 1983) and the slope in F is too large to be a result of thermal expansion which has a coefficient of $0.8 \times 10^{-4}\mathrm{K}^{-1}$ on the surface (Suzanne and Bienfait 1972). These however do not rule out an anomolous prevacancy rise. Because F is calculated from a ratio about the peak it can be a measure of *p*-Ps. The self-annihilation radiation from *p*-Ps contributes only to a few channels about the peak. Figure(8.4.1.2) shows the A/C-parameter (R-parameter). This by definition (chapter 6) is sensitive to *o*-Ps. The decline in A/C with increasing temperature indicates increasing positronium formation. These results agree qualitively with lifetime measurements of Jean *et al* (1984). In their temperature study they found the intensity of the *o*-Ps component to rise from 1.5 to 7% between 300 and 850K. The rise in positronium production was mirrored by a fall in surface positron intensity.

§8.4.2 Lineshape Analysis

The peaks were fitted with an inverted parabola and gaussian convoluted with the instrumental resolution function. The subtraction of error function backgrounds before convolution against background inclusion as additional fit components resulted in a much enhanced rate of convergence in the least squares minimisation routine. The inclusion of a free fifth component for common centroid

further improved final χ^2/ν values. The results are presented in figures(8.4.2.1 - 3). The χ^2/ν, figure(8.4.2.1a), ranged from 3 - 4, tending to the higher values for increasing temperature. The parabola and gaussian widths, figure(8.4.2.2), are found to be quite different from those obtained in metals (Khangi 1980, Berry 1982). Here for low temperatures the parabola at 20 channels (94 eV/channel) is a little wider than the gaussian at 19 channels. The electron Fermi energy from this parabola width being 7.4eV. Both widths decline with increasing temperature, reaching some 16 channels at 440K. Figure(8.4.2.3) shows component intensities. The parabola percentage is seen to drop from 35% at 90K to under 10% at 440K with a concomitant increase in the intensity of the, more narrow, gaussian. These sharp variations like those of the F-parameter cannot be explained by bulk effects or surface positrons. The rise in the gaussian (narrow) component intensity is perhaps in sympathy to increased *p*-Ps production. If this is so its presence may be explained by thermal detrapping of surface bound positrons (Mills 1979b) which on escape capture an electron from the medium to form positronium. The effect is similar to that observed with low energy positron beams (Mills 1979a, Lynn and Welch 1980, Lynn *et al* 1985).

Later an attempt based upon the successful detection of *p*-Ps in oxygen adsorption (chapter 13), involving the addition of a second gaussian component was performed. The width of this component was fixed at a low 4 channels (see later chapters). The results are presented in figures(8.4.2.1b) and (8.4.2.4 - 6). The new χ^2/ν at $\sim$2.6 ,figure(8.4.2.1b), lacks the temperature trend of the two component analysis. A more striking change is shown in the parabola and gaussian. Both have widths of $\sim$20 channels, figure(8.4.2.4), and are deprived of a temperature dependence. This width compares well with the lowest temperature values in the two component case. The same goes for intensities, figure(8.4.2.5), which remain at roughly 40% for parabola and 60% for gaussian. Again these intensities are to be compared with the two component low temperature results. The cause of these dramatic changes is seen in figure(8.4.2.6) where the narrow component intensity approaches 4.5% at the highest temperatures from a background near zero level. These three component results are indicative of a temperature dependence in positronium production.

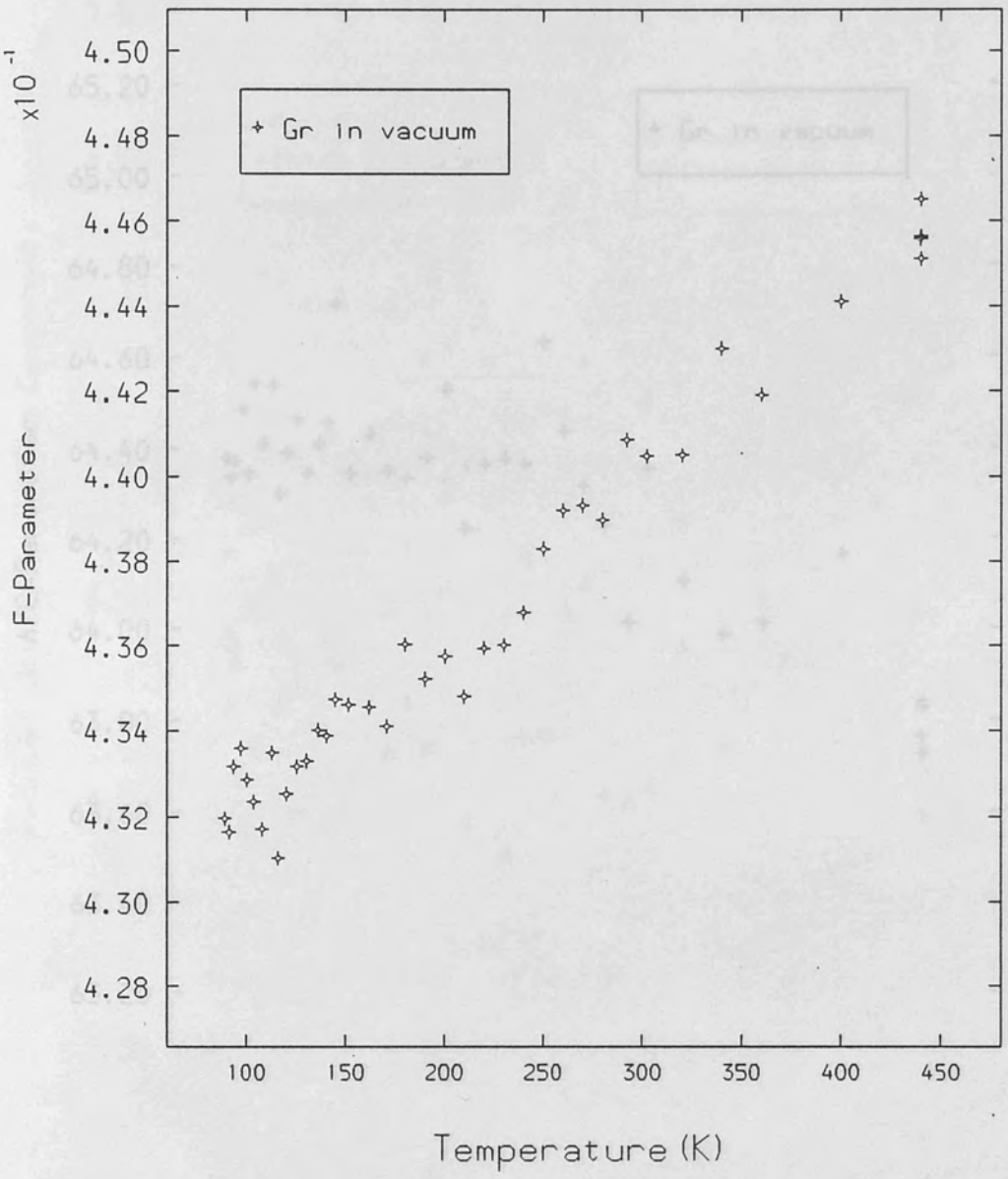

Figure(8.4.1.1) Grafoil (Gr) in vacuum.

Lineshape F-parameter as a function of temperature.

Results shown of a [7 + 1 + 7] definition.

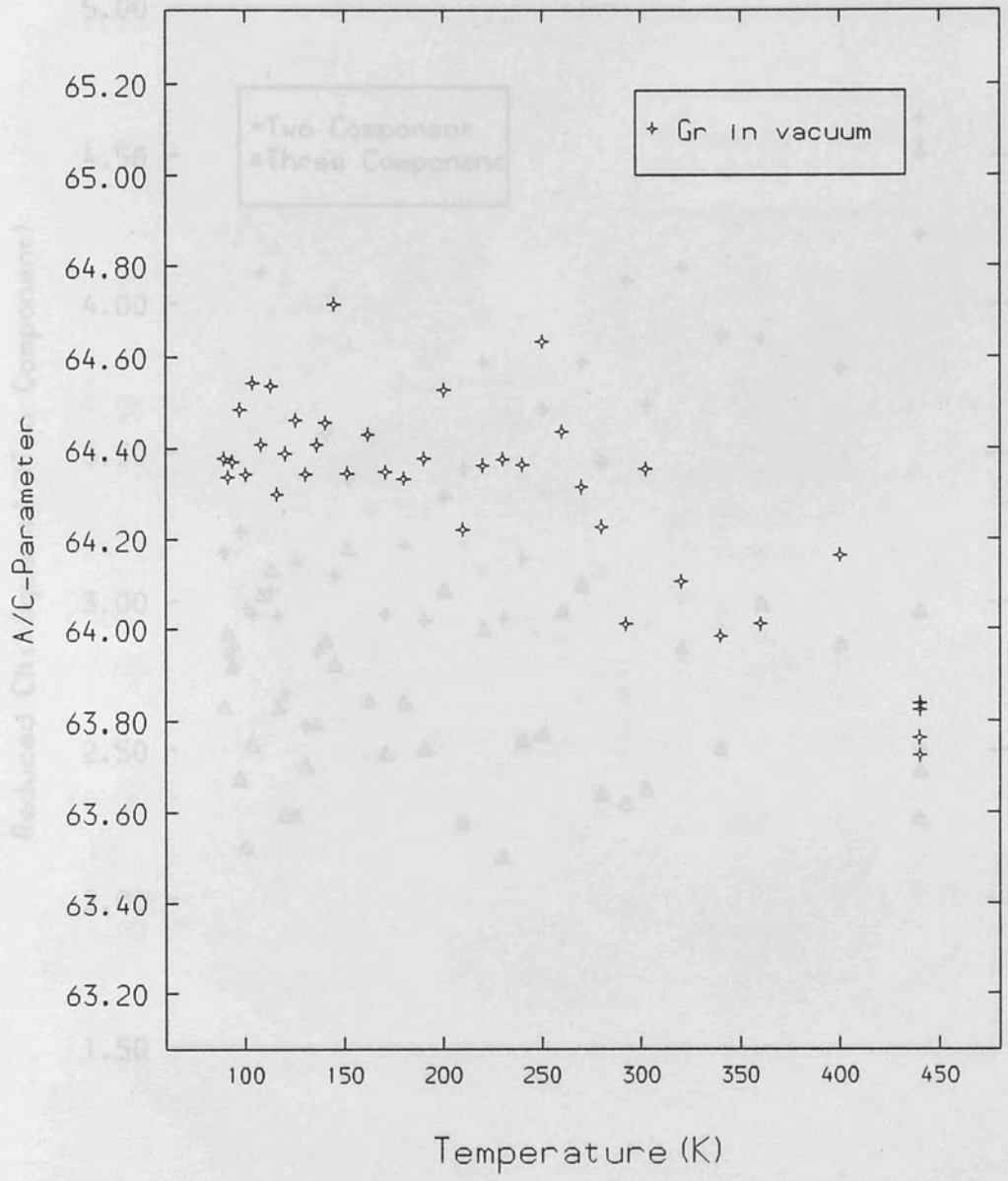

Figure(8.4.1.2) Grafoil (Gr) in vacuum.

Positronium parameter (A/C) as a function of temperature.

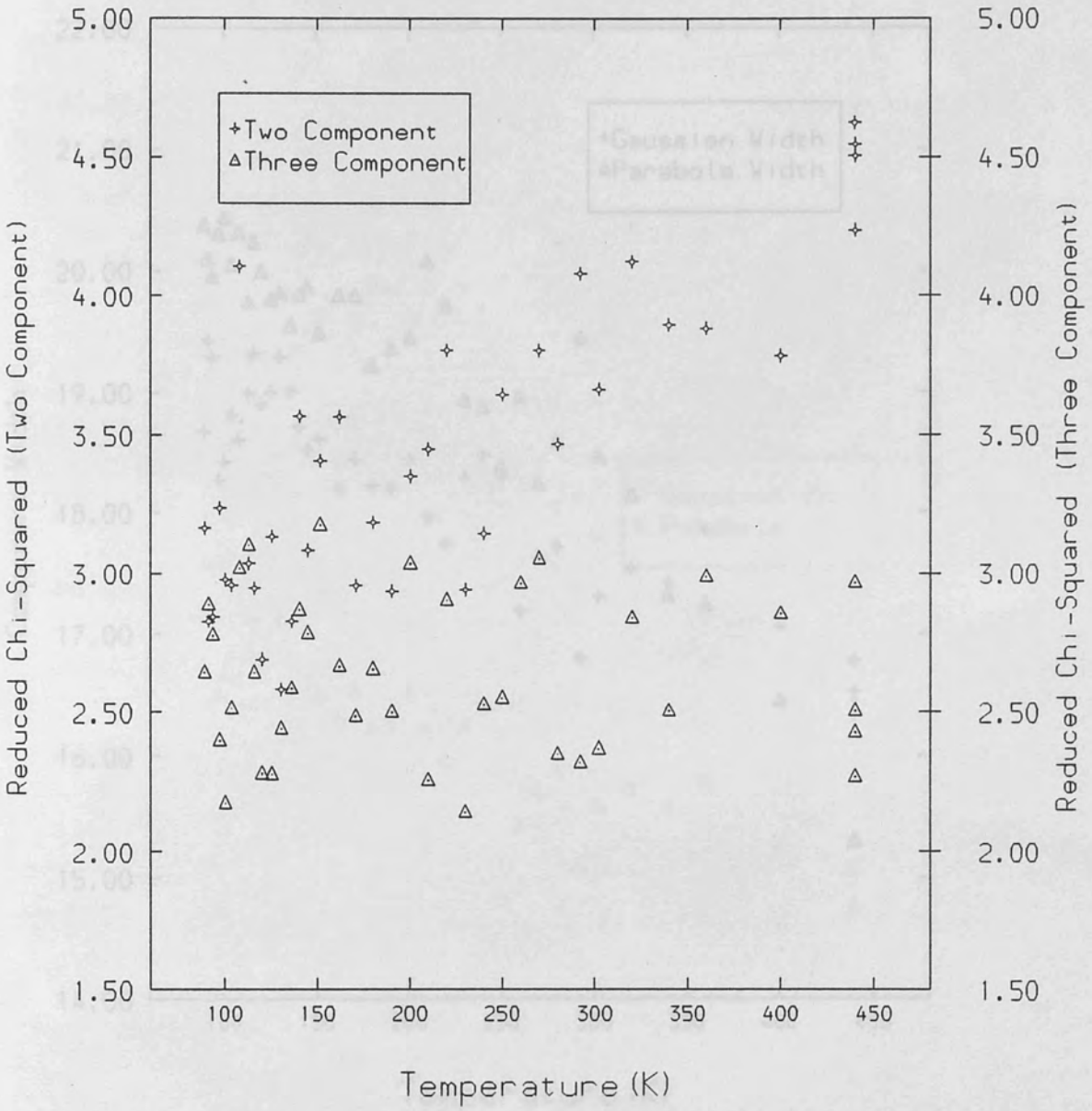

Figure(8.4.2.1) Grafoil in vacuum. χ^2/ν.

(a) From two component analysis (left ordinate).

(b) From three component analysis (right ordinate).

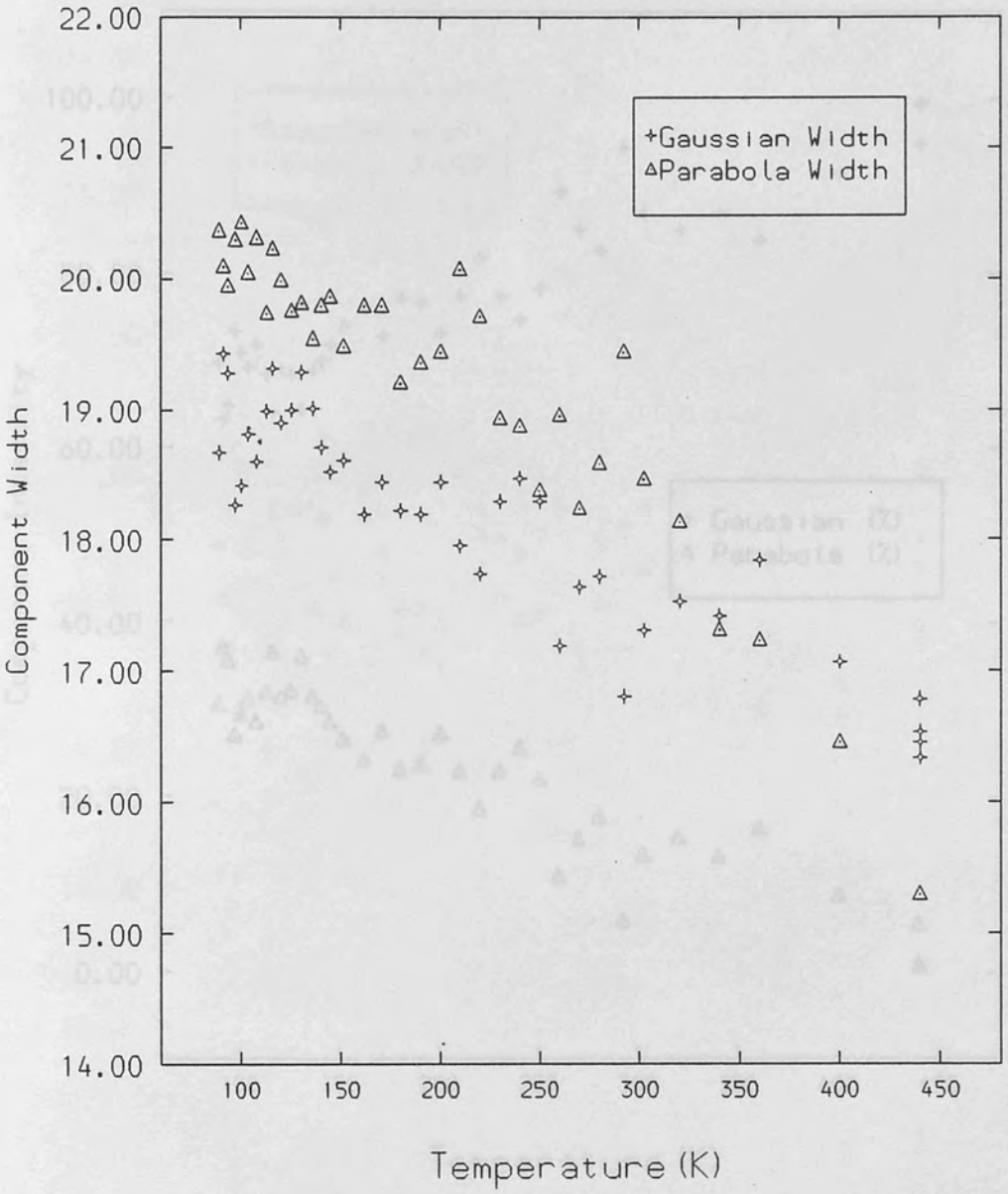

Figure(8.4.2.2) Grafoil in vacuum. Parabola and Gaussian Width from two component analysis.

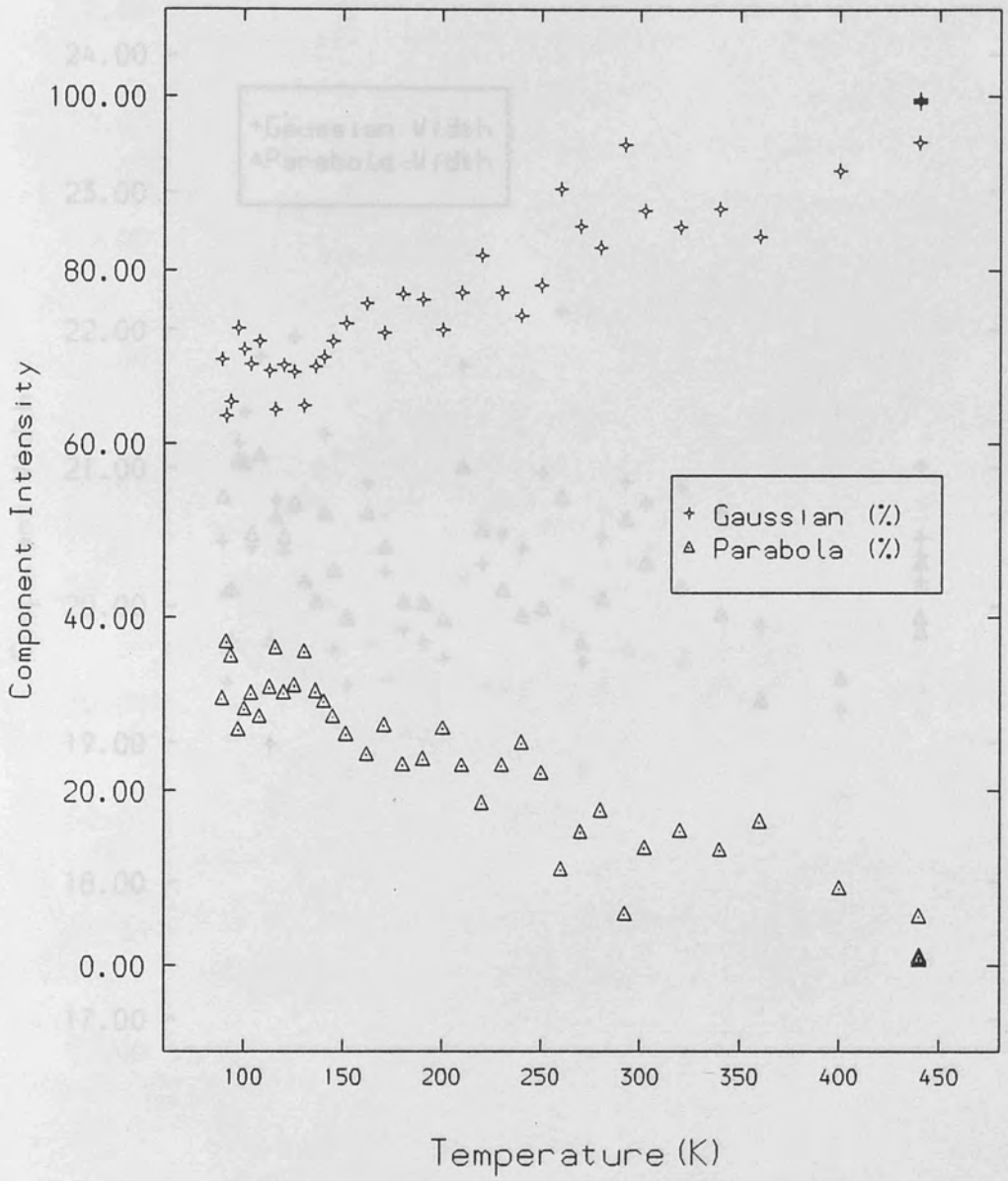

Figure(8.4.2.3) Grafoil in vacuum. Parabola and Gaussian Intensity from two component analysis.

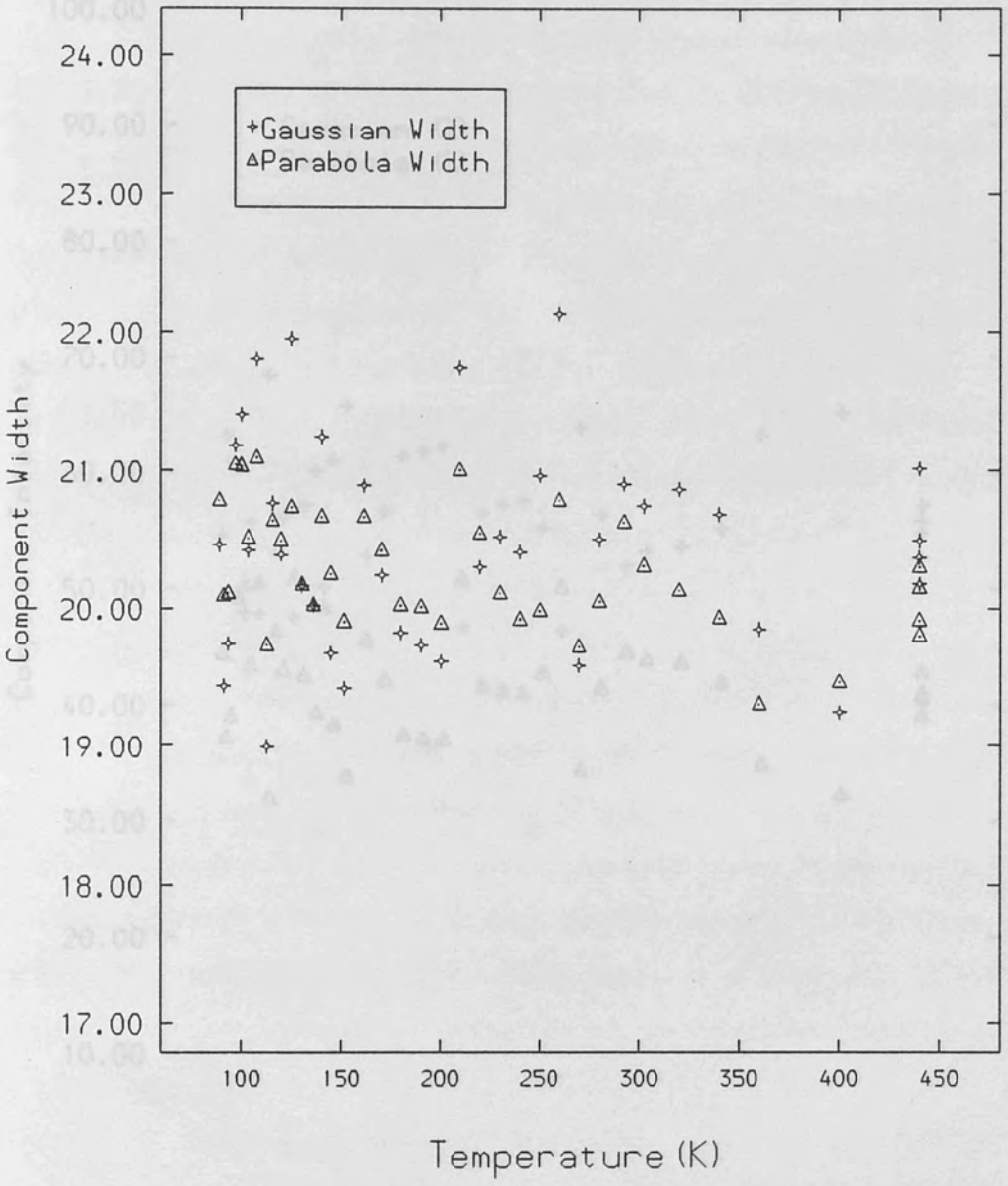

Figure(8.4.2.4) Grafoil in vacuum. Parabola and first Gaussian Width from three component analysis.

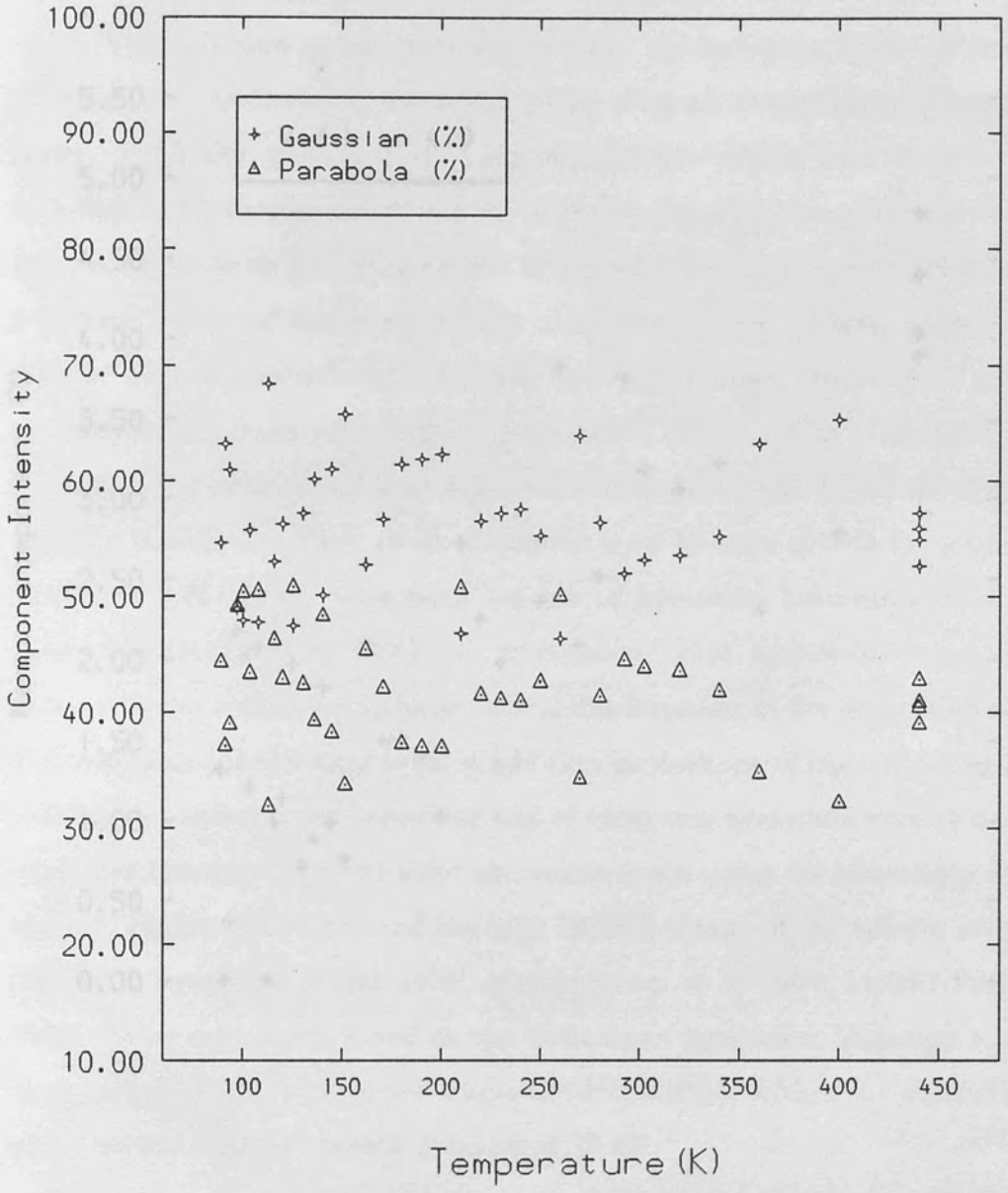

Figure(8.4.2.5) Grafoil in vacuum. Parabola and first Gaussian intensity from three component analysis.

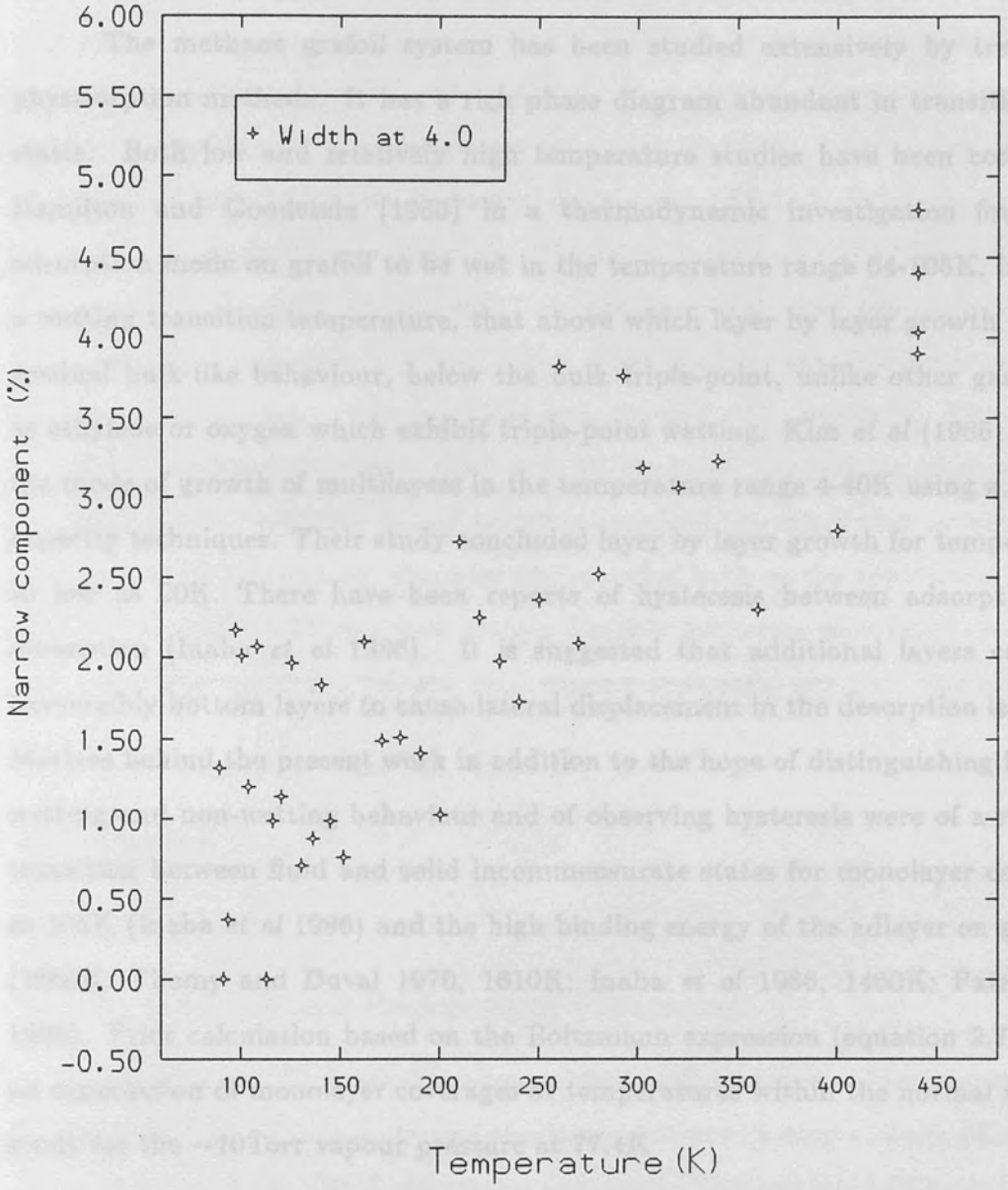

Figure(8.4.2.6) Grafoil in vacuum. Narrow component intensity (width fixed at 4 channels).

Chapter IX Methane on Grafoil

§9.1 Introduction

The methane grafoil system has been studied extensively by traditional physisorption methods. It has a rich phase diagram abundant in transitions and states. Both low and relatively high temperature studies have been conducted. Hamilton and Goodstein (1983) in a thermodynamic investigation found the adsorption mode on grafoil to be wet in the temperature range 64-105K, implying a wetting transition temperature, that above which layer by layer growth leads to gradual bulk-like behaviour, below the bulk triple-point, unlike other gases such as ethylene or oxygen which exhibit triple-point wetting. Kim *et al* (1986) studied the mode of growth of multilayers in the temperature range 4-40K using a.c. heat-capacity techniques. Their study concluded layer by layer growth for temperatures as low as 20K. There have been reports of hysteresis between adsorption and desorption (Inaba *et al* 1986). It is suggested that additional layers compress irreversibly bottom layers to cause lateral displacement in the desorption isotherm. Motives behind the present work in addition to the hope of distinguishing between wetting and non-wetting behaviour and of observing hysteresis were of a reported transition between fluid and solid incommensurate states for monolayer coverages at 105K (Inaba *et al* 1986) and the high binding energy of the adlayer on graphite (1660K: Thomy and Duval 1970, 1610K: Inaba *et al* 1986, 1460K: Patrykiejew 1983). Prior calculation based on the Boltzmann expression (equation 2.7) led to an expectation of monolayer coverages at temperatures within the normal range of study for the ~10Torr vapour pressure at 77.4K

§9.2 Method

Following sample heat treatment at 470K and vacuum runs from 470-100K the cooled sample chamber was charged with an excess of methane gas (99.995% pure, supplied by British Oxygen Special Gases). The 77.4K vapour pressure of this solid methane as read by the DTC-Transmitter arrangement and Genevac 0-20Torr gauge was 9.7±0.5Torr. Two hour measurements were begun spanning 300-80K, followed by repeat runs from 78-350K. A procedure of halving gas pressure and taking sets of measurements was adopted. From the fourth set, pressure measurement was with the DPI101 indicator and 0-52Torr transducer. The transducer sensitivity was 0.01Torr and accuracy, after zeroing and factory span setting, better than 0.05Torr. After these positron annihilation experiments, isotherms were taken. The gas store was charged with methane. The cryostat allowed to warm, under evacuation and 36 hrs later, the sample allowed to cool to 130K. A high pressure in the gas store required the small shot pressure to be reduced before application. Pressure was recorded both on the application of a shot and at the end of a 10 min wait period. Further isotherms were taken at 110, 100 and 80K. The same shot volume, with varying pressures, was used throughout.

§9.3 Results

§9.3.1 Lineshape and Positronium Parameters

Figure(9.3.1.1) shows a most prominent positronium production peak with a grafoil in vacuum variation. Drawn also is an arbitrary fit derived from a Lorenztian with gaussian wings. The A-parameter gave a 4% effect but the A/C ratio is seen to be 5%. A discrepancy between high temperature go back points and the initial set was later attributed to detector drift. Around the peak itself, at 135K there was no sign of hysteresis. The relative to vacuum 5% change gives minimum proportions for Ps decays. Total positronium production is higher as one third of positronium is produced in the singlet state and there is some o-Ps contribution to the lower

energy side of the 511keV photon peak. An expression derived from the two state trapping model (see appendix A) was used to fit the right hand side of the *o*-Ps peak

$$R = \frac{R_l - R_h A t^{-\frac{3}{2}} \exp(\epsilon_0/t)}{1 - A t^{-\frac{3}{2}} \exp(\epsilon_0/t)} \tag{9.1}$$

where R_l and R_h are the low and high limits of R respectively, ϵ_0 adatom-substrate binding energy, t temperature, A a constant and where the Boltzmann approximation (valid for low coverages, chapter 2) has been inserted. The fit, figure(9.3.1.2), yielded 1550±30K for ϵ_0. The F-parameter results, figure(9.3.1.3), show a change of some 4% and indicate the presence of *p*-Ps. Figure(9.3.1.4) shows the A/C parameter for the full set of methane peaks. The gentle downwards trend of the minima and right hand side levels is a result of detector drift. The peak broadening from high to low temperatures is a consequence of pressure variation within sets of runs. Only the vapour pressure peak, owing to the nature of the experiments was conducted at a fixed pressure. For the rest, the pressure declined with sample temperature and drew the minimum to lower temperatures. The lower the start pressure the larger the change across a peak and so the greater the broadening. Another observation is the sudden failure for peaks at or below 100K to produce a left hand side rise. Although the possibility of a lack of gas for adsorption beyond the peak cannot be ruled out (as pressure does tend towards zero, figure 9.3.2.3) it could signal a phase change. The generally accepted phase diagram for monolayer adsorption, figure(9.3.1.5), shows the first layer melting curve to start above ~0.75 commensurate layer coverage at ~60K and tend towards above monolayer coverage for increasing temperature. This implies that if the positronium peak's occur at half-coverage (see later) their attainment would be uneffected by the fluid→incommensurate solid phase change. This in fact appears to be the case, the S-form variations above 78K show the same ~5% effect. The peaks above 100K do not show any sign of the transition perhaps because they cross the transition temperature at the (low) vacuum level of positronium. The failure for a rise to progress for the peak at 100K appears to occur a little to the left suggesting a transition coverage of above one half (~0.6). Data for pressure and temperature at maximum positronium was collected for the sets of runs and an attempt made

to fit the resultant pressure versus temperature variation. The central assumption was that the adlayer state, in particular coverage and binding energy, was the same at each peak. Although adlayer binding energy is known to vary with coverage, as a result of preferential adsorption sites on real substrates (Dash 1975, Piper and Morrison 1984, Inaba *et al* 1986), a temperature independence on the premise of constant coverage seems reasonable. The Boltzmann approximation for gas adsorption in the Henry law region was used. Equation(2.7), after insertion of methane mass and nearest-neighbour distance becomes

$$P = 1798 x t^{\frac{3}{2}} \exp\left(-\frac{\epsilon_0}{kt}\right) \tag{9.2}$$

in which x is monolayer fraction, P adlayer vapour pressure(Torr), t temperature(K) and ϵ_0 adatom-substrate binding energy(kK). For the supposed fluid state a methane nearest-neighbour distance of 4.10Å is used (Kim *et al* 1986). This is the same as that of the bulk where methane molecules form a triangular structure with a lattice constant of 5.8Å and is to be compared with the effective size for commensurate $\sqrt{3}\times\sqrt{3}$ packing, 4.26Å(from $\sqrt{3}\times 2.46$Å, 2.46Å being the separation of minimum potential sites in the hexagonal graphite structure). This expression, which essentially ignores adatom-adatom interactions, yielded 1600 ± 30K for ϵ_0 and ~0.5 for x, figure(9.3.1.6). An attempt was made to improve on this value of ϵ_0 with the modified Boltzmann expression (equations 2.10 and 2.11),

$$P = 1798 x t^{\frac{3}{2}} \exp\left(-\frac{\epsilon_0}{kt}\right) \exp\left[2x\left(b - \frac{a}{kt}\right)\right] \tag{9.3}$$

In (9.3) the constants a, b account for the adatom felt attractive, large separations, and repulsive, short separations, forces respectively. The attractive term dominates at low coverage and/or low temperature and to a first approximation may be ignored. For further simplicity, b which relates to maximum packing before repulsion can be set at monolayer capacity, i.e. 1 in relation to x. When the extra term ($\exp[2x \times 1]$) is inserted in (9.2) ϵ_0 rises to ~1720K for the same coverage.

It must be borne in mind that coverage values relate to the fluid state and must be increased by some 5% before comparision with figure(9.3.1.5).

§9.3.2 Pressure Results

Figure(9.3.2.1) presents the pressure record for the fourth methane peak. An S-shape is apparent the inflexion point of which coincides with the positronium peak minimum. The nonzero gradient of either wing is the background pressure trend, the change of slopes indicate gas adsorption to the completion of a monolayer and hence the point of inflexion half coverage. Figure(9.3.2.2) shows more clearly the striking resemblance between pressure variation and an unfolded positronium peak. In figure(9.3.2.3) the peak at 100K is plotted side by side with pressure which appears to duplicate the anomalous behaviour of the positronium peak. An attempt was made to fit the pressure variation with the expression used for positronium peak right hand sides (9.1). In (9.1) the low and high parameter constants were replaced by temperature dependent terms which represented the underlying wing trends. The analysis produced a reasonable value for ϵ_0 (1530 ± 30K) and is shown in figure(9.3.2.4).

The attempted isotherms proved rewarding with those at 80K and 110K showing very clear form, figures(9.3.2.5) and (9.3.2.6) respectively. The isotherm at 110K, at the temperature of one of the Doppler experiments, figure(9.3.2.6) resembles closely the pressure variation of that measurement (figure 9.3.2.1). With an inflexion at 0.83 ± 0.02Torr this isotherm also asserts a positronium maximum at half-coverage. Locating the point of slope change in the isotherm at 80K, figure(9.3.2.5), reveals the pressure of monolayer coverage at an almost unmeasurable 0.04Torr. Using 0.02Torr as the pressure for half-coverage in the Langmuir formula for a registered adlayer (equation 2.4)

$$P = 1264 t^{\frac{5}{2}} \frac{x}{1-x} \exp\left(-\frac{\epsilon_0}{t}\right) \tag{9.5}$$

yielded $\epsilon_0 = 1760 \pm 30$K. Again this assumes no interaction between adatoms. As an exercise the modified Boltzmann expression (9.3) with the attractive component

assumed negligible and the repulsive component written to act at separations approaching those of full coverage (i.e. b, the effective collision area, replaced by one, in the present notation) was used for a corrected value. This produced $\epsilon_0 = 1540 \pm 30$K.

The small effect in these isotherms is due to the amount of grafoil (0.54gr) which with a specific adsorption area of $9.68 m^2/gr$ can be expected to reach commensurate monolayer capacity at only 61μmoles or 1.4CC at STP.

§9.3.3 Convolution Analysis

A single gaussian and parabola analysis produced results similar to the other gases (see for example chapter 10). Following this a second, narrow, gaussian was added. After a free fit, its width was fixed at the value yielded for spectra of maximum F-parameter (see chapter 13 for detail). Figures(9.3.3.1 - 3) show the results for a χ^2/ν ranging between 1.4 and 2.2. Unlike oxygen (chapter 13) the maximum *p*-Ps component is only 3-4%, however the variation shows a definite peak and underlying background, figure(9.3.3.3) . A clause in the fitting routine which set the narrow component intensity to zero if it fell below a threshold was found to greatly improve the speed of convergence, as it gave the minimisation routine the freedom to choose essentially a two component fit for the low F-parameter or positronium content points. An attempt similar to that performed for oxygen to pin point optimum narrow component width was made. Figure(9.3.3.4) shows the χ^2/ν over peak centroid channels for the cluster of runs over the positronium peak as a function of narrow component width. Unlike oxygen (chapter 13) there is no definite form to the variation, this is most likely a result of the low intensity of the third component.

§9.4 Conclusion

Refined pressure measurements have led to the assertion that maximum positronium emission occurs at half and not full coverage (Rice-Evans *et al* 1986) and that it could be due to maximum surface irregularity at half-coverage (Jean *et al* 1986). Fitting of the right hand side of the V.P. positronium peak yields 1550±30K for the binding energy of the first layer which compares favourably to that found by other groups. Methane has the highest binding energy in the group of gases studied and this appears to relate to the highest percentage change encountered in *o*-Ps parameters (5%). A direct mapping between pressure variation and positronium emission for adlayer formation has been made. Adsorption has been studied in the temperature range 80-135K and isotherm measurements presented for 110, 80K. Anomalous positronium peak and pressure variation behaviour has been recorded for measurements at and below 100K, the closest normal peak measurement being at 110K. The explanation of a phase transition from fluid to incommensurate solid for coverages above half has been proposed. No evidence for hysteresis has been observed but this is quite natural as adsorption to monolayers only was investigated.

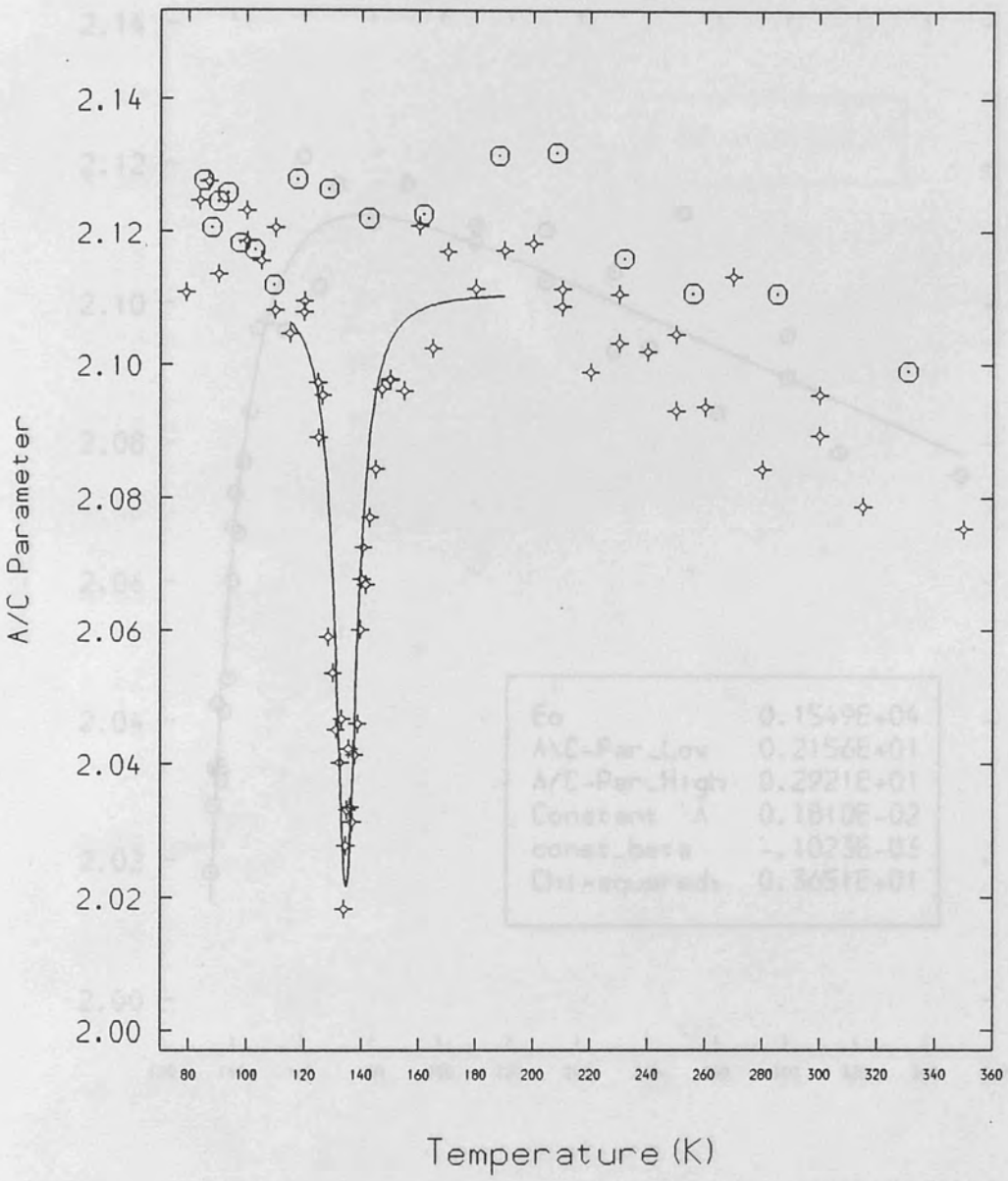

Figure(9.3.1.1) Grafoil in vacuum (circles) and plus methane. The positronium (A/C) parameter for the methane peak has been traced by a Lorentzian. The A/C methane parameter follows the vacuum background trend at higher temperatures.

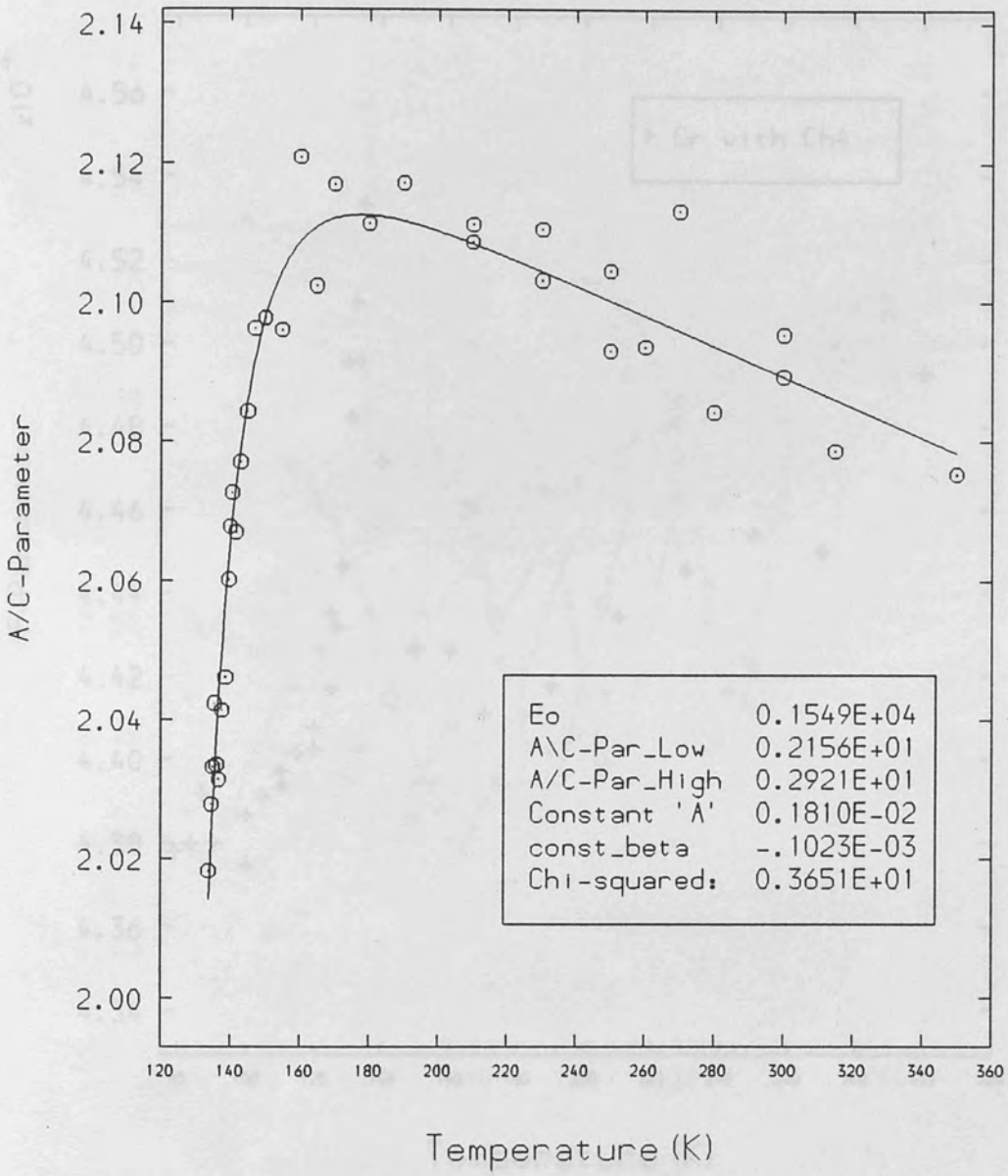

Figure(9.3.1.2) Grafoil with methane. A fit of the positronium (A/C) parameter by equation(9.1). An extra constant has been introduced to extrapolate background vacuum trend: $R_{low} \rightarrow R_{low}(1 + \beta t)$.

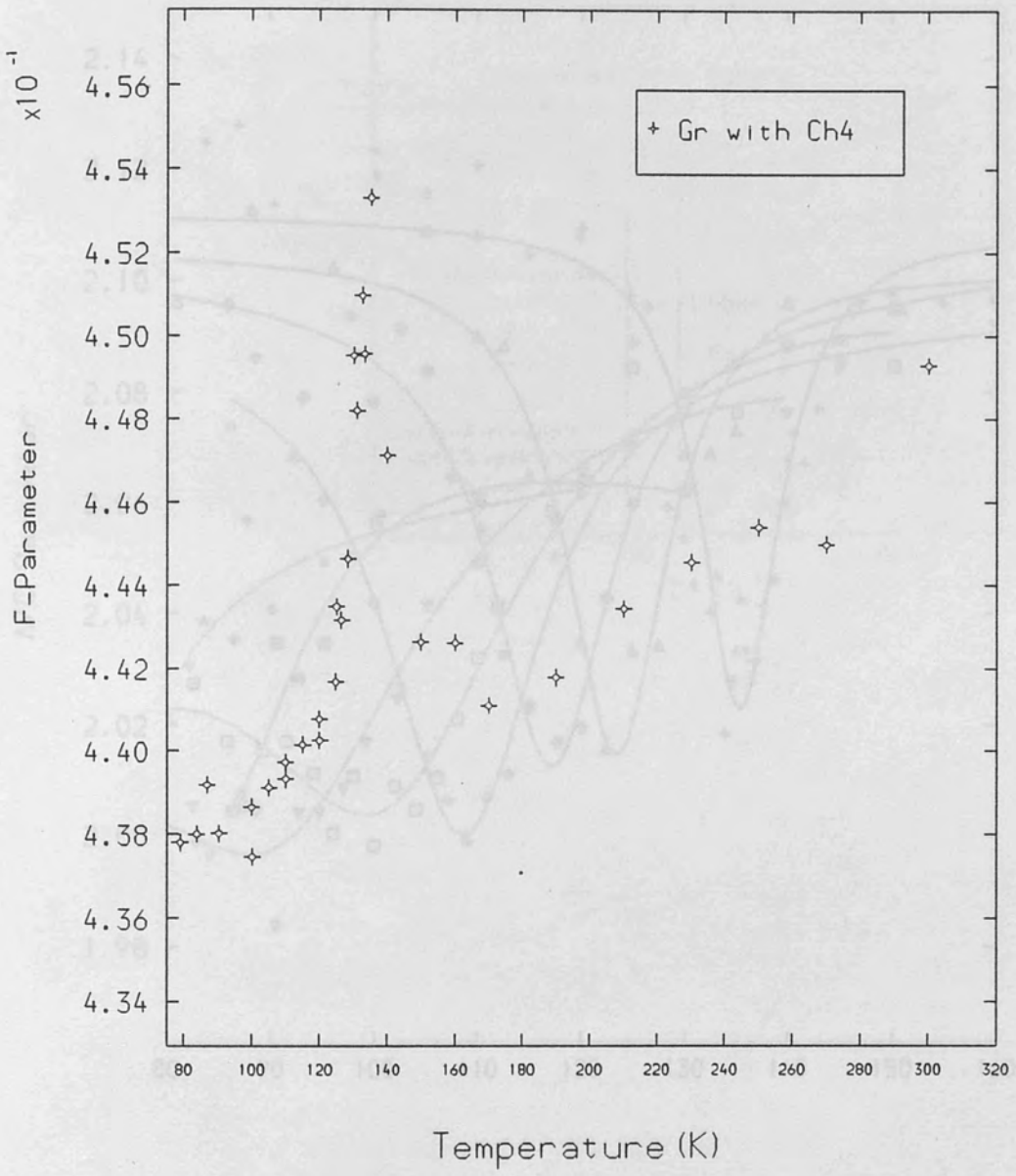

Figure(9.3.1.3) Grafoil with methane.

The F-parameter vs temperature for V.P. peak.

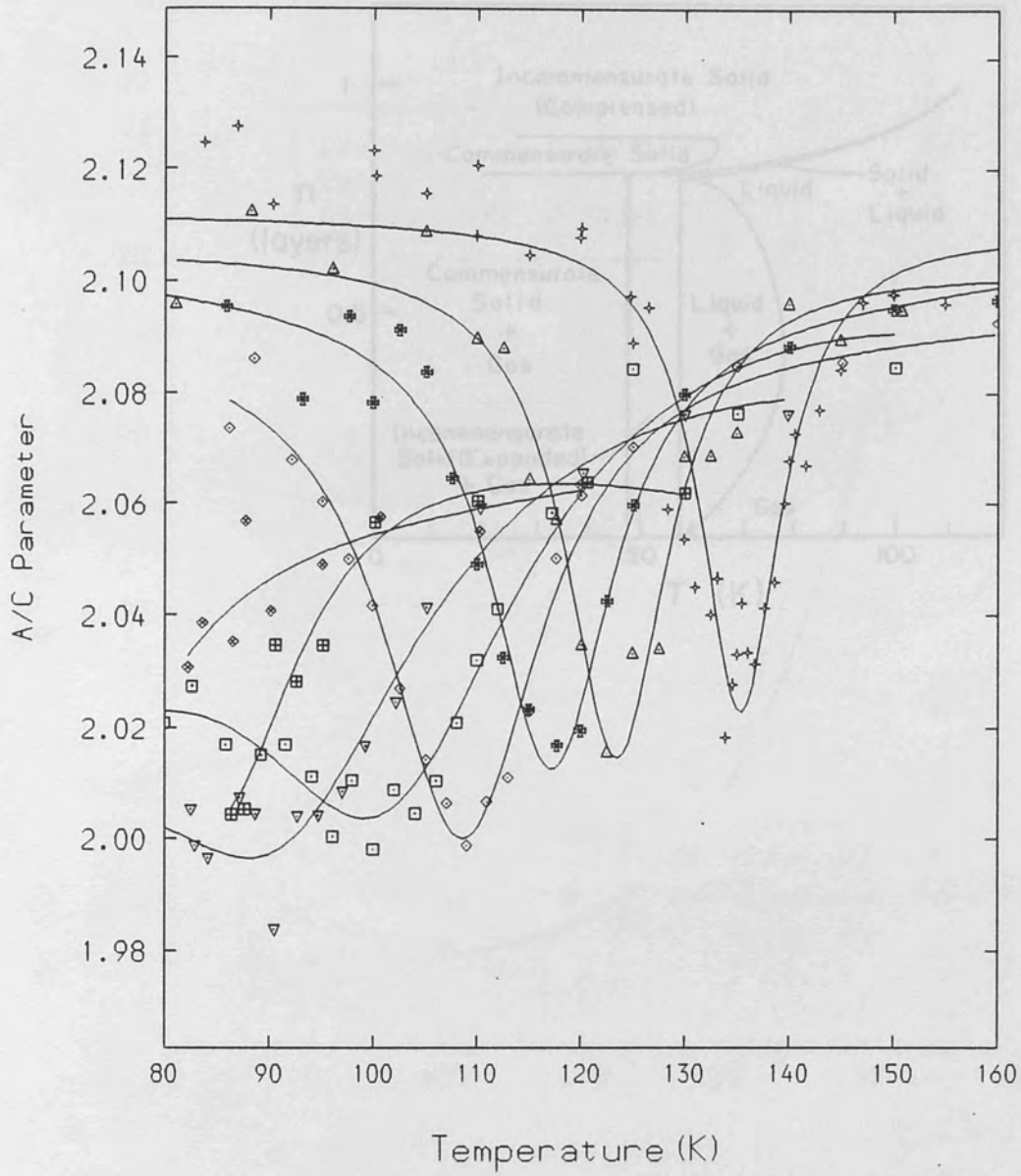

Figure(9.3.1.4) Grafoil with methane.

Display of the methane sets taken.

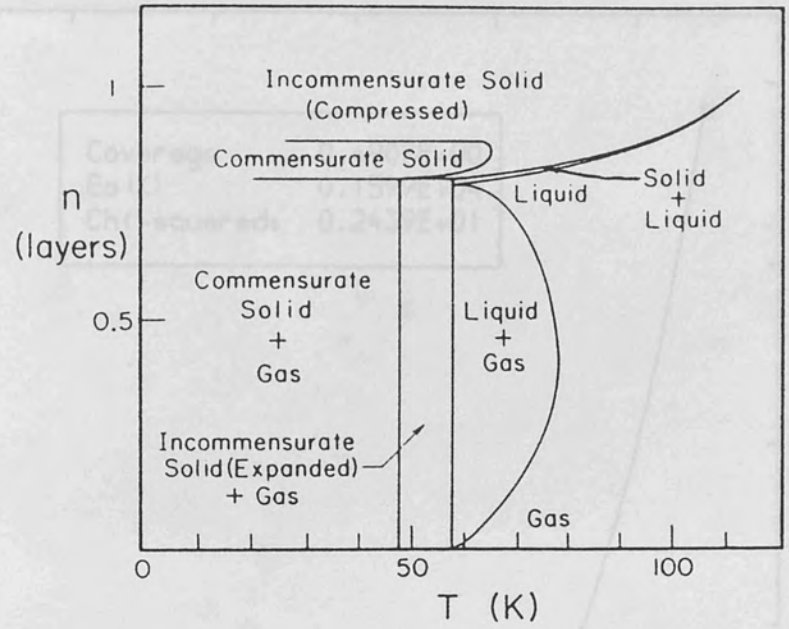

Figure(9.3.1.5) First layer phase diagram for methane adsorbed on graphite (Hamilton and Goodstein 1983). n= 1 is a commensurate monolayer.

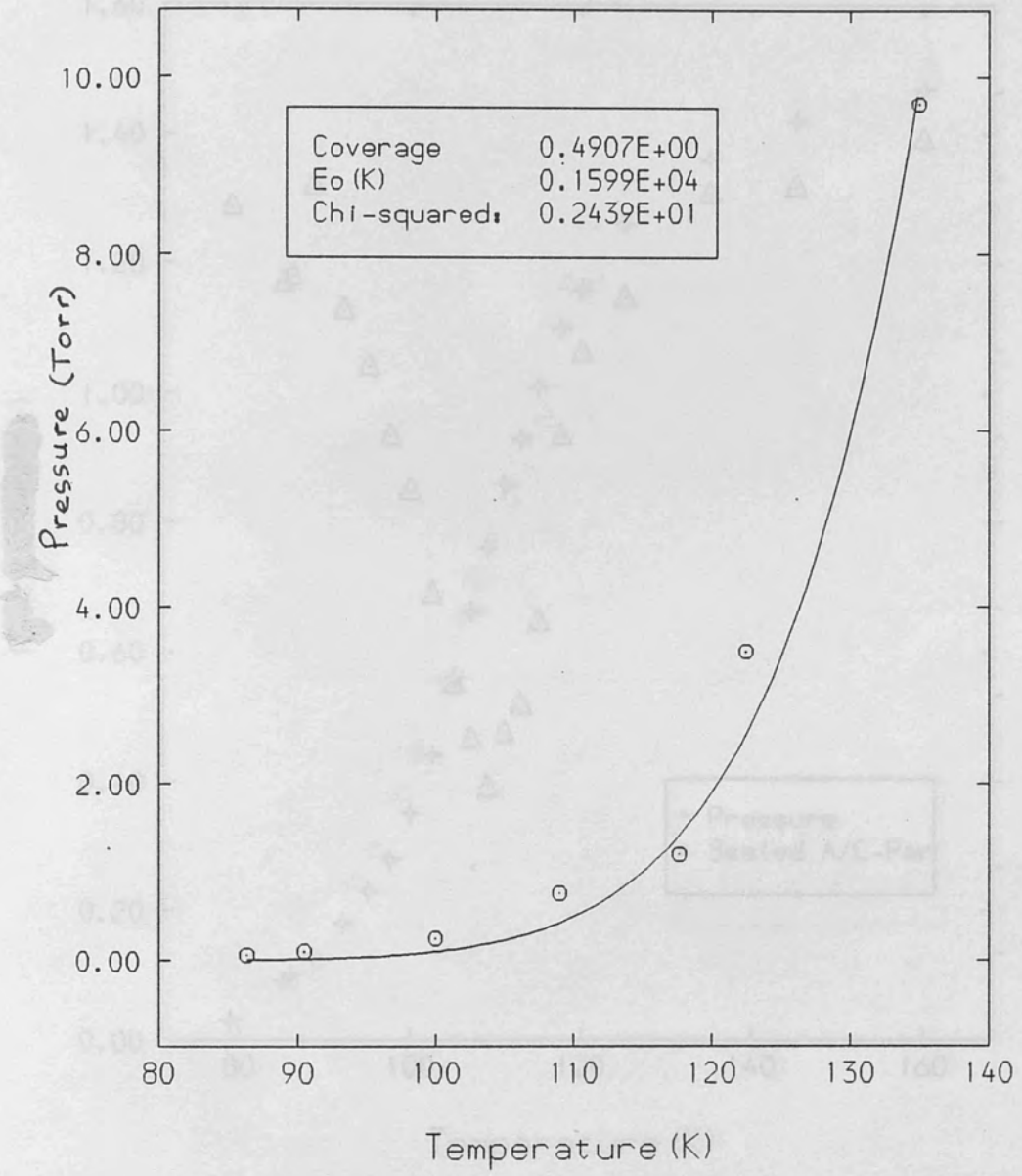

Figure(9.3.1.6) Pressure at maximum positronium vs temperature fitted with the Boltzmann approximation to yield coverage at peak and ϵ_0.

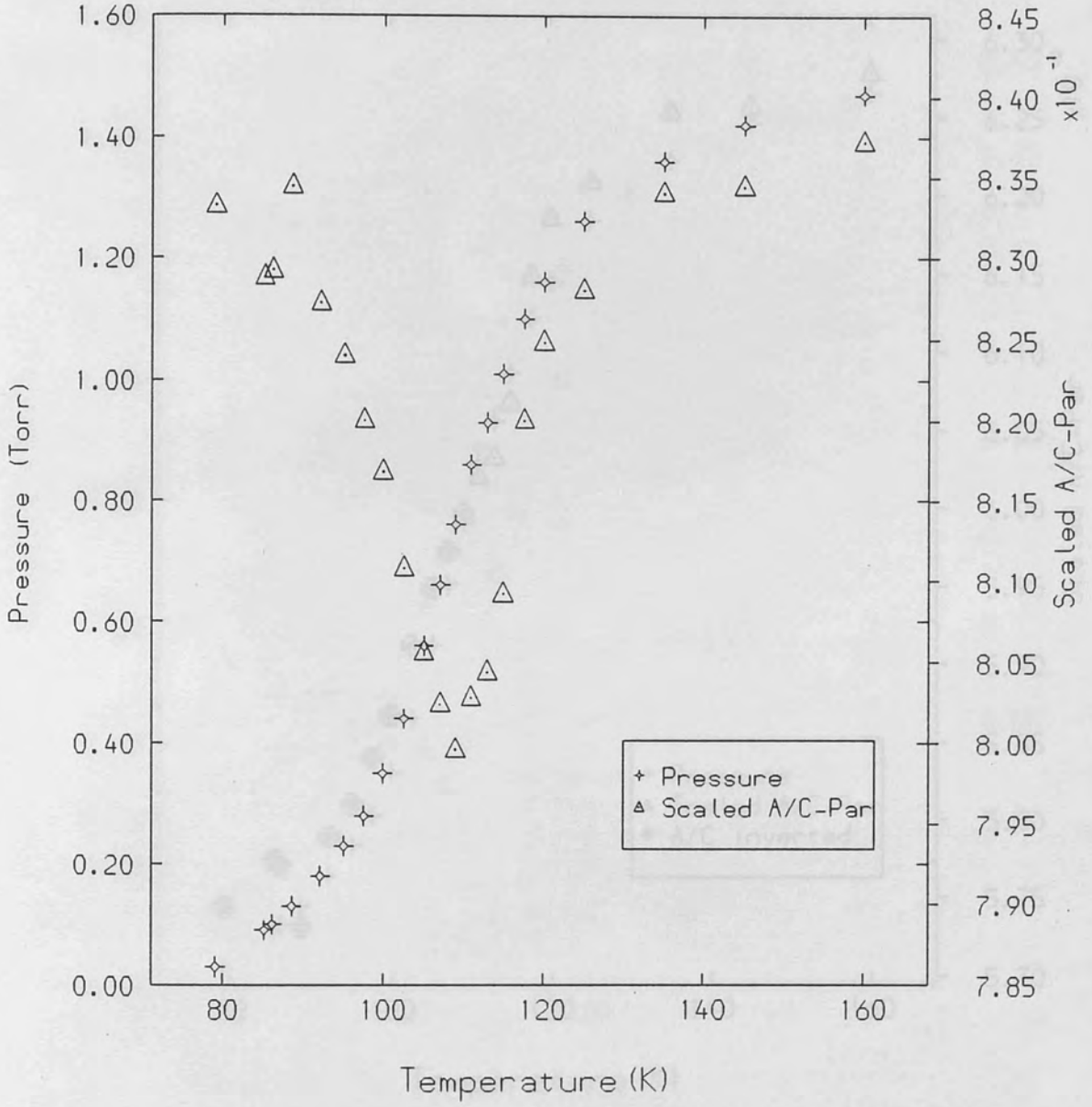

Figure(9.3.2.1) Simultaneously recorded pressure variation and positronium parameter. The S-form indicates adlayer formation to a monolayer. The *o*-Ps maximum is seen to lie at the point of inflexion or at half-coverage. The nonzero slope at either pressure wing is the underlying temperature variation.

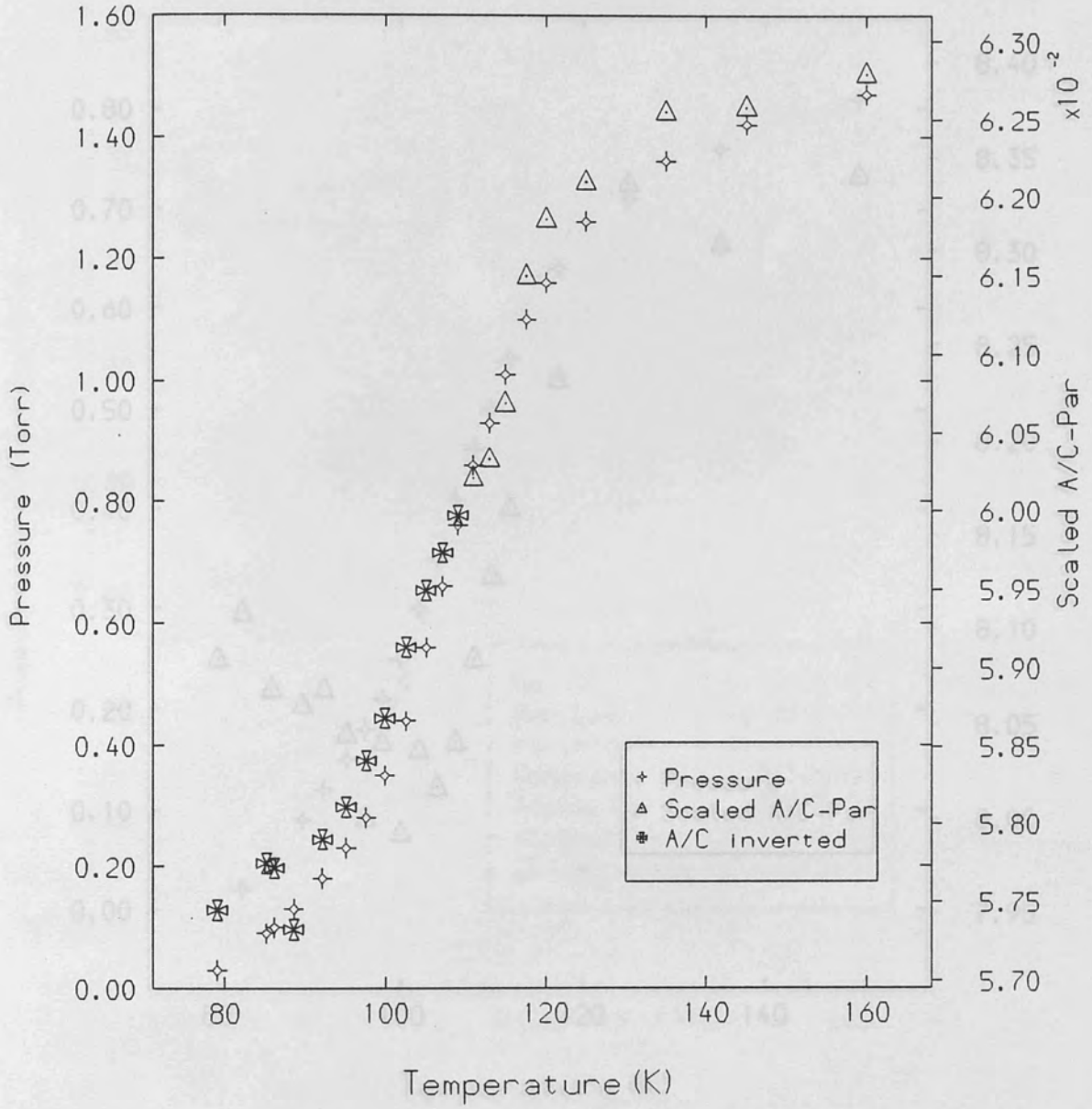

Figure(9.3.2.2) The same as figure(9.3.2.1) but with the Ps parameter unfolded about the maximum. This shows the striking similarity between the response of the two methods.

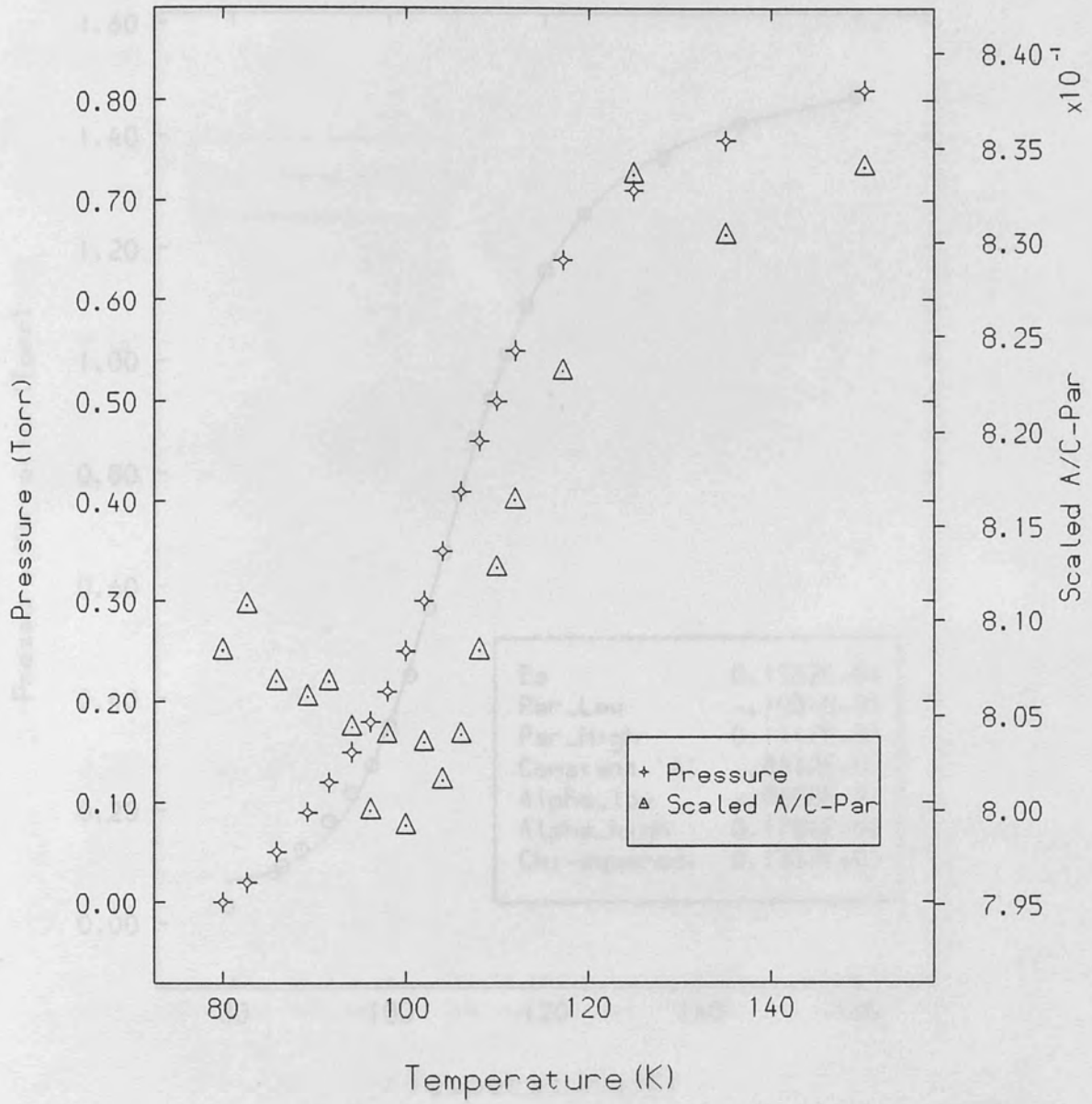

Figure(9.3.2.3) The pressure variation for the anomalous peak at 100K. Its form appears to be different compared to the 110K variation and may indicate a phase transition. However the effect could also be the result of gas exhaustion.

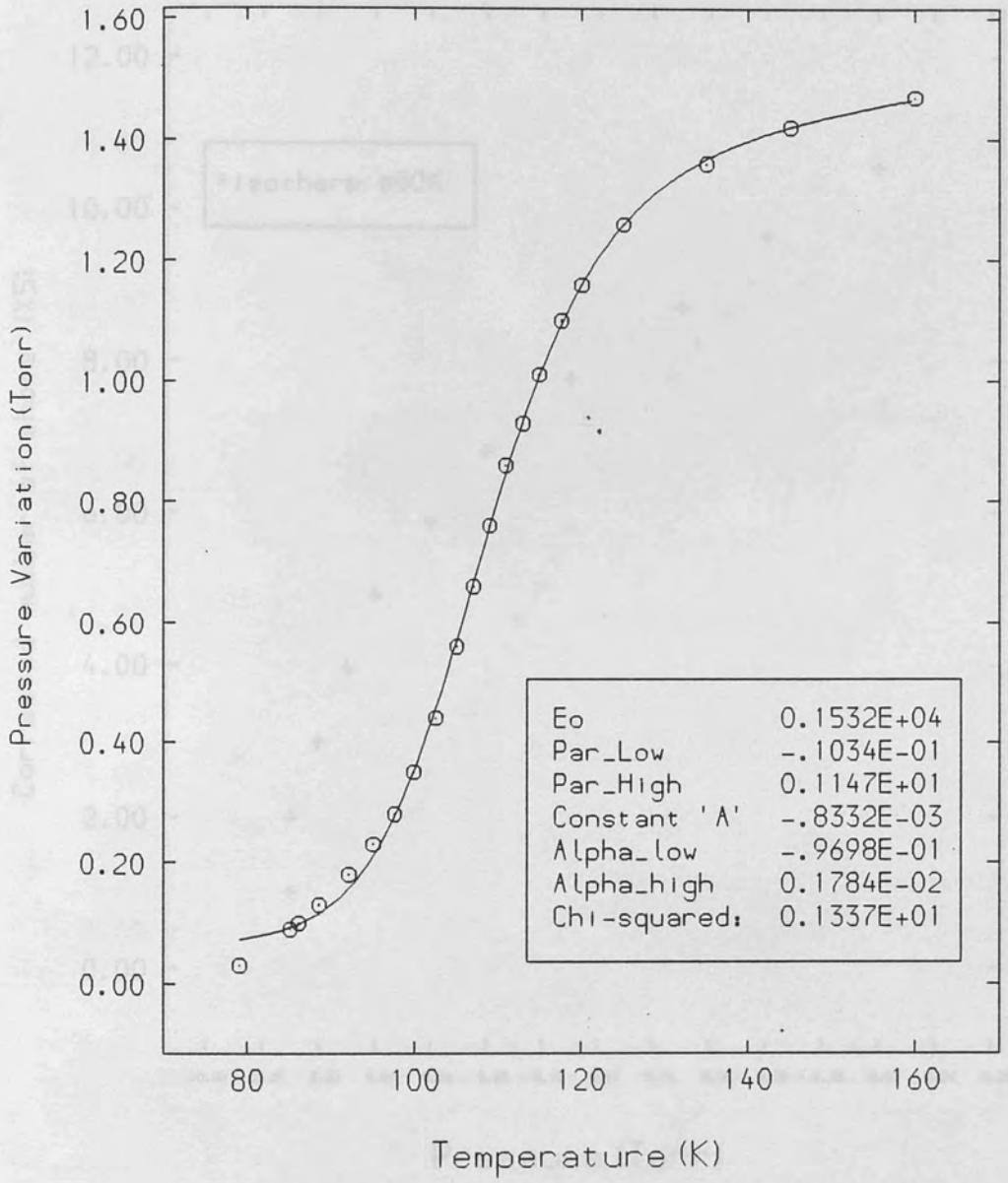

Figure(9.3.2.4) Fit of pressure variation for peak at 110K. Equation(9.1) modified for the S-form left and right wing backgrounds in the manner $R_l \rightarrow R_l(1 + \alpha_{low} t)$ and $R_h \rightarrow R_h(1 + \alpha_{high} t)$

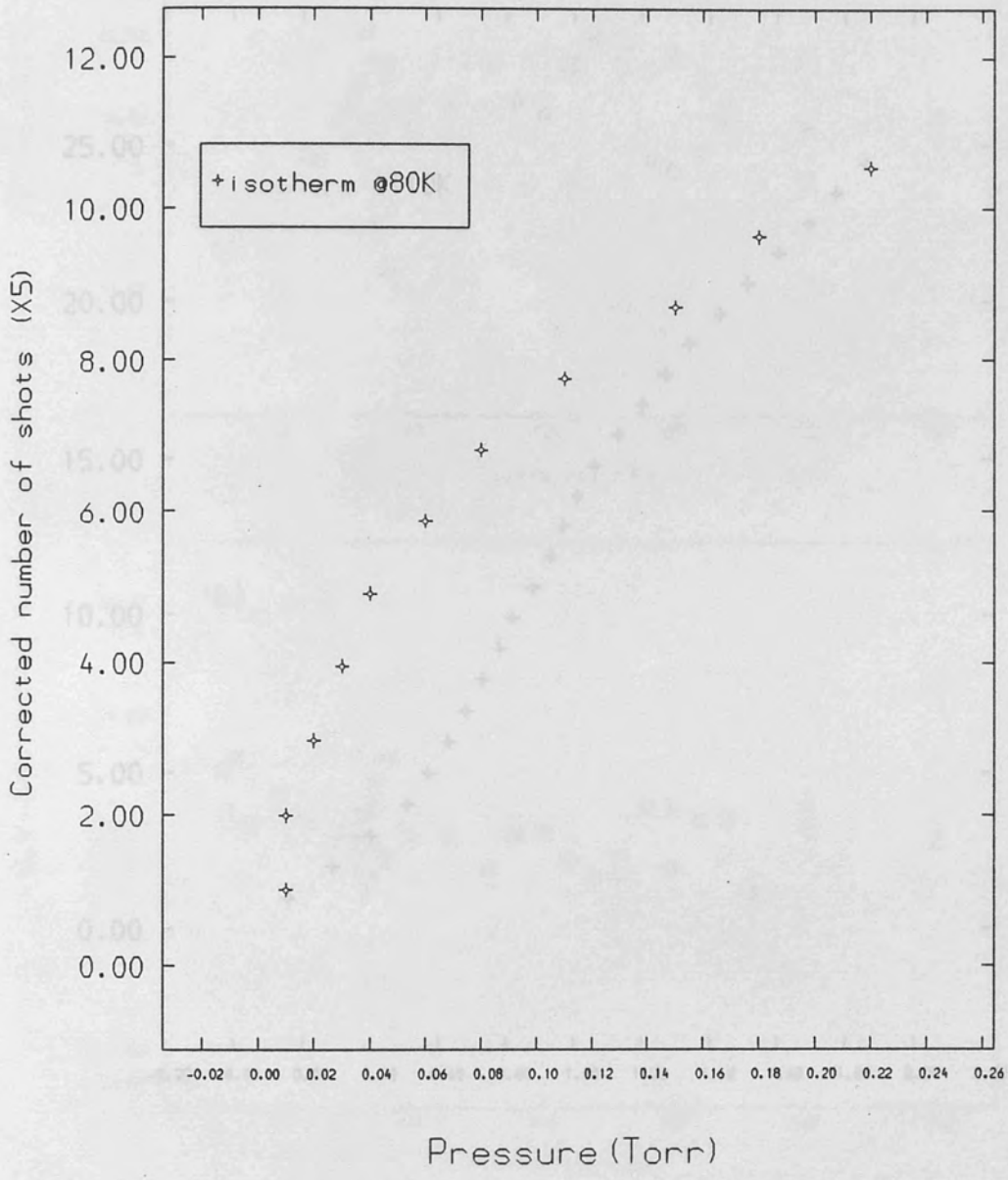

Figure(9.3.2.5) Isotherm taken at 80K for start shot pressure 1.24Torr.

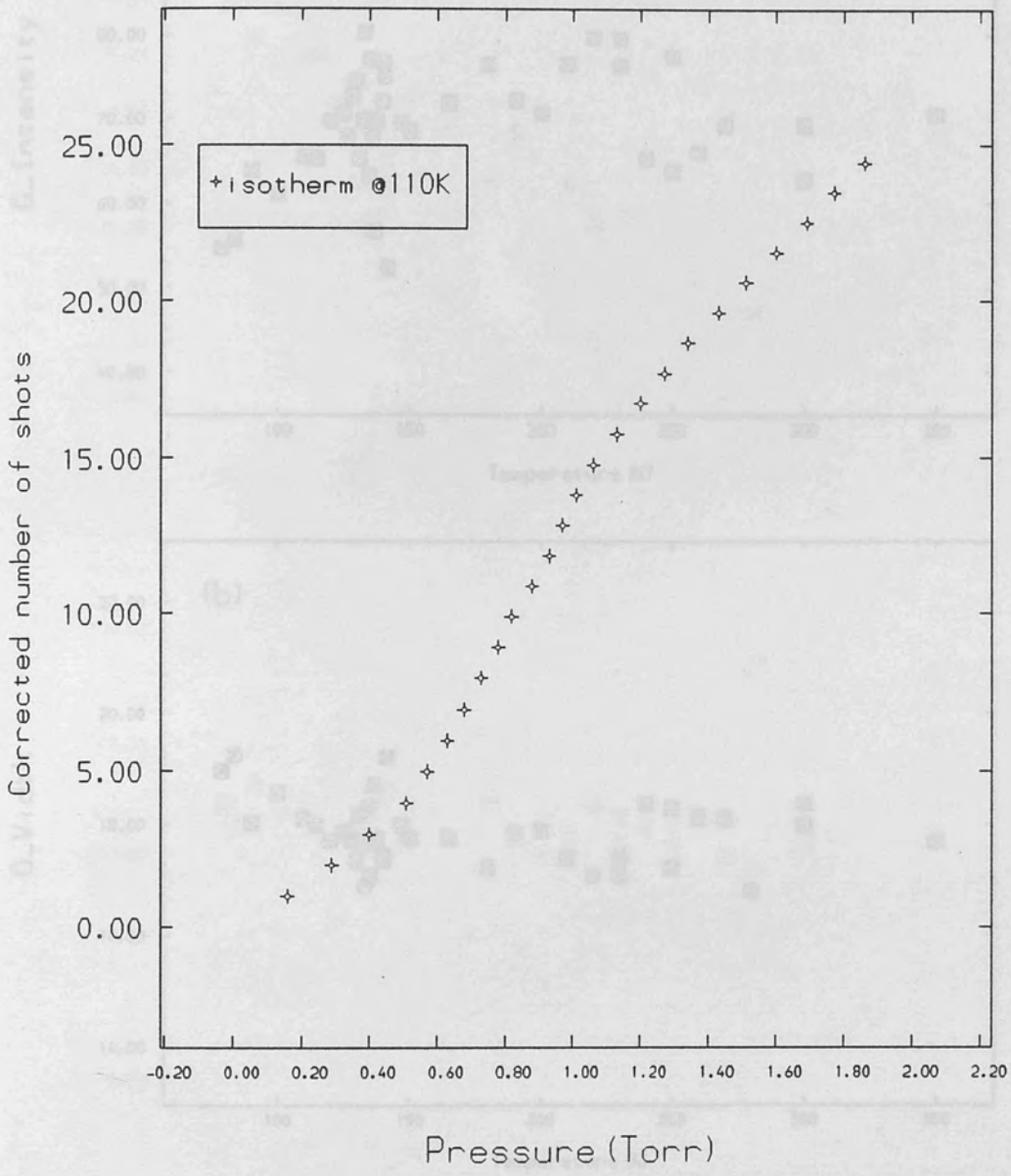

Figure(9.3.2.6) Isotherm taken at 110K for start shot pressure 4.08Torr.

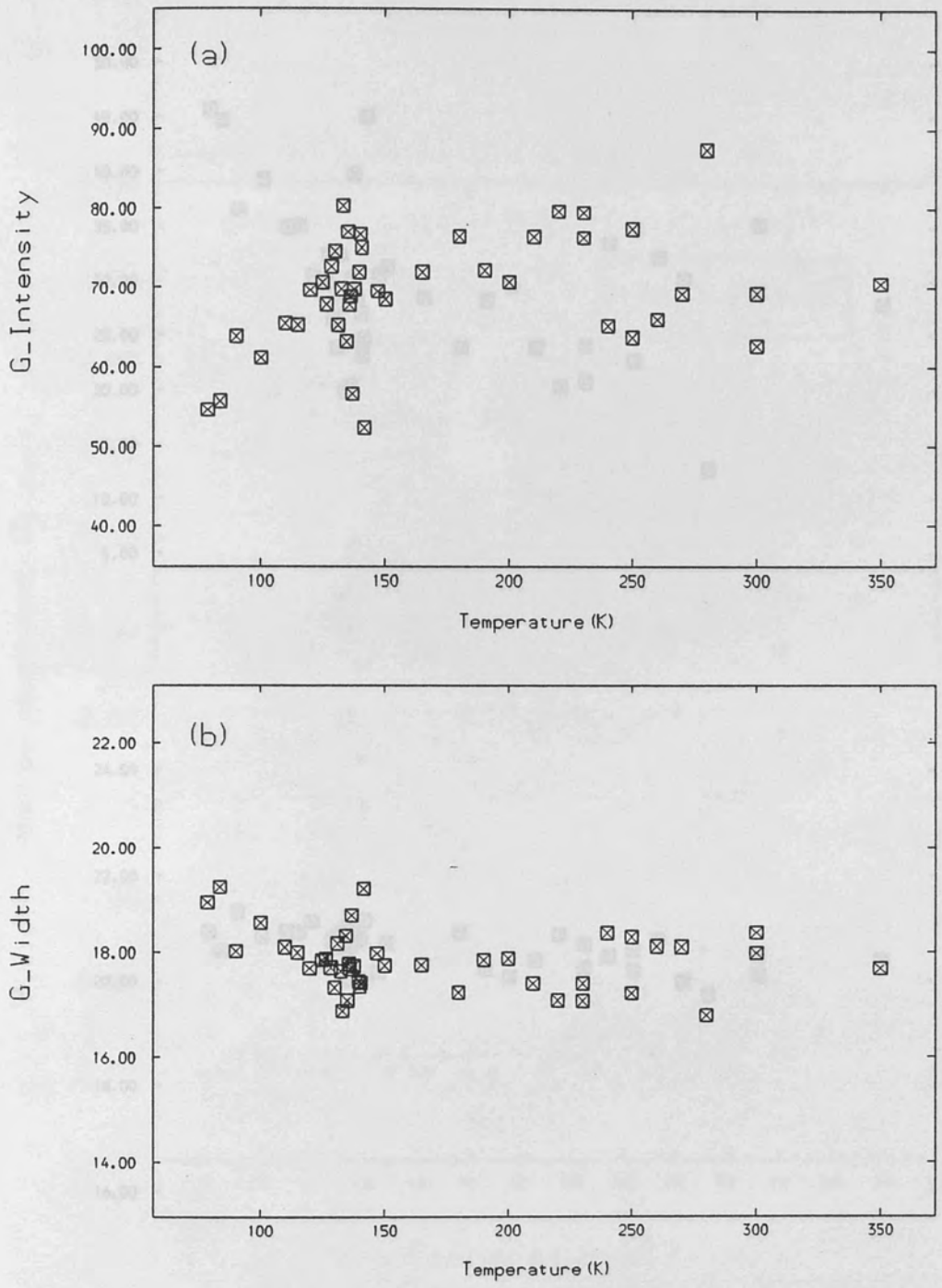

Figure(9.3.3.1) Three component analysis of Grafoil + methane.

(a) First gaussian intensity.

(b) First gaussian width.

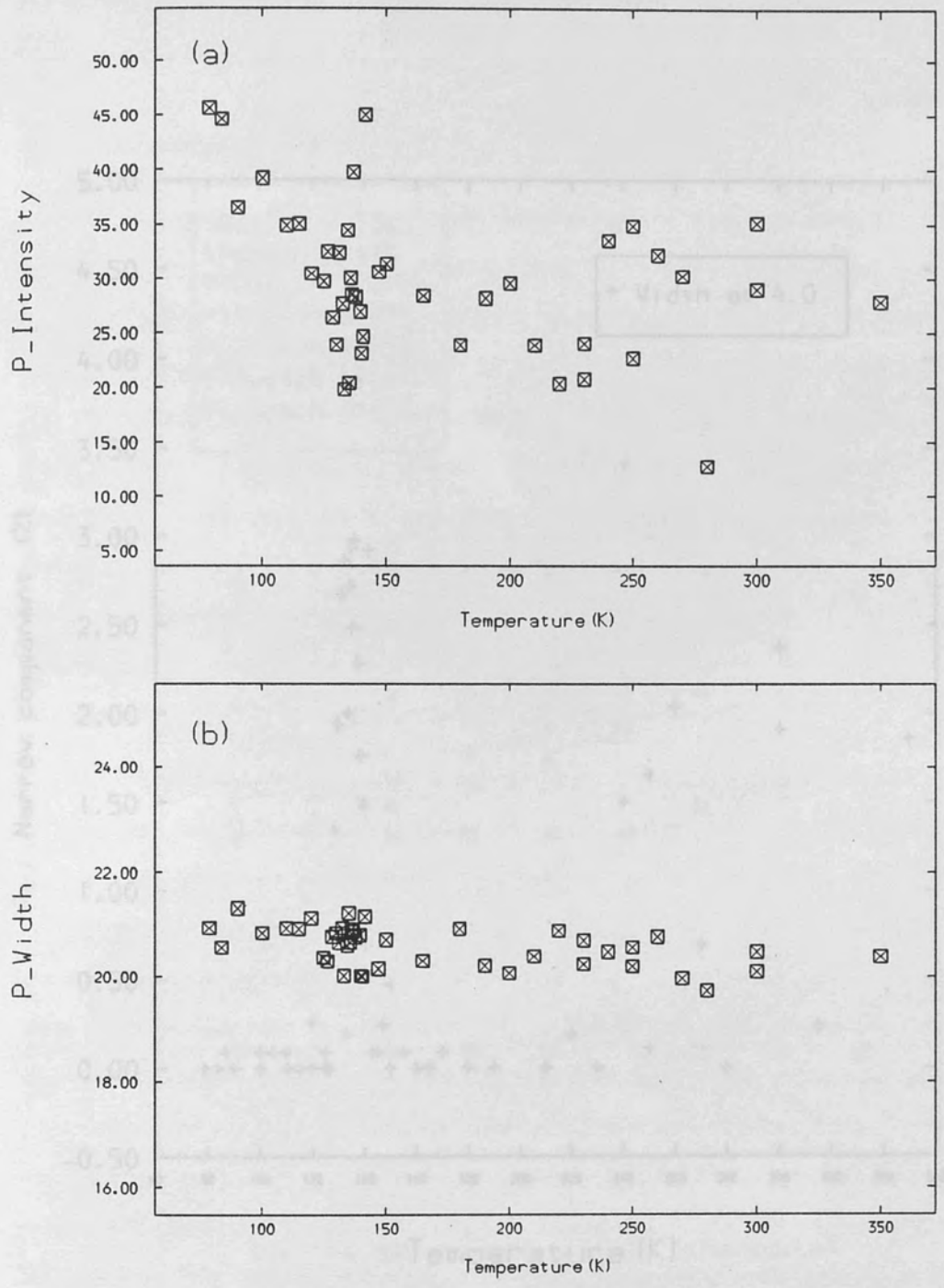

Figure(9.3.3.2) Three component analysis of Grafoil + methane.

(a) Parabola intensity.

(b) Parabola width.

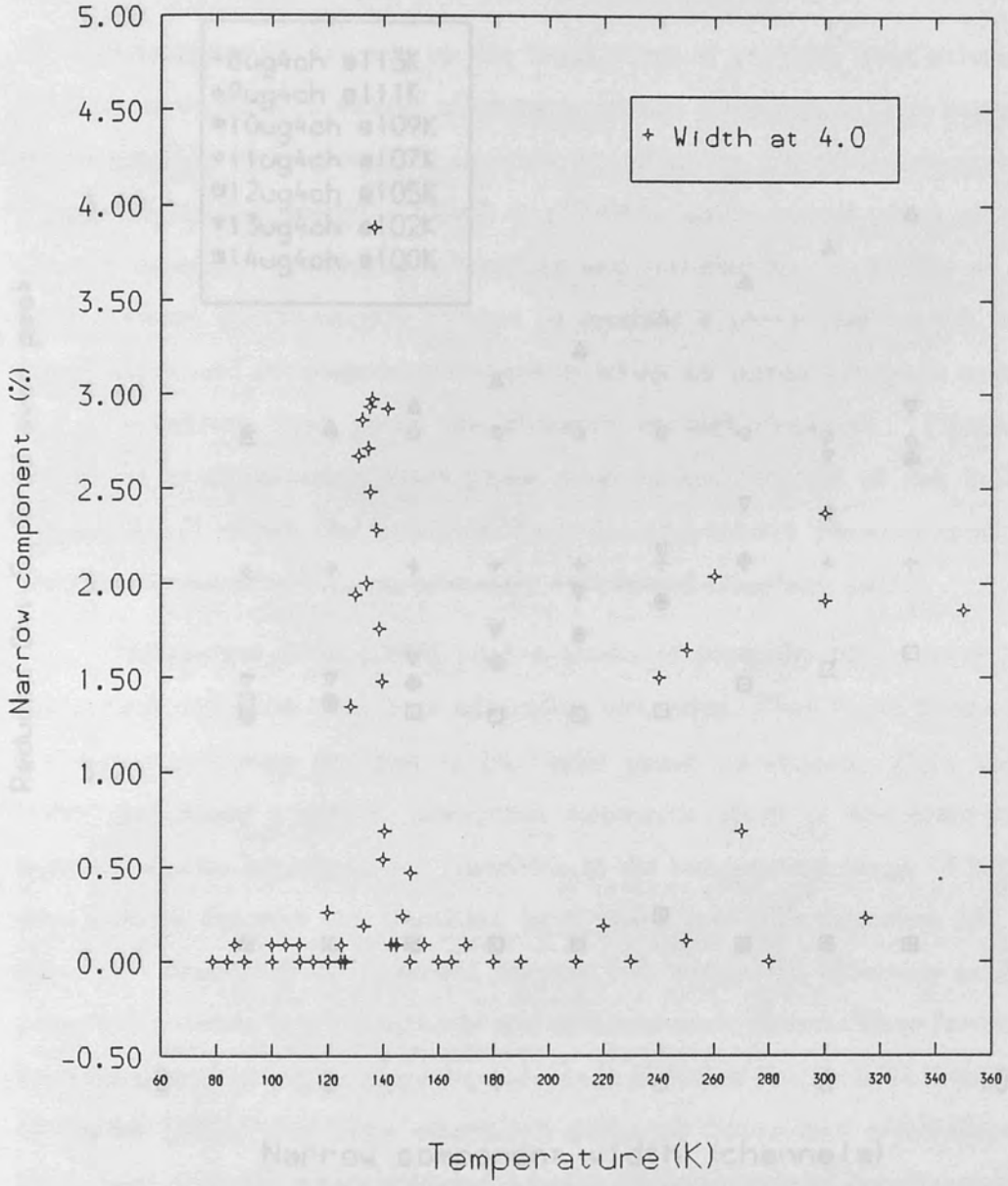

Figure(9.3.3.3) Three component analysis of grafoil + methane. Second gaussian intensity when width fixed at 4 channels. High temperature increase is the underlying emission due to graphite.

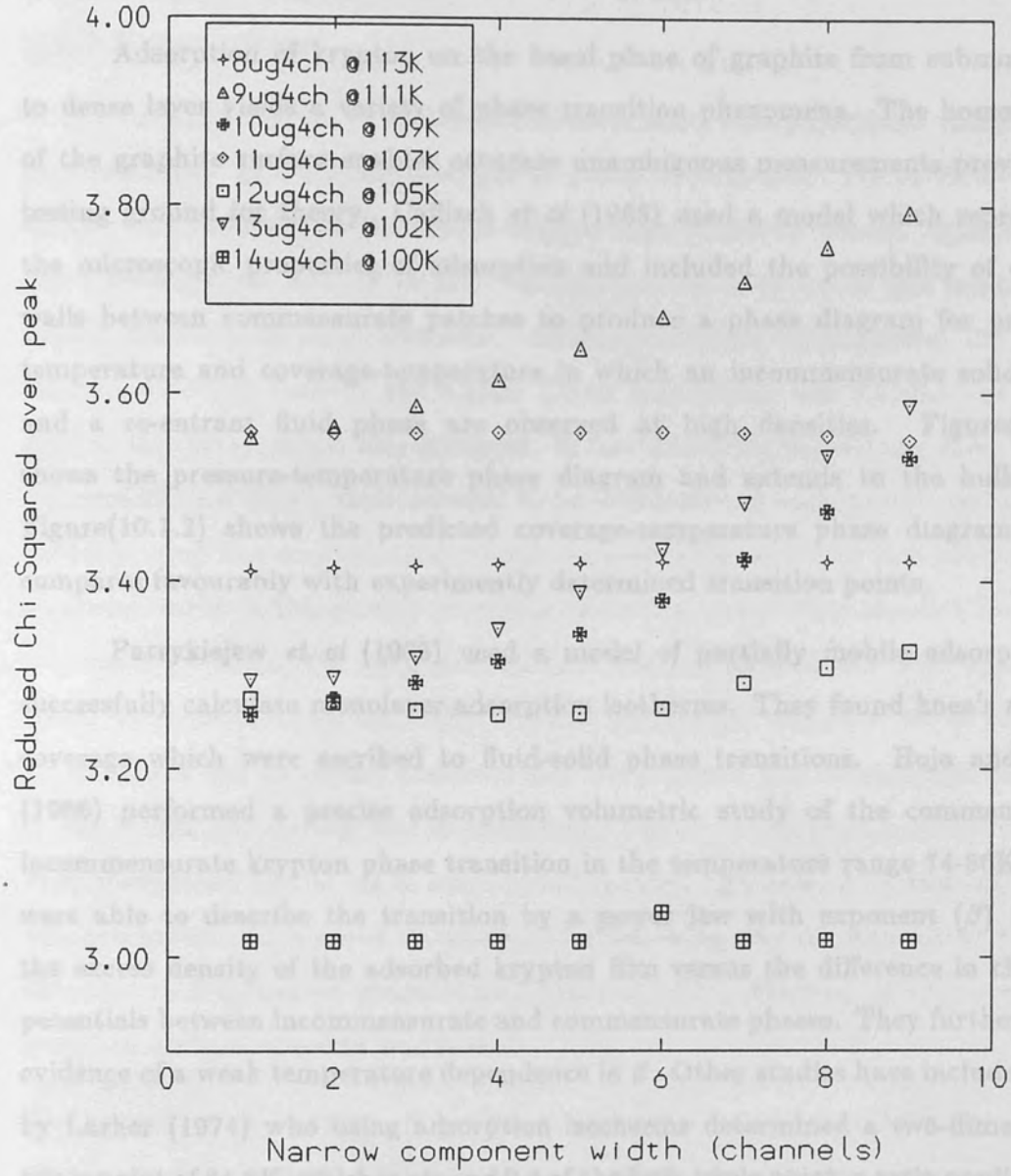

Figure(9.3.3.4) Three component analysis of fourth peak at 110K. Shown is the χ^2/ν over peak centroid as a function of second gaussian width for seven spectra about the positronium peak. The lack of a form (optimal width) is most likely due to the small <4% *p*-Ps content.

Chapter X Krypton on Grafoil

§10.1 Introduction

Adsorption of krypton on the basal plane of graphite from submonolayer to dense layer yields a variety of phase transition phenomena. The homogeneity of the graphite surface enables accurate unambiguous measurements providing a testing ground for theory. Caflisch *et al* (1985) used a model which represented the microscopic properties of adsorption and included the possibility of domain walls between commensurate patches to produce a phase diagram for pressure-temperature and coverage-temperature in which an incommensurate solid phase and a re-entrant fluid phase are observed at high densities. Figure(10.1.1) shows the pressure-temperature phase diagram and extends to the bulk state. Figure(10.1.2) shows the predicted coverage-temperature phase diagram which compares favourably with experimently determined transition points.

Patrykiejew *et al* (1983) used a model of partially mobile adsorption to successfully calculate monolayer adsorption isotherms. They found knee's at ~0.9 coverage which were ascribed to fluid-solid phase transitions. Hoja and Marx (1986) performed a precise adsorption volumetric study of the commensurate-incommensurate krypton phase transition in the temperature range 74-86K. They were able to describe the transition by a power law with exponent (β) 1/3 for the excess density of the adsorbed krypton film versus the difference in chemical potentials between incommensurate and commensurate phases. They further found evidence of a weak temperature dependence in β. Other studies have included work by Larher (1974) who using adsorption isotherms determined a two-dimensional triple point of 84.8K, which is around 0.4 of the bulk triple point, a ratio predicted by simple theory. Bienfait *et al* (1984) used a reflection high energy electron diffraction technique to study the wetting behaviour of krypton and oxygen on graphite and found complete wetting in the case of krypton.

In the present work with grafoil, krypton was the first gas investigated known to have phase transitions within scope of the liquid nitrogen coolant. It was intended

to scan temperatures at fixed pressures and observe the positron signal under a variety of adsorbed states.

§10.2 Experimental

Two sets of krypton adsorption measurements were performed. After sample heat treatment at 470K, krypton gas of purity 99.99% (supplied by BOC Special Gases) was allowed into the cooled sample chamber to an excess. Bulk krypton has a boiling point at STP of 123K and so exhibits at or below this temperature vapour pressures up to atmospheric. At liquid nitrogen temperatures the vapour pressure (V.P) as read by the 0-1Bar Druck transmitter was 2.7±0.5Torr. After runs at this pressure gas was decanted. In fact decanting proved too slow, the low pressure allowed only a small amount to be withdrawn at each decant, and a rotary vacuum pump was employed for continuous evacuation at a flow rate controlled by a vacuum valve. Although this process took ~8 hrs, a seemingly steady 1Torr being eventually obtained, the measurement that was commenced was later abandoned owing to pressure build up. After further pumping a complete set of runs was taken. These had an almost unmeasurably low pressure, and considerable zero drift in the Druck transmitter was encountered. The uncertainty in pressure coupled with unexpected results led to suspicion of vacuum tightness. As a test the system was evacuated and allowed to warm. The following day air was allowed in and decanted to a measured pressure of 1.1Torr at 250K. Starting at this pressure a grafoil in air measurement was taken.

The second set of krypton on grafoil measurements was taken with the DPI101 pressure indicator and 0-52Torr transducer. After heat treatment and a grafoil in vacuum measurement, sets of runs were taken below the 77.4K V.P. The first set was at a start pressure of 1.00±0.03Torr at 200K. Lastly a V.P. peak was attempted, the sample chamber was charged with excess Kr and runs taken from 200-78K. A decline in pressure was noticed someway through and the chamber was further charged.

§10.3 Results

§10.3.1 Positronium and Lineshape Parameters

The A-parameter for the first V.P. peak with a Lorentzian derived fit is shown in figure(10.3.1.1). A peak of some 2.5% at 117K is observed. (This fit performed over just peak points is used for peak position and as a measure of width.) A distinct downwards trend is noticed at is normally a left hand side plateau. Figure(10.3.1.2) shows the parameter between 78-160K. The two-state trapping model coupled with the Boltzmann expression for adsorbate V.P., (equation 9.1), was fitted to the peak right hand side, figure(10.3.1.3). The fit produced (1460 ± 40)K, for adatom-substrate binding energy (ϵ_0), which compares favourably with other groups (1400K: Patrykiejew *et al* 1983, 1460K: Caflisch *et al* 1985, 1560K: Thomy and Duval 1970). The F-parameter, figure(10.3.1.4), produces a 3.8% effect and indicates the presence of *p*-Ps. The A-parameter for the grafoil in air run is shown in figure(10.3.1.5). There is a sharp decline which appears to reach a minimum at 82K with lower points showing a rise. This test proved of value in interpretation of grafoil with argon results.

For krypton the Boltzmann approximation for adsorbate V.P., (equation 2.7), is

$$P = 4174 x t^{\frac{3}{2}} \exp\left(-\frac{\epsilon_0}{t}\right) \qquad (10.1)$$

where P is in Torr, x is fractional coverage, t temperature (K) and ϵ_0 adlayer binding energy (K). In evaluating the premultiplier a packing density for the fluid state of 7.69×10^{18}atoms/m^2, based on krypton's natural lattice spacing, 4.07Å (Larher 1974), has been assumed. When half-coverage is asserted for the 2.7Torr V.P. peak at 117.5K, (10.1) produces $\epsilon_0 = 1614 \pm 30$K. This value is rather high but would be reduced if the attractive term, $(-a/kt)$, in the modified Boltzmann expression (equations 2.10 and 2.11) dominated. In a way of course calculation when x is set at monolayer coverage, $\epsilon_0 = 1695$K is found. Additionally with the reasonable assumption (see chapter 9) that the positronium peak is completed at

full coverage, figure(10.3.1.2) may be used to place x= 1 at 108K. Then (10.1) yields $\epsilon_0 = 1550 \pm 40$K. The anomalous increase in positronium beyond the left hand side riser may be looked at from the point of view of bilayer appearance. Caflisch *et al* (1985) performed a calculation for bilayer formation on a commensurate monolayer. Although strictly, from figure(10.1.2), this situation cannot arise (adsorption beyond a commensurate monolayer leads first to a maximally packed incommensurate structure) the value for second layer binding energy obtained serves as a useful guide. They assumed the bilayer energy (ϵ_2) to have two components *viz.* a bilayer-substrate binding force (192K) and the attractive force due to second layer adatom placement in a "nook" of minimum potential provided by three first layer adatoms (3×144K). A figure of ϵ_2= 624K thus arrived. When this is placed in equation(10.1) together with x= 0.5 and P= 2.7Torr a temperature for half bilayer coverage is yielded, ~50K. In view of this the low temperature increase in positronium may be in sympathy to bilayer formation and had temperatures below 78K been approached may have shown a broad peak in the vicinity of 50K.

§10.3.2 Pressure Results

The mean pressure for each run as read by the Druck transmitter for the first sets of runs did not show any form. This can be attributed to the inadequate ±0.5Torr best accuracy. This is not the case for the 0-52Torr transducer pressures, as figure(10.3.2.1) illustrates. In this alongside the pressure variation is drawn the corresponding A-parameter, suitably scaled. An S-shape as obtained for methane is apparent, however the peak minimum lies not at the point of inflexion but closer to the lower pressure wing. It was thought this implied maximum positronium emission at coverage closer to that of monolayer than half. However on further inspection it is evident that there is a rapid fall to zero pressure which would produce an artificial levelling. Indeed the S-shape is not symmetrical and thus not like those obtained for methane. Figure(10.3.2.2) shows a pressure and A/C-parameter variation for

a lower pressure run. The asymmetry in the pressure variation is greater, the approach to zero pressure occuring more rapidly.

§10.3.3 Convolution Analysis

A two component *viz.* inverted parabola and gaussian lineshape fit was performed on the first V.P. runs. Error function backgrounds were subtracted from both Doppler and resolution lineshapes prior to convolution. It was found that allowing the common centroid freedom to move improved the reduced chi-squared and convergence rate. The addition of a residual background term as a sixth component for convolution although further reduced minimisation times, usually produced greater scatter in component intensities. A gentle, logarithmic, weighting favouring peak points was applied. The $1/\sqrt{\text{count}}$ weighting used prior to this work (El Khangi 1980, Berry 1982, Moussavi-Madani 1986) placed emphasis on the wings of a photopeak and resulted quite often in poor fits to peak channels. Likewise the inverse weighting, $\sqrt{\text{count}}$, was found too harsh and lead to the fit sometimes ignoring wing points. In an extreme analysis for a narrow *p*-Ps content this heavy weighting may be appropiate but in normal practise best results were obtained with a log(count) weighting. The fits produced χ^2/ν of 1.8-3.4, with the higher values occuring at F peak temperatures. The results are presented in figure(10.3.3.1) and (10.3.3.2) which show component intensity and width respectively. The components show large variations at F and positronium parameter peak temperatures. The gaussian at a background width of 18 channels (90eV/channel) behaves as a narrow component whose intensity increases and width decreases at peak points, figure(10.3.3.2). A decline in width is also shown by the 20 channel parabola. These two component variations although assert the presence of a third component cannot in themselves quantify *p*-Ps contributions. In the three component analysis a third component width of 4 channels was selected, based on methane and oxygen results, with a gentle weighting for peak points. The results were most satisfactory, with the χ^2/ν ranging from 1.6-2.4. Figure(10.3.3.3) and (10.3.3.4) show the results for the first gaussian and parabola. The sharp variations at the positronium peak

have all but disappeared. On the other hand the narrow component intensity, figure(10.3.3.5), shows a ~4.5% peak at 117K. This maximum compares to a 1.5% high temperature (vacuum) level and a mean below 1% for points to the left.

§10.4 Summary

Krypton adsorption to monolayer coverages on graphite has been mapped by positron annihilation and pressure measurements. A low vapour pressure of 2.7Torr at 78K precluded measurements across phase transitions and all results are for a fluid adlayer. A peak in positronium production was observed with a maximum at half-coverage and a fall attributed to monolayer completion. An increase at lower temperatures was also found, indicative perhaps of bilayer formation. A discrepancy in positronium emission between vapour pressure and free pressure measurements is explained by insufficient gas for adlayer formation in the latter. The V.P. temperature of maximum o-Ps emission yielded 1610K $\pm$ 30K for adatom-substrate binding energy when placed in the the Boltzmann formula for adsorbate vapour pressure, and the peak right hand side produced $\epsilon_0 = 1460\text{K} \pm 40\text{K}$. The increase, relative to grafoil in vacuum, of 2.5% in o-Ps production is the second highest in the gases studied. Only methane shows a larger effect and, perhaps corresponding, higher binding energy. A three component lineshape analysis revealed p-Ps at 4.5% maximum intensity for a width of 4 channels.

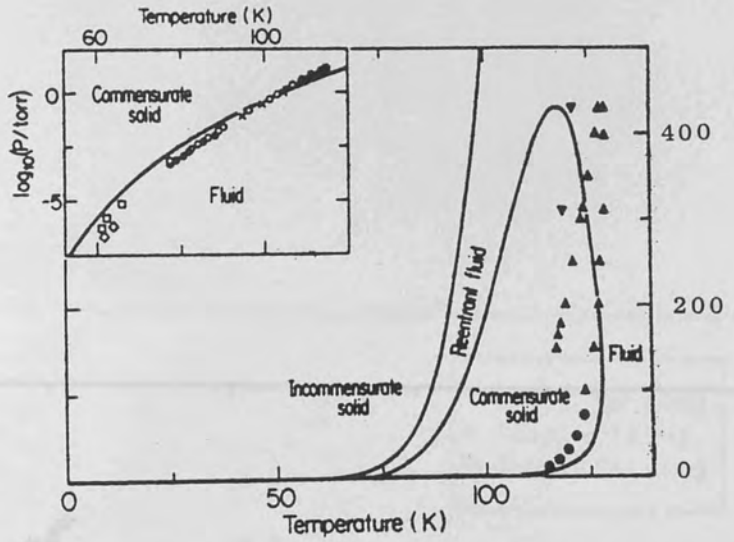

Figure(10.1.1) Pressure vs temperature diagram showing the re-entrant fluid phase. The symbols mark experimentally determined transition points (Caflisch *et al* 1985).

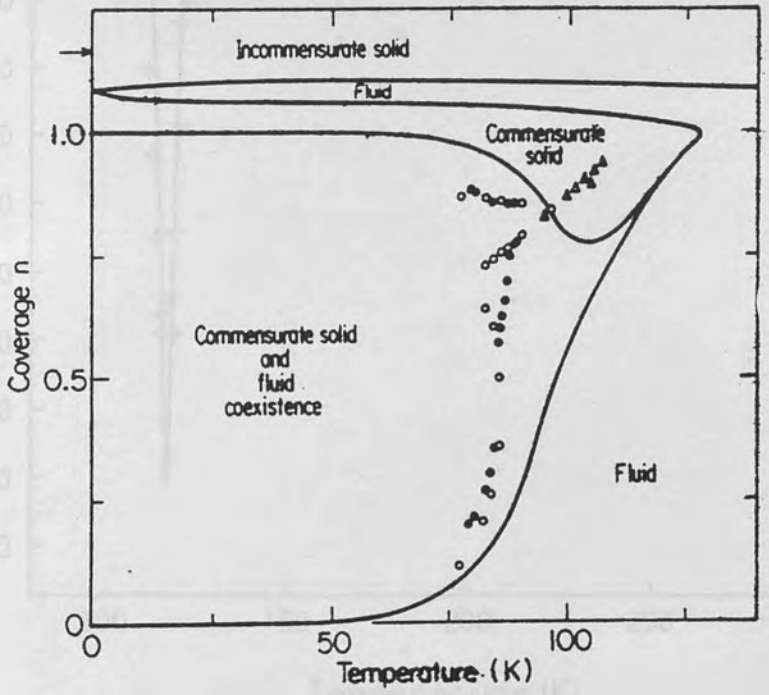

Figure(10.1.2) Krypton on graphite phase diagram in coverage and temperature according to Caflisch *et al* (1985). Symbols are expermentally obtained transition points. The arrow indicates equivalent commensurate packing (n) of maximally dense layer (at n= 1.17).

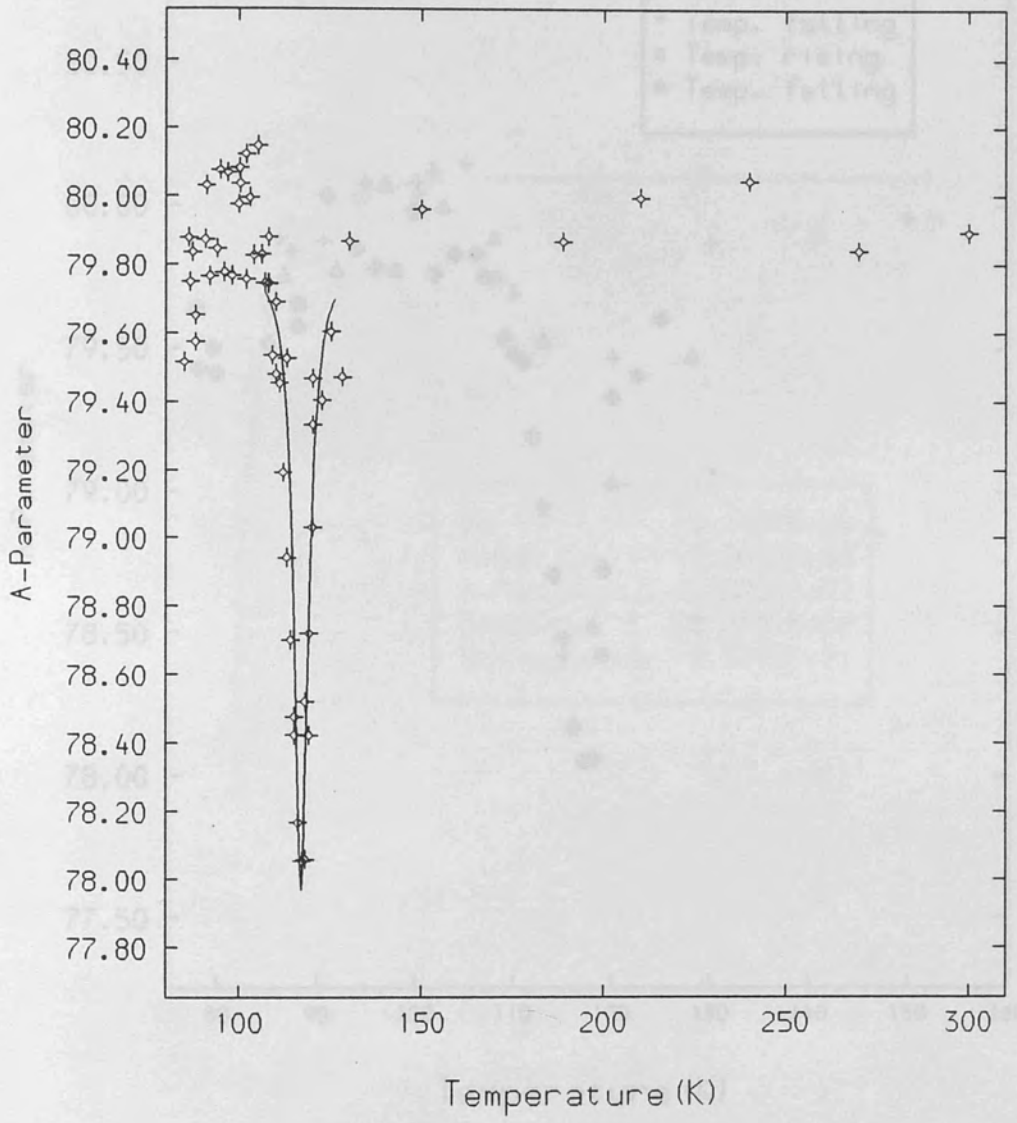

Figure(10.3.1.1) A-Parameter of Grafoil with Krypton 77.4K Vapour Pressure run (2.7Torr). A Breit-Wigner function has been used to trace peak. This A-Parameter shows a $\sim 2\frac{1}{2}\%$ effect

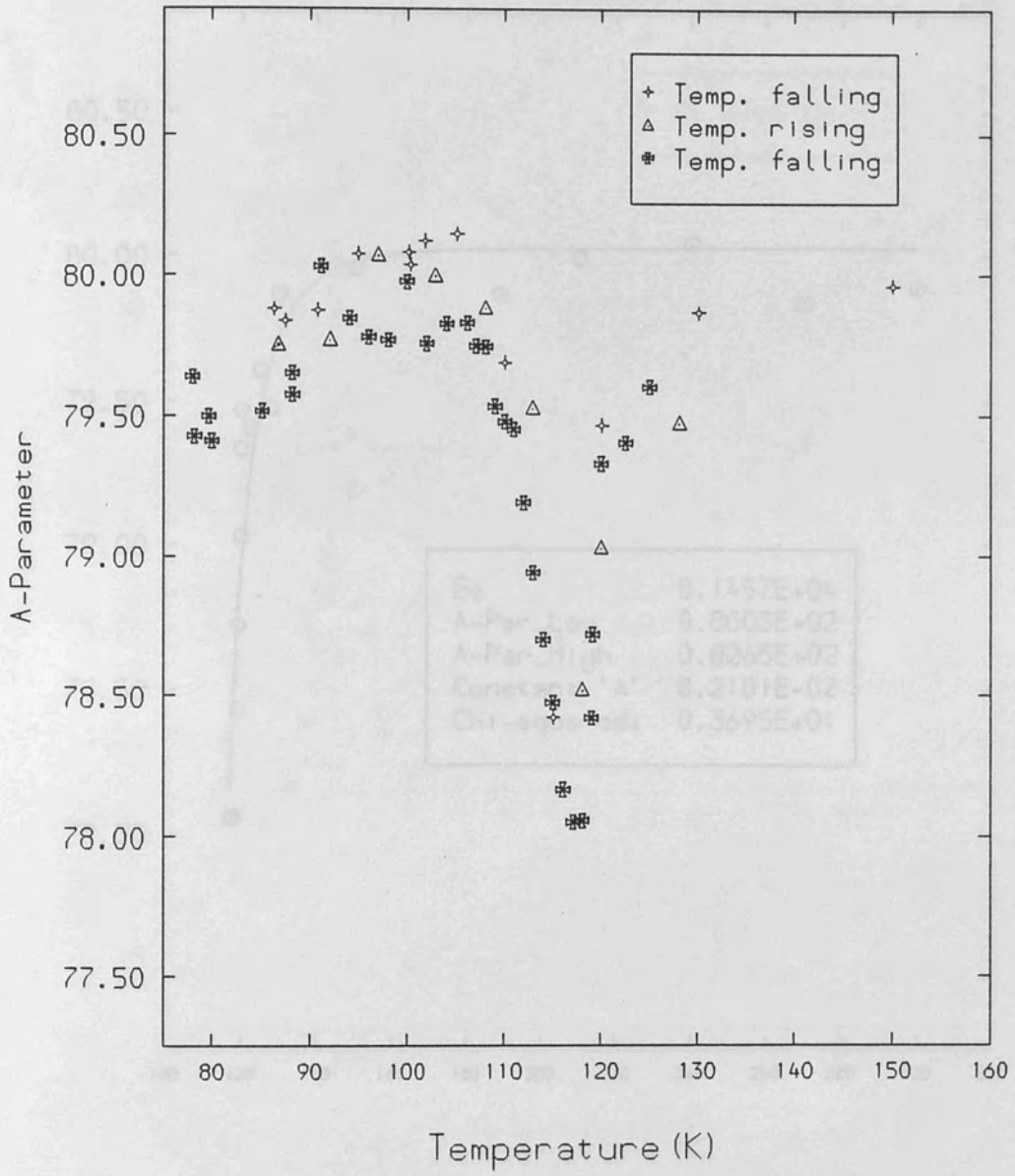

Figure(10.3.1.2) Grafoil with krypton, V.P. peak.
The A-parameter over 80-160K. Symbols mark changes in temperature flow.

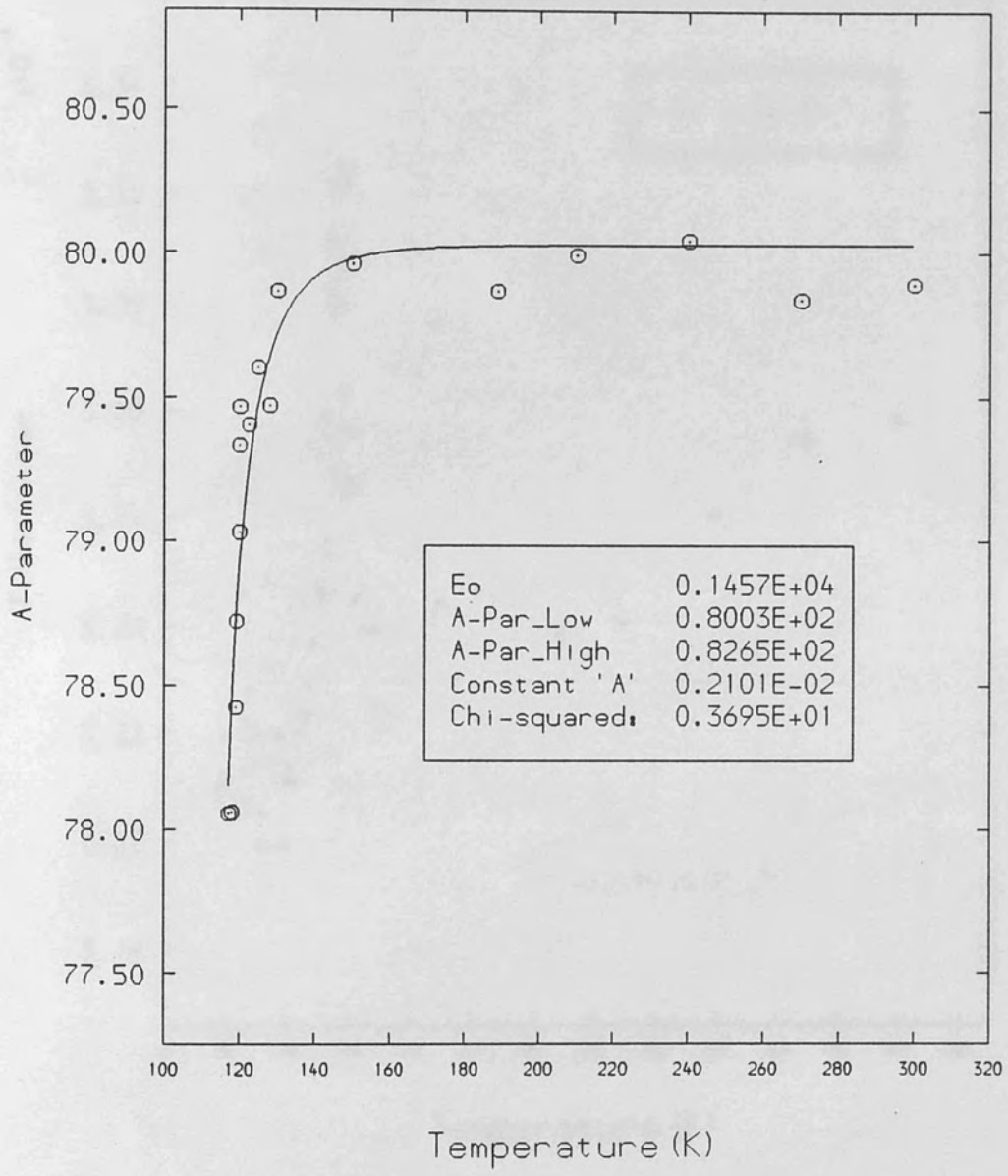

Figure(10.3.1.3) Grafoil with krypton, V.P. peak.

Fit of equation(9.1) to the A-parameter peak RHS to yield ϵ_0.

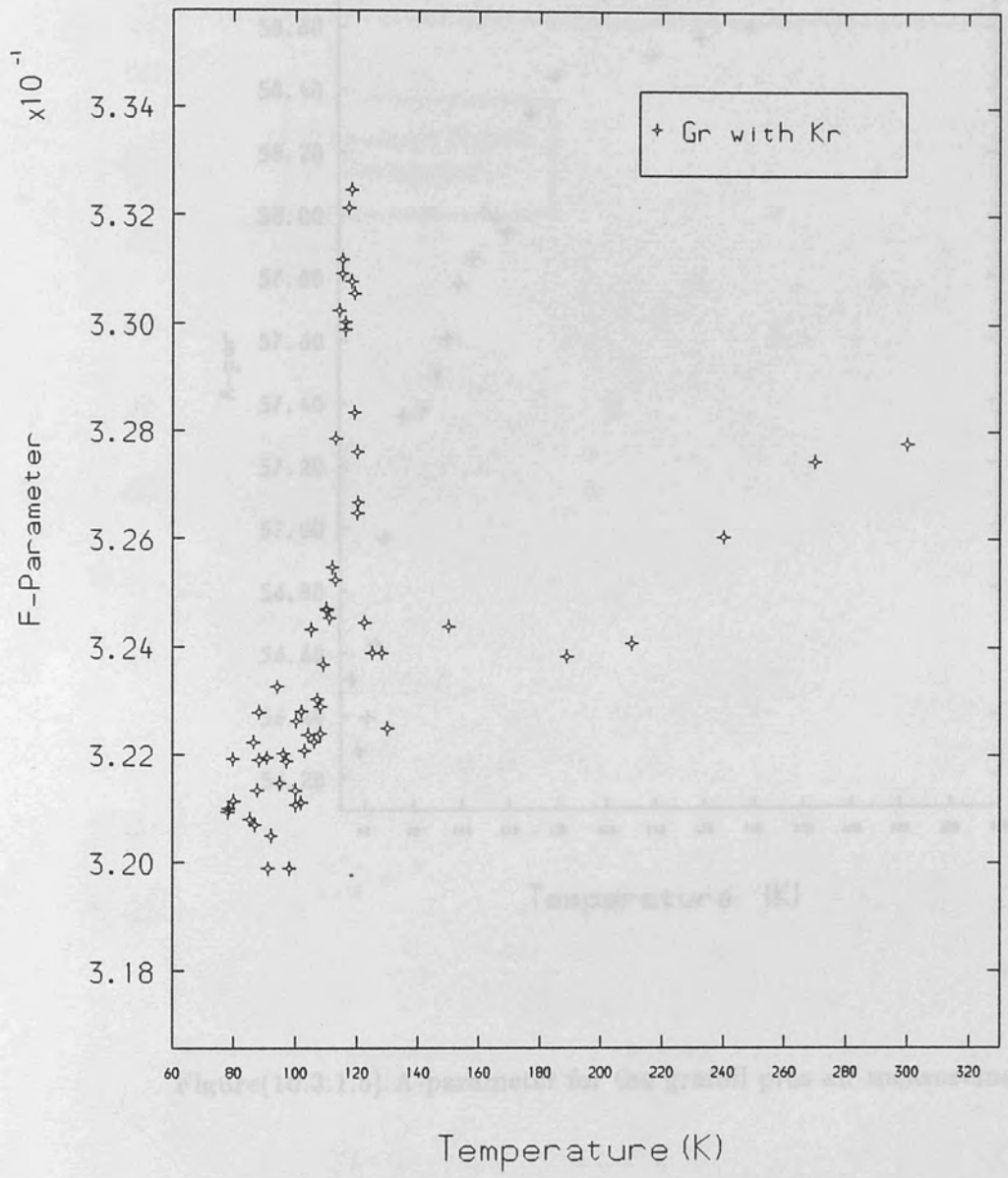

Figure(10.3.1.4) F vs temperature of grafoil with krypton.

Results shown are of a [5 + 1 + 5] definition.

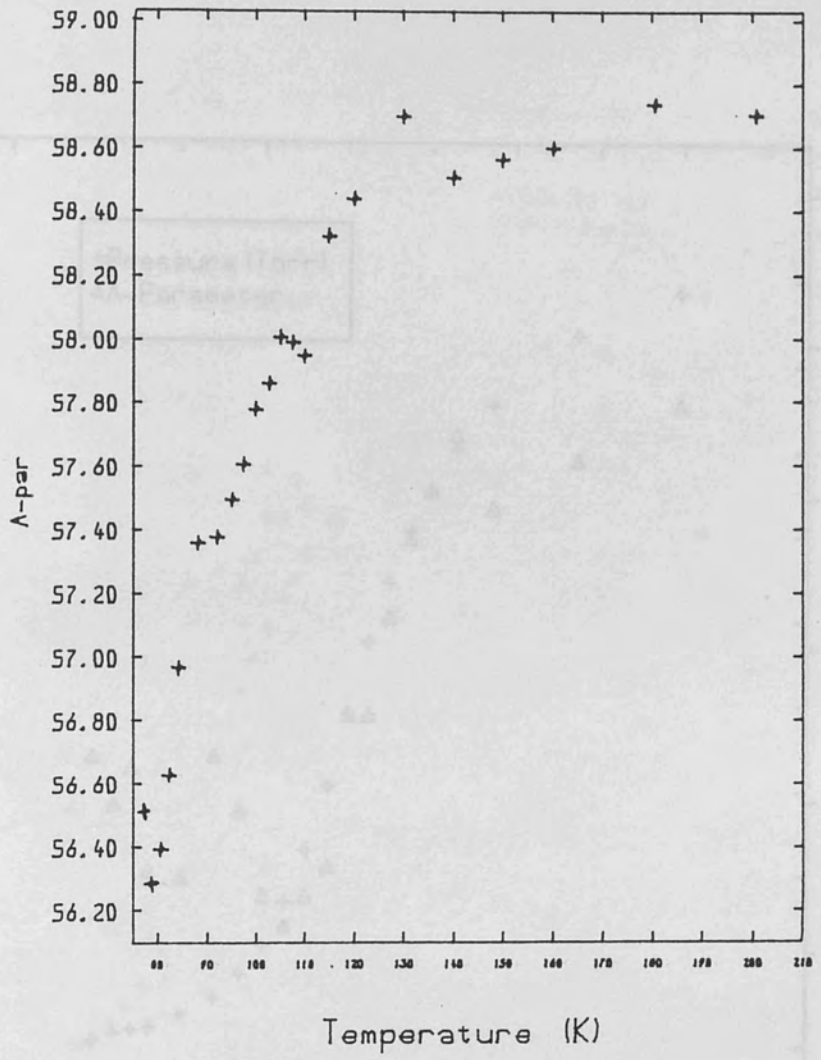

Figure(10.3.1.5) A-parameter for the grafoil plus air measurement.

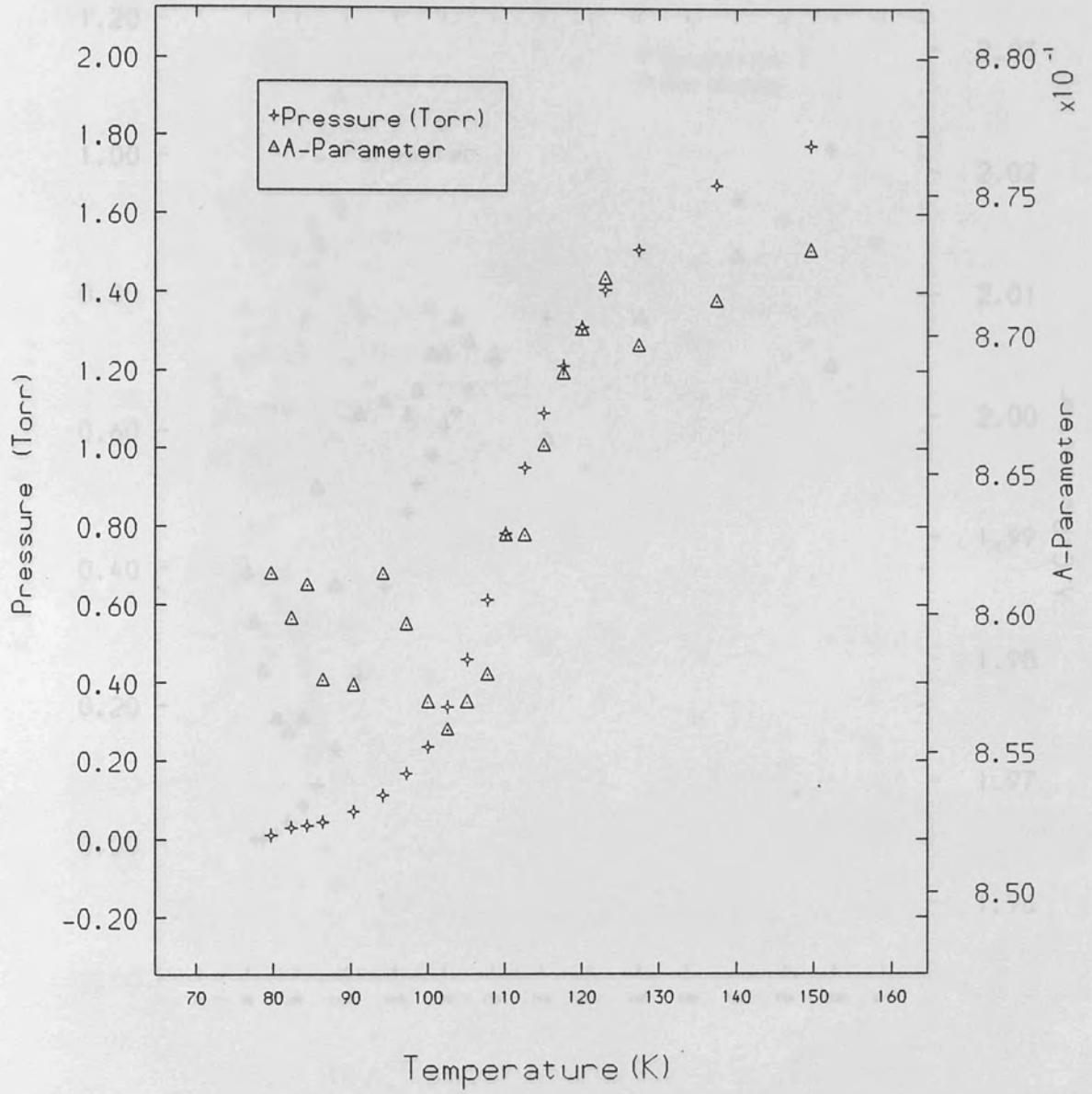

Figure(10.3.2.1) Grafoil with krypton.
Pressure and scaled A-parameter drawn together for a peak at below the 77.4K V.P. A gas deficiency is apparent from the fall to zero pressure.

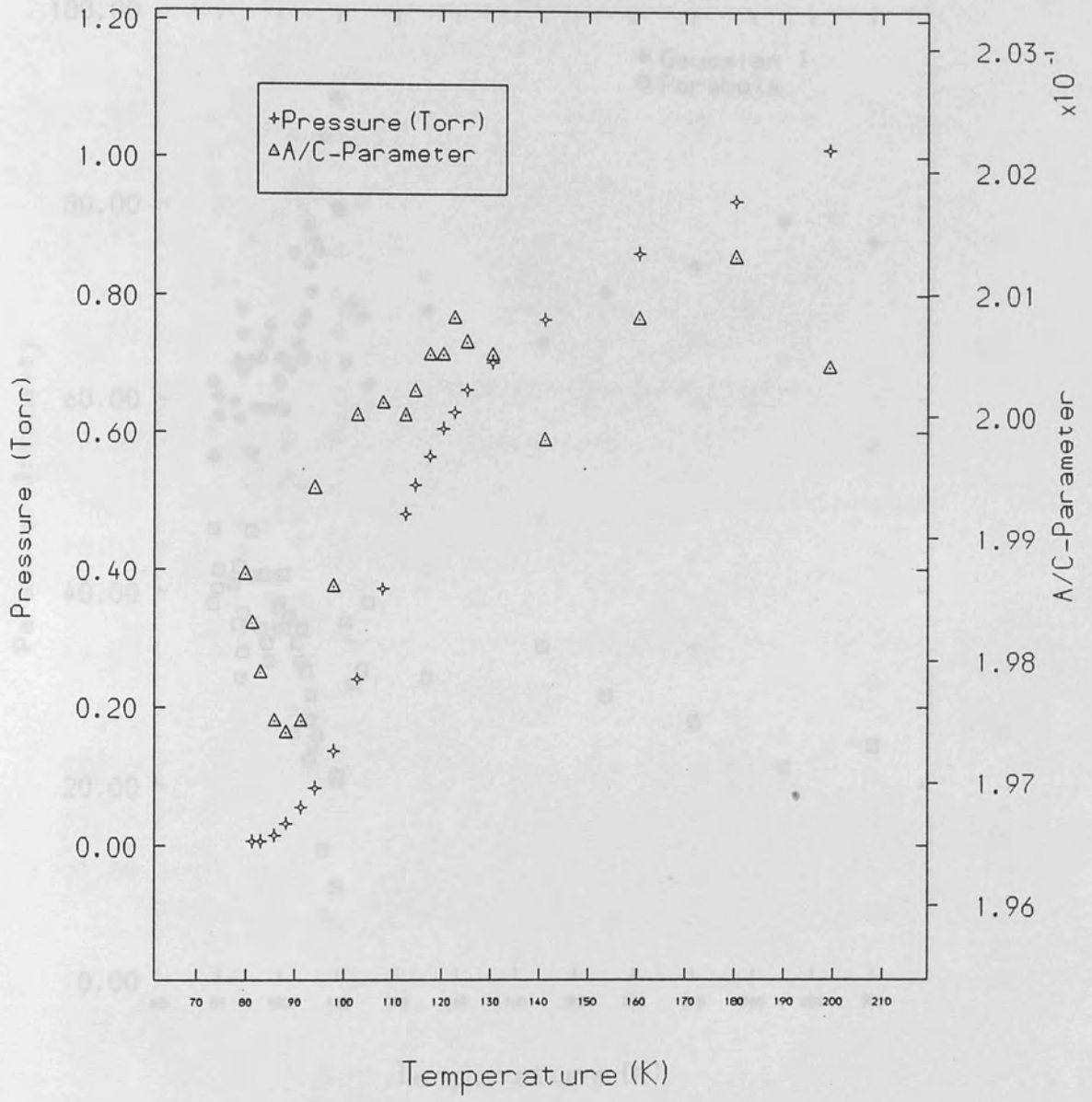

Figure(10.3.2.2) Grafoil with krypton.
Pressure and scaled A/C-parameter drawn together for a start pressure of 1Torr. The decline to zero pressure is more rapid than in figure(10.3.2.1) and this increases the asymmetry of the variation.

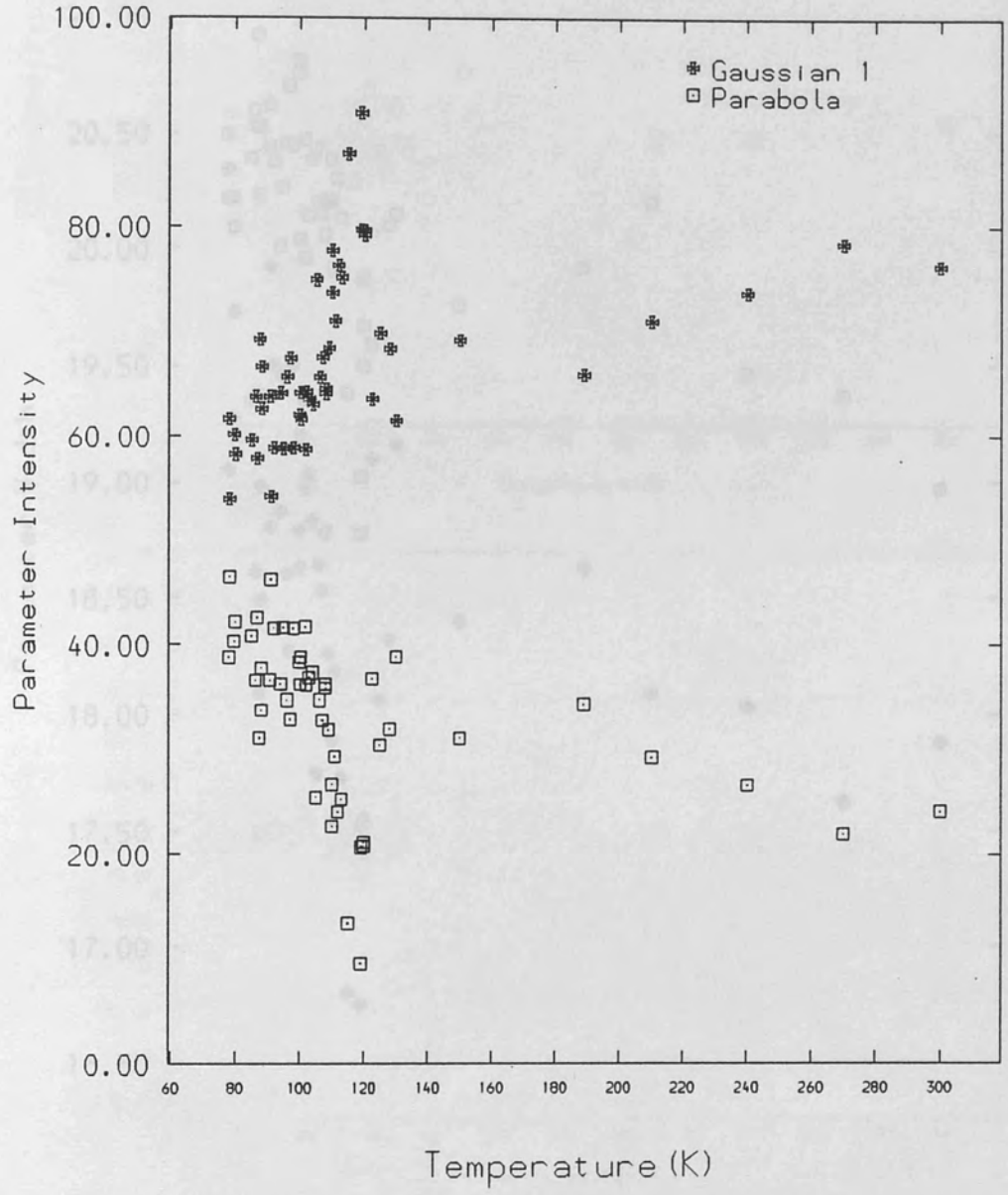

Figure(10.3.3.1) Two component analysis of Grafoil + Krypton Parabola and single gaussian intensity. Sharp rise of gaussian (narrow) component indicates presence of *p*-Ps.

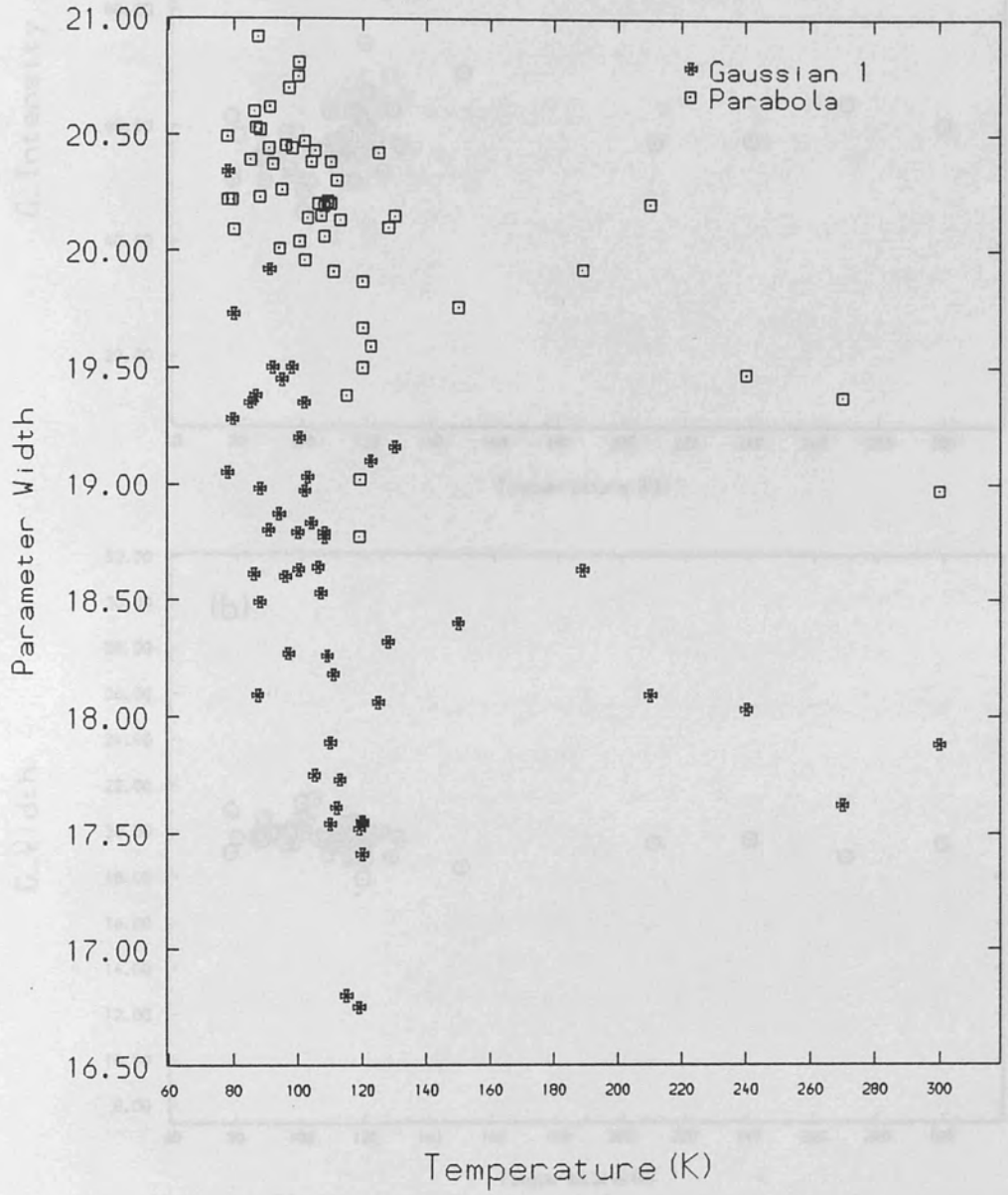

Figure(10.3.3.2) Two component analysis of Grafoil + Krypton. Parabola and single gaussian width.

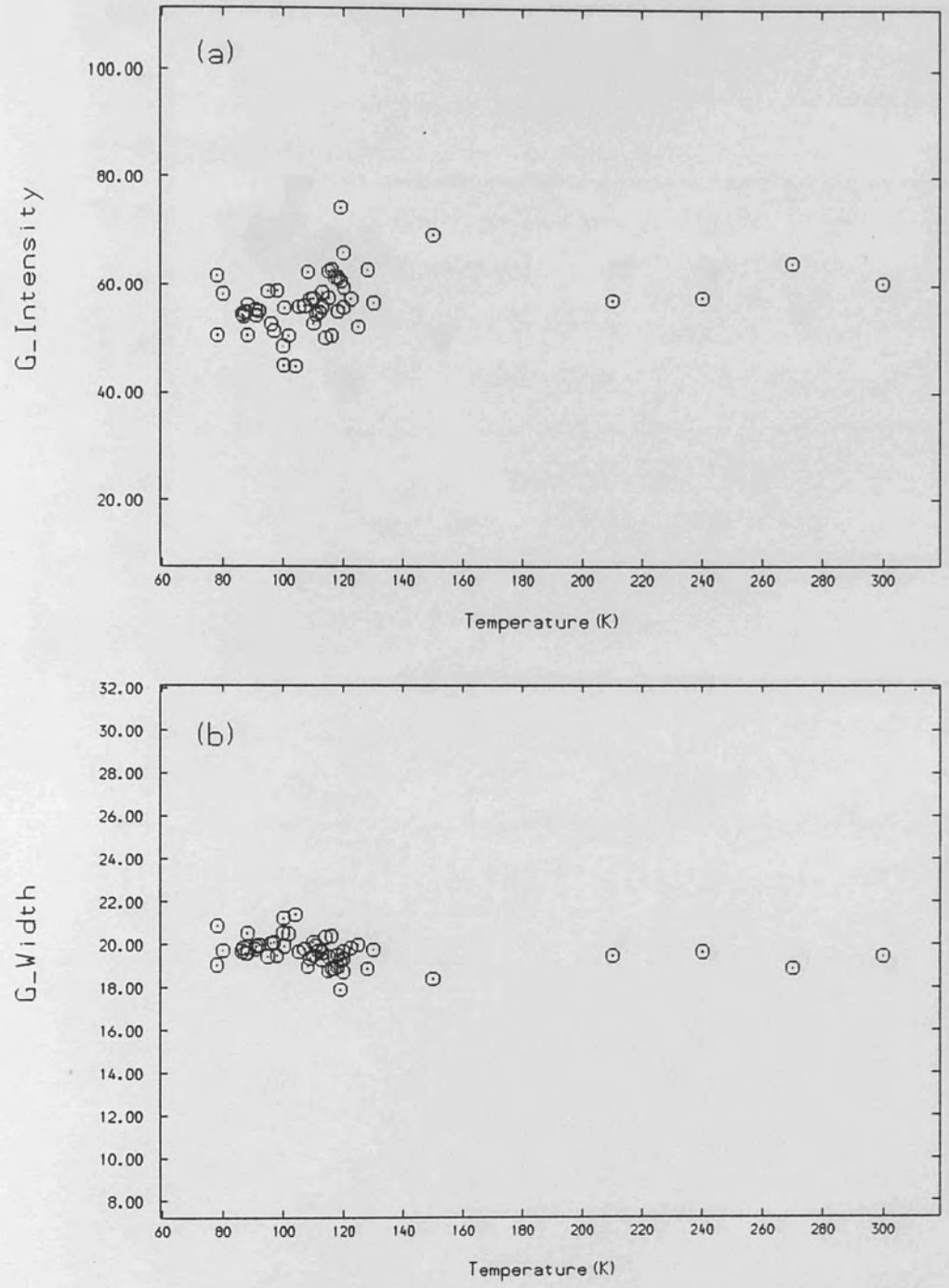

Figure(10.3.3.3) Three component analysis of Grafoil + Kr.

(a) First gaussian intensity.

(b) First gaussian width.

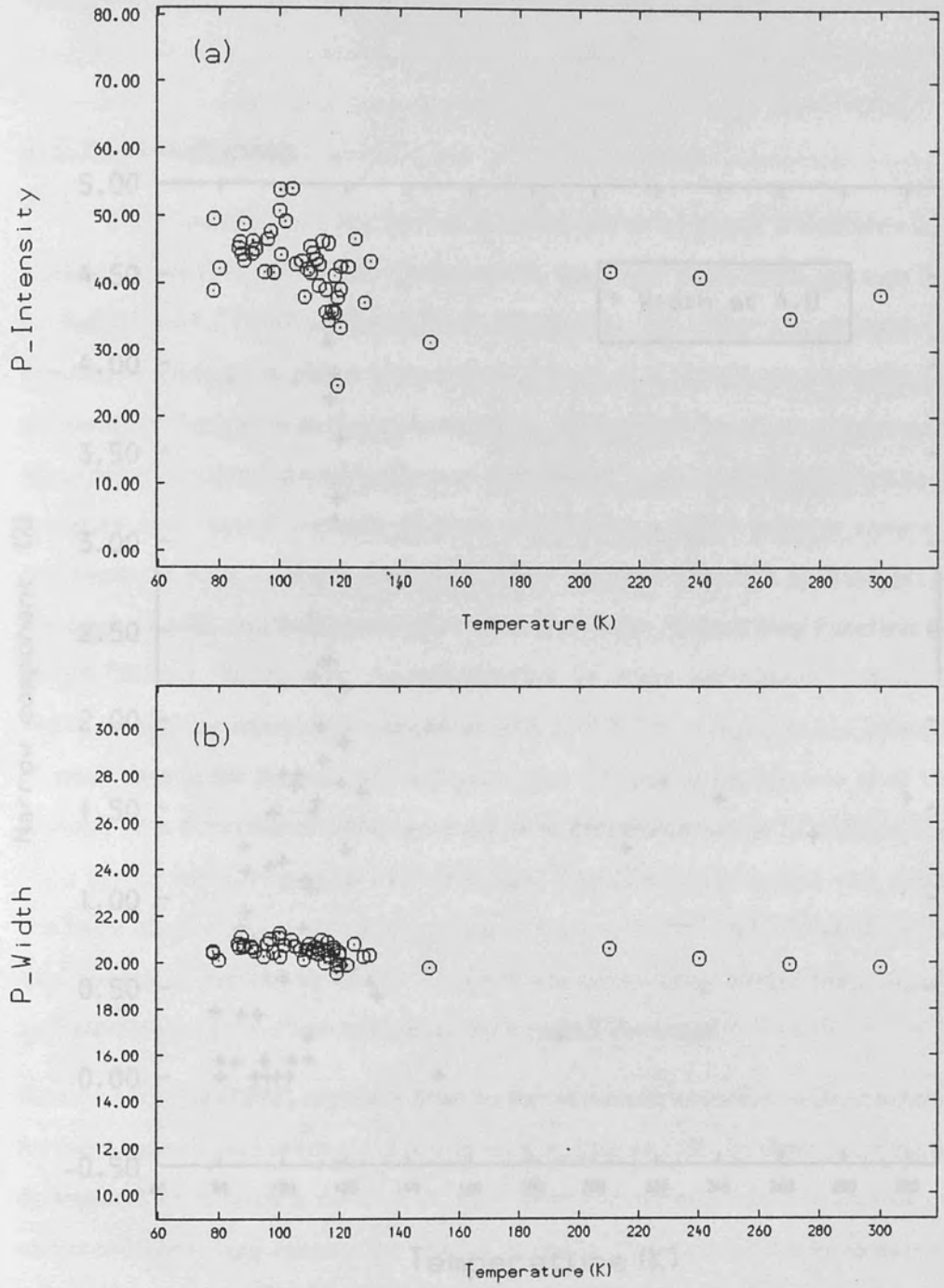

Figure(10.3.3.4) Three component analysis of Grafoil + Kr.

(a) Parabola intensity.

(b) Parabola width.

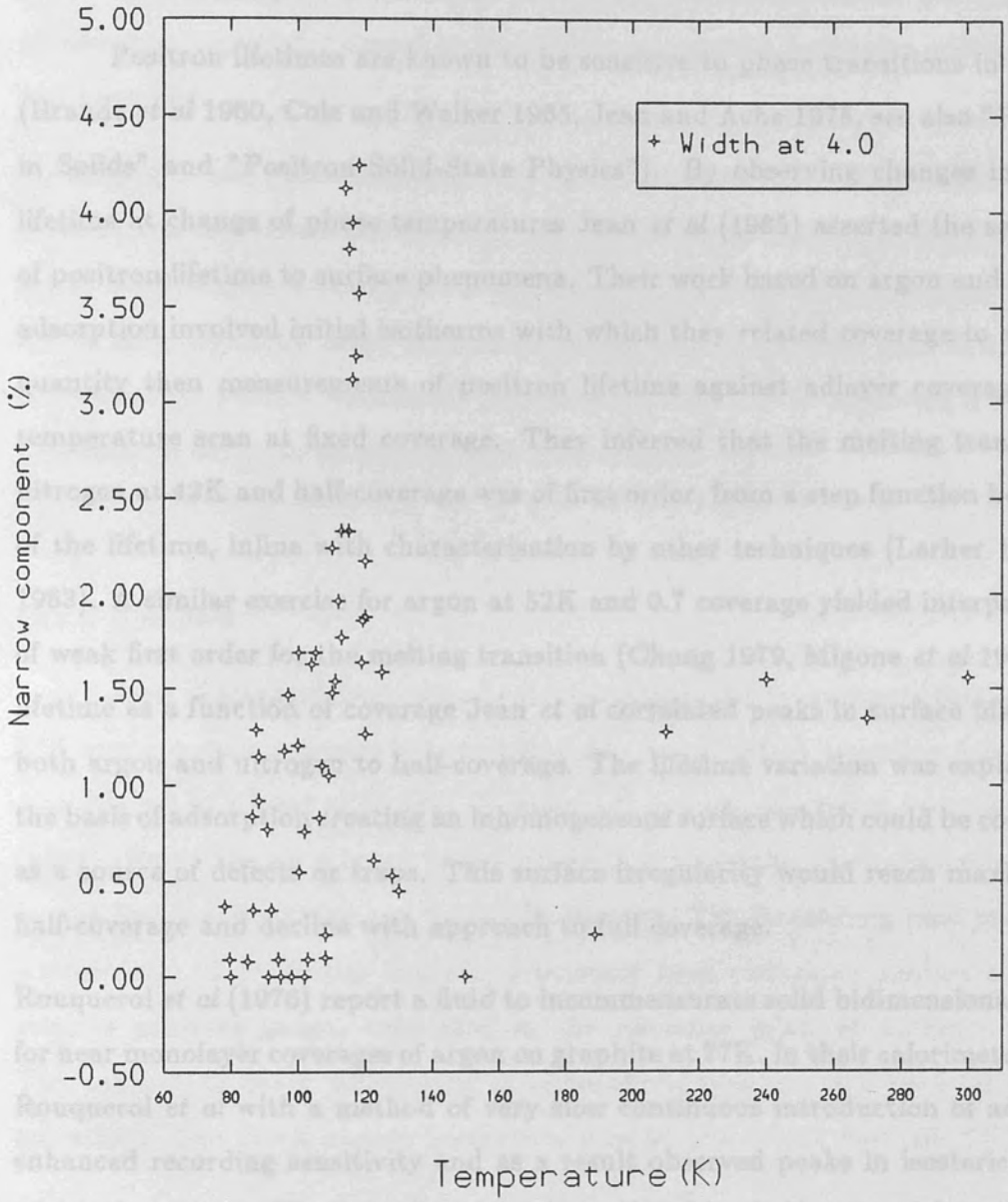

Figure(10.3.3.5) Three component analysis of Grafoil + Kr.
Second gaussian intensity when width fixed at 4 channels.

Chapter XI Argon Adsorption on Grafoil

§11.1 Introduction

Positron lifetimes are known to be sensitive to phase transitions in the bulk (Brandt *et al* 1960, Cole and Walker 1965, Jean and Ache 1978, see also "Positrons in Solids" and "Positron Solid-State Physics"). By observing changes in surface lifetime at change of phase temperatures Jean *et al* (1985) asserted the sensitivity of positron lifetime to surface phenomena. Their work based on argon and nitrogen adsorption involved initial isotherms with which they related coverage to adsorbed quantity then measurements of positron lifetime against adlayer coverage and a temperature scan at fixed coverage. They inferred that the melting transition of nitrogen at 42K and half-coverage was of first order, from a step function behaviour of the lifetime, inline with characterisation by other techniques (Larher 1978 and 1983). A similar exercise for argon at 52K and 0.7 coverage yielded interpretations of weak first order for the melting transition (Chung 1979, Migone *et al* 1984). For lifetime as a function of coverage Jean *et al* correlated peaks in surface lifetime for both argon and nitrogen to half-coverage. The lifetime variation was explained on the basis of adsorption creating an inhomogeneous surface which could be considered as a source of defects or traps. This surface irregularity would reach maximum at half-coverage and decline with approach to full coverage.

Rouquerol *et al* (1976) report a fluid to incommensurate solid bidimensional change for near monolayer coverages of argon on graphite at 77K. In their calorimetric study Rouquerol *et al* with a method of very slow continuous introduction of adsorbate enhanced recording sensitivity and as a result observed peaks in isosteric heat of adsorption curves. These peaks were substantiated by isotherms performed to the same sensitivity in which substeps at the critical coverage were recorded. Migone *et al* (1984) performed precision ac heat-capacity scans and proposed a phase diagram of argon on graphite. This is reproduced in figure(11.1.1), extended from 65K to 77K. From their work Rice-Evans *et al* (1986) concluded that maximum positronium emission occured at monolayer and not half-layer coverages. A coverage of 103±17%

was presented for nitrogen. This figure was based upon triangular incommensurate packing with nitrogen nearest-neighbour separation at 4.1Å and by Henry law fitting of pressure at maximum emission versus temperature. A mechanism of electron capture from adlayer by emerging positrons to form maximum positronium at monolayer completion followed by inability to escape with increasing adlayer density was proposed.

By making detailed measurements over the temperature range 80-150K of maximum positronium emission it was sought in the present study to acertain the positronium state. Additionally bulk argon has a melting temperature of 85K and as coverages above monolayer can often be likened to the bulk state (Wei and Bruch 1981), dependent on wetting behaviour, there was a possibility of observing a change in positronium emission on crossing this temperature.

§11.2 Method

A set of measurements after heat treatment and a vacuum run, starting at the 77K argon vapour pressure were commenced. A method of decanting was adopted and this led to a total of 18 sets. A repeat set and corresponding vacuum run was taken, after soldering a break in the Au-Fe thermocouple. Pressure was measured by the Druck transmitter and 0-1Bar Budenberg. The Budenberg read pressure to a sensitivity of $\pm$0.5mBar and had previously been calibrated against a Penwalt relative pressure gauge, evacuated at the reference inlet, of accuracy 0.1Torr. The calibration offset by changes in atmospheric pressure was used for pressure correction. The 77.4K vapour pressure as read by the Druck was 210$\pm$5Torr.

§11.3 Results

§11.3.1 Positronium and Lineshape Parameters

A characteristic positronium emission peak, obtained for the vapour pressure run, is shown by the A/C-parameter in figure(11.3.1.1). The peak of some 2% shows maximum positronium emission to occur at 124±1K. Again the high temperature trend is the background grafoil in vacuum variation with the peak corresponding to adlayer formation to what was believed to be a monolayer followed by an emission progressively subdued with bilayer formation to meet again, on the left, the graphite level. As in earlier chapters the R-parameter variation was fitted for peak position, depth and width. Figure(11.3.1.2) shows the fit and A-parameter for the second set. All 19 sets were fitted in this manner. The Druck transmitter measurement for the first free pressure set, figure(11.3.1.3), displays only a temperature dependent variation without the now characteristic S-form at the positronium peak (see earlier chapters). The fits to the positronium emission are shown together in figure(11.3.1.4), where for the sake of clarity data points have not been drawn. The collection is quite striking. Three stages are visible: a lowering of peak temperature with pressure at constant positronium emission, a sudden disappearance of the left hand side riser and a trend of increasing maximum positronium. It may be noted that whilst, in the third stage, the peak minimum value is changing, a constant right hand side level appears to be maintained. It may thus be inferred that maximum positronium production increases for these lower temperature peaks. The second stage starts with the measurement at 97K and 12±2Torr, figure(11.3.1.5), and the change to increasing emission at 90K and 1±1torr. It is seen that the peaks were chased until only the RHS decline was visible before the cut-off at 77K, figure(11.3.1.4). The F-parameter was calculated, without background substractions, for each set and fitted with the same arbitrary function. Figure(11.3.1.6) shows these, with data points omitted, again for clarity. Three regions are noticed. These confirm those of the R-parameter, first constant maximum *p*-Ps production then an S-form followed by gradually increasing

emission. Peak temperature and pressure data were used to form a pressure at peak versus temperature relation and a fit attempted with the Boltzmann expression for adsorbate vapour pressure (equation 2.7). At the higher temperatures the adlayer is fluid (figure 11.1.1) and hence not in registry with the graphite. Using an effective argon diameter of 3.85Å (Larher 1974) for the film and placing mass gives

$$P = 3221 x t^{\frac{3}{2}} \exp\left(-\frac{\epsilon_0}{t}\right) \tag{11.1}$$

where P is the adsorbate vapour pressure (Torr), x monolayer fraction, t temperature (K) and ϵ_0 adatom-substrate binding energy (K). The unweighted fit, figure(11.3.1.7), over the full set yielded x = 52% ± 10% and $\epsilon_0 = 1160 \pm 30$K and a χ^2/ν of 3.9.

§11.4 Conclusion and Discussion

Physisorption of argon on exfoliated graphite has been followed by Doppler broadening of annihilation radiation, over the temperature range 80-125K. A three stage effect was observed spanning constant positronium production to increasing positronium yield. At the time the measurements were performed maximum emission was thought to occur at monolayer coverages and the LHS fall through bilayer formation. This supposition led to an explanation of the sudden loss of the peak riser for intermediate runs crossing 84K as due possibly to bulk melting. This melting transition however does not explain the final effect which starts at submonolayer coverages. It is possible that the increased positronium emission stage is a reflection of the fluid-incommensurate solid phase transition at 77K reported for near monolayer coverages (Migone *et al* 1984). In the light of recent pressure results and realization that maximum positronium formation occurs not at monolayer but half-layer coverages the following observations are made:

(a) The S-form positronium variations are reminiscent of the krypton results, where the gas available for adsorption was exhausted. The pressures are indeed very low for the second stage and quite within an extreme zero drift in the measuring transmitter. Furthermore the coverages at which the effect occurs are submonolayer and so cannot duplicate bulk transitions.

(b) The peaks at the third stage could be an indication of the fluid-incommensurate phase change. If the incommensurate structure has a smaller packing density it would require less gas for equivalent fluid layer coverages. This said, there is a similarity between these third stage peaks and grafoil plus air (chaper 10) which perhaps implies a leakeage of air.

The Henry law fit to pressure at peak versus temperature gave a reasonable value for the adatom-substrate binding energy of $\epsilon_0 = 1160 \pm 30$K (*cf.* 1380K: Wei and Bruch 1981, 1180K: Diehl and Fain 1982).

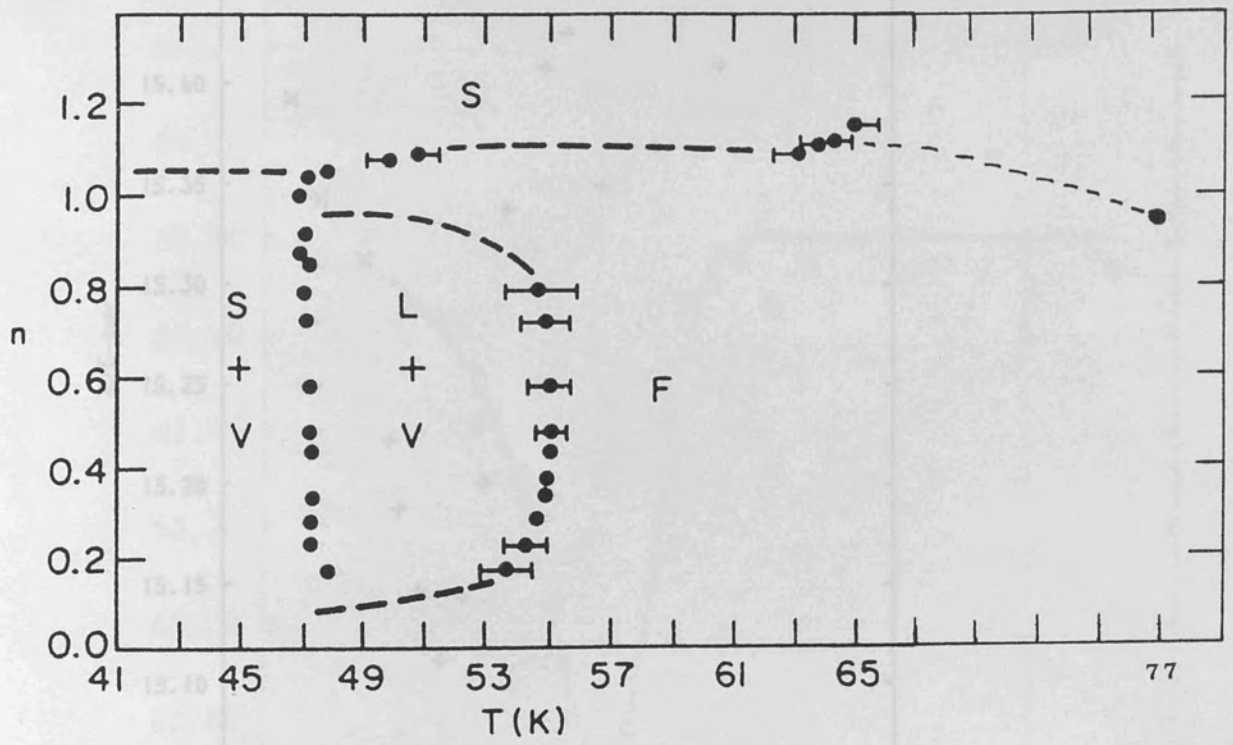

Figure(11.1.1) Phase diagram for argon on graphite (Migone 1984). S, L, V, and represent solid, liquid (registered fluid), vapour and fluid phases respectively. An additional point due to Rouquerol *et al* (1976) for near monolayer coverage has been added at 77K.

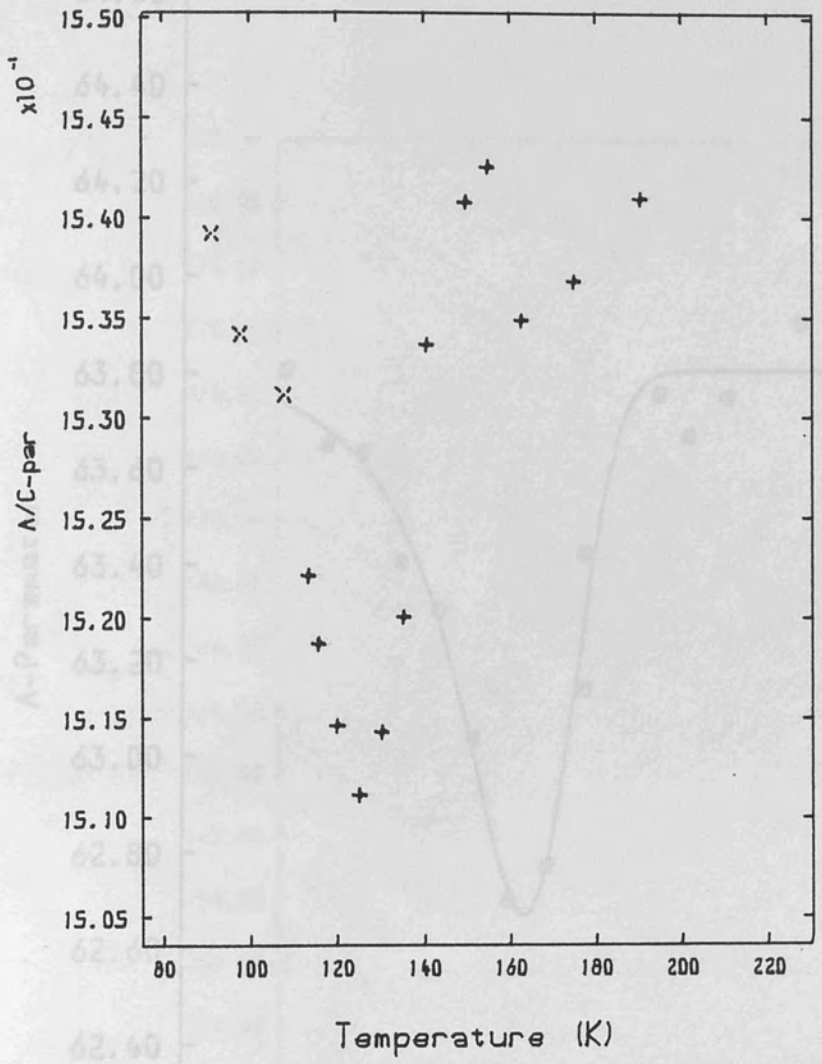

Figure(11.3.1.1) Positronium parameter for the 210Torr vapour pressure run.

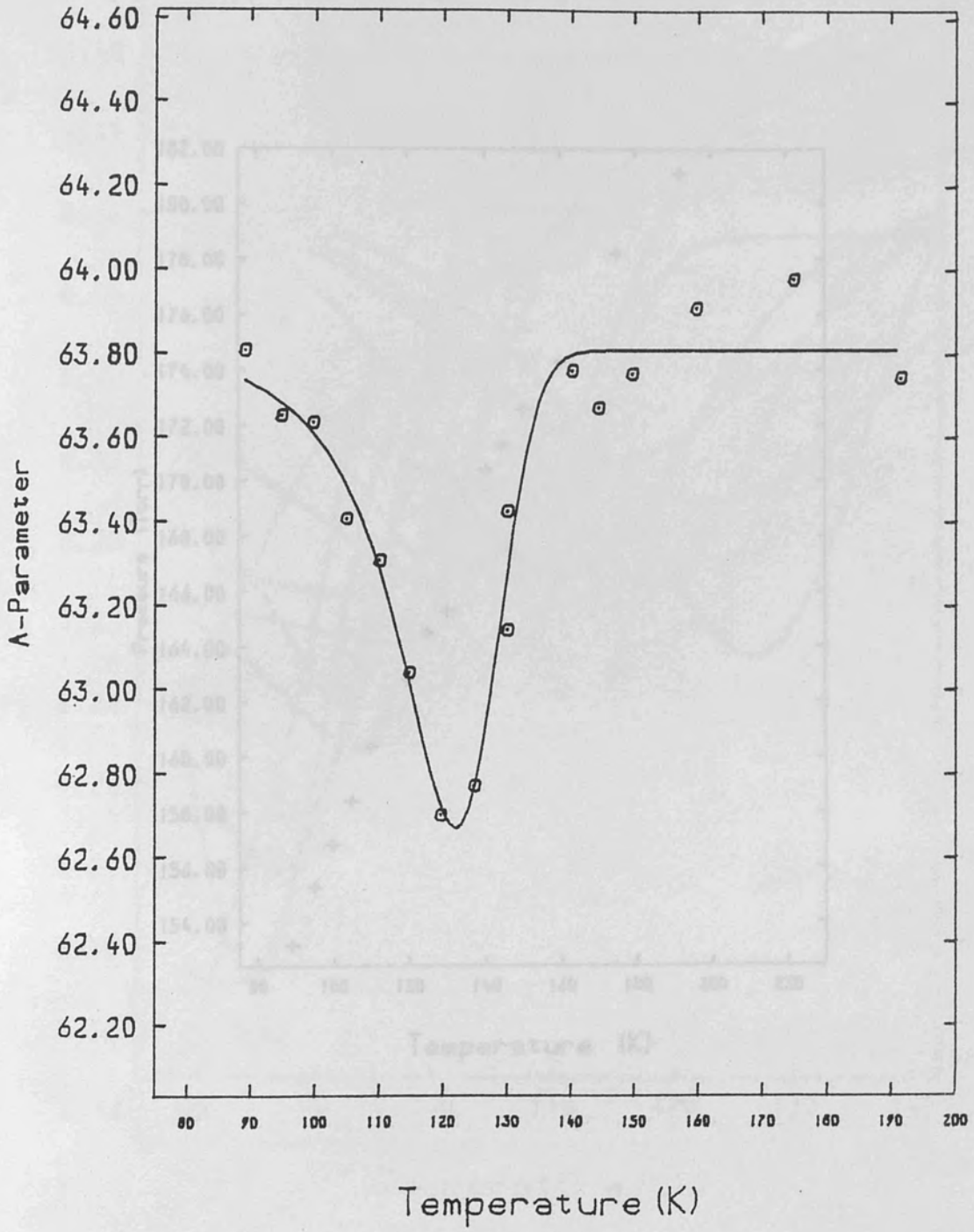

Figure(11.3.1.2) The A-parameter for the second set at 122K and 160Torr fitted with an arbitary function.

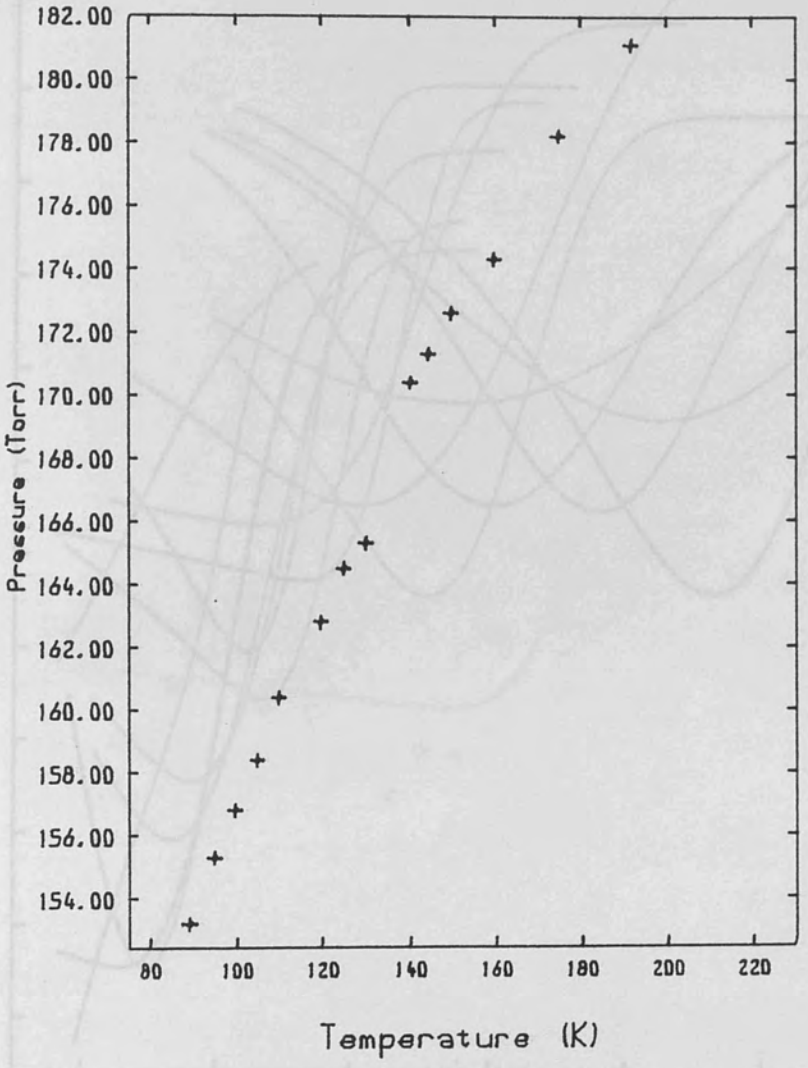

Figure(11.3.1.3) Pressure variation as recorded by the 0-760Torr transmitter for the second argon peak. The variation lacks the S-form, indicative of monolayer formation, of later measurements with the 0-52Torr transducer.

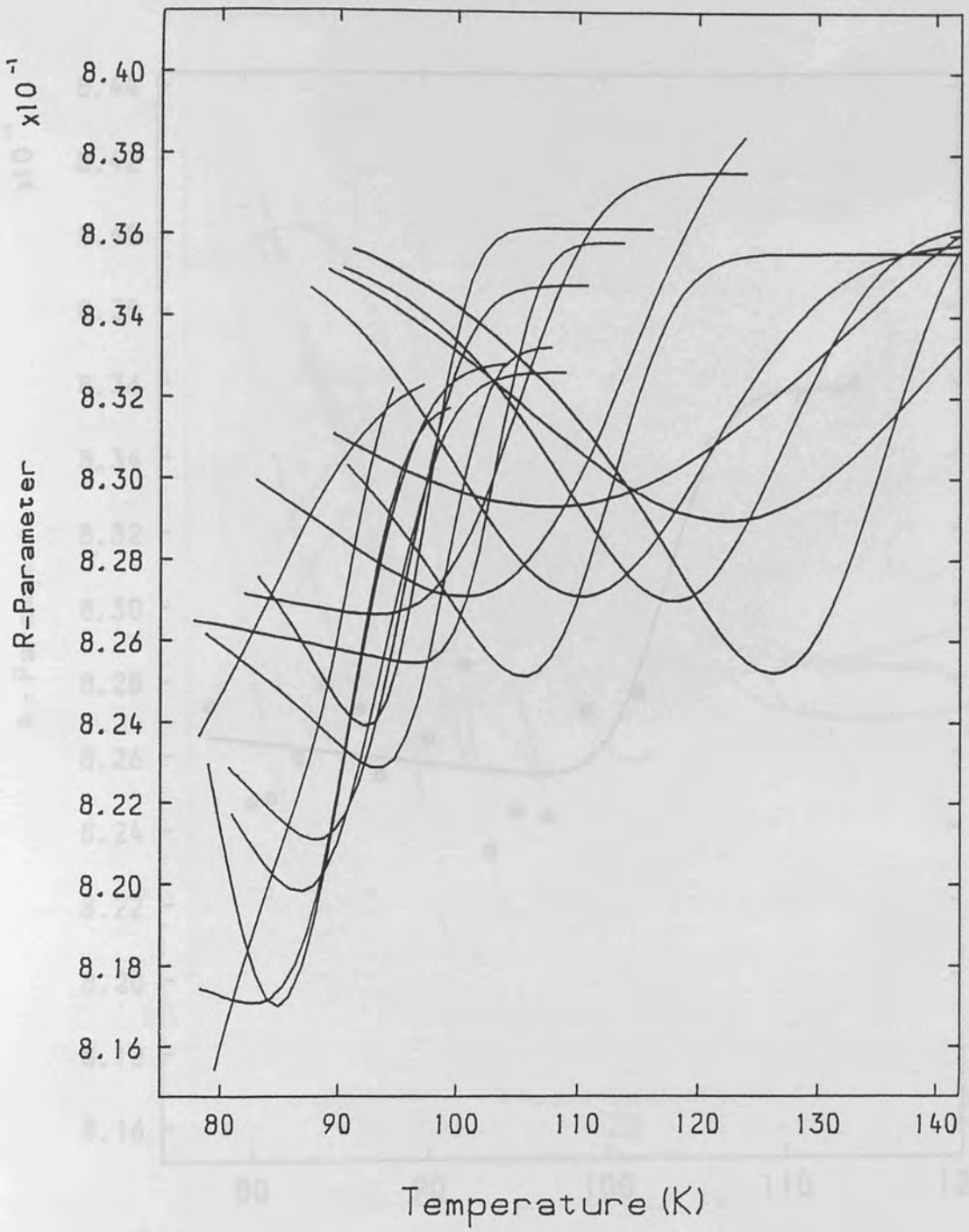

Figure(11.3.1.4) Complete set of fits for the recorded R-parameter. For the sake of clarity, data points have been omitted. A region of constant maximum positronium production is followed by one of increasing emission with a loss of the left hand side riser for intermediate peaks.

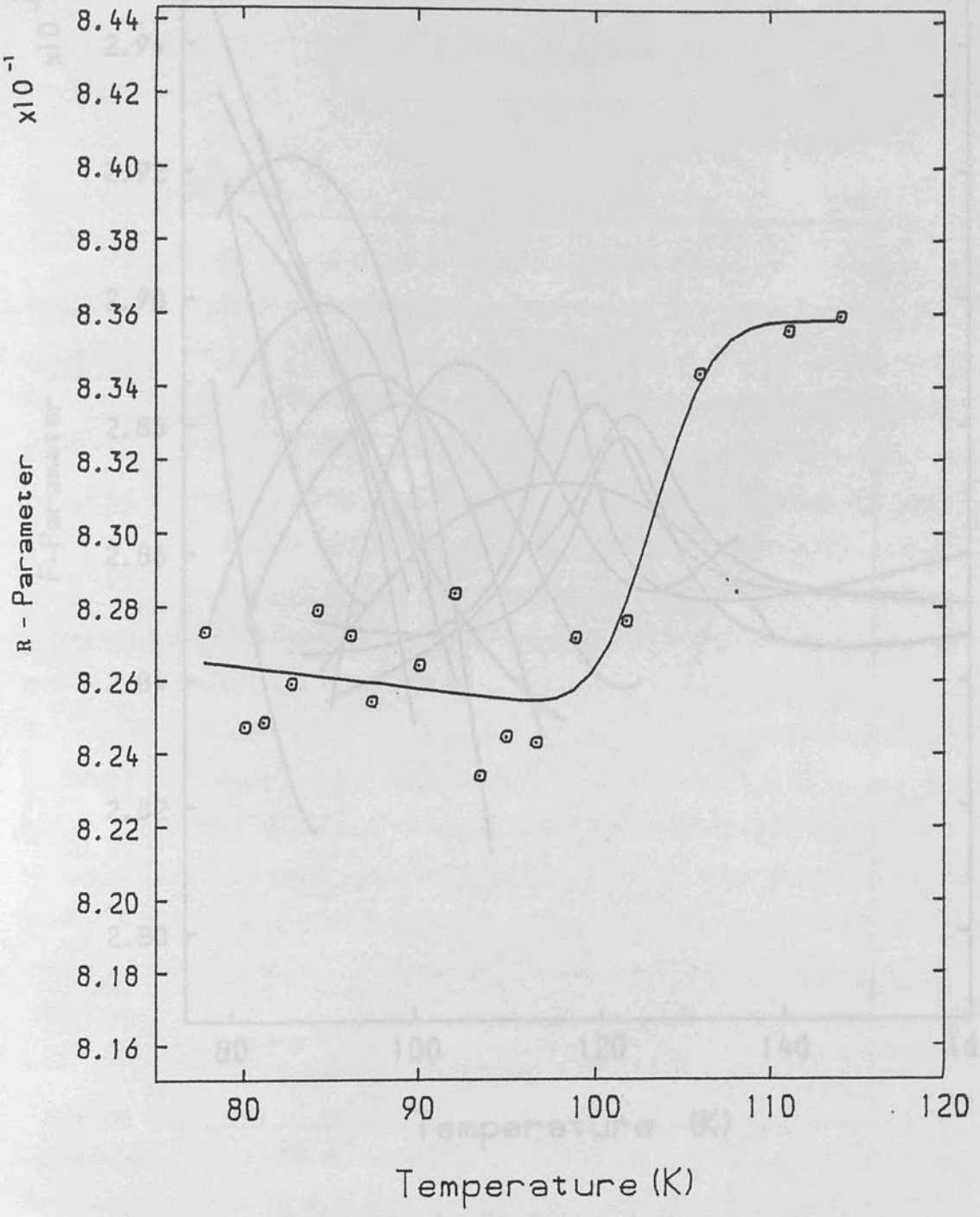

Figure(11.3.1.5) A representative S-form variation for the intermediate sets. Shown is the ninth run with a start pressure at 77K of 5Torr.

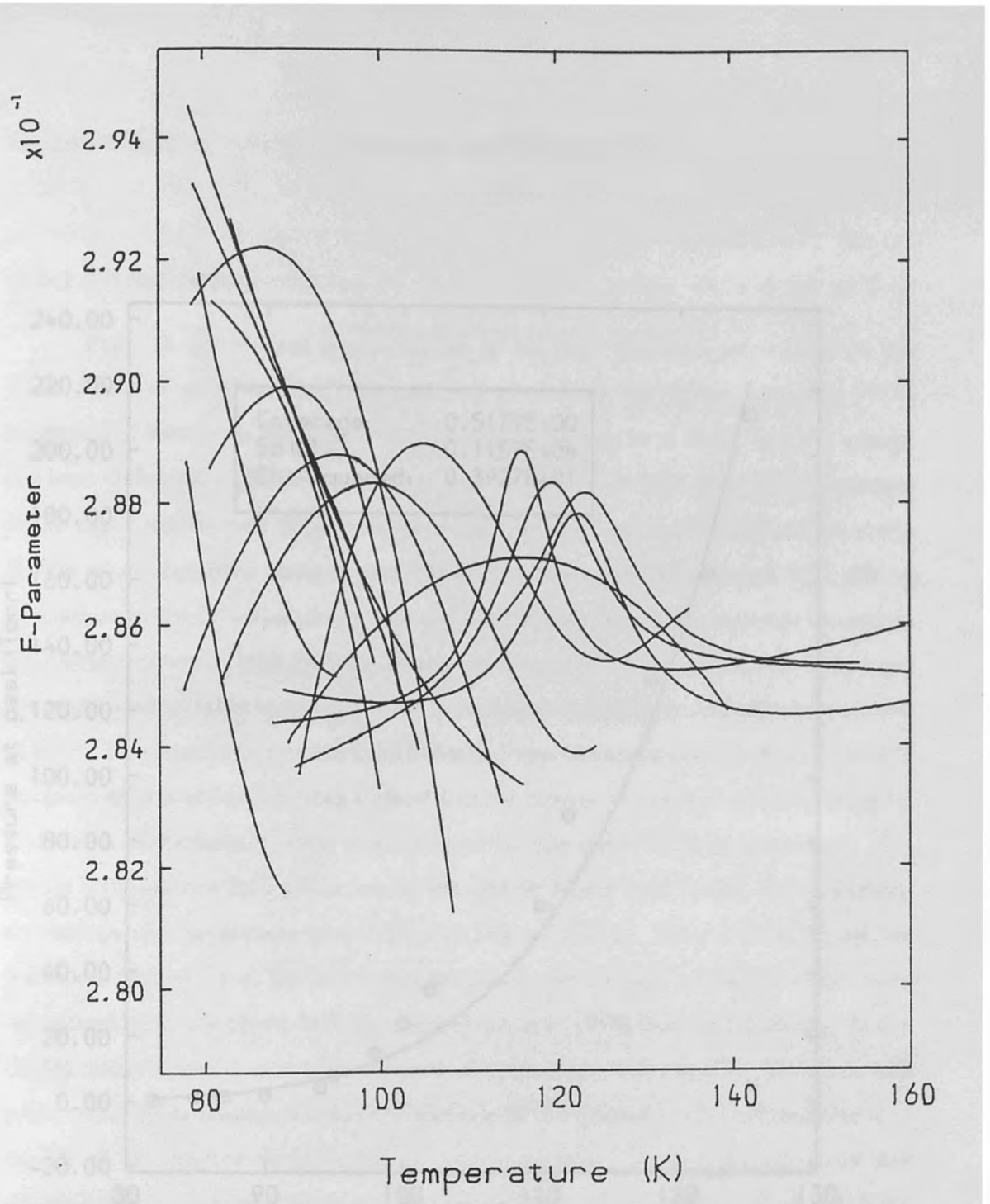

Figure(11.3.1.6) The fitted F-parameters. These also show the three phase effect.

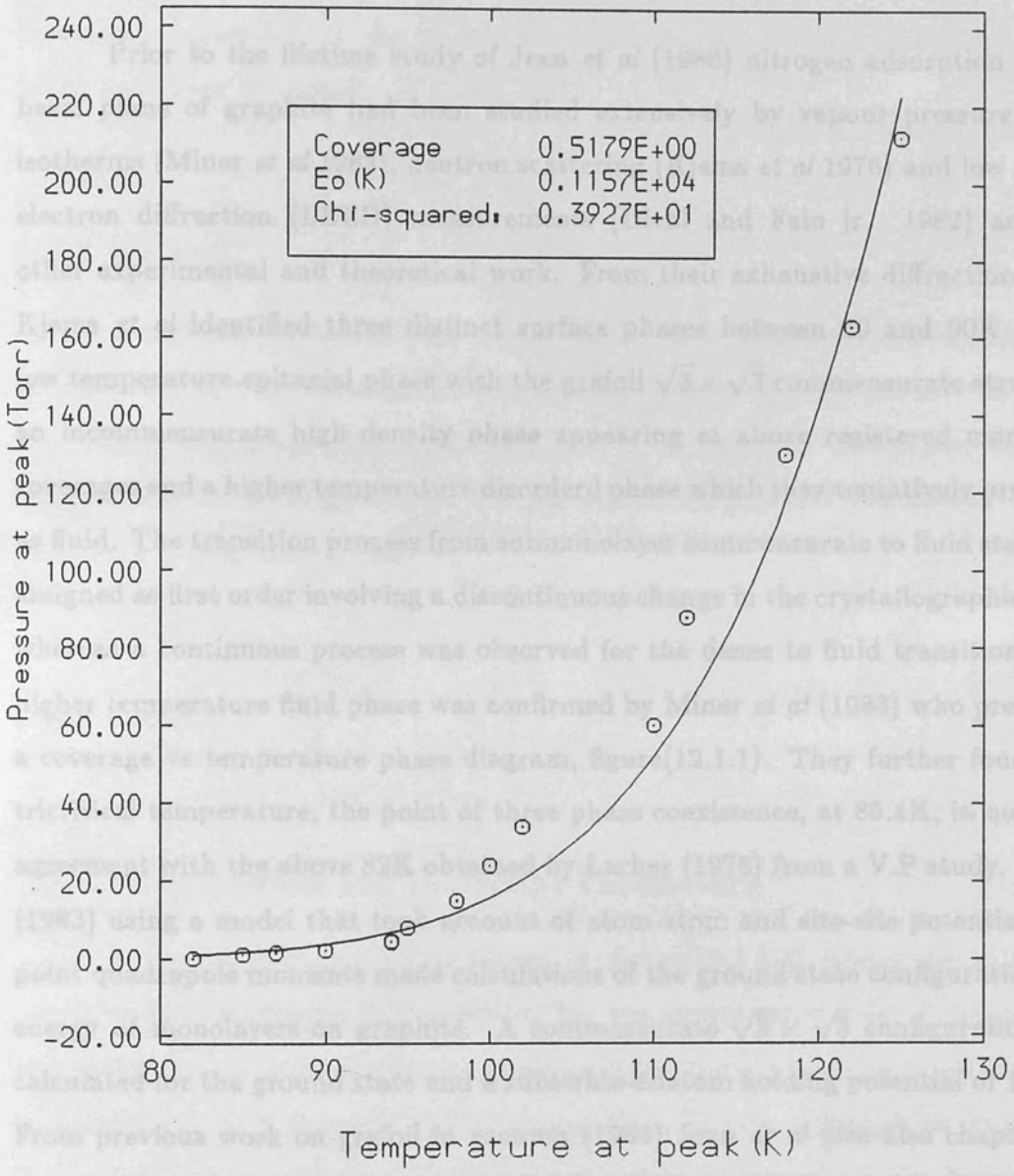

Figure(11.3.1.7) Peak pressures vs temperatures fitted with the Boltzmann's expression to yield ϵ_0 and coverage(x).

Chapter XII Nitrogen on Grafoil

§12.1 Introduction

Prior to the lifetime study of Jean *et al* (1986) nitrogen adsorption on the basal plane of graphite had been studied extensively by vapour pressure (V.P) isotherms (Miner *et al* 1983), neutron scattering (Kjems *et al* 1976) and low energy electron diffraction (LEED) measurements (Diehl and Fain jr. 1982) amongst other experimental and theoretical work. From their exhaustive diffraction study Kjems *et al* identified three distinct surface phases between 10 and 90K *viz.* a low temperature epitaxial phase with the grafoil $\sqrt{3} \times \sqrt{3}$ commensurate structure, an incommensurate high density phase appearing at above registered monolayer coverages and a higher temperature disorderd phase which they tentatively proposed as fluid. The transition process from submonolayer commensurate to fluid state was assigned as first order involving a discontinuous change in the crystallographic order whereas a continuous process was observed for the dense to fluid transition. The higher temperature fluid phase was confirmed by Miner *et al* (1983) who presented a coverage vs temperature phase diagram, figure(12.1.1). They further found the tricritical temperature, the point of three phase coexistence, at 85.4K, in qualitive agreement with the above 82K obtained by Larher (1978) from a V.P study. Bruch (1983) using a model that took account of atom-atom and site-site potentials and point quadrupole moments made calculations of the ground state configuration and energy of monolayers on graphite. A commensurate $\sqrt{3} \times \sqrt{3}$ configuration was calculated for the ground state and a substrate-adatom holding potential of 1159K. From previous work on grafoil in vacuum (1984) Jean *et al* (see also chapter 11) after fixing background *o*-Ps intensity (1%) and lifetime (1.3nsec) followed surface positron lifetimes under varying adsorbate coverages. For both argon and nitrogen at 77K the surface positron lifetime, with coverage increasing to monolayer, was found to rise from 0.38nsec to ~0.41nsec then fall again to 0.38nsec, the maximum occuring at half-coverage. This maximum lifetime was attributed to maximum surface irregularity at half-coverage giving rise to maximum positron trapping. The

work of Rice-Evans *et al* (1986) followed the production of positronium with adlayer formation on graphite, by use of a $2\gamma/3\gamma$ ratio. Positronium emission was found to increase with coverage to reach a maximum then fall. Recently with the aid of accurate pressure measurements the maximum has been pin-pointed to half-coverage (chapter 9). In the present work these measurements (Rice-Evans *et al* 1986) have been extended.

§12.2 Method

A method similar to that described in earlier chapters was employed to produce sets of measurements at varying start pressures from 290Torr to 2Torr. The Budenberg gauge measured the higher pressures with a 0-20Torr Genevac incorporated for lower pressures. For the second set pressure was measured with the Druck 0-1Bar transmitter.

§12.3 Results

§12.3.1 Positronium and Lineshape Parameters

A typical R-Parameter is shown in figure(12.3.1.1) where the minimum corresponds to maximum *o*-Ps emission. For the second set of measurements there was drift in the detector electronics resulting in the Doppler peak position dropping by some 0.1% (or 6 channels at 90eV/channel= 0.5KeV). Although to obtain the R-parameter the peak area is computed relative to peak position the 3γ windows are fixed and hence are susceptible to spectrum drift. The effect of changing peak position was exacerbated by an apparent decline in detector efficiency which caused a reduction in the integral of peak counts at a rate not accountable by source half-life. The collection is shown in figure(12.3.1.2) as a function of time and against temperature in figure(12.3.1.3).

Peak pressures and temperatures were fitted by the Boltzmann expression (equation 2.7)

$$P = 2377 x t^{\frac{3}{2}} \exp\left(-\frac{\epsilon_0}{t}\right) \tag{12.1}$$

in which P is adsorbate V.P (Torr), x coverage as a fraction of monolayer capacity, t temperature (K) and ϵ_0 adatom-substrate binding energy (K) and where the effective nitrogen area is set at $12.2 Å^2$. A value which assumes negligible effects from substrate corrugation potential on a triangular packing arrangement with a nitrogen nearest-neighbour distance of 4.1Å (Steele 1977). The fit yielded $x = 0.6 \pm 0.1$ and $\epsilon_0 = 1120 \pm 30$K, figure(12.3.1.4)

§12.4 Conclusion

A complete set of positronium emission peaks between 127-80K has been taken a value of 1120K for the adatom-substrate binding energy being obtained from a fit by the Boltzmann expression. This value compares reasonably with that reported by other groups (1159K: Bruch 1983, 1100K: Avgul and Kiselev 1970, 1060K: Steele 1977). The corresponding value for coverage was 0.6 and stands to correct the 103% found from the initial set alone (Rice-Evans *et al* 1986). At the start of the measurements it was hoped to see a positron effect for the phase transition at the 85.6K tricritical point (Miner *et al* 1983) but the absence of firm signals is explained by the now accepted knowledge of only half-coverage at maximum positronium emission. This implies, (figure 12.1.1), a requirement to traverse temperatures in the region of 50K in order to observe the fluid to commensurate solid transition at maximum positronium sensitivity. An anomolous tendency for the peak left hand side not to reach the pre-peak level was noted and may be, if not detector induced, evidence of a weak positronium sign of the transitions at near monolayer coverages at 85.4K tricritical point.

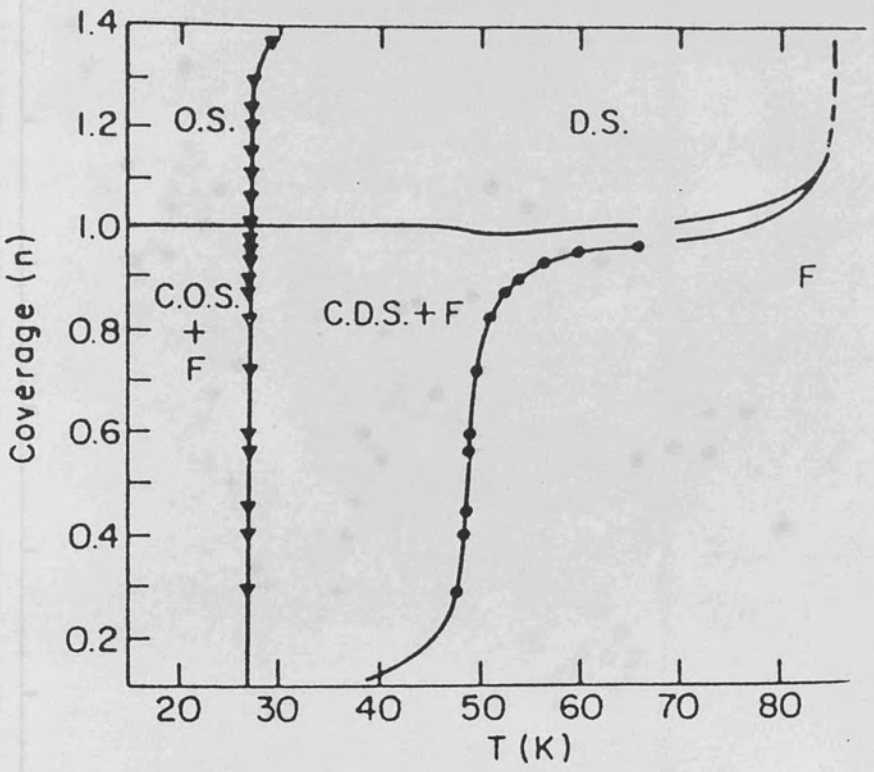

Figure(12.1.1) Phase diagram for first layer nitrogen on graphite according to Miner *et al* (1983). n= 1 is completed commensurate layer; O, S, D, C and F refer respectively to ordered, solid, disordered, commensurate and fluid.

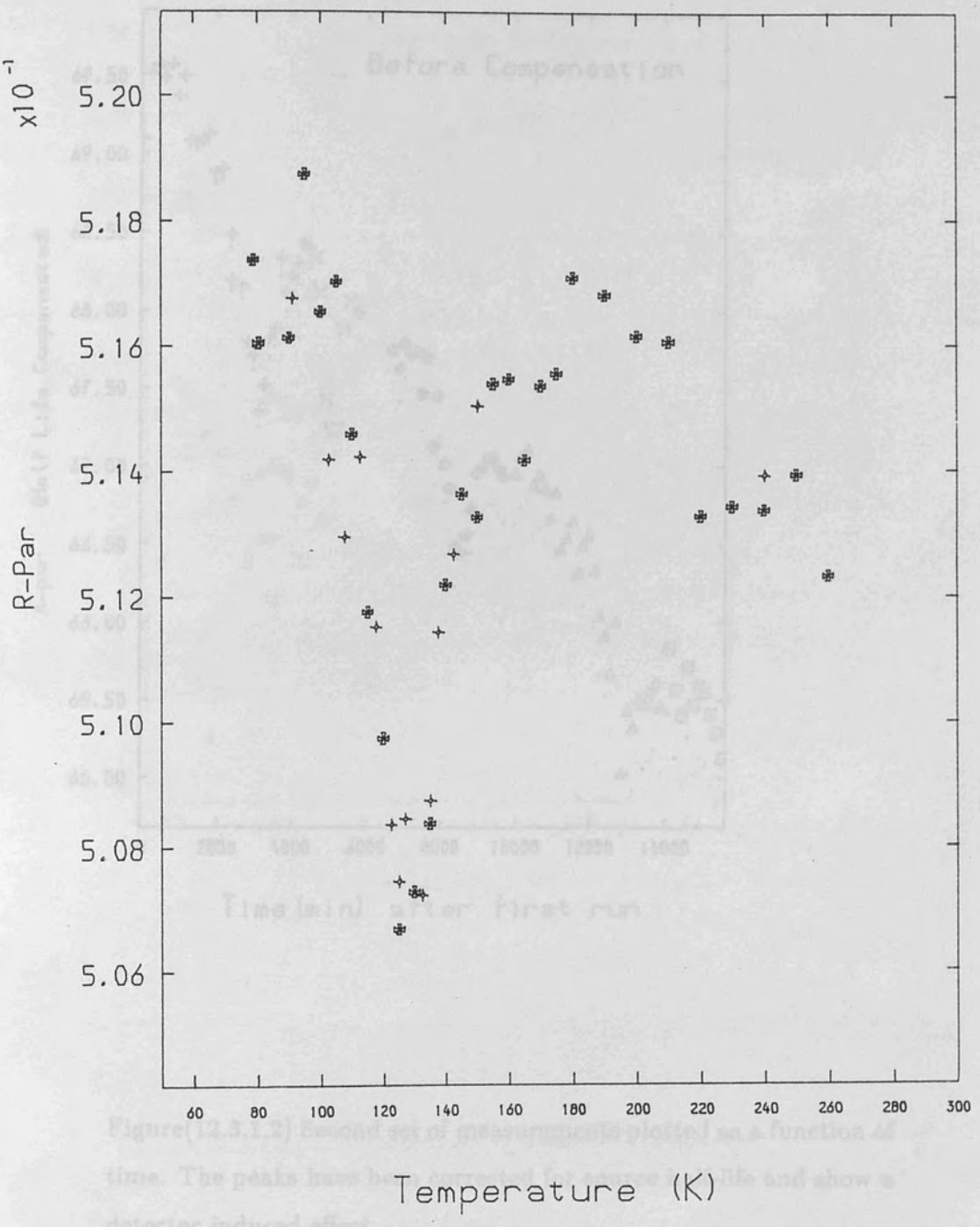

Figure(12.3.1.1) The R-parameter for the peak at 127K.

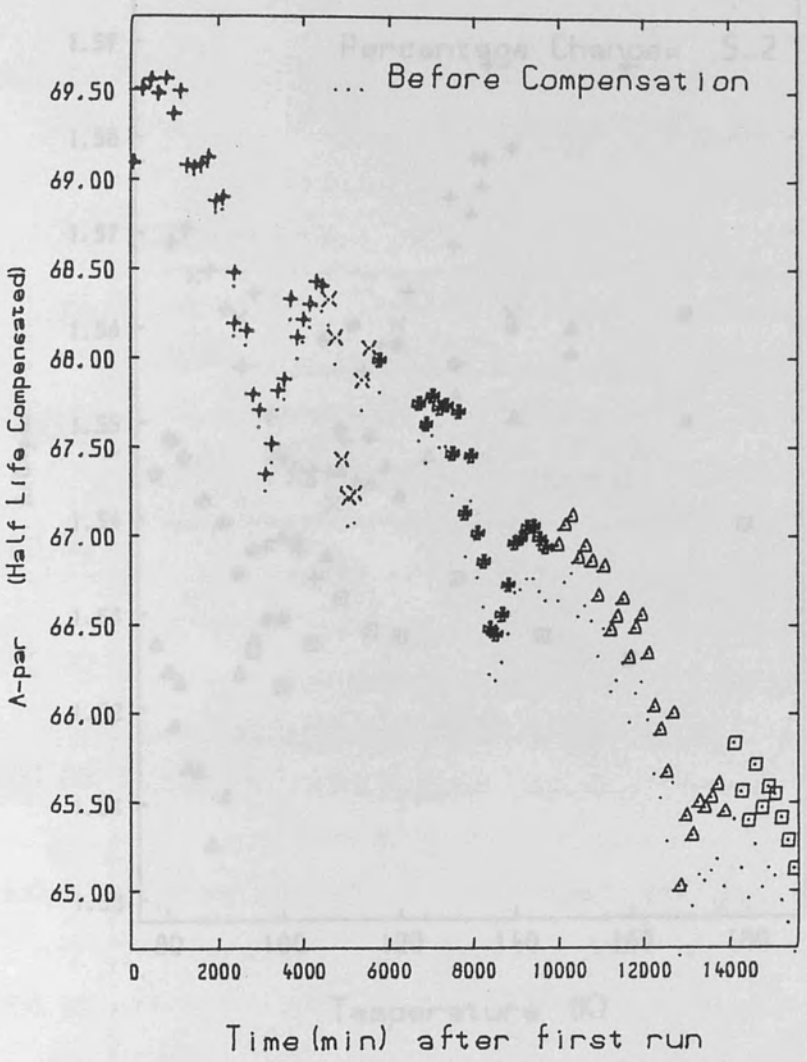

Figure(12.3.1.2) Second set of measurements plotted as a function of time. The peaks have been corrected for source half-life and show a detector induced effect.

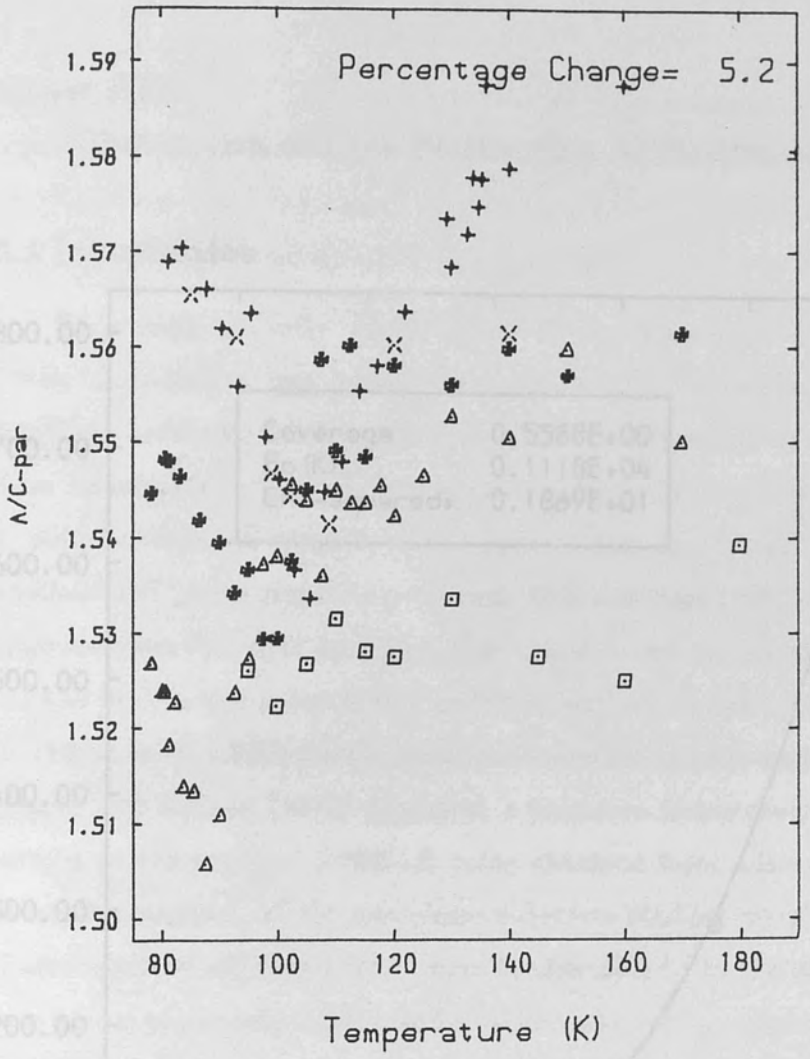

Figure(12.3.1.3) The second set of peaks vs temperature.

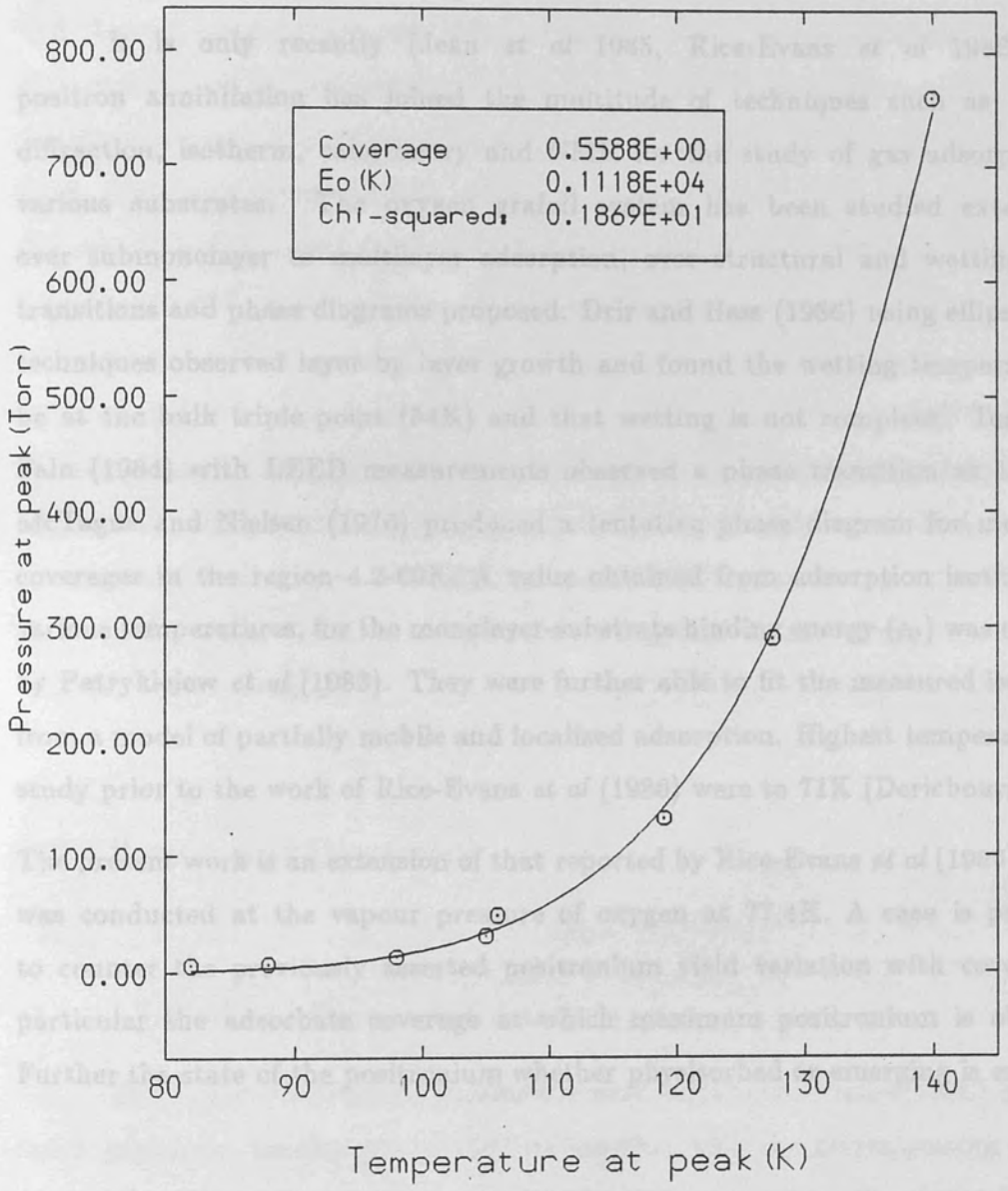

Figure(12.3.1.4) Pressure at peak vs temperature fitted with the Boltzmann expression.

Chapter XIII

Observation of Para-Positronium in Oxygen on Grafoil

§13.1 Introduction

It is only recently (Jean *et al* 1985, Rice-Evans *et al* 1986), that positron annihilation has joined the multitude of techniques such as neutron diffraction, isotherm, calorimetry and NMR for the study of gas adsorption on various substrates. The oxygen grafoil system has been studied extensively, over submonolayer to multilayer adsorption, over structural and wetting phase transitions and phase diagrams proposed. Drir and Hess (1986) using ellipsometric techniques observed layer by layer growth and found the wetting temperature to be at the bulk triple point (54K) and that wetting is not complete. Toney and Fain (1984) with LEED measurements observed a phase transition at 18K and McTague and Nielsen (1976) produced a tentative phase diagram for monolayer coverages in the region 4.2-60K. A value obtained from adsorption isotherms at various temperatures, for the monolayer-substrate binding energy (ϵ_0) was reported by Patrykiejew *et al* (1983). They were further able to fit the measured isotherms from a model of partially mobile and localized adsorption. Highest temperatures of study prior to the work of Rice-Evans *et al* (1986) were to 71K (Dericbourg 1976).

The present work is an extension of that reported by Rice-Evans *et al* (1986), which was conducted at the vapour pressure of oxygen at 77.4K. A case is presented to counter the previously asserted positronium yield variation with coverage in particular the adsorbate coverage at which maximum positronium is obtained. Further the state of the positronium whether physisorbed or emerging is explored.

§13.2 Experimental Method

After heat treatment for 12 hours at 470K a set of grafoil vacuum runs was taken between 470-90K. Before sample chamber charging with oxygen the gas feed line was evacuated and flushed. Enough oxygen gas (research grade of 99.97% purity) was allowed into the cooled sample chamber to ensure collection of a pool

at the bottom. For the first set of measurements the Druck pressure transmitter with readout on a furnace DTC was employed. The Druck read vapour pressure was 156±2Torr. Sample temperature was maintained throughout the charging process at 250K. Two hour runs were begun from this 250K to 78K. Lowest temperature runs were taken with the temperature controlling DTC disconnected, as its residual output would have prevented attainment of 78K. At the same pressure, repeat measurements were taken starting at 150K and reaching 300K. This completed the first oxygen on grafoil experiment. For the next set the oxygen pressure was reduced to 91Torr by decanting at 300K and runs taken between 300-80K. A process of pressure ~halving was repeated to a final pressure of 1.5±1.0Torr at 170K, providing a set of 9 peaks, including a repeat measurement. After a break a final peak accompanied by a vacuum measurement was taken. The DPI101 pressure indicator and 0-52Torr transducer were employed for measurement of pressure. After initial charging to vapour pressure, oxygen was decanted in an attempt to obtain a pressure only just under 156Torr, acheiving 135±0.5Torr at 300K and a single direction sweep between 300-80K taken. Mean run pressures were recorded throughout.

§13.3 Results and Discussion

§13.3.1 Lineshape Parameter Analysis

The F and positronium parameters were calculated. Figure(13.3.1.1) shows the F-parameter for the run at 156Torr together with the corresponding vacuum runs. The shown F-parameter was calculated from a centroid area of (7+1+7) channels, without prior background subtractions. Under these channels F essentially measures the ratio of free to core electron contributions. The percentage change of some 9% increased when fewer centroid area channels, such as (5+1+5) or even (3+1+3) were chosen; however the scatter also increased. This increase with narrowing centroid area indicates that the effect is due to a narrow component and

not from changes in conduction electron density. The consistently above grafoil in vacuum F is attributed to the surrounding gaseous oxygen. The F-parameter from 300-160K shows a trend similar to the vacuum line, from 160-105K it rises, 105K-90K appears to be a plateau which is followed by a sudden drop. One may note that the left hand side fall is more abrupt than the rise. Presumably if measurements could have continued to below 78K, F would have approached a level below the lowest right hand side points. Figure(13.3.1.2) shows F for the first two oxygen sets. The second peak is seen to shift leftwards by ~10 deg. as the pressure is dropped from 156 to 91Torr. Figure(13.3.1.3) is the F-parameter for later sets. The leftwards movement was chased until for the lowest pressure peak there was only a hint of a rise. Figure(13.3.1.4) shows the o-Ps parameter variation for the ninth set with a start pressure at 250K of 16torr which included a repeat, temperature rising, scan. The characteristic sign of o-Ps production is observed with a change of some 2%. The F-parameter for the same set, figure(13.3.1.5), shows no sign of hysteresis in the go back points indicating perhaps low adlayer coverage. An attempt was made to fit the F-parameter based upon the two-state trapping model and with the assumption of a fluid state for the adsorbed film, *i.e.* using the Boltzmann relation for vapour pressure. The expression derived was (see appendix A)

$$F = \frac{F_l(1+\alpha t) + A\,F_h t^{-\frac{3}{2}} \exp(\ \epsilon_0/t)}{1 + A\,t^{-\frac{3}{2}} \exp(\ \epsilon_0/t)} \qquad (13.1)$$

where F_l, F_h are the low and high limits respectively of F, t temperature, ϵ_0 adatom-substrate binding energy and A and α constants. The $(1+\alpha t)$ term is included for extrapolation of the high temperature trend. Figures(13.3.1.6) and (13.3.1.7) show two attempts at fitting. In the second fit the plateau points are not included. The value of ϵ_0, 2101K, for the first attempt is far too high when compared to reported values (1050K: Patrykiejew *et al* 1983, 1065K: Pan *et al* 1982, Bienfait *et al* 1984) but a more reasonable 1109K is obtained in the second. The Boltzmann expression (chapter 2) was also used directly to fit the pressure at the start of each rise against temperature

$$P = C\frac{N_a}{A} t^{\frac{3}{2}} \exp(-\epsilon_0/t) \qquad (13.2)$$

where C is a constant and N_a/A the number of molecules per unit area. A nearest neighbour distance of 3.5Å may be used (Patrykiejew and Jaroniec 1980), which compares to the 4.26Å of a registered $\sqrt{3} \times \sqrt{3}$ adlayer. Below 3.5Å the Lennard-Jones 6-12 potential for oxygen becomes repulsive. The effective area of oxygen is thus taken to be $13.6Å^2$ so that (13.2) may be written

$$P = 2370xt^{\frac{3}{2}} \exp(-\epsilon_0/t) \tag{13.3}$$

where x is coverage as a fraction of 100% and P pressure(Torr). Figure(13.3.1.8) shows a most satisfactory fit which produced an attractive value for ϵ_0, 1040 ± 30K, together with an expected low coverage.

§13.3.2 Pressure Variation

The pressure variation for the final measurement is shown in figure(13.3.2.1) with the corresponding F-parameter peak. A broad step is discerned which is interpreted, by comparision to an isotherm of adsorbed volume versus pressure (chapter 2 and 9) as the formation of a monolayer, the point of inflexion indicating half-coverage. The nonzero slope at higher temperatures is the background pressure variation. It is seen that, with temperature decreasing, the rise in F corresponds to the change of slope in pressure and that F reaches a maximum at the point of inflexion in the pressure curve. Additionally on closer inspection the abrupt lower temperature drop of F appears to coincide with a sharper decline in pressure. It follows that positronium emission increases with the formation of an adlayer to reach a maximum at half-coverage and to fall again with further adsorption. This conclusion is in qualitive agreement with the work of Jean *et al* (1985) who observed a peak in the lifetime of surface positrons (but who fixed the *o*-Ps component). However it contradicts earlier work (Rice-Evans *et al* 1986, Moussavi-Madani 1986). A fit was performed on the pressure data of figure(13.3.2.1) using a variant of equation(13.1) (see chapter 9) and this produced $\epsilon_0 = 1050 \pm 30$K, figure(13.3.2.2). The very brisk left hand side fall of F makes the peak asymmetrical and is in contrast to the other gases. The fall may indicate a positronium decline not caused

by monolayer build up. It may be the case that a configurational change in the adlayer occurs above a critical coverage (between 0.5-1) leaving insufficient space for positronium to form.

§13.3.3 Convolution Analysis

Following an initial two component analysis efforts were concentrated on three component fits. In the analysis error function backgrounds were subtracted prior to fitting from both the resolution and experimental lineshapes. Figure(13.3.3.1) shows for the vapour pressure run first gaussian intensity and width and figure(13.3.3.3) parabola intensity and width. Figure(13.3.3.2) shows the third component intensity and width. The narrow or *p*-Ps component peak is evident at a width of ~3 channels reaching a maximum intensity of ~12%. In general the addition of the third component was found to increase disproportionately the computing time required and all but those at the F-parameter peak failed to converge satisfactorily. This difficulty in fitting is illustrated by the large scatter in the narrow component width and intensity. A method of fixing the third component width was adopted for maximum efficiency and this lead not only to rapid convergence but minimised scatter. Figure(6.4.2) shows a typical three component fit. Figure(13.3.3.4) shows the intensity variation when the width is fixed at 4 channels. This intensity variation was also fitted with equation(13.1), figure(13.3.3.5), and gave $\epsilon_0 = 1070 \pm 30$K. The lineshape analysis was carried out for the remaining oxygen sets and figure(13.3.3.6) shows several results together.

Lynn and Lutz (1980) studied oxygen chemisorption on aluminium with a low energy positron beam and made the observation that a high percentage of Ps is formed in the para state, because of a spin exchange process. *O*-Ps quenching may also result from chemical reaction with strong reagent molecules (Eldrup *et al* 1975, Anisimov and Molin 1976, Jean *et al* 1984). The present work is corroborative, a high *p*-Ps yield is obtained without the expected *o*-Ps level (some three times the *p*-Ps level), leading to an assertion of chemical quenching by the triplet oxygen. Analysis was performed to determine the state of the *p*-Ps on annihilation, namely whether it

is trapped or moving, fast, positronium. Platzmann and Tzoar (1985) propose a model for Ps in which it stands away, physisorbed, from the substrate at a distance of some twice the Ps diameter (4Å) and on annihilation has only zero point motion energy in a direction normal to the surface and thermal motion parallel to the surface. Figure(13.3.3.7) from Platzmann, shows the localized Ps. The model of a positron bound by its 'image-correlation-potential' well (Nieminen and Manninen 1974, Hodges and Stott 1973) also produces anisotropy between surface normal and parallel directions. An alternative approach (Lynn *et al* 1985) is of desorbed, fast Ps. Actual creation of positronium may be from electron capture by thermally detrapped surface positrons. Indeed positronium formation because of the release of 6.8eV binding energy may be the only means of escape of the positron from surface traps at temperatures not sufficiently high for thermal desorption. Fast Ps may also be produced by emerging 'hot' positrons (Gullikson and Mills 1986).

An optimal width was determined for the *p*-Ps component. For a given measurement spectra about the F-parameter peak were selected and the χ^2/ν over the centroid evaluated for second gaussian widths of 1-7 channels. Figure(13.3.3.8) shows the results for the seven sets analysed. The peaks with lower χ^2/ν have higher F-parameter values and hence greater narrow component content. There appears to be an inclination for a minimum at ~4 channels. Figure(13.3.3.9) shows the variation for the peak at 105K where a minimum is more obvious.

Based on this optimal width a calculation was performed (see also Rice-Evans *et al* 1981) to obtain the positronium velocity (v_{ps}). Similar to equations(7.1 - 3)

$$v_{ps} = \frac{\Delta E}{m_o c} \tag{13.3}$$

where ΔE is the energy spread (2×4 channels, at 90eV/channel), m_o in this case the positronium rest mass and c the velocity of light. (13.3) gives $v_{ps} = 2.1 \times 10^5 m/s$. Using this in

$$E_{ps} = \frac{1}{2} m_o v_{ps}^2 \tag{13.4}$$

yields 0.25eV for the positronium energy (E_{ps}). Additionally the uncertainty principle

$$\Delta p \Delta x = \hbar \tag{13.5}$$

where Δp is the uncertainty in momentum, Δx that in position and $\hbar = h/2\pi$ (h being Planck's constant) produces $\Delta x = 2.76$Å. The 0.25eV energy for positronium seems to favour Ps trapping at the surface as it is of the correct order of magnitude for zero-point motion. However it is still an order of magnitude above thermal energies so that the possibility of flying Ps cannot be ruled against.

Positronium formation at solid surfaces is conventionally described by the Born approximation. Ishii (1987) included higher order contributions in a quantum mechanical treatment to calculate the Ps distribution. He arrived at an equation which by varying initial conditions encompassed experimental results from a range of materials. In a simple solid the Ps spectrum due to electronic band structure may be described as in figure(13.3.3.10) where ϕ_{ps} is the Ps workfunction which, from chapter 1, is essentially $\phi_+ + \phi_- - 6.8$eV (ϕ_+ and ϕ_- being positron and electron workfunctions respectively and 6.8eV Ps binding energy). It is seen that electrons having an energy between E_F and $E_F + \phi_{ps}$ may be picked up to form Ps. An inability of the first-order Born approximation to explain experimental results was found by Howell *et al* (1987) from work on Ni(100), figure(13.3.3.11) where solid circles mark experimental data and the dotted line the calculated distribution. Likewise the Born approximation may be expected to break down for the present grafoil work and a model which produces maximum Ps intensity at only 0.25eV require formulation.

The rise then fall in Ps annihilations observed for the gases studied may have an alternative explanation to that of maximum surface trapping at half coverage. It may be that surface trapping in particular Ps formation would rise if unhindered up to full coverage but that the yield diminishes as a result of insufficient space for formation above a critical adlayer density, figure(13.3.3.12). If this is the case the coverage of maximum emission may be found to be a function of molecular size and ordering. Further simultaneous pressure and Doppler measurements would be required to pin-point more accurately these critical coverages.

It would also in the case of oxygen be interesting to perform measurements as a function of grafoil orientation at maximum *p*-Ps yield as the high *p*-Ps content would make possible the detection of anisotropy in Ps energy.

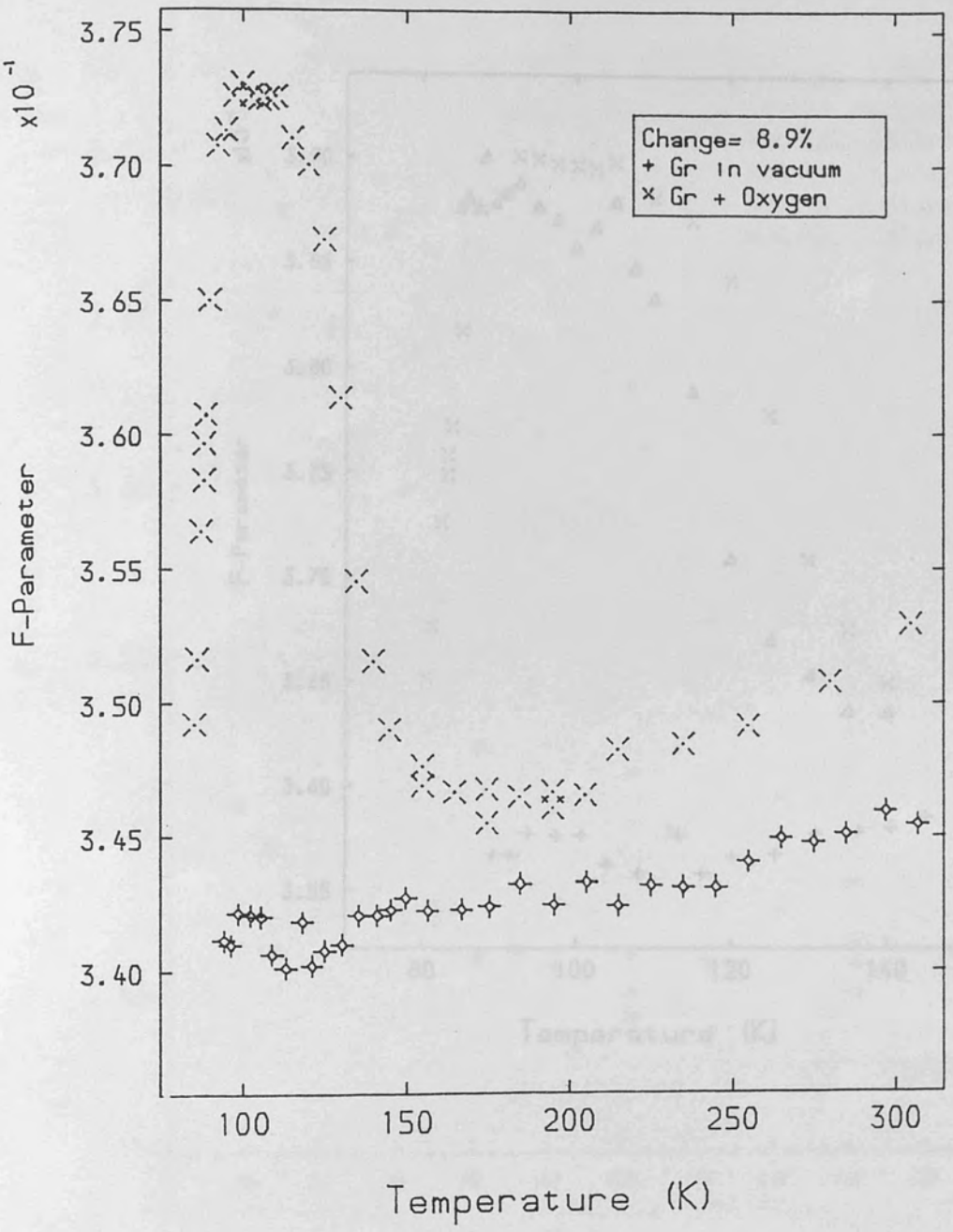

Figure(13.3.1.1) F-parameter for the V.P. peak and underlying graphite trend.

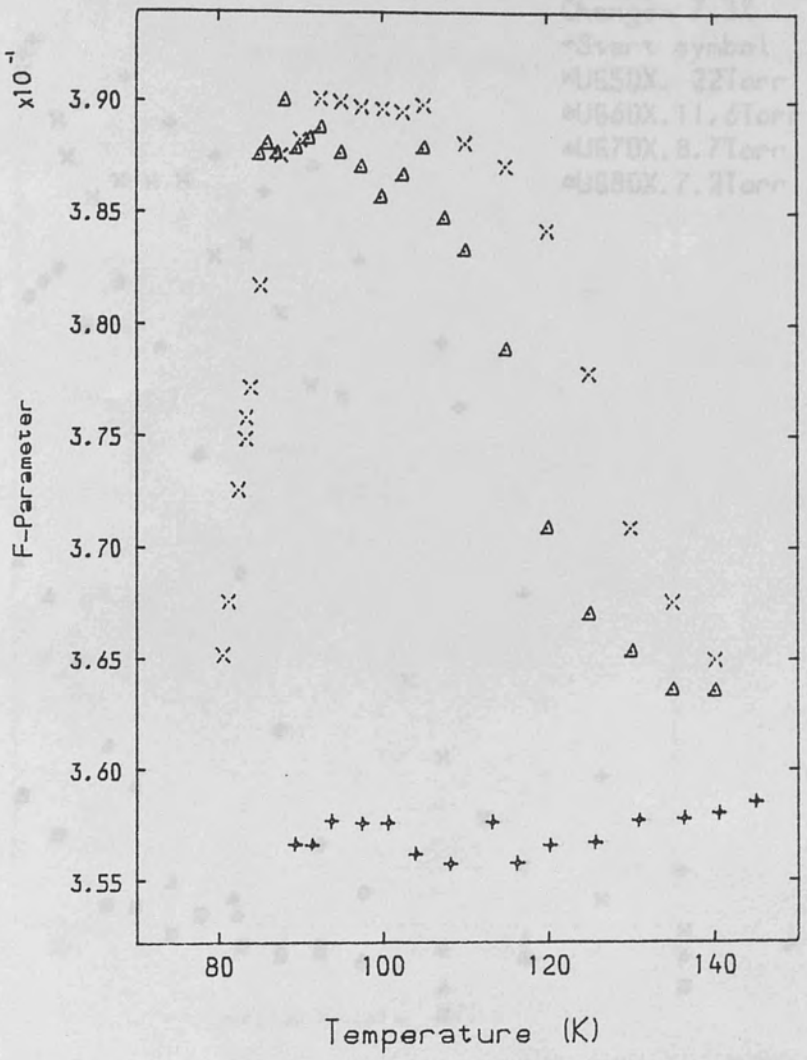

Figure(13.3.1.2) V.P. pressure F and an immediate free pressure run.

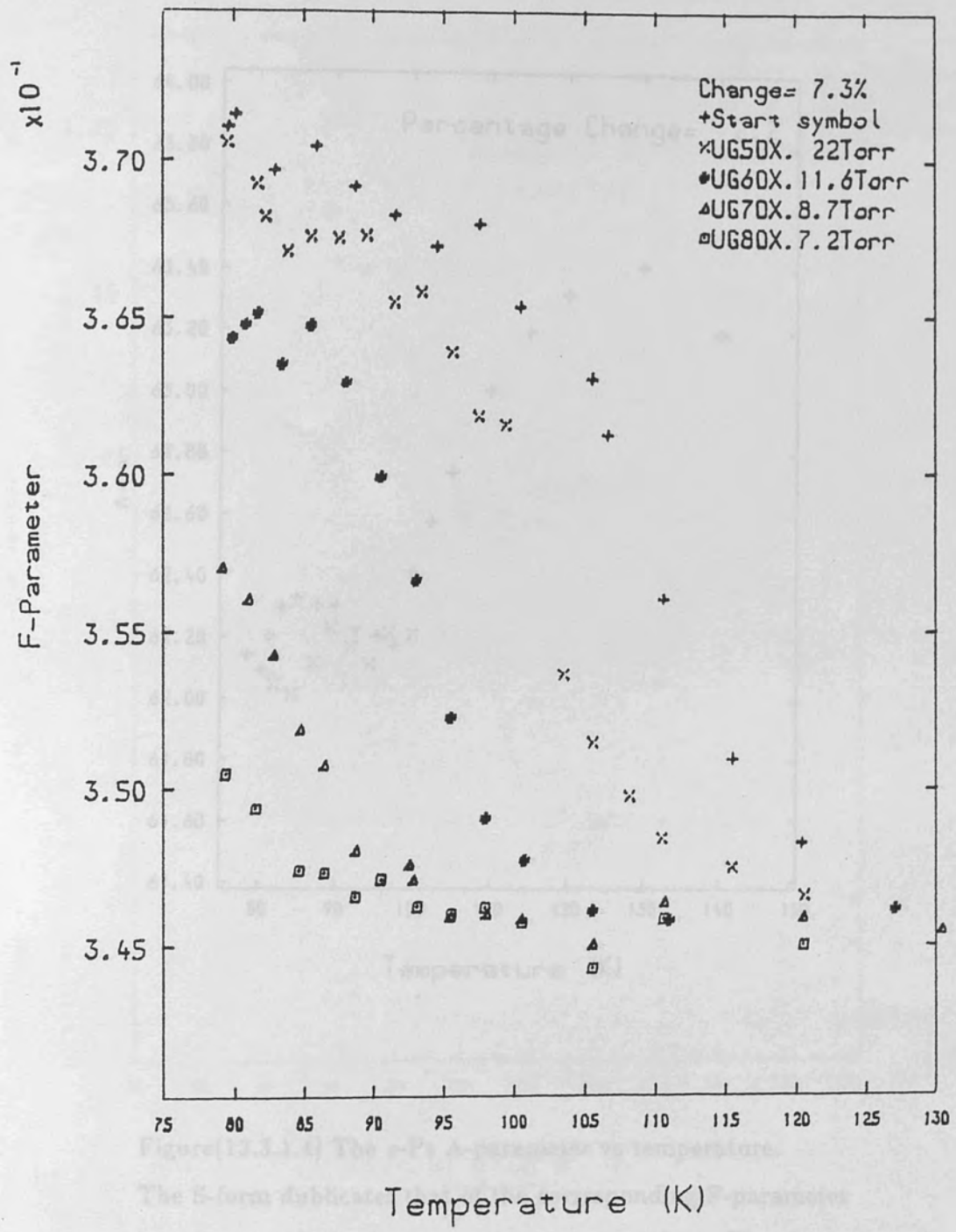

Figure(13.3.1.3) F-parameter for the lower pressure sets. The movement left was pursued until only a few points showed a rise before the 78K limit.

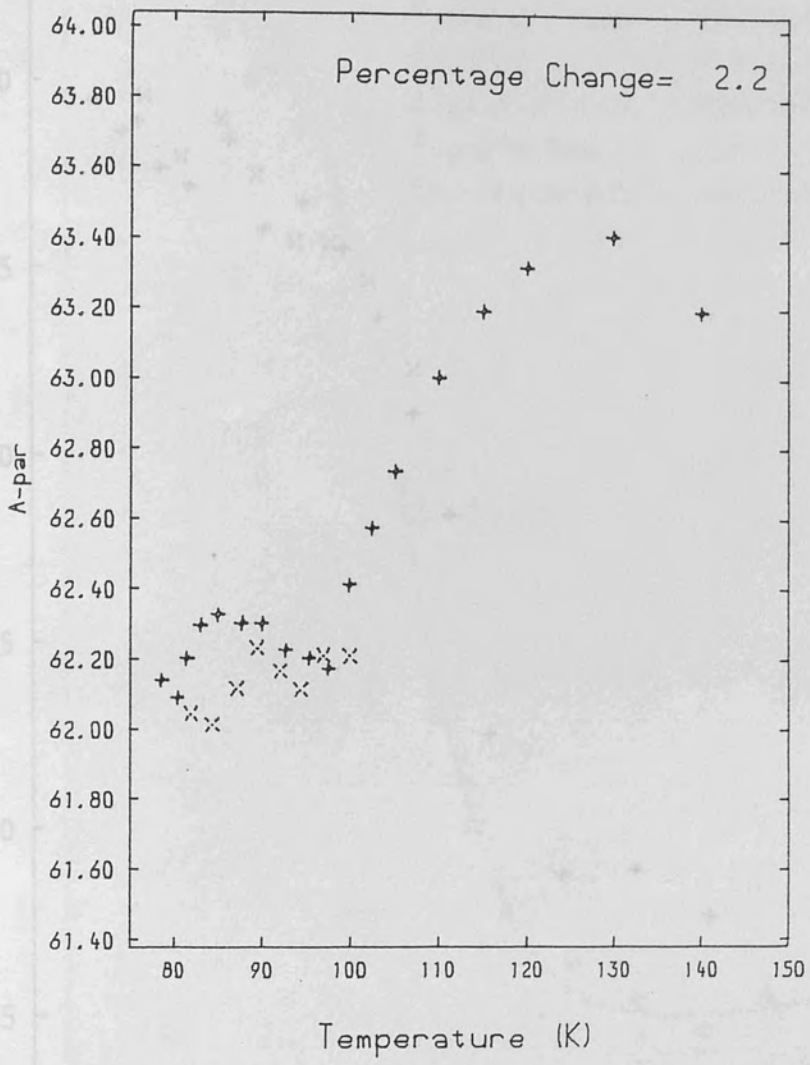

Figure(13.3.1.4) The o-Ps A-parameter vs temperature.
The S-form dublicates that of the corresponding F-parameter but does not show the expected percentage effect. The ninth set is shown, with a start pressure of 16±2Torr at 250K and which included go back points (crosses).

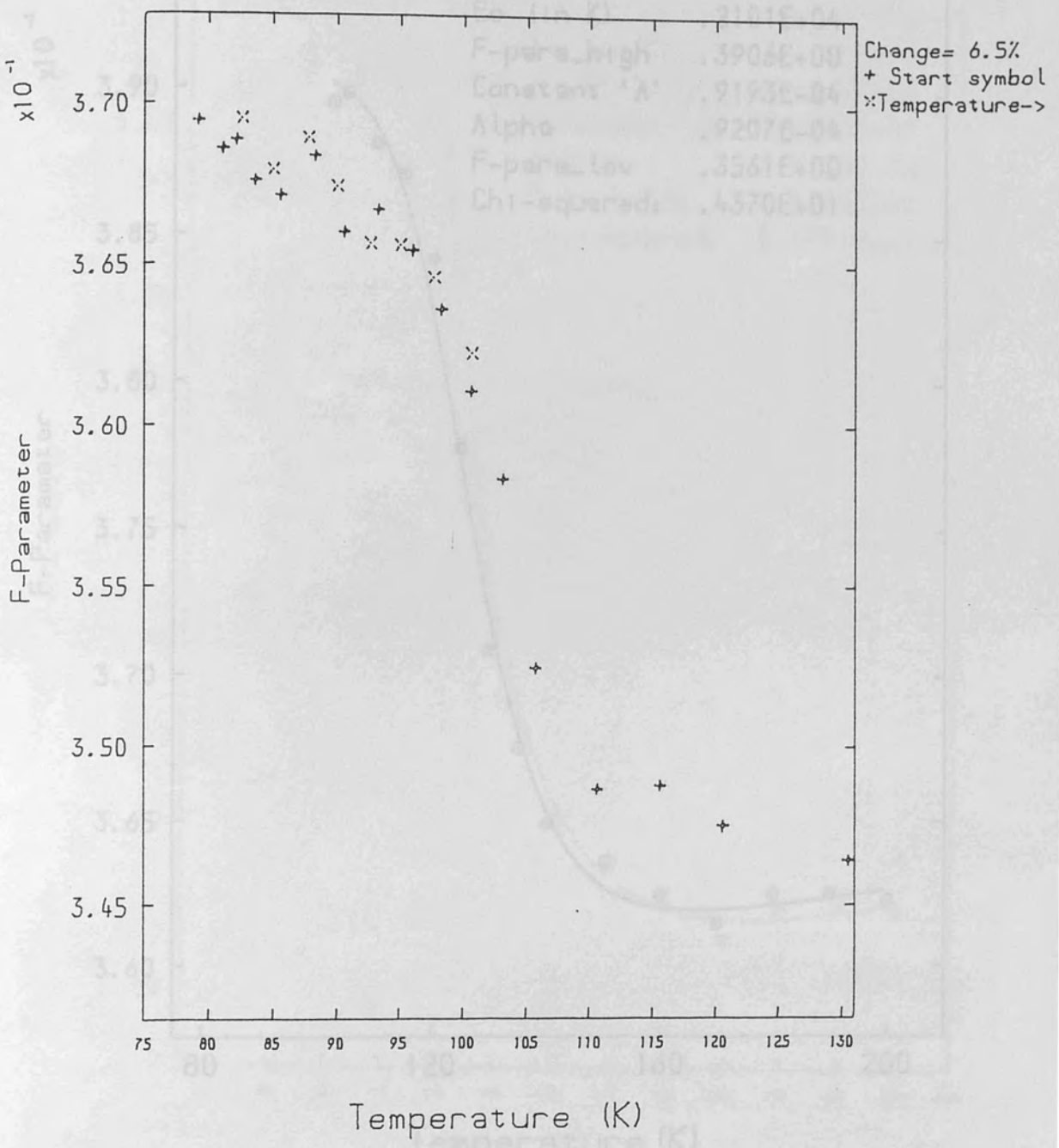

Figure(13.3.1.5) The F-parameter for the set shown in figure(13.3.1.4). F shows no hysteresis in the go back points (crosses) which perhaps indicates low (submonolayer) coverages.

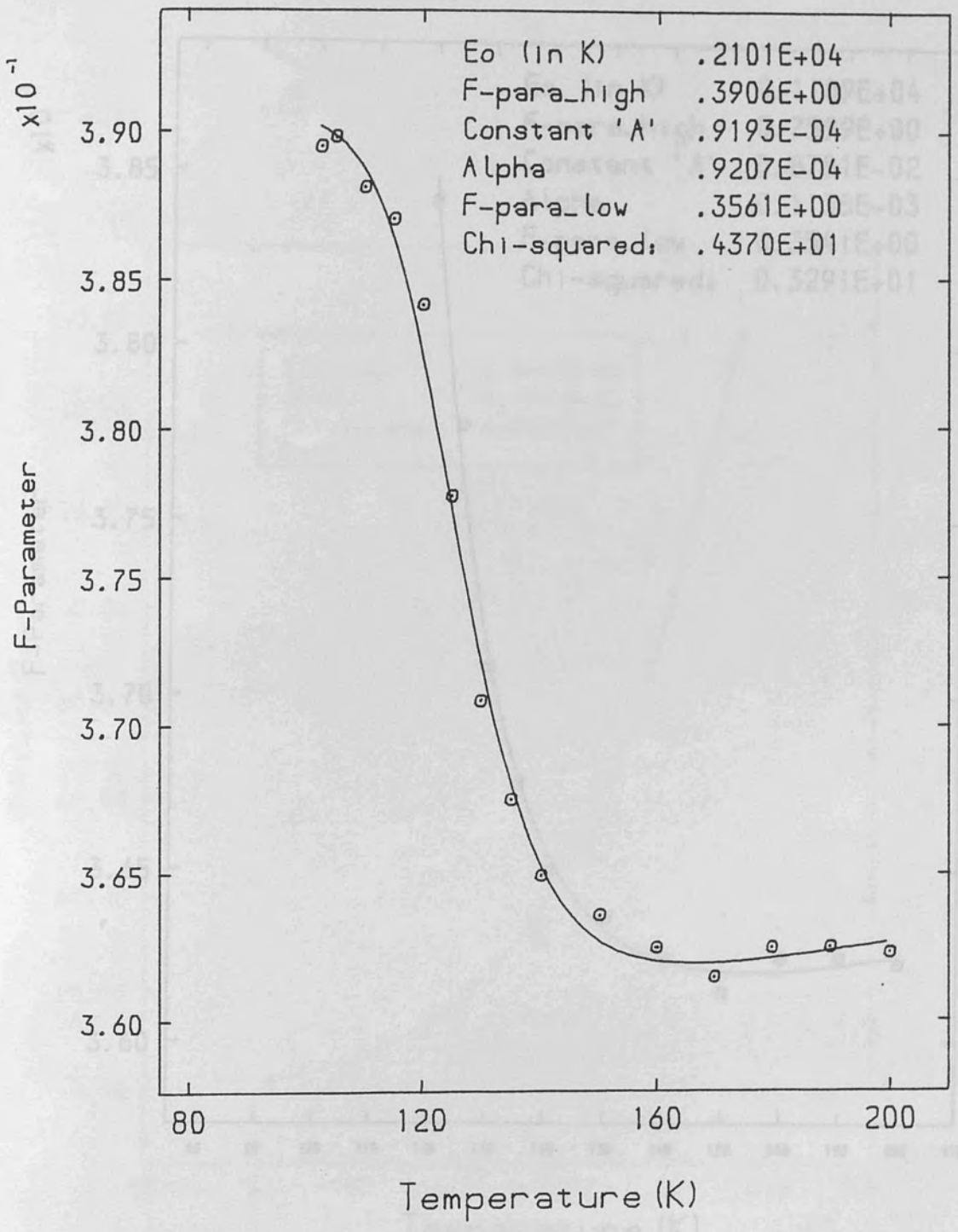

Figure(13.3.1.6) An attempt made at fitting the V.P. F-parameter with equation(13.1). The high value for ϵ_0 is a result of forced curvature at high F.

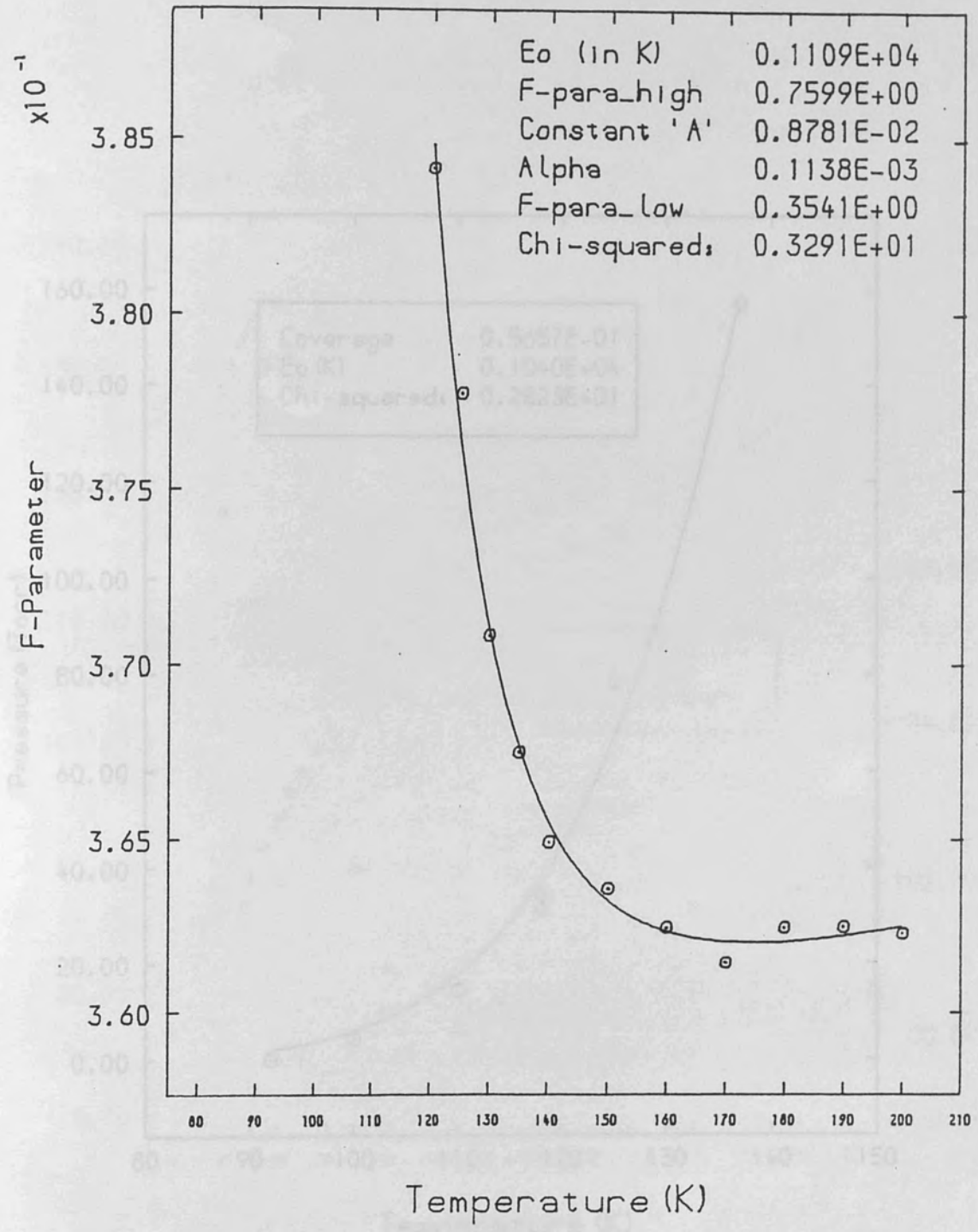

Figure(13.3.1.7) The same fit of figure(13.3.1.6) but omitting the highest F points. This results in a reasonable value of ϵ_0.

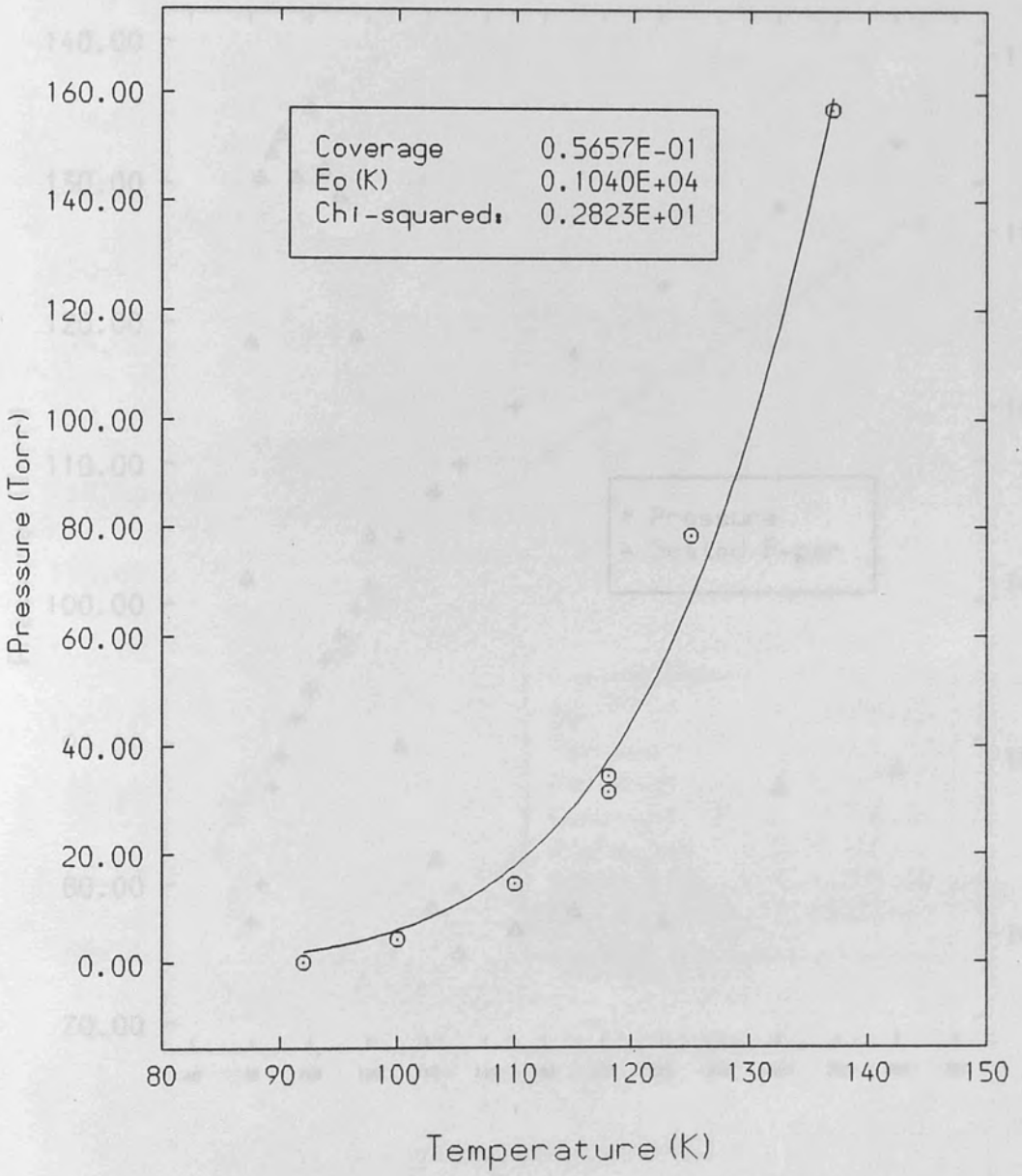

Figure(13.3.1.8) Pressure at F rise vs temperature. An unweighted fit to the Boltzmann expression has been attempted.

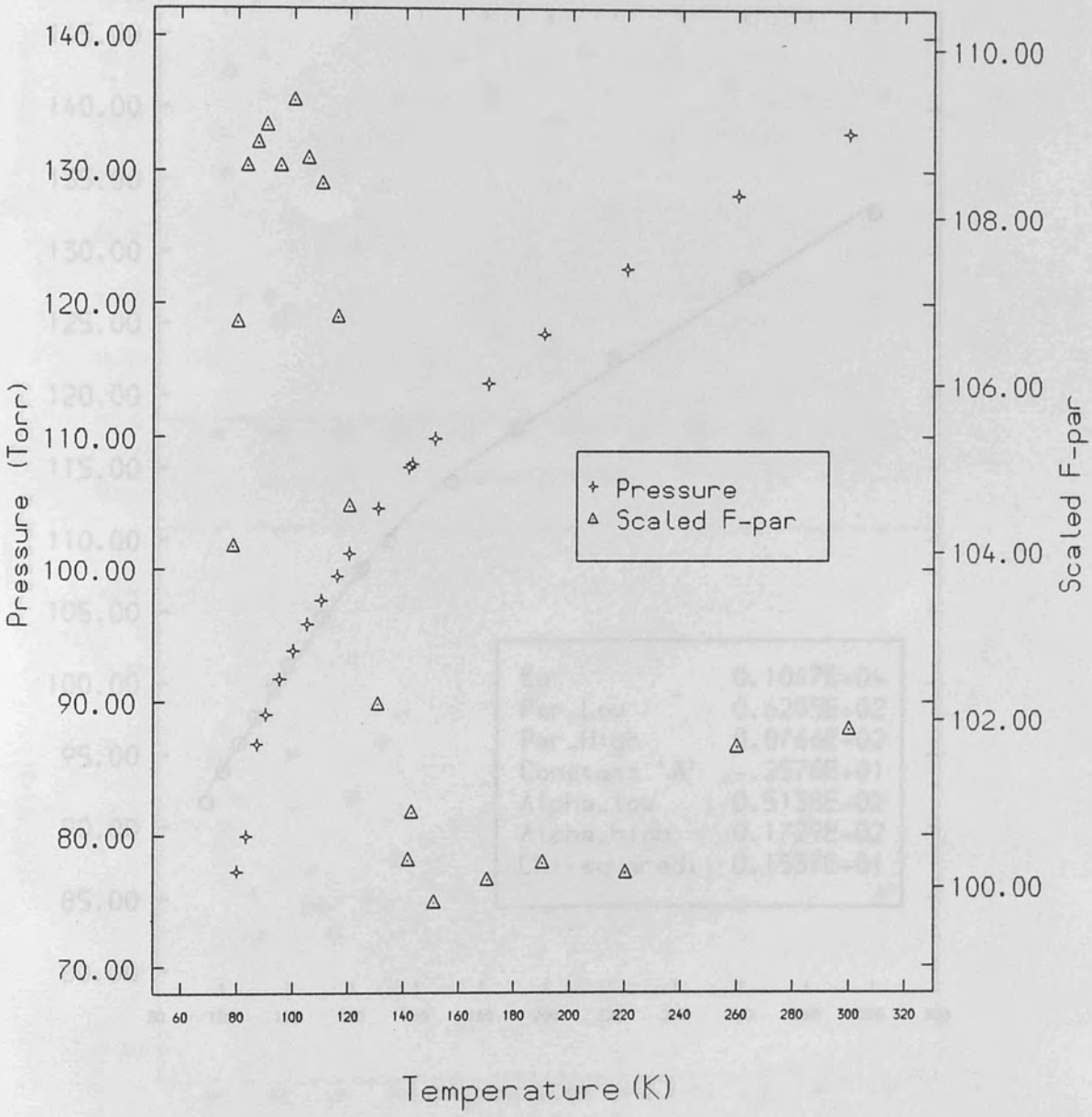

Figure(13.3.2.1) Pressure variation and F for final oxygen set.

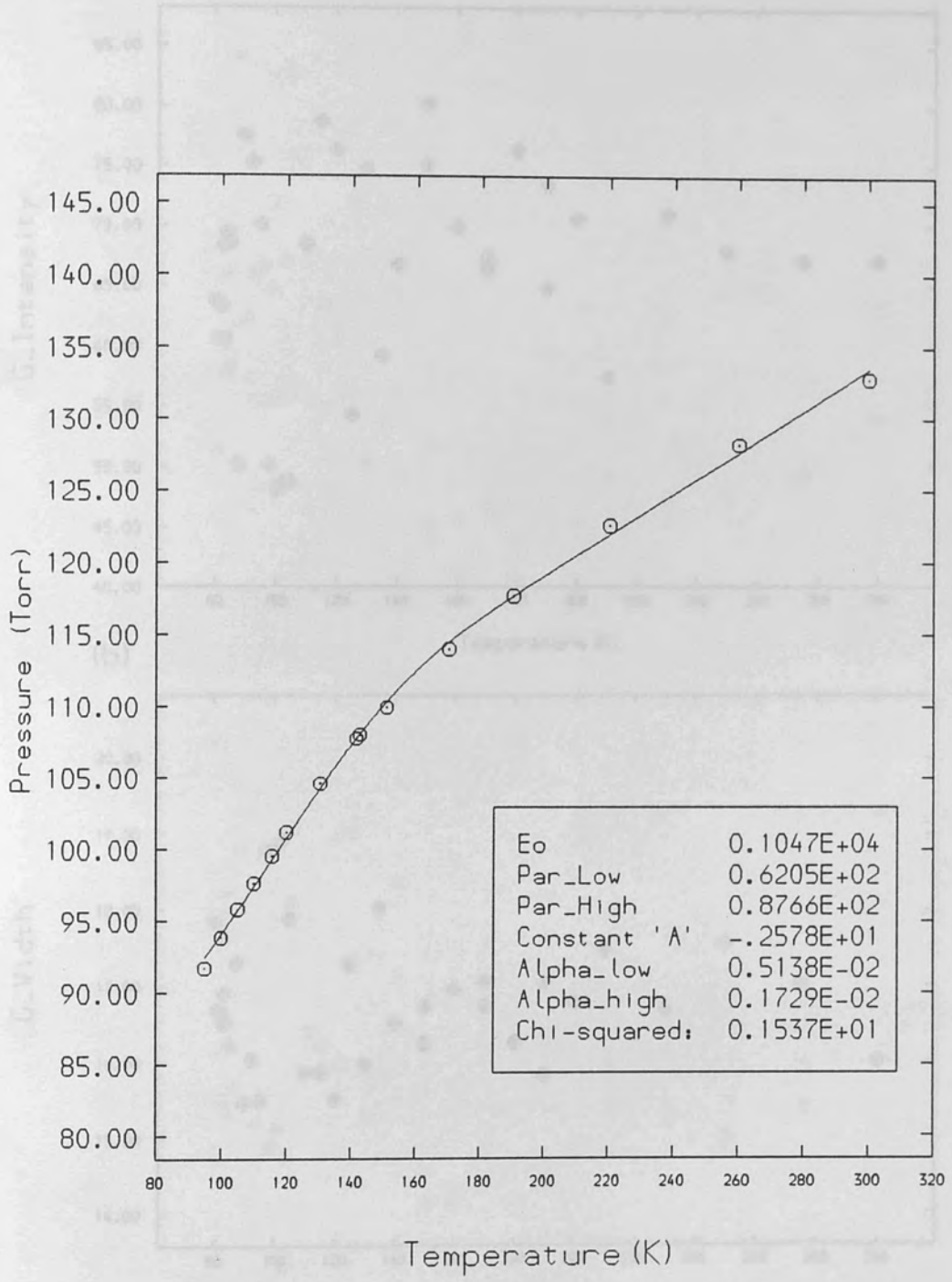

Figure(13.3.2.2) Pressure variation of final oxygen set fitted to yield ϵ_0. Only data above the sharp pressure drop have been included.

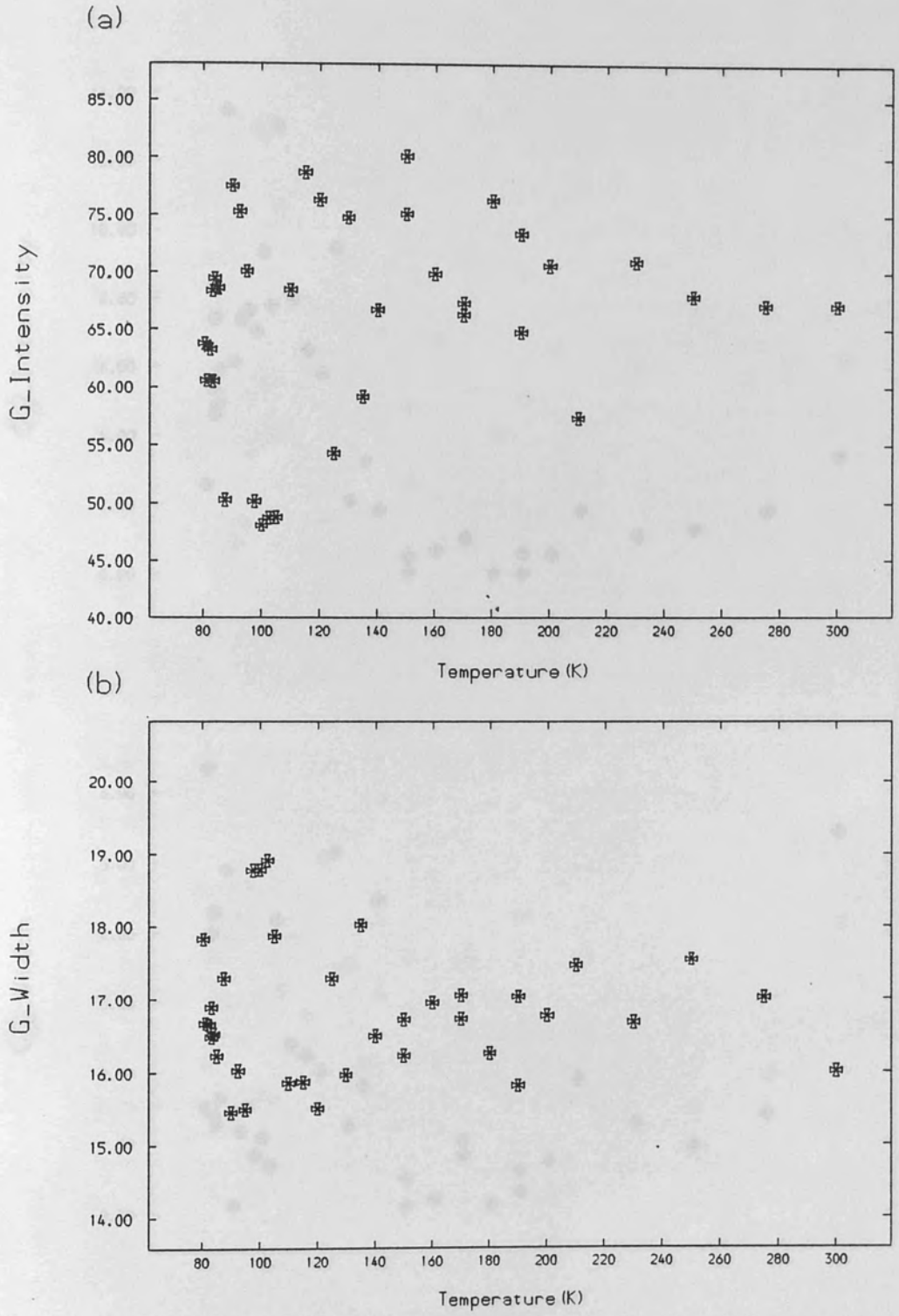

Figure(13.3.3.1) Three component analysis of grafoil + oxygen.

(a) First gaussian intensity.

(b) First gaussian width.

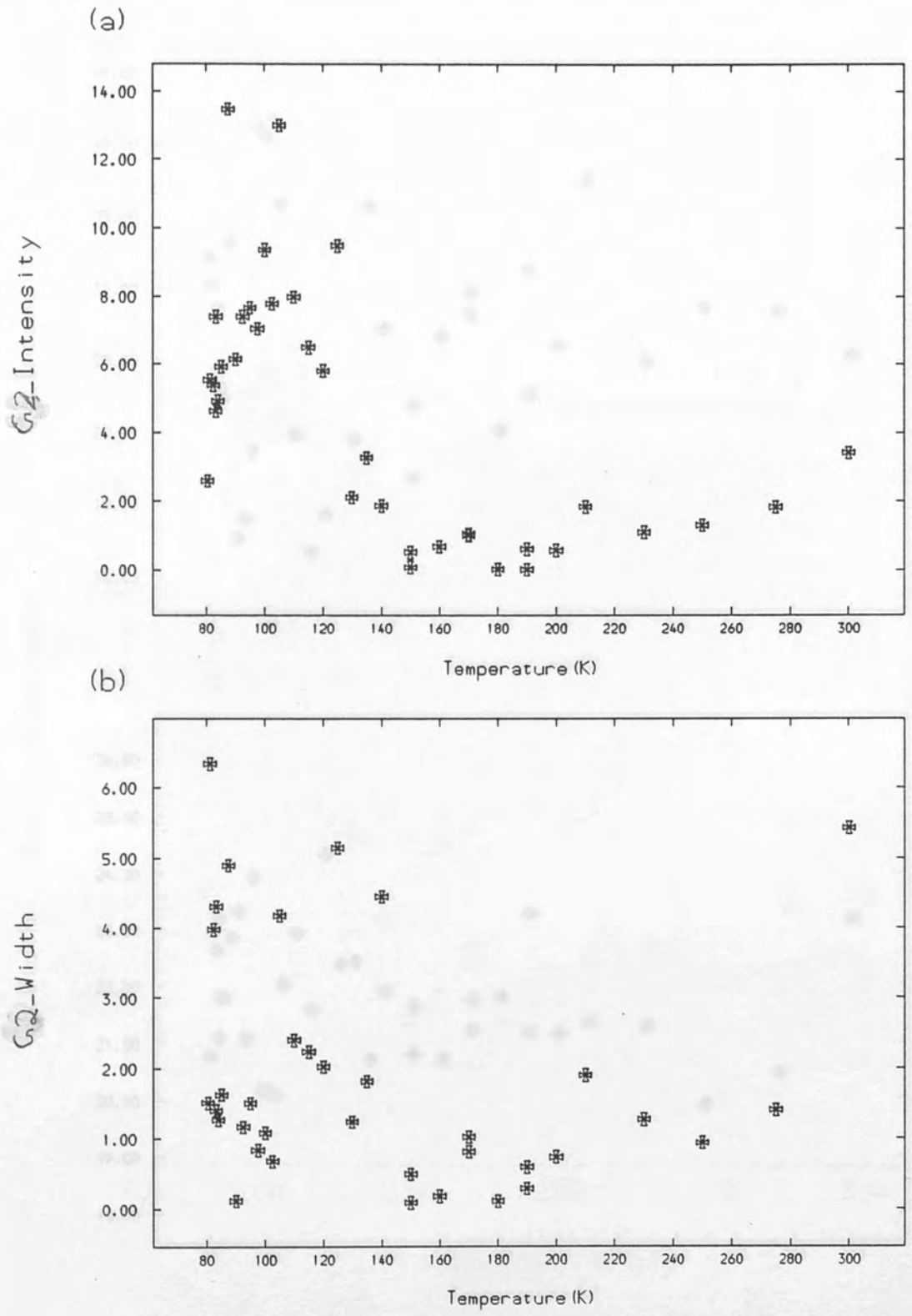

Figure(13.3.3.2) Three component analysis of grafoil + oxygen.

(a) Parabola intensity.

(b) Parabola width.

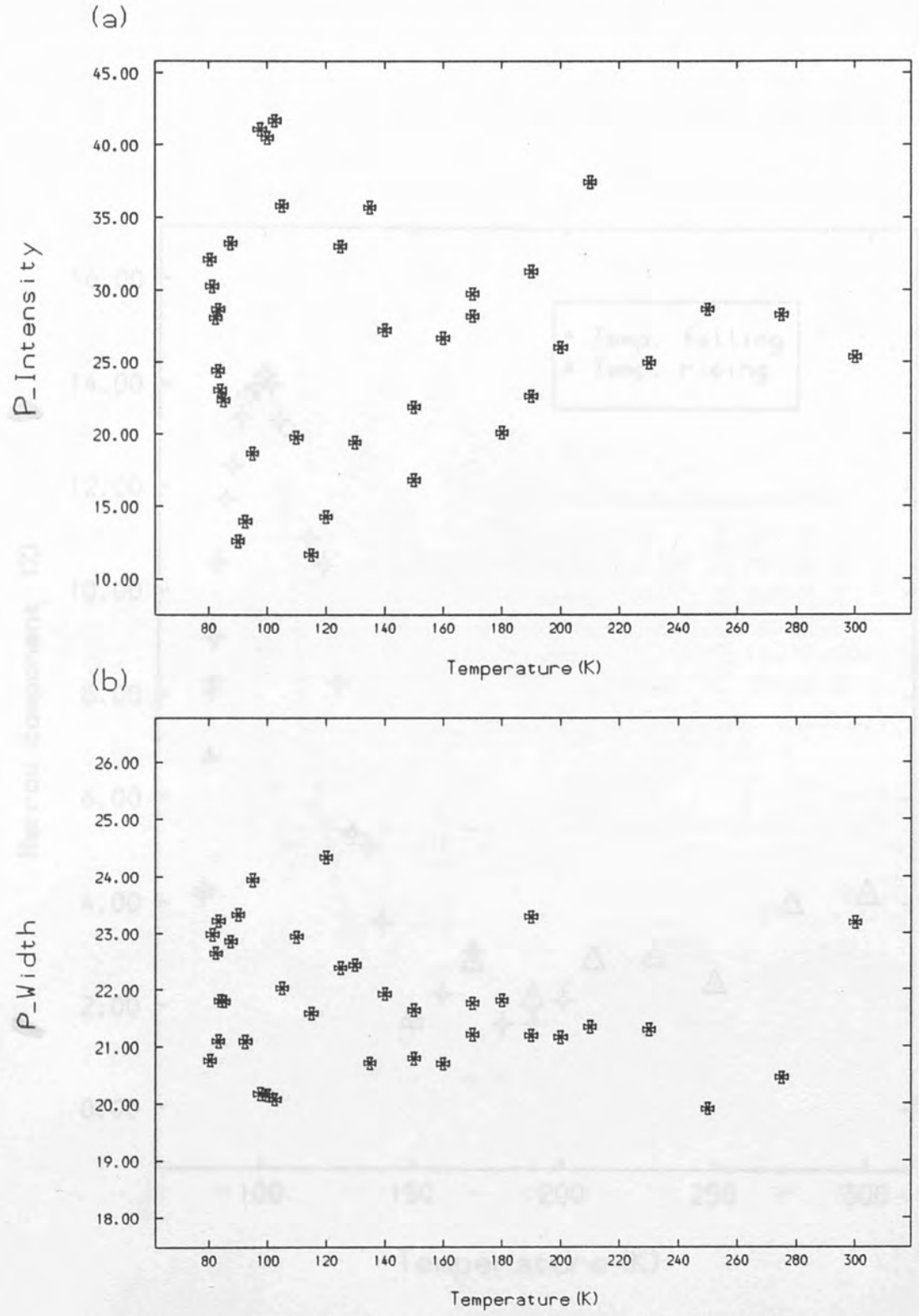

Figure(13.3.3.3) Three component analysis of grafoil + oxygen.

(a) Second (narrow) gaussian intensity.

(b) Narrow component width.

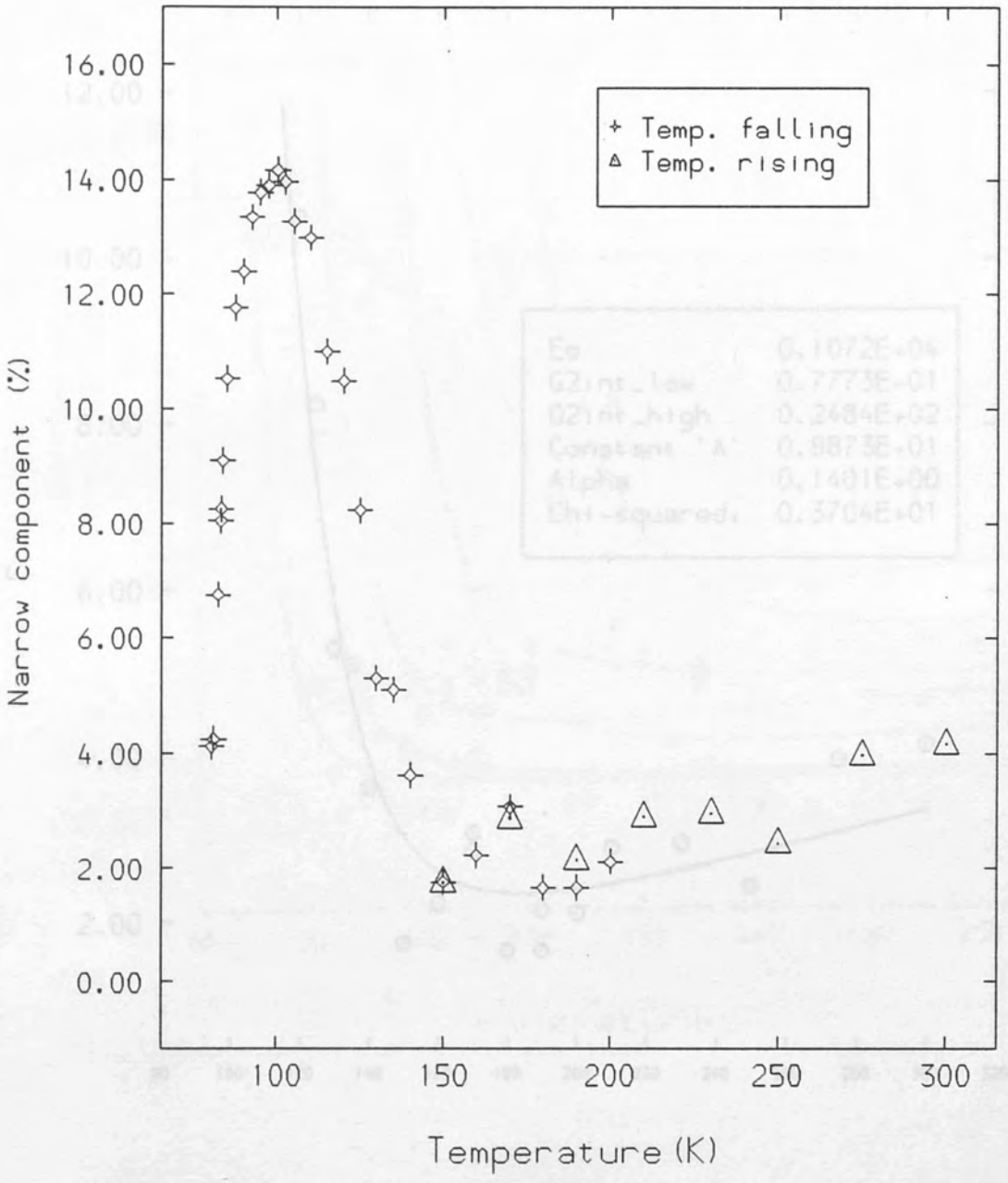

Figure(13.3.3.4) Narrow component intensity in oxygen with width fixed at 4 channels. The lack of a plateau at high intensity is in contrast to the F-parameter.

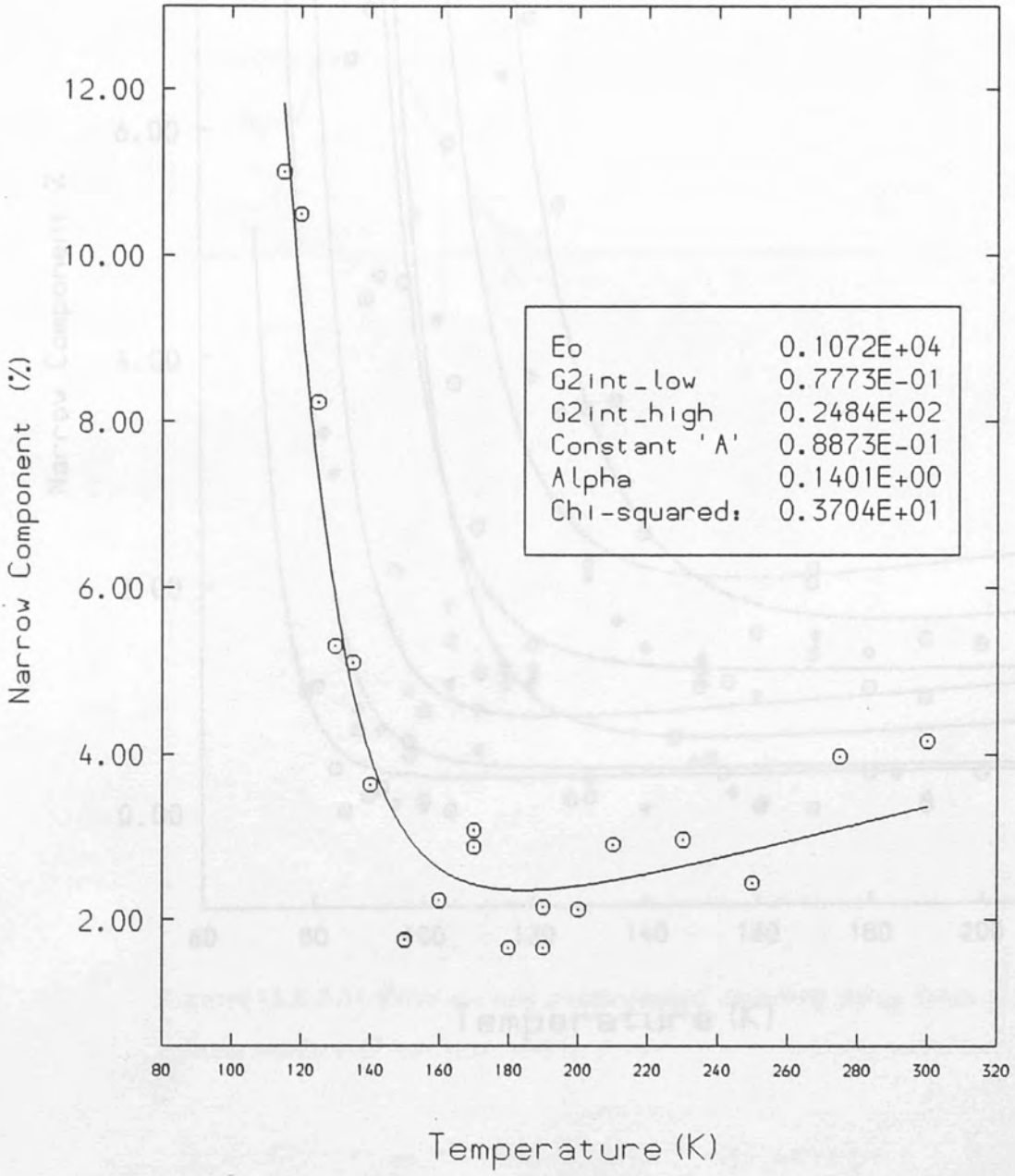

Figure(13.3.3.5) The narrow component intensity variation and trapping model derived fit.

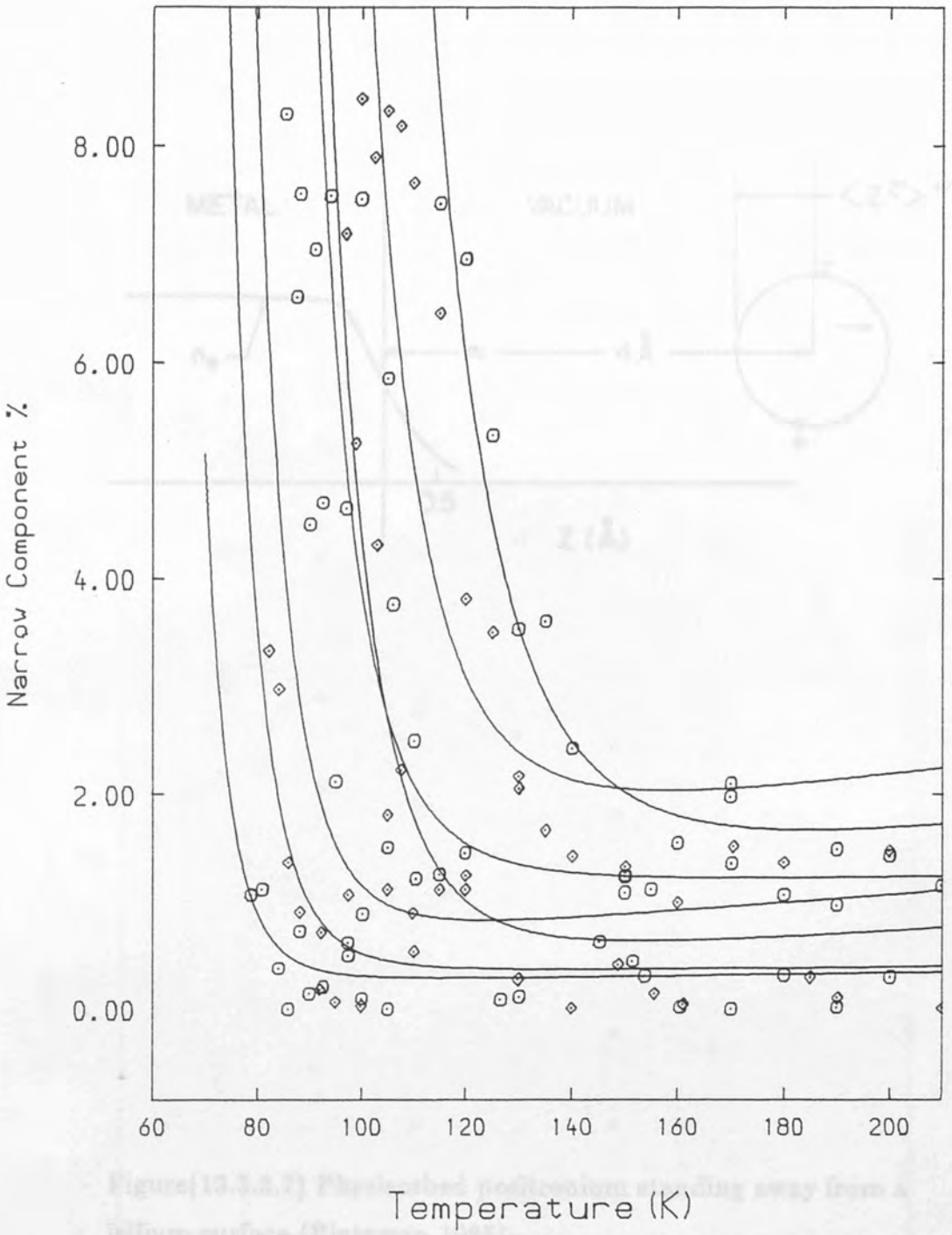

Figure(13.3.3.6) Narrow component intensity variations for several sets (width fixed at 2 channels).

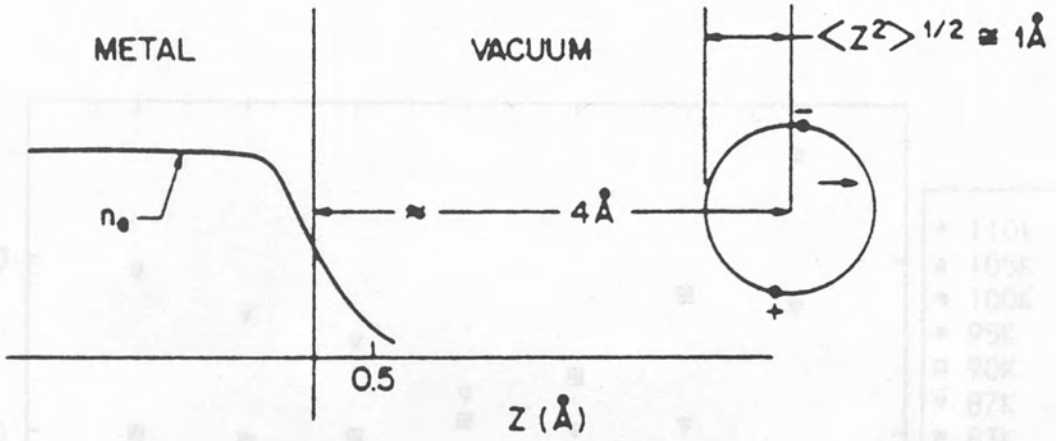

Figure(13.3.3.7) Physisorbed positronium standing away from a jellium surface (Platzman 1985).

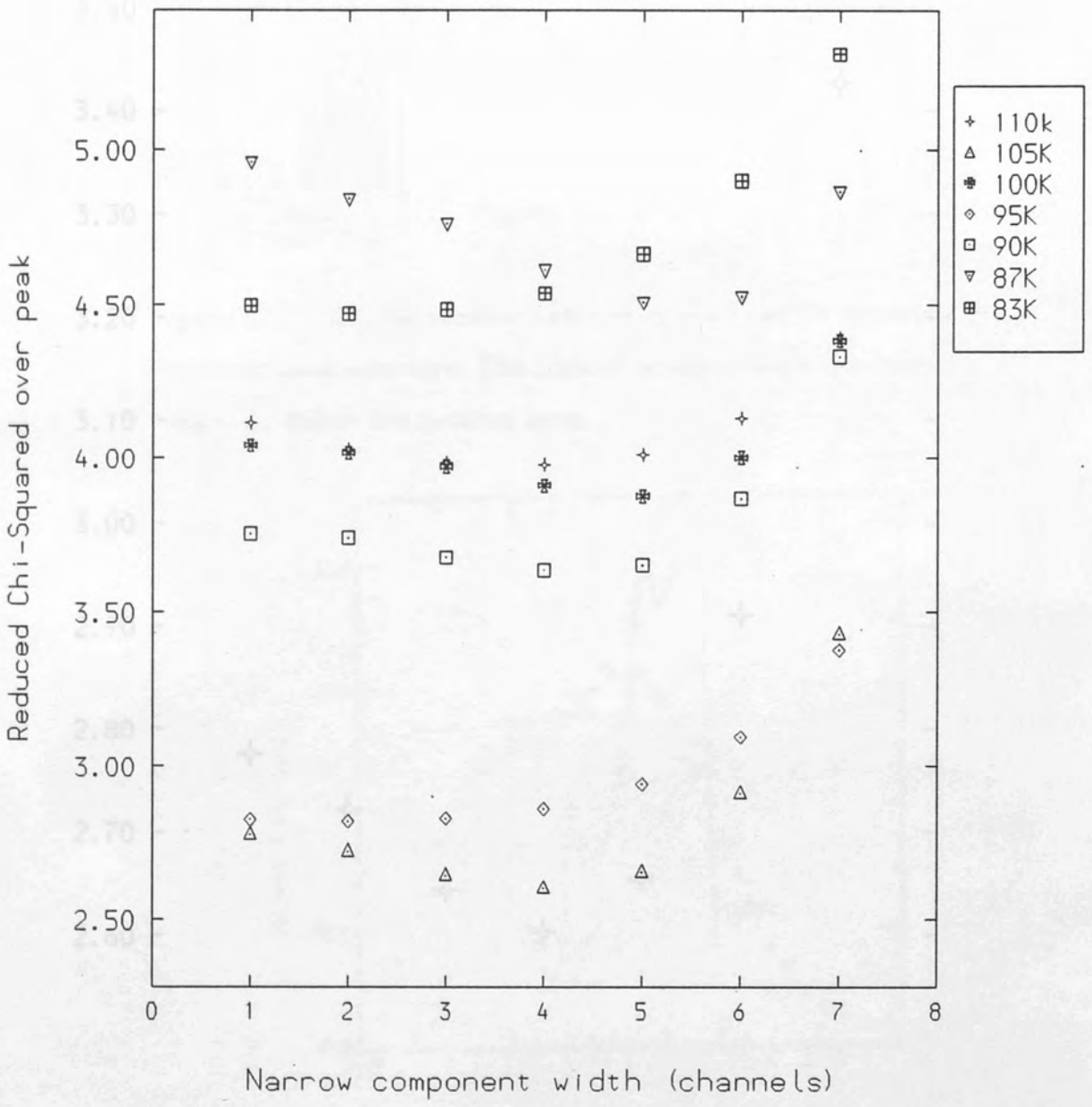

Figure(13.3.3.8) χ^2/ν over centroid channels as a function of narrow component width for seven high F-parameter spectra of the final oxygen measurement.

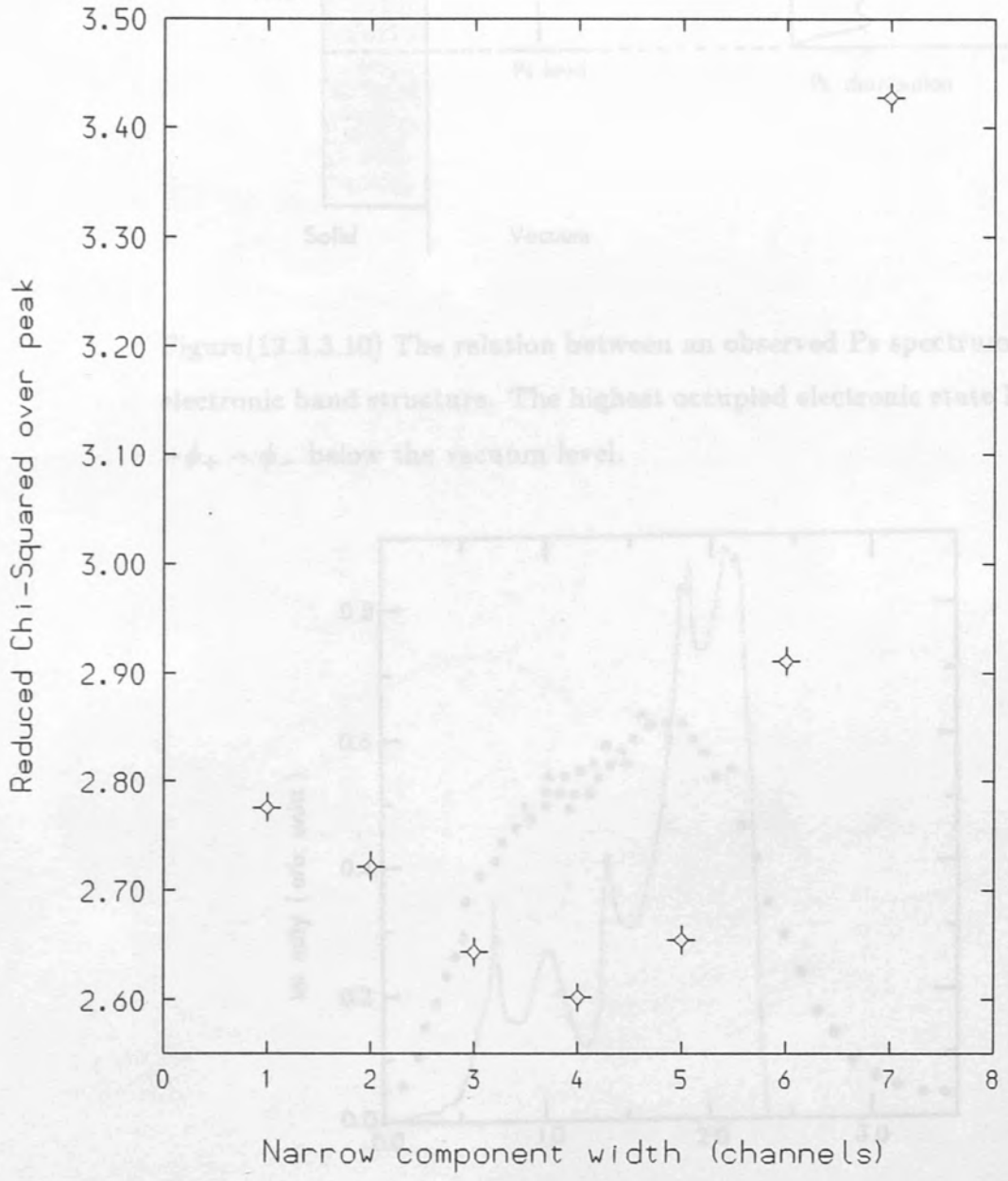

Figure(13.3.3.9) χ^2/ν over centroid channels calculated for various widths of the *p*-Ps due narrow component for the run at 105K showing more clearly the optimal width.

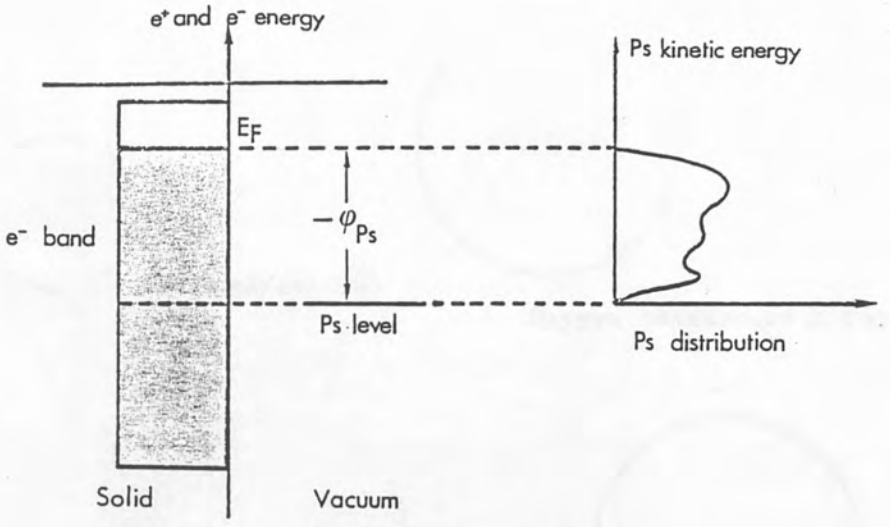

Figure(13.3.3.10) The relation between an observed Ps spectrum and electronic band structure. The highest occupied electronic state E_F is $-\phi_+ - \phi_-$ below the vacuum level.

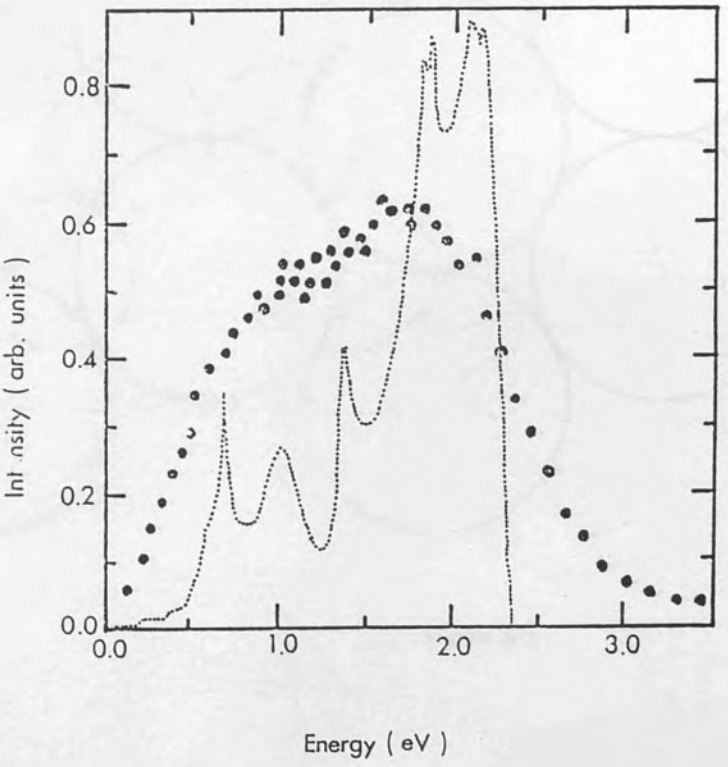

Figure(13.3.3.11) Ni(100) results of Howell *et al* (1987). The dotted line is their calculation using the first-order Born approximation.

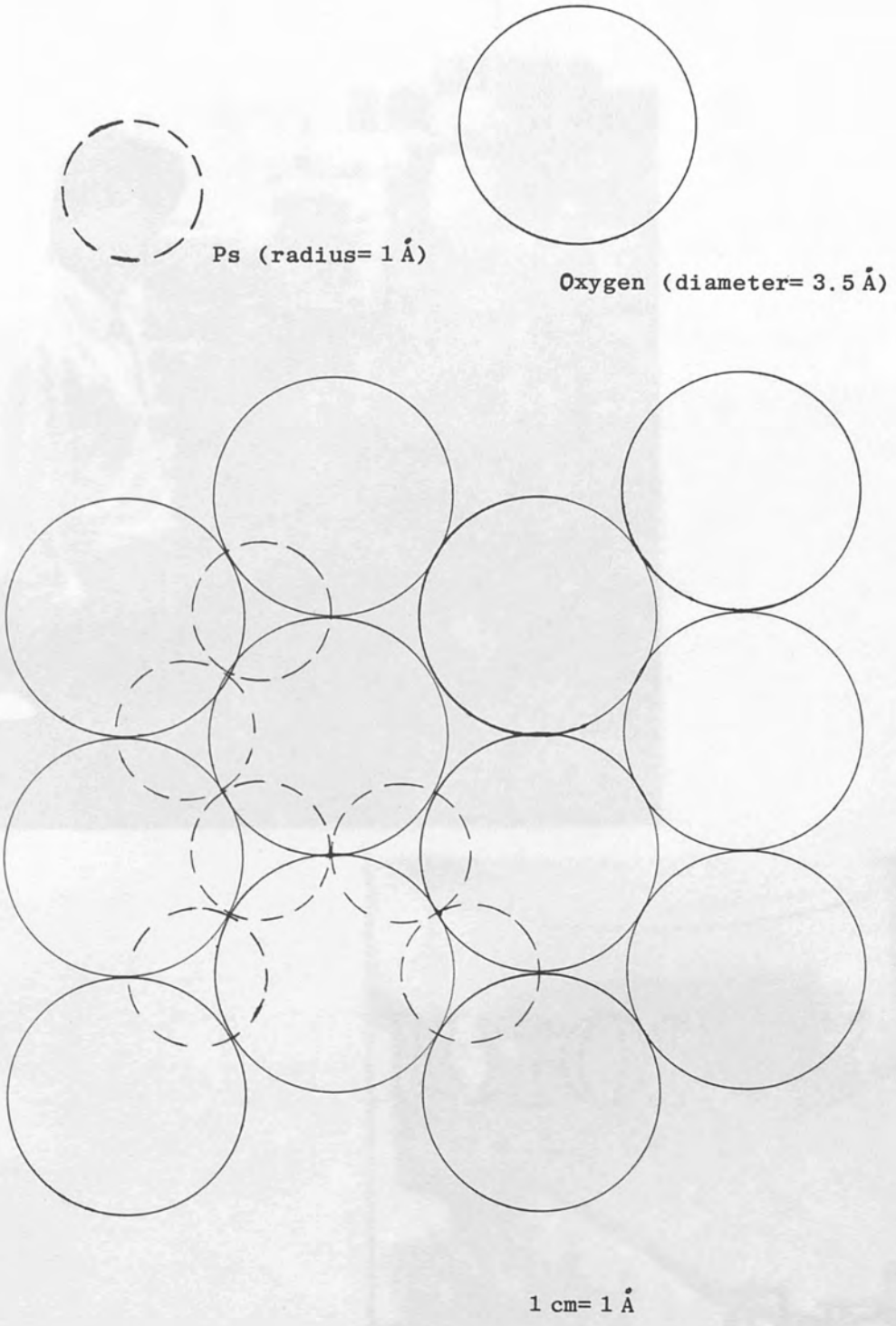

Figure(13.3.3.12) At full coverage a maximally packed adlayer leaves insufficient space for Ps to form. For convenience only the effective diameter of the oxygen molecule has been drawn.

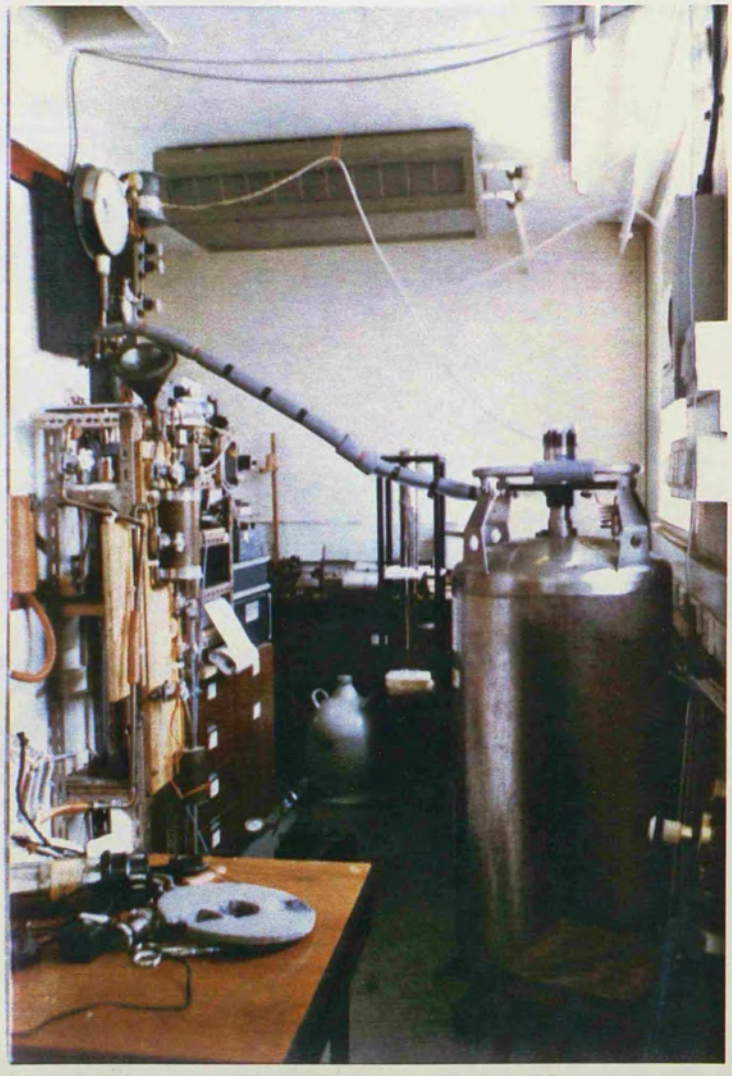

Appendix A

Formulae for F and Ps parameter fit

Assume two states *viz.* no Ps production (l) and Ps production (h), rate equations are

$$\frac{d\,n_l}{d\,t} = -\lambda_l n_l - \sigma C n_l + N = 0$$
$$\frac{d\,n_h}{d\,t} = \sigma C n_l - \lambda_h n_h = 0$$

where σ= Ps formation rate, C= density of formation sites, taken to be the density of adsorbed atoms and λ_l, λ_h the annihilation rates.

Probabilities for free and Ps annihilations are then

$$P_l = \lambda_l \left(\frac{n_l}{N}\right) = \frac{\lambda_l}{\lambda_l + \sigma C}$$
$$P_h = \lambda_h \left(\frac{n_h}{N}\right) = \frac{\sigma C}{\lambda_l + \sigma C}$$

Assuming F is a linear parameter

$$F = F_l P_l + F_h P_h = F_l(1 - P_h) + F_h P_h$$

therefore

$$F = F_l \left(1 - \frac{\sigma C}{\lambda_l + \sigma C}\right) + F_h \left(\frac{\sigma C}{\lambda_l + \sigma C}\right)$$

or

$$F = \frac{F_l \lambda_l + F_h \sigma C}{\lambda_l + \sigma C} = \frac{F_l + F_h C.const}{1 + C.const}$$

From the Boltzmann expression

$$n = \frac{\lambda P}{kT} \exp\left(\frac{\epsilon_0}{kT}\right)$$

where n is the number of adsorbed atoms and is $\propto$ C, then

$$F = \frac{F_l + F_h A T^{-\frac{3}{2}} \exp(\epsilon_0/kT)}{1 + A T^{-\frac{3}{2}} \exp(\epsilon_0/kT)}$$

where A is a constant. For fits to $2\gamma/3\gamma$ parameters this becomes

$$R = \frac{R_l - R_h A T^{-\frac{3}{2}} \exp(\epsilon_0/kT)}{1 - A T^{-\frac{3}{2}} \exp(\epsilon_0/kT)}$$

Appendix B

MCA-380Z data transfer routines

```
          ;*Master receive*
              ORG 4826
          XON     EQU 11H
          XOFF    EQU 13H
          MENREQ  EQU 18
          OUTC    EQU  1
          LPOUT   EQU  5
          KBDIN   EQU 29
          FCB     EQU 005CH
          RESET   EQU 13
          BDOS    EQU 0005
          BUFF    EQU 80H
          BUFFL   EQU 128
          COUNT   EQU 255
          CTRLZ   EQU 1AH
          CLOSE   EQU 16
          WRITE   EQU 21
          MAKE    EQU 22
          WAIT    EQU 4000H
          INTEST  EQU 0C9H
          PORT    EQU 0C8H
          TEST    EQU 2
          WAIT2   EQU 1000H
          KBDTF   EQU 32
          OPEN    EQU 0FH
          FILSIZ  EQU 23H
          READ    EQU 14H
          RCADDR  EQU 6BH
          CRADDR  EQU 7CH
          ERROR   EQU 1
          SUCCES  EQU 0
          CTRLE   EQU 5

          LD C,RESET
          CALL BDOS
          LD DE,FCB
          LD C,OPEN
          CALL BDOS
          CP 255
          JR Z,EXITEN
DISPLAY:  LD DE,FCB       ;open data file and display header
          LD C,READ
          CALL BDOS
          CP 0
          JR NZ,EOF
          LD HL,BUFF
          LD B,BUFFL
DISPREC:  LD A,(HL)
          CP CTRLZ
          JR NZ,CONTDIS
FILZERO:  LD (HL),0       ;expand buffer with ASCII nulls
          INC HL
          DEC B
          JR NZ,FILZERO
          LD A,(CRADDR)
          DEC A
          LD (CRADDR),A
          LD A,(RCADDR)
          DEC A
          LD (RCADDR),A
          LD DE,FCB
          LD C,WRITE
          CALL BDOS
          JR EOF
CONTDIS:  EMT OUTC
          EMT KBDTF
```

```
          EMT KBDIN
          CP MENREQ       ;check for menu-request
          JR Z,EXITEN
          INC HL
          DEC B
          JR NZ,DISPREC   ;continue display checking for eof
          JR DISPLAY
EOF:      JR START
          LD DE,FCB
          LD C,FILSIZ
          CALL BDOS
;
START:    LD HL,BUFF      ;collection from slave begun
          LD B,BUFFL
START2:   LD A,XON
          EMT LPOUT
READS:    LD DE,WAIT
READ1:    EMT KBDIN
          CP MENREQ
          JR NZ,SKIPEX

EXITEN:   JR EXIT
;
SKIPEX:   IN A,(INTEST)
          AND A,TEST
          JR NZ,READ2
          DEC DE          ;wait for (DE) time for data to arrive
          LD A,D
          OR E
          JR NZ,READ1
          JR EXIT         ;wait expired exit
READ2:    IN A,(PORT)     ;read byte
          CP CTRLZ
          JR Z,EXIT       ;if eof exit
          LD (HL),A       ;dump byte into buffer
          INC HL
          DEC B
          JR NZ,READS     ;back for another byte
;
          LD A,XOFF       ;buffer full, send xoff
          EMT LPOUT
          POP HL
          PUSH HL
          LD C,0
STARTB:   LD DE,WAIT2
CHECKB:   IN A,(INTEST)
          AND A,TEST
          JR NZ,CONTB
          DEC DE
          LD A,D          ;deal with hanging bytes
          OR E
          JR NZ,CHECKB
          LD B,BUFFL
          LD A,B
          SBC C
          LD B,A
          PUSH BC
          JR BUFF1
CONTB:    IN A,(PORT)
          LD (HL),A
          INC HL
          INC C
          JR STARTB
BUFF1:    LD C,WRITE
          LD DE,FCB
          LD HL,BUFF
```

```
         LD B,BUFFL
OUTCHAR: LD A,(HL)
         EMT OUTC          ;write (buffer) to vdu
         INC HL
         DEC B
         JR NZ,OUTCHAR
         CALL BDOS         ;write (buffer) to data file
         CP 0
         JR NZ,EXITER      ;exit with error condition if write unsuccessful
         POP BC
         LD A,C
         CP 0
         JR Z,START        ;repeat if no hanging bytes
         LD DE,BUFF
         POP HL
         PUSH HL
         PUSH BC
         LD B,0
         LDIR              ;place hanging bytes at buffer start
         PUSH DE
         POP HL
         POP BC
         JR START2
EXITER:  POP BC
         LD A,CTRLE
         EMT LPOUT         ;send error flag
ERREX2:  POP HL
         LD (HL),ERROR
         CALR SYNC         ;wait for synchronization
         LD A,ERROR
         EMT LPOUT
         JR EXIT3
EXIT:    LD (HL),CTRLZ     ;fill buffer with eof
         INC HL
         DEC B
         JR NZ,EXIT
         LD HL,BUFF
CONTOP:  LD A,(HL)
         CP CTRLZ
         JR Z,EXIT2
         EMT OUTC          ;write excess bytes to vdu
         INC HL
         JR CONTOP
EXIT2:   LD C,WRITE
         LD DE,FCB
         CALL BDOS         ;write excess bytes to data file
         LD C,CLOSE
         LD DE,FCB
         CALL BDOS         ;close data file
         POP HL
         LD (HL),SUCCES    ;flag succesful data transfer
         CALR SYNC
         LD A,SUCCES
         EMT LPOUT
EXIT3:   RET
SYNC:    LD A,CTRLE        ;synchronize with slave
         EMT LPOUT
         EMT KBDIN
         CP MENREQ
         JR Z,SYNCEXI
         IN A,(INTEST)
         AND A,TEST
         JR Z,SYNC
         IN A,(PORT)
         CP CTRLE
         JR NZ,SYNC
         RET
SYNCEXI: POP HL
         RET
```

```
        ;*Memout (spectrum output from slave 380Z to master)*
        ORG     00100H
        S4KTL   EQU     47
        S4KIN   EQU     48
        LPOUT   EQU     5
        KBDTF   EQU     32
        KBDIN   EQU     29
        OUTC    EQU     1
        CTRLZ   EQU     01AH
        CTRLD   EQU     4
        RETREQ  EQU     18
        XOFF    EQU     013H
        XON     EQU     011H
        CR      EQU     13
        LF      EQU     10
        CTRLE   EQU     5
        ERROR   EQU     1
MSTART: POP     DE              ;get BASIC passed parameters
        POP     HL
        PUSH    HL
        PUSH    DE
START0: EMT     KBDIN
        CP      RETREQ
        JR      Z,JPEXIT        ;check for user intervention
        EMT     KBDTF
        EMT     S4KTL
        JR      Z,START0
        EMT     S4KIN
        EMT     OUTC
        CP      XON             ;wait for xon from master
        JR      NZ,START0

START:  EMT     KBDIN           ;begin transfer
        CP      RETREQ
        JR      Z,EXIT
        EMT     KBDTF
        EMT     S4KTL
        JR      NZ,TSTXOFF
        JR      CONT
JPEXIT: JR      EXIT
JPSTART:JR      MSTART
CONT:   LD      A,(HL)
        EMT     LPOUT           ;write byte to output port
        EMT     OUTC            ;write byte to vdu
        INC     HL
        CP      CTRLZ           ;check for eof
        JR      Z,BEGEND
CONT2:  PUSH    HL
        SBC     HL,DE           ;check for end of storage buffer
        POP     HL
        JR      NZ,START
        LD      A,CTRLZ
        EMT     LPOUT
        JR      BEGEND
TSTXOFF:                        ;check byte for xoff
        EMT     S4KIN
        CP      XOFF
        JR      Z,WAITXON
        EMT     OUTC
        JR      CONT
WAITXON:                        ;xoff received, wait now for xon
        EMT     KBDIN
        CP      RETREQ
        JR      Z,EXIT
        EMT     KBDTF
        EMT     S4KTL
```

```
        JR      Z,WAITXON
        EMT     S4KIN
        CP      XON
        JR      Z,CONT
        CP      CTRLE           ;test for synch request from master
        JR      Z,BEGEND
        EMT     OUTC
        JR      WAITXON
BEGEND: EMT     KBDIN           ;exit code
        CP      RETREQ
        JR      Z,EXIT
        EMT     KBDTF
        EMT     S4KTL
        JR      Z,BEGEND
        EMT     S4KIN
        CP      CTRLE           ;exit only when in synch with master
        JR      NZ,BEGEND
TRYSYNC:LD      A,CTRLE
        EMT     LPOUT
WAITFLG:EMT     KBDIN           ;wait while checking user abort and synch flag
        CP      RETREQ
        JR      Z,EXIT
        EMT     KBDTF
        EMT     S4KTL
        JR      Z,WAITFLG
        EMT     S4KIN
        CP      ERROR           ;if error flag sent start data transfer afresh
        JR      Z,JPSTART
        CP      CTRLE
        JR      Z,TRYSYNC
        POP     DE
        POP     HL
EXIT:   RET                     ;return to BASIC control
```

```
          ;*MCA read utility*
          ORG     00100H
          S4KTL   EQU     47
          S4KIN   EQU     48
          LPOUT   EQU     5
          KBDTF   EQU     32
          KBDIN   EQU     29
          OUTC    EQU     1
          CTRLZ   EQU     01AH
          CTRLD   EQU     4
          CTRLCL  EQU     01FH
          NLINES  EQU     11
          RETREQ  EQU     18
          CR      EQU     13
          LF      EQU     10
          TIMEOUT EQU     03000H
          POP     DE
          DEC     DE
          POP     HL
          LD      A,NLINES
          LD      (DE),A
START:    LD      BC,TIMEOUT
CHKINP:   EMT     KBDIN
          CP      RETREQ          ;check for user abort
          JR      Z,EXITREQ
          EMT     KBDTF
          EMT     S4KTL
          JR      NZ,GETBYTE      ;wait 'timeout' to receive byte
          DEC     BC
          LD      A,B
          OR      C
          JR      NZ,CHKINP
          JR      SETEXIT         ;exit if input timed out
GETBYTE:  EMT     S4KIN
          LD      (HL),A          ;read and store byte
          EMT     OUTC            ;write byte to vdu
          EMT     LPOUT           ;write byte to serial port
          CP      CR
          JR      NZ,CONT4        ;check for 'nlines' carriage returns
          LD      A,(DE)
          DEC     A
          JR      Z,CONT3
          LD      (DE),A
          JR      CONT4
CONT3:    LD      A,CTRLCL        ;clear screen when full (at nlines)
          EMT     OUTC
          LD      A,NLINES
          LD      (DE),A
CONT4:    INC     HL
          PUSH    HL
          SBC     HL,DE
          POP     HL
          JR      Z,MEMEX         ;check against memory limit
          JR      START
MEMEX:    JR      EXITREQ
          LD      (HL),CTRLZ      ;if memory limit surpassed force exit
          JR      EXIT
SETEXIT:
          LD      (HL),CTRLZ      ;write eof to buffer
WCTRLD:   EMT     S4KTL           ;wait for exit byte
          JR      NZ,CTRLDCK
          EMT     KBDIN
          CP      RETREQ
          JR      Z,EXITREQ
          EMT     KBDTF
          JR      WCTRLD

CTRLDCK:
          EMT     S4KIN
          CP      CTRLD
          JR      NZ,WCTRLD
EXIT:     RET                     ;exit when, in a normal transfer, exit byte
                                   received
```

Appendix C

Core backup MCA code

```
        ;*Backup MCA  timer subroutine*
        CTCH1   EQU     13
        RETREQ  EQU     18
        KBDIN   EQU     29
        KBDTC   EQU     30
        KBDTF   EQU     32
        OUTC    EQU      1
        OPNWT   EQU     11
        CLOSE   EQU     12
        DEOUT   EQU     20
        GETJP   EQU     38
        OUTF    EQU     43
        A1FIX   EQU     48000
        RATE    EQU     A1FIX+12
        TIME    EQU     A1FIX+14
        CNTS    EQU     A1FIX+16
        CHNUM   EQU     A1FIX+18
        RATEPSN EQU     A1FIX+20
        TIMPSN  EQU     A1FIX+22
        CNTSPSN EQU     A1FIX+24
        CHPSN   EQU     A1FIX+26
        RUNDUR  EQU     A1FIX+28
        RUNEND  EQU     30
        RETBAS  EQU     31
        POWERS  EQU     A1FIX+34
        ASCZERO EQU     '0'
        SPACE   EQU     ' '

        IM2
        EI
        PUSH IY
        PUSH AF
        PUSH BC
        PUSH DE
        PUSH HL
        LD IY,A1FIX
        LD DE,(TIME)
        INC DE
        LD (TIME),DE
        LD IY,(RATEPSN)
        LD DE,(RATE)
        LD HL,10000
        SBC HL,DE
        JR Z,RATE5
        JR C,RATE5
        LD BC,00100H
        CALR ASCII
        JR SKP5
RATE5:  CALR ASCOUT
SKP5:   LD DE,0
        LD (RATE),DE
        LD IY,(TIMPSN)
        LD DE,(TIME)
        LD HL,10000
        SBC HL,DE
        JR Z,TIME5
        JR C,TIME5
        LD BC,00100H
        CALR ASCII
        JR SKPTM5
TIME5:  CALR ASCOUT
SKPTM5: LD IY,(CNTSPSN)
        LD DE,(CNTS)
        LD HL,10000
        SBC HL,DE
        JR Z,CNTS5
```

```
        JR C,CNTS5
        LD BC,00100H
        CALR ASCII
        JR SKPCT5
CNTS5:  CALR ASCOUT
SKPCT5: LD IY,(CHPSN)
        LD DE,(CHNUM)
        LD BC,00100H
        CALR ASCII
        LD IY,A1FIX
        LD HL,(RUNDUR)
        LD DE,(TIME)
        SCF
        CCF
        SBC HL,DE
        JR NZ,EXIT
        SET 0,(IY+RUNEND)
        JR EXIT
ASCOUT: LD BC,0
ASCII:  LD A,B
        LD HL,POWERS
        EMT GETJP               ;(HL)<=(POWERS+A)
        EX DE,HL
RPTSUB: PUSH HL
        SCF
        CCF
        SBC HL,DE
        JR C,DISPASC
        POP AF
        INC C                   ;(C)=DIGIT
        JR RPTSUB
DISPASC:LD A,ASCZERO
        ADD A,C
        PUSH IY
        POP HL                  ;LOAD HL WITH IY
        DI
        EMT OUTF                ;WRITE DIGIT TO SCREEN AT (HL)
        IM2
        EI
        INC IY
        LD C,0
        POP DE
        INC B
        LD A,B
        CP 4
        JR NZ,ASCII
        LD A,ASCZERO
        ADD A,E                 ;OUTPUT UNARY DIGIT
        PUSH IY
        POP HL
        DI
        EMT OUTF
        INC HL
        LD A,SPACE
        EMT OUTF
        IM2
        EI
        RET
EXIT:   POP HL
        POP DE
        POP BC
        POP AF
        POP IY
        RETI
```

```
          ;*Backup MCA accumulator subroutine*
          PIO1AI   EQU     0
          PIO1BI   EQU     1
          PIO2AI   EQU     4
          PIO2BI   EQU     5
          RETREQ   EQU     18
          KBDIN    EQU     29
          KBDTC    EQU     30
          KBDTF    EQU     32
          OUTC     EQU     1
          STRETCH  EQU     16384
          STREADD  EQU     16394
          INIMEM   EQU     1
          ENINTER  EQU     2
          DSINTER  EQU     3
          AFIX     EQU     48000
          RATE     EQU     AFIX+12
          LETTER   EQU     65

          PUSH AF
          PUSH BC
          PUSH HL
          LD BC,(RATE)
          INC BC
          LD (RATE),BC
CYCLE:    IN A,(PIO1AI)
          CPL
          LD L,A
          IN A,(PIO1BI)
          CPL
          AND 31
          LD H,A
          ADD HL,HL
          LD BC,(AFIX)
          ADD HL,BC
          LD C,(HL)
          INC HL
          LD B,(HL)
          INC BC
          LD (HL),B
          DEC HL
          LD (HL),C
EXIT:
          POP HL
          POP BC
          POP AF
          IM2
          EI
          RETI
```

```
          ;*Backup MCA enable *MCA accumulator* subroutine*
          RETREQ  EQU     18
          KBDIN   EQU     29
          KBDTC   EQU     30
          KBDTF   EQU     32
          OUTC    EQU     1
          STRETCH EQU     16384
          STREADD EQU     16394
          INIMEM  EQU     1
          ENINTER EQU     2
          DSINTER EQU     3
          AFIX    EQU     50000
          CANCNT  EQU     50500

          LD IX,AFIX
          POP DE
          POP BC
          LD (AFIX+8),BC
          POP BC
          LD (AFIX+2),BC
          LD (AFIX+4),BC
          LD (IX+6),0
          LD (IX+7),0
          POP HL
          PUSH HL
          LD (AFIX),HL
          LD (AFIX+10),DE
          LD A,E
          CP INIMEM
          JR NZ,INTABLE
INITIL:   POP HL
          PUSH  HL
          LD BC,STRETCH
FILZER:   LD (HL),0
          INC  HL
          DEC BC
          LD A,B
          OR  C
          JR NZ,FILZER
INTABLE:  POP HL
          POP BC
          PUSH BC
          PUSH HL
          LD A,B
          LD I,A
          LD A,(AFIX+10)
          CP ENINTER
          JR NZ,WAIT
          IM2
          EI
WAIT:     LD A,(AFIX+10)
          CP ENINTER
          JR NZ,AUTOCYC
          LD DE,(AFIX+2)
          LD A,D
          OR E
          JR NZ,WAIT
          JR CYCLE
AUTOCYC:  CALL CANCNT
CYCLE:    LD DE,(AFIX+8)
          LD A,D
          OR E
          JR Z,EXIT
          DEC DE
          LD (AFIX+8),DE
          LD DE,(AFIX+4)
          LD (AFIX+2),DE
          LD A,(AFIX+10)
          CP ENINTER
          JR NZ,WAIT
          IM2
          EI
          JR WAIT
EXIT:     POP HL
          POP BC
          DI
RETRN:    RET
```

PHILOSOPHICAL MAGAZINE A, 1985, VOL. 52, NO. 4, 431–439

Positron annihilation study of lattice defects and phase transitions in tin

By P. C. RICE-EVANS, M. MOUSSAVI-MADANI, F. A. R. EL KHANGI and K. U. RAO

Department of Physics, Bedford and Royal Holloway Colleges (University of London), Regent's Park, London NW1 4NS, England

[*Received 2 January 1985 and accepted 15 March 1985*]

ABSTRACT

Positron annihilation in tin has been studied as a function of temperature. The Doppler broadening of the 511 keV line has been measured with a germanium photon detector system. For annealed white tin the positron parameters show only a small increase on approach to melting. For the tin sample plastically deformed at 77 K, the grey–white phase transitions are strikingly manifested at 240 and 300 K.

§ 1. INTRODUCTION

This study concerns positron annihilation in tin. Measurements on annealed tin are reported which shed light on the creation of lattice vacancies as temperatures approach the melting point, and measurements on plastically deformed tin are reported which illuminate the nature of the phase transitions from white to grey to white tin as the temperature is varied.

It is well known that the Doppler broadening of the 511 keV photon line arising from positron annihilation is a sensitive indicator of characteristics of the site of a positron at the instant of its annihilation (West 1979, Brandt and Dupasquier 1983). The technique reveals information about the momentum distributions of electrons selected for annihilation, which in turn can yield information on the nature of the lattice, and on the existence or creation of defects such as vacancies, dislocations and voids. Parameters such as the vacancy formation enthalpies and entropies may be determined with some confidence.

§ 2. DOPPLER BROADENING METHOD

The shape of the 511 keV photopeak measured with a high-resolution germanium detector can indicate the relative proportions of conduction and core electrons that participate in the annihilations. The geometry of a typical experiment is to sandwich a carrier-free positron-emitting radioactive source such as ^{22}NaCl between two specimen metal plates. The energetic positrons are rapidly thermalized within the metal in about 10^{-12} s, which is short compared with the typical positron lifetime of about 10^{-10} s. A consequence is that, compared with the electron velocities, the positron has a negligible speed; hence any Doppler broadening arising from the motion of the centre-of-mass of the e^+e^- pair is mainly attributable to the electron velocity.

Figure 1 shows the line shapes corresponding to positron annihilation in deformed tin at two different temperatures, together with the line shape for the monochromatic 514 keV gamma ray from ^{85}Sr which indicates the intrinsic resolution of the system. The Doppler broadening of the line is easily visible and it can be reasonably expressed

Fig. 1

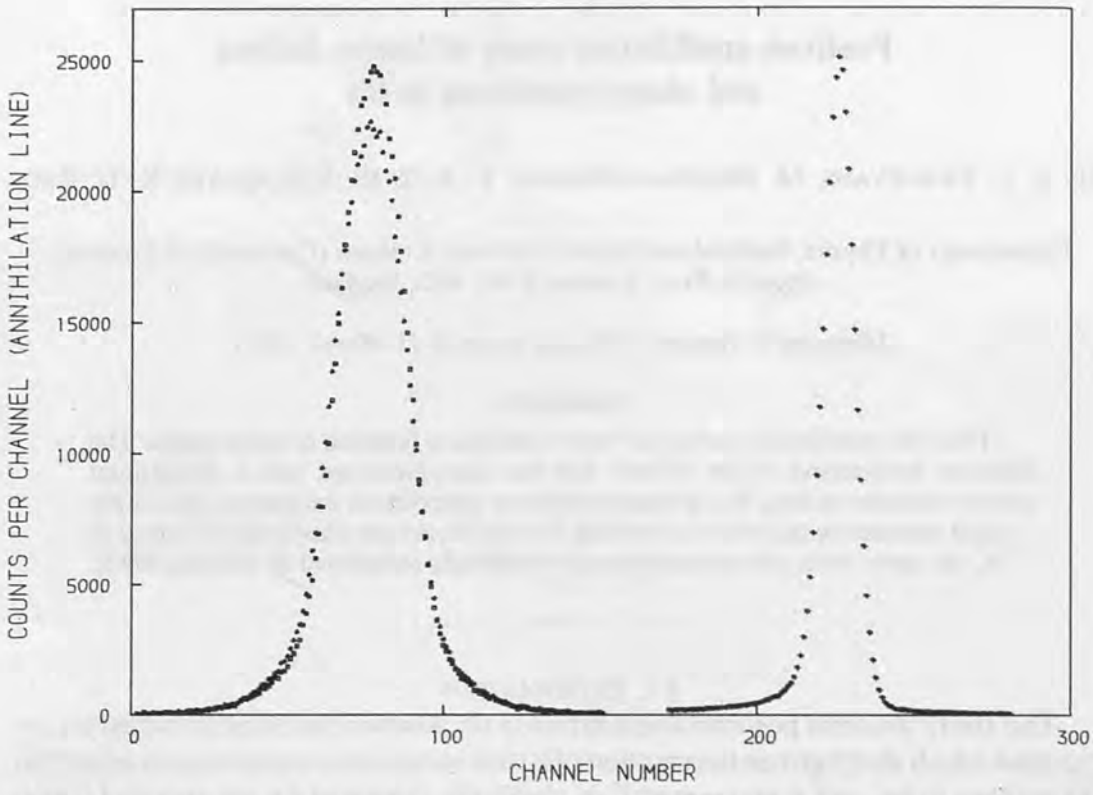

Examples of line shapes. To the right is the response of the photon detector to a monochromatic gamma ray at 514 keV. To the left are two Doppler-broadened 511 keV lines for white tin and grey tin.

as the sum of two components, a parabolic curve representing annihilations with free conduction electrons, and a Gaussian representing essentially annihilations with bound core electrons in the metal. The observed curve is given by these components convoluted with the resolution function (Rice-Evans, Chaglar and El Khangi 1981)

$$f(x)=A\int_{-\infty}^{+\infty}\exp\left[-(x'-\bar{x})^2/2\sigma_g^2\right]R(x-x')\,dx'$$

$$+B\int_{-\sigma_p\sqrt{2}}^{\sigma_p\sqrt{2}}\left[1-(x'-\bar{x})^2/2\sigma_p^2\right]R(x-x')\,dx.$$

The simplest linear parameter which can be used to characterize changes in the line shape is the line-height parameter F (some physicists use S), the ratio of the counts in a selected band of channels in the centre of the line to the counts in the whole line. Thus, an increase in F indicates a narrowing of the line, which usually signifies an increase in the proportion of the parabolic component.

In the present experiments the annealed sample consisted of two $15\times15\times1\,\mathrm{mm}^3$ pieces of 99·999% pure tin, supplied by Metals Research Ltd., which were spark cut and then etched in a mixture of nitric acid and alcohol. After direct deposition of the source within a central circle of diameter 3 mm, and composition into a sandwich, the sample was annealed at 450 K in a vacuum of 3×10^{-6} mbar for 15 hours and allowed to cool slowly to room temperature over 8 hours. It was then transferred to a vacuum cryostat, the temperature of which could be accurately controlled in the range 4·2–430 K. The

higher temperature range (300–500 K) was studied by placing the sample in a vacuum furnace.

The plastically deformed specimen was two $10 \times 10 \times 2\,\mathrm{mm}^3$ pieces of the same tin. After production of the radioactive sandwich, the whole sample was placed in a bath of liquid nitrogen which lay between the jaws of a hydraulic press. The application of 10 tons pressure resulted in a reduction of sample thickness at 77 K from 2 mm to 1 mm. The sample was immediately transferred to the cryostat at 77 K during which operation the temperature was monitored and seen not to rise above 90 K.

§ 3. Positron trapping by lattice defects

Defects such as vacancies appear as attractive potential wells that trap slow positrons diffusing through a lattice. Positrons annihilating in traps experience an electron environment that differs from the bulk lattice and hence a different F parameter signature is likely to result. This has been exploited in the so-called trapping model, on which several excellent reviews have been written (see for example, West 1979, Brandt and Dupasquier 1983). The model has been especially successful in monitoring the creation of vacancies as the sample temperature is raised. Furthermore, the dimensions and depths of the wells vary according to the type of defect (vacancy, dislocation, void, etc.) and thus in many cases the F parameter may distinguish them.

The concentration of thermally created vacancies as the temperature of the crystal is raised is given by

$$C_v = \exp(S_v/k)\exp(-H_v/kT),$$

where S_v and H_v are the entropy and enthalpy of vacancy formation.

The parameter F may indicate linearly the proportion of positrons trapped

$$F = F_f P_f + F_v P_v,$$

where F_f corresponds to $P_f = 1$, that is 100% of positrons annihilating in the free state, and F_v corresponds to P_v, that is, 100% trapping; $P_f + P_v = 1$. F_v is expected to exceed F_f because positrons trapped in vacancies will be more likely to annihilate with conduction electrons.

It follows (Rice-Evans *et al.* 1978 that

$$\frac{F - F_f}{F_v - F} = (\sigma\tau_f)\exp(S_v/kT)\exp(-H_v/kT),$$

where σ is the trapping rate, and τ_f is the lifetime of the free positron in the lattice. This expression may be fitted to data to yield values of H_v and S_v.

In practice it is observed that in the temperature region below the onset of vacancy production, the F parameter exhibits an approximately linear 'prevacancy rise'. This is naturally associated with the thermal expansion of the lattice; however, it remains to be properly explained (see, for example, Stott and West 1978 on lattice vibrations; Rice-Evans, Chaglar, Khangi and Berry 1981 on orientational effects; and Smedskjaer 1983 on positron detrapping). In any event, it is customary to write $F_f = F_f^\circ\,(1 + \beta T)$ and extrapolate it into the vacancy region; in other words, to fit the data to

$$F = \frac{F_f^\circ(1 + \beta T) + F_v A \exp(-H_v/kT)}{1 + A\exp(-H_v/kT)}.$$

The positron annihilation signature has also been exploited in elucidating the nature of annealing processes as a function of rising temperature, for example the migration of vacancies to form clusters in quenched samples (West 1979, Nieminen and Manninen 1979). Also, studies on a variety of plastically deformed metals in the temperature range 4–400 K have revealed a number of distinctive features associated with altering defect distributions (Rice-Evans *et al.* 1978 b).

The wavefunction of a positron trapped in a well is localized and the uncertainty principle therefore leads to some zero-point motion. This motion causes an extra Doppler broadening of the shape of the 511 keV photopeak. Jackman, Schulte, Campbell, Lichtenberger, MacKenzie and Wormald (1974) have shown that trapping in deep wells can be accommodated by fitting with an extra Gaussian broadening term, and this has also been achieved by Rice-Evans *et al.* (1981) with cadmium.

§4. Phase transitions in tin

The first scientific report of a low-temperature phase of tin was given by Erdman in 1851. For more than a century, extensive studies were conducted on the transformations leading to this non-metallic grey (α phase) tin from the commonly known white (β phase) tin, and these have been summarized by Busch and Kern (1960). The α phase, which is stable below 286·4 K, forms spontaneously if metallic β tin is kept below this temperature for sufficiently long periods (days to years). The transformation is accompanied by a 27% increase in volume, and a piece of white tin becomes a powdery mass of grey tin. Typically, after a certain incubation period, the transformation starts at one or several points on or near the surface and spreads out spherically until the whole piece is transformed, although there are indications that a small percentage remains untransformed (Burgers and Groen 1957). Grey tin converts back to white tin in a shorter time if it rises above the equilibrium temperature. Alpha tin has a diamond structure with a density of 5·76 g cm^{-3} and the β phase has a body-centred tetragonal structure with a density of 7·29 g cm^{-3}.

It has been accepted (Busch and Kern 1960) that the transition from β to α requires two processes: an incubation period in which α nuclei are formed, followed by a period of spherical growth at a linear rate. Various factors influence the processes, for example impurities or previous treatments such as cold-working and annealing. The atomic mechanism for the β to α transition has not been established, but some observations indicate that the α to β process is of the diffusionless or martensitic type.

Traditionally, quantitative information on the transformations has been obtained (*a*) by dilatometric measurements on the change of volume, and (*b*) by direct observation of the motion of the phase boundary; but recently more modern techniques have been used to study the phases, such as X-ray crystallography (Burgers and Groen 1957) and Mössbauer isomeric shifts (Nikolaev, Mar'in, Panayishkin and Pavlynkov 1973). The phases of tin have also been studied with annihilating positrons. Badoux, Heinrich and Kallmeyer (1967) used the angular correlation method to establish the different momentum distributions of the electron participating in the annihilations for α and β samples and Puff, Mascher, Kindl and Sormann (1983) used positron lifetime measurements to indicate that the β to α transformation occurred at 230 K.

Fig. 2

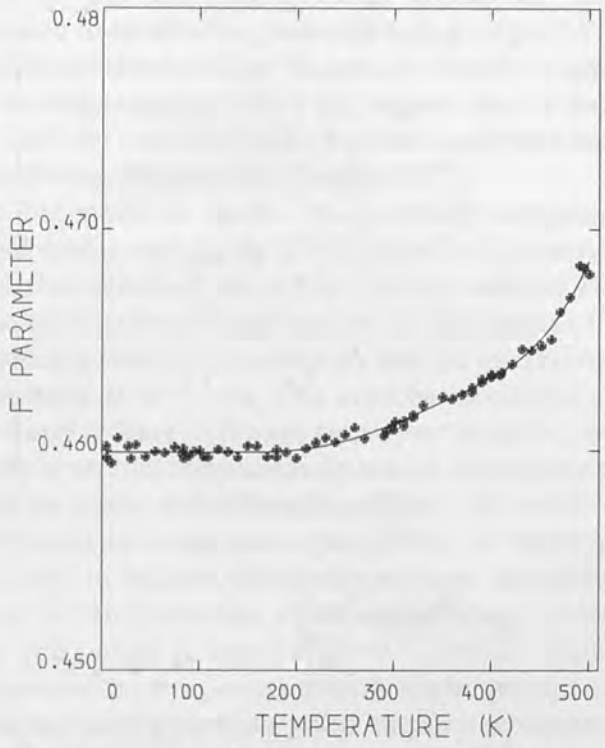

The variation of the F parameter as a function of temperature for annealed tin, showing only a modest rise at high temperatures resulting from the creation of vacancies.

§ 5. Results and discussion

5.1. *Results for annealed tin*

Figure 2 shows the curve of F parameter versus temperature plotted over the range 4·2 K to the melting point. Each point corresponds to a run of 2 hours with intervals of 30 min for adjusting and stabilizing the temperature.

The curve appears flat up to 200 K, then rises apparently linearly between 200 and 400 K with what is presumably the customary prevacancy rise. Thereafter the curve rises more steeply, corresponding, one assumes, to the trapping of positrons in an increasing concentration of thermally produced point vacancies. In contrast with many other metals, there is little evidence of a saturation pattern (i.e. a plateau) as the melting point at 509 K is approached.

The curve has been fitted with the expressions outlined in § 3. When the prevacancy rise is fitted with a straight line from 200 K upwards and extrapolated into the vacancy region (>450 K) the value obtained for the vacancy formation enthalpy (H_v) is $0{\cdot}56 \pm 0{\cdot}01$ eV. The slope (β) of the prevacancy rise is $(28{\cdot}0 \pm 4) \times 10^{-6}$. When the analysis includes self-trapping the value of H_v reduces to $0{\cdot}52 \pm 0{\cdot}02$ eV. It is estimated that the proportions of positrons trapped at 500 K are 67% and 63% for the two cases, respectively (El Khangi 1980).

5.2. *Results for deformed tin*

Figure 3 shows the line-height parameter (F) plotted as a function of temperature, the sequence of measurements being indicated alphabetically. The white tin sample was compressed at 77 K and the 2 hour runs started, as indicated at A. No change is seen for

Fig. 3

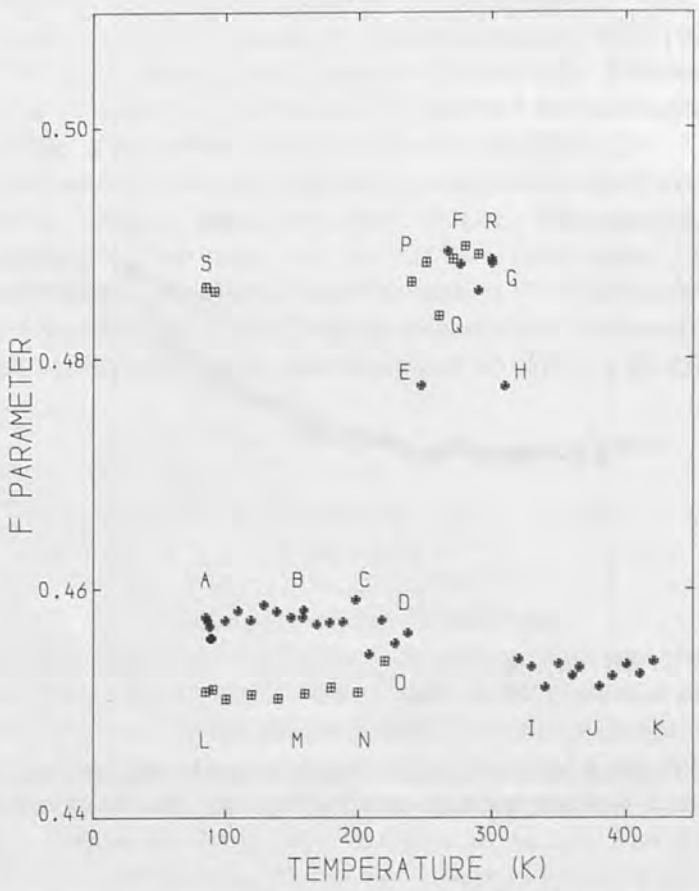

The variation of the F parameter as a function of temperature for tin plastically deformed at 77 K. The measurements are indicated sequentially A to S. The high values ($\approx 0{\cdot}48$) indicate grey tin; the low values ($\approx 0{\cdot}46$) correspond to white tin.

A–B–C–D, but after 235 K F suddenly increases (D–E–F). This demonstrates the rapid transition from white to grey tin which corresponds to the reduced metallic density. The sample remains grey until 300 K (F) when it quickly reverts (G–H–I) to white tin. The sample was further raised in temperature (I–J–K) during which a thorough annealing must have occurred, the melting temperature being 505 K.

The sample was reduced again to 77 K and a similar sequence of measurement started. It may be seen in the figure that the F values for annealed white tin (L–M–N–O) are significantly lower than (A–B–C). This can be ascribed to the high concentration of defects in the early life of the sample. These defects, introduced by the compression, act as traps for the positrons and produce higher values in F; but just as tin is unusual in yielding small values of F_v for saturation trapping in vacancies at high temperatures (§ 3), so too the change in F corresponding to high concentrations of defects at low temperatures is also small, say, compared with cadmium (Rice-Evans *et al.* 1978).

The white tin transforms to grey once more (O–P) at about 230 K and remains so until 290 K (P–Q–R). The experiment was concluded at 290 K (R) by lowering the temperature of the sample to 80 K, at which temperature two more runs were taken (S). The high F values at S indicate that the sample remained in the grey tin state.

Finally, the sample was extracted from the cryostat and the metal was discovered to have been reduced to a fine powder.

5.3. *Defects in tin*

In his model of the positron trapping process at vacancies, applying the Schrödinger equation to an effective potential well, Hodges (1970) did not discern any anomalous results for positrons in tin. Whereas he found a trapping potential of 5·2 eV and a positron binding energy of 1·4 eV for traps in tin, he found virtually the same values (4·9 and 1·4 eV) for indium which is known to exhibit a large trapping effect (see, for example, Rice-Evans, Hlaing and Chaglar 1977).

Both indium and white tin have a body-centred tetragonal structure and their valences are 3 and 4, respectively. In his discussion of the curious case of tin, Seeger (1973) points out that although the higher valence of β-Sn should favour positron trapping, three other features militate against it. The radius of the Sn^{4+} ion is 0·71Å (Pauling 1968), which is small compared with half the interatomic distances (1·4 Å and 1·51Å). Thus, in spite of its $4d^{10}$ core, β-Sn must be considered as a metal with narrow cores, and hence likely to have shallower traps. Furthermore, inward relaxation of the atoms surrounding a vacancy may seriously reduce the trapping probability at such a site. The value of the tracer self-diffusion coefficient of $5 \times 10^{-11}\,cm^2\,s^{-1}$ (Nachtrieb and Coston 1965) leads to a very low value of 0·25 for the monovacancy formation volume in tin (cf. 0·45 in indium, 0·8 in copper), and this should result in a smaller potential well to attract the positrons. Finally, Seeger contrasts the above self-diffusion coefficient for tin with typical values of 10^{-8}–$10^{-7}\,cm^2\,s^{-1}$ for most other metals and, assuming that the mobility of vacancies near the melting point of tin is similar to other metals, he estimates that the melting point vacancy concentration in β-Sn is three orders of magnitude less than in many other metals; tin melts too early, judged by the equilibrium concentration of vacancies.

The values of F for deformed white tin at low temperatures (fig. 3) (A–B–C) are 3·5% higher than the values for samples when annealed (L–M–N). This may be compared with the rise of 0·8% when the annealed specimen was taken to high temperatures (fig 1). In cadmium, where saturation trapping is seen at high temperatures, the equivalent figures are 6·6% and 7·0%, respectively (Rice-Evans *et al.* 1978). The present authors are not aware of any arguments that would link a low concentration of vacancies at the highest temperatures with a low frozen defect concentration in deformed states at low temperatures; one might imagine them to be independent of each other. In this event one would expect ΔF to be much greater in the case of frozen traps. Thus we do not find the arguments from positron annihilation for a low C_v on approach to the melting point conclusive.

However, evidence of another sort comes from the comparison of macroscopic thermal expansion with X-ray measurements of lattice expansion. Balzer and Sigvaldason (1979) found them indistinguishable in tin, from which they concluded that the vacancy concentration at the melting temperature was low: less than 3×10^{-5}. Nevertheless the result might have other explanations, such as the possibility of displaced atoms becoming interstitials.

The findings for H_v (§ 5.1) agree reasonably with results from other laboratories: 0·57 eV (MacKenzie and Fabian 1980); 0·51 eV (Dedoussis, Charalambous and Chardalas 1977); 0·58 eV (Puff *et al.* 1983); 0·51 eV (Shah and Catz 1984); 0·54 eV (Segers, Dorikens-Vanpraet and Dorikens 1980). The curve concurs with the results of MacKenzie and Fabian who observed that the ratio of the threshold temperature for trapping by vacancies (450 K) to the temperature of melting is 0·88, in contrast with the value of 0·63 found for most close-packed metals.

Puff *et al.* (1983), on the basis of lifetime measurements, believed they could

distinguish two regions in the prevacancy rise; the first, 230–370 K, being attributable to thermal expansion and the second, 380–450 K, which is steeper, corresponding to a temporary localization of positrons in dilation zones of the lattice. The present results do not indicate this distinction of two regions, and in accord with our previous findings (see, for example, Rice-Evans *et al.* 1981) in the present authors' opinion the major theoretical question of the origin of the prevacancy rise remains unresolved.

5.4. *Discussion on phase transitions in tin*

Whereas the annealed sample showed no signs of the α–β phase transition as the temperatures were varied, it is clear from the results on the deformed specimen that a high concentration of defects promotes the transitions. Assuming the overall effect corresponds to a 100% transition, it is seen that approximately 85% of the white tin is transformed to grey in 2 hours (O–P), the F parameter being a linear indicator. Similarly the grey to white transition (G–H–I) is seen to occur in 4·5 hours, with 61% transforming in about 2 hours (H–I). Thus, the positron annihilation method can indicate the phase transition rates and transition temperatures for tin rather accurately, and possibly uniquely. The method could be further refined by conducting a series of measurements with various degrees of plastic deformation and correlating defect concentrations with rates of phase transition.

Acknowledgments

It is a pleasure to thank Dr J. H. Evans of AERE, Harwell, and Dr Ian Butler of the Tin Research Institute for valuable discussions; and the Science and Engineering Research Council for its financial support.

Note added in proof

W. Puff, P. Mascher, P. Kindl and H. Sormann reported observations in the phase transitions in tin at the Seventh International Conference on Positron Annihilation in Delhi, January 1985. Their results are to be published.

References

Badoux, F., Heinrich, F., and Kallmeyer, G., 1967, *Helv. phys. Acta*, **40,** 815.
Balzer, R., and Sigvaldason, H., 1979, *Phy. Stat. Sol.* (b), **92,** 143.
Brandt, E., and Dupasquier, A., (editors), 1983, *Positron Solid State Physics* (*Fermi School, Varenna*) (Amsterdam: North-Holland).
Burgers, W. G., and Groen, L. J., 1957, *Discuss. Faraday Soc.*, **23,** 183.
Busch, G. A., and Kern, R., 1960, *Solid St. Phys.*, **11,** 1.
Dedoussis, S., Charalambous, S., and Chardalas, M., 1977, *Phys. Lett.* A, 359.
El Khangi, F. A. R., 1980, Ph.D Thesis, University of London.
Erdmann, O. L., 1851, *J. prakt. Chem.*, **52,** 428.
Hodges, C. H., 1970, *Phys. Rev., Lett.*, **25,** 284.
Jackman, T. E., Schulte, C. W., Campbell, J. L., Lichtenberger, P. C., MacKenzie, I. K., and Wormald, M. R., 1974, *J. Phys.* F, **4,** L1.
MacKenzie, I. K., and Fabian, J., 1980, *Can. J. Phys.*, **58,** 1635.
Nachtrieb, N. H., and Coston, C., 1965, *Physics of Solids at High Pressure*, edited by C. T. Tomizuko and R. M. Emrick (Academic Press: New York), pp. 336–48.
Nieminen, R. M., and Manninen, M. J., 1979, *Positrons in Solids*, edited by P. Hautojärvi (Berlin: Springer-Verlag) pp. 145–196.
Nikolaev, I. N., Mar'in, V. P., Panyishkin, V. N., and Pavlynkov, L. S., 1973, *Sov. Phys. solid St.*, **14,** 2022.
Pauling, L., 1968, *Die Natur der Chemischen Bindung*, Vol. 3 (Weinheim/Bergstrasse: Verlag Chemie), p. 479.

PUFF, W., MASCHER, P., KINDL, P., and SORMANN, H., 1983, *Appl. Phys.* A, **32,** 183.
RICE-EVANS, P., CHAGLER, I., EL KHANGI, F. A. R., 1978 a, *Phil. Mag.*, **38,** 543; 1978 b, *Phys. Rev. Lett.*, **40,** 716; 1981, *Phys. Lett.* A, **81,** 480.
RICE-EVANS, P., CHAGLAR, I., EL KHANGI, F. A. R., and BERRY, A. A., 1981, *Phys. Rev. Lett.*, **47,** 271.
RICE-EVANS, P., HLAING, T., and CHAGLER, I., 1977, *Phys. Lett*, A, **60,** 368.
SEEGER, A., 1973, *J. Phys.* F, **3,** 248.
SEGERS, D., DORIKENS-VANPRAET, L., and DORIKINS, M., 1980, *Phys. Stat. Sol.* (a), **59,** 543.
SHAH, N., and CATZ, A. L., 1984, *Phys. Rev.* B, **30,** 2498.
SMEDSKJAER, L. C., 1983, *Positron Solid-State Physics*, edited by W. Brandt and A. Dupasquier (Amsterdam: North Holland) pp. 597–608.
STOTT, M. J., and WEST, R. N., 1978, *J. Phys.* F, **8,** 635.
WEST, R. N., 1979, *Positrons in Solids*, edited by P. Hautojärvi (Berlin: Springer-Verlag), pp. 89–145.

POSITRON ANNIHILATION
edited by P. C. Jain, R. M. Singru & K. P. Gopinathan

POSITRON ANNIHILATION IN THE SEMICONDUCTING ALLOY $Pb_{.93}Ge_{.07}Te$

P.C. Rice-Evans*, K.U. Rao*, M. Moussavi-Madani*, He Yusheng**, and A.D.C. Grassie***

* Department of Physics, Bedford and Royal Holloway Colleges, Regent's Park, London, NW1 4NS, England.

** Department of Physics, Tsinghua University, Peking, China.

*** Department of Physics, Sussex University, Brighton, England.

(PbGe)Te is a narrow gap chalcogenide semiconductor material that is of interest technologically because it is easily obtained in the crystalline state and because it has a structural phase transition with a transition temperature that is dependent on the carrier concentration and the germanium composition. The Doppler-broadening of the 511 keV radiation arising from positrons annihilating in the semiconductor has been studied as a function of temperature. The results failed to show any indication of the phase transition, expected to occur at about 150 K, but the role of the defect structures was signified as the temperature was varied. A detrapping phenomenon was seen in the region 77K - 300K, and a slow clustering of shallow defects commenced at 300 K, reached a maximum at 450 K, after which annealing was evident.

The chalcogenide (Pb,Ge)Te is a narrow gap semiconductor. It is of considerable interest in the physics and technology of semiconductors due to the fact that it is easily obtained in the crystalline state, and that it has a structural phase transition with a transition temperature that is dependent on carrier concentration and germanium composition. Positron annihilation measurements have already proved to be a valuable approach to this class of semiconductors (1,2) and they might be expected to yield information on phase transitions, on trapping sites and on defect concentrations.

Mokrushin et al (1) undertook lifetime and angular correlation studies on various chalcogenides (e.g. $As_{42}Te_{58}$ and $Ge_{15}Te_{85}$) in both crystalline and glassy states. They observed a single lifetime component, τ = 0.35 ± .03 ns, for all compounds and both states. The angular distributions indicated a predominance of positron annihilation with chalcogen atoms; and the authors concluded that the annihilation was essentially of positrons bound in vacancy defects.

The polycrystalline sample for the present study, made in Sussex from a melt with weighed proportions of pure (5N) elements, was $Pb_{1-x}Ge_xTe$ with x = 0.07; after melting in an rf-furnace, the sample was quenched in iced water. Figure 1 shows a resistivity measurement on the material. The anomalous peak at 150K is taken to indicate a ferroelectric phase transition,

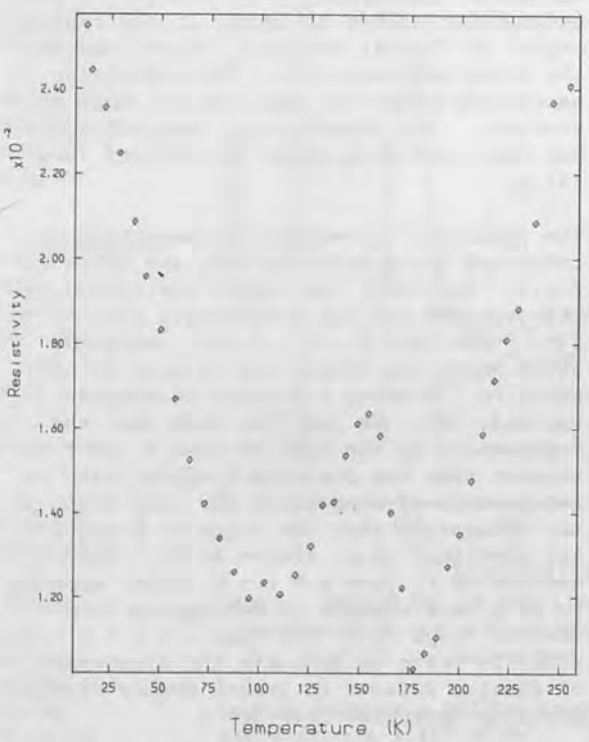

Fig.1. The resistivity of the sample of (Pb,Ge)Te plotted as a function of temperature.

from a rhombohedral to a cubic structure, associated with a decrease in the relaxation time of the free carrier. The sample had lain for several years at room temperature prior to this experiment; hence any defects initially present at 77K would be those that

could survive at 300K.

Positron annihilation in the semiconductors has been investigated with the Bedford-Doppler-broadening spectrometer. Two 1 mm. thick slices sandwiched 100 μc of $^{22}NaCl$, and the sample was subjected to temperatures ranging from 77-400K in a cryostat and 300-600K in a vacuum furnace. The germanium photon detector recorded 511 keV line shapes, with two hours for each temperature. The intrinsic resolution of the system was 1.05 keV at 514 keV. Each spectrum was accumulated in two hours.

The method relies on assessing the shape of the 511 keV photon annihilation line. Energetic positrons from the radioactive source are assumed to be rapidly thermalised to negligible velocities and the Doppler-broadening is mainly due to the electron momentum of the e^+e^- pair. The conventional line-height parameter F has been employed which is taken essentially to indicate changing proportions of annihilations with outer (lower momentum) and inner (higher momentum) electrons. F is defined as the accumulated number of counts in the central region of the 511 keV peak, normalised to the total peak area (3). The underlying background below the peak has not been subtracted. The conventional trapping model has been used to analyse the results (see (4)).

The results of a sequence of measurements, indicated alphabetically A→S, are shown in Fig.2. Initially the sample was placed in the cryostat and the temperature reduced to 77K. The runs A → C → E were recorded, after which the sample was allowed to cool again to 77K where a further measurement was made (F). We take the fact that the F-parameter is the same at both E and F to suggest that the positron trapping rate is independent of temperature for deep traps on the assumption that the traps at E and F are identical (i.e. frozen at F). The decline in F, from A → B → C (350K) appears to be a rare example of detrapping from shallow traps (5). The rise C → D → E (370-430K) is taken to indicate the clustering of shallow defects to create deeper traps, possibly vacancies (see (6)).

On transfer to the furnace, commencing at 300K the rise G → H → I occurs. This rise is surprising. It rather suggests the clustering was not complete at E, but continued to occur at a relatively slow rate over the same temperature range in the furnace.

The decline in F from I → J → K → L we take to represent the annealing of the defects.

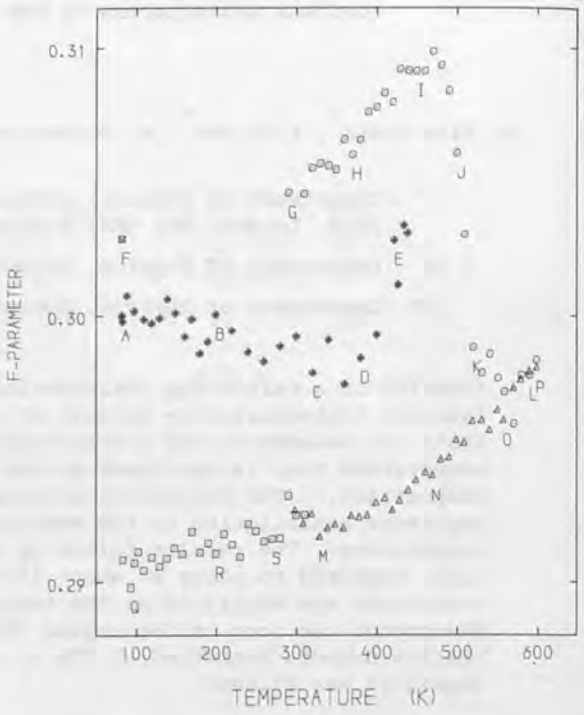

Fig.2. The positron annihilation Doppler line-height parameter F plotted as a function of temperature. The sequence of measurements is indicated alphabetically.

This is confirmed by taking the sample down to 300K and taking points MNOP which have the characteristic appearance of results for an annealed crystal.

The annealed crystal was replaced in the cryostat and the range Q → R → S studied. The absence of any significant feature at about 150K means the phase transition is not observable although the scatter of points might hide a small effect.

References

1. Mokrushin A., Prokop'ev E., Minaev V., Kisekka B., and Kupriyanova R., Sov. Phys.Semicond.14, 751 (1980).
2. Kobrin B., Shantarovich V., Mikhailov M., Tukina E., Physica Scripta 29, 276 (1984)
3. Rice-Evans P., Chaglar I., and El Khangi F., Phil.Mag. 38, 543 (1978).
4. Brandt W. and Dupasquier A., (Ed) Positron Solid-State Physics [Fermi School, Varenna]. North Holland, Amsterdam, 1983.
5. Smedskjaer L.C., Manninen M., and Fluss M.J., J.Phys.F. 10, 2237 (1980).
6. Petersen K., chapter in ref.(4).

Acknowledgement

The authors thank the Science & Engineering Research Council for its financial support.

POSITRON ANNIHILATION
edited by P. C. Jain, R. M. Singru & K. P. Gopinathan

SEARCH FOR A MONOLAYER SURFACE OF OXYGEN ON EXFOLIATED GRAPHITE AT LOW TEMPERATURES

P.C. Rice-Evans, M. Moussavi-Madani, K.U. Rao and B.P. Cowan

Department of Physics, Bedford College,
Regent's Park, London NW1 4NS, England.

The results are presented of a pilot study devised to demonstrate the growth of a monolayer surface of oxygen due to van der Waals forces. Exfoliation of graphite involves the formation of intercalation complexes within layer-structured crystals, and subsequent heating which explodes the layers apart. It forms a uniform substrate with a large area/volume ratio [9.1 x 10^6 m^2/m^3].

A standard sandwich sample containing ^{22}NaCℓ was prepared and placed in a cryostat and the annihilation radiation studied with the Bedford Doppler spectrometer. An orthodox graph of the line-height parameter was obtained with temperature when the sample chamber was evacuated. The introduction of oxygen allows the formation of a monolayer on the substrate at appropriate low temperatures, and this is clearly indicated with the line-height values. Further line-shape analysis suggests the formation of positronium at the monolayer, although some features remain unexplained.

Positrons have been valuable probes in Solid State Physics for many years. They have enabled important advances to be made in our knowledge of the bulk properties of solids including Fermi surface studies and in the investigation of lattice-defects such as vacancies, voids, dislocations (Hautojärvi, 1979) etc. Recently the techniques of positron annihilation have been extended to surfaces with the development of beams of low energy positrons, and rich pastures remain to be grazed (Brandt and Dupasquier, 1983).

However, low energy positron beams require high vacuum, usually ultra high vacuum. This fact militates against some types of surface investigation. In cases where the surface condition is in equilibrium with gas at a relatively high pressure a beam of positrons with energies of the order of 1 eV could not easily be transported to the surface.

In this paper we report initial work on a system which allows surfaces to be studied, without the use of a beam. We have exploited the special properties of exfoliated graphite (known as grafoil, commercially available from Union Carbide) namely a huge surface area, in the expectation that a large proportion of positrons may be induced to interact with a monolayer surface of oxygen laid down at low temperature.

Exfoliation of graphite involves the formation of intercalation complexes within layer-structured crystals, and subsequent heating which explodes the layers apart. It forms a uniform substrate with a large area/volume ratio of 9.1 x 10^6 m^2/m^3. Its use is an extension of the idea of using powder samples as a means of enhancing the area/volume ratio.

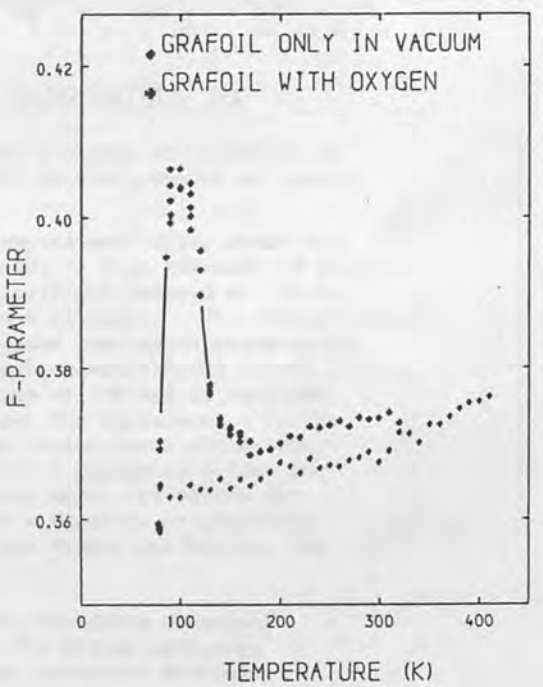

Fig.1. Variation of the line-height parameter *F*, as a function of temperature, for grafoil in vacuum and in oxygen.

A conventional sandwich sample containing ^{22}NaCℓ was prepared. Because of the low density (0.94 gm cm^3) of grafoil the source

was deposited directly at the centre of a stack of 12 pieces of grafoil, each 1 x 1 x 0.07 cm^3, the number being determined by the need to stop all the positrons. After preparation the sample was transferred to a cryostat capable of maintaining controlled temperatures in the range 77-430K and the annihilation radiation studied with the Bedford photon spectrometer (Rice-Evans et al, 1978). Shimotomai et al (1983) have already studied Doppler effects in pure graphite as a function of crystal orientation.

For the preliminary analysis, we have employed the usual Doppler line-height parameter, *F*, defined in our case as the contents of the central 15 channels in the 511 keV peak normalised to the total area of the peak. It is assumed that the positrons will rapidly thermalise in the carbon, and the Doppler-broadening will be a consequence of the motion of the annihilating electron. Figure 1 shows the response of the annihilation line to varying sample temperatures. For graphite in high vacuum of about 10^{-6} Torr, the points display a not unexpected gentle rise in temperature, that is commonly seen with many materials and often associated with thermal expansion and other prevacancy effects.

The graph also shows the effects of introducing oxygen into the sample chamber. The procedure adopted was to insert the

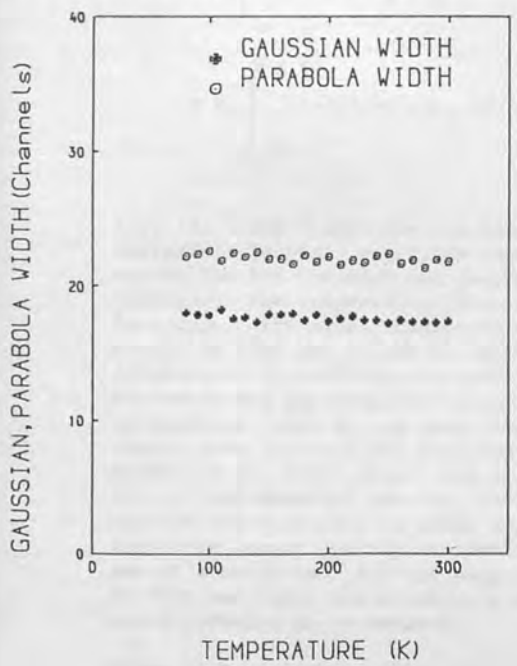

Fig.2. Results of analysis of annihilation peak for grafoil only.

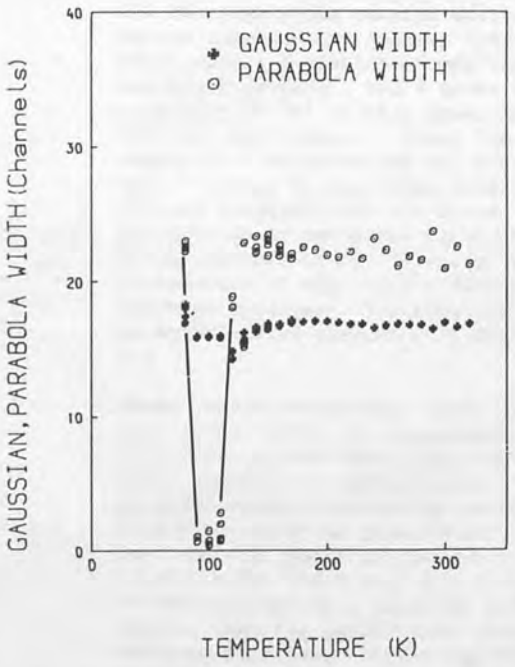

Fig.3. Results of analysis of annihilation peak for grafoil in the presence of oxygen.

oxygen at room temperature; after which the cryostat was cooled, so that the wall of the sample chamber itself was reduced to 77K by contact with liquid nitrogen. The effect of this was to reduce the oxygen pressure to 160 Torr, the expected equilibrium vapour pressure for oxygen at 77K and it remained constant throughout the experiment. In the graph, for sample temperatures above 160K, it is seen that the *F* parameter values for oxygen lie slightly above the values for carbon indicating a fraction of positrons annihilating in the oxygen gas between the graphite layers.

As the temperature decreases we expect physisorption of the gas to commence, initially with an increasing monolayer coverage (Dash, 1975). We are not certain at what temperature bilayers and more could be laid down, but below the boiling point of oxygen (90.1K) we assume that the crevices within the grafoil will be completely filled with liquid oxygen.

In Fig.1 we see that below 160K, with oxygen present, the value of *F* rises sharply, but further reduction below 90K causes a sharp diminution of *F*. It seems sensible to associate the rise with the physisorption of a monolayer of oxygen.

To examine the origin of the magnified value of *F* between 90 and 150K we analysed the

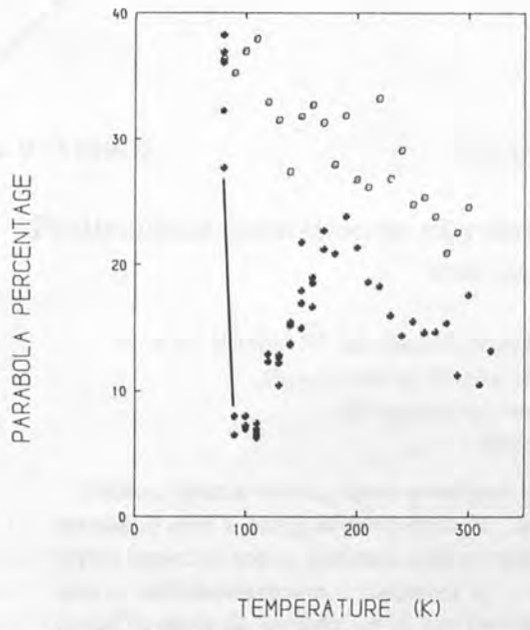

Fig.4. Results of analysis: open circles refer to grafoil only, stars to grafoil in presence of oxygen.

annihilation peaks into a parabolic and a Gaussian component (Rice-Evans et al, 1981). This relies on convoluting the intrinsic resolution (R) of the system determined with the ^{85}Sr gamma line at 514 keV and fitting with the expression

$$f(x) = A \int_{-\infty}^{+\infty} \exp[-(x'-\bar{x})^2/2\sigma_g]R(x-x')dx'$$

$$+ B \int_{-\sigma_p\sqrt{2}}^{\sigma_p\sqrt{2}} [1-(x'-\bar{x})^2/2\sigma_p]R(x-x')dx'.$$

Figs. 2, 3 and 4 show the results of this analysis. In Fig.2 one finds rather steady values for the Gaussian and parabolic widths throughout the temperature range for grafoil in vacuum. The usual interpretation for metals is that the parabolic component corresponds to annihilation with conduction electrons and the Gaussian to core electrons. In graphite there is one free electron per carbon atom [Ganguli and Krishnan, 1940]. Normal to the basal plane, and in the direction of our detected photons, the effective mass of the electrons is large and one therefore cannot justify theoretically the use of a parabola. For our purposes it may be that any curve would actually suffice - and a parabola is convenient.

Below 130K, in the presence of oxygen, one sees a sharp reduction in the width of the parabola to a mere couple of channels, while the Gaussian width remains unaltered. This narrow component we suggest indicates preferential formation of positronium at the monolayer surface. Fig.4 shows that the intensity (6-7%) of this positronium peak at 100K not negligible. Below 90K, the narrow component disappears and the fittings indicate a return to the wider parabola. From this we conclude that the formation of positronium is inhibited either by relatively thick adsorbed oxygen layers or by the total elimination of empty space between the graphite surfaces. The fits are all reasonable with reduced χ^2/ν between 0.9 and 1.3.

These studies complement those of Lyn and Lutz (1980, 1983) who observed positronium fractions emitted from aluminium surfaces, after exposure to various levels of oxygen at 300K, using a low energy positron beam. They detected ortho positronium by observing the 3-photon region of the spectrum. Our results below 90K - i.e. the disappearance of the positronium - coincide with Lyn's finding that the positronium fraction declines with large oxygen exposures. Nevertheless, in view of several unexplained features, our conclusions must be only tentative at this stage, and obviously further work is called for.

Acknowledgement

We wish to thank the Science and Engineering Research Council for their support.

References

1. P.Hautojarvi (Ed), Positrons in Solids, Topics in Current Phys. 12, (Springer, Heidelberg, 1979).
2. W. Brandt and A. Dupasquier (Eds), Positron Solid State Physics (North-Holland, Amsterdam, 1983).
3. P.Rice-Evans, I. Chaglar and F.A.R. El Khangi, Phys.Rev.Lett. 40 716 1978.
4. M. Shimotamai, T. Iwata, T. Takahashi and M. Doyama, J.Phys.Soc.Japan, 52 694 1983.
5. J.G. Dash, Films on Solid Surfaces (Academic Press, New York, 1975).
6. P. Rice-Evans, I. Chaglar and F.A.R. El Khangi, Phys.Lett. 81A 480 1981.
7. N. Ganguli and K.S. Krishnan, Proc.Roy. Soc.(Lond), A177 168 1941.
8. K.G.Lynn and H. Lutz, Phys.Rev.B, 22 4143 1980.
9. K.G.Lynn - chapter in reference (2) 1983.

PROOF 57 BS1-LH-3136B

Page 6117

PHYSICAL REVIEW B VOLUME 34, NUMBER 9 1 NOVEMBER 1986

Positronium formation at physisorbed monolayer surfaces of argon, nitrogen, and oxygen on graphite

P. Rice-Evans, M. Moussavi-Madani, K. U. Rao, D. T. Britton, and B. P. Cowan
Department of Physics, Royal Holloway & Bedford New College (University of London), Egham, Surrey, England
(Received 4 June 1986)

Photon spectra arising from positrons annihilating at surfaces in exfoliated graphite have been measured over a range of temperatures. The role in the annihilation process of physisorbed equilibrium layers of argon, nitrogen, and oxygen has been observed. With argon and nitrogen the formation of orthopositronium is indicated by a three-to-two γ ray ratio; for nitrogen maximum o-Ps was found to occur on completion of one monolayer. In contrast, a Doppler analysis shows that oxygen yields parapositronium. In the case of nitrogen, the results allow the estimation of the coverage, the binding energy of the molecule to the carbon substrate, and the activation energy for the process of Ps emission from the surface traps.
MS code no. LH3136B 1986 PACS number(s): 71.60. + z, 68.45. − v

The invention of monochromatic low-energy positron beams[1–3] has been important, and early advances are being made in our knowledge of positron interactions at solid surfaces.[4] For example, the fact that positrons may be trapped in surface states has been confirmed by the observations of enhanced thermally desorbed positronium at increasing temperatures.[2,3] However, the theory of the positron surface state is still incomplete; indeed, recently reported 2γ angular correlation results[5] on an aluminium surface indicating an isotropic momentum distribution have not been consistent with either a positron bound by its "image correlation potential"[6,7] or a positronium atom weakly bound to the surface.[8] It is clear that more evidence on the behavior of positrons under a variety of surface conditions is needed to resolve the theoretical uncertainties. One such condition is the two-dimensional layer of gas condensed on a known substrate for which positron trapping sites are, in principle, capable of being well characterized. In this paper we show that positrons respond sensitively to monolayer coverages of argon, nitrogen, and oxygen on graphite.

Physisorption is governed by van der Waals forces and information on the growth, phases, and registration of thin films[9] as a function of temperature has been acquired from isotherm and calorimetry studies[10,11] neutron diffraction,[12] NMR,[13] and low-energy electron diffraction[14] methods amongst others. It remains to be seen whether annihilating positrons will provide new insights into the thermodynamics of low-dimensional systems.

Beam studies require UHV to facilitate positron transport and ensure uncontaminated surfaces. Equilibrium monolayer systems are more easily investigated by thermalizing fast positrons within a solid substrate and relying on a large surface-to-volume ratio to ensure that positrons have a high probability of annihilating at the surface. High ratios are possible in powder samples, but they are also obtained in graphite that has been exfoliated—a process that involves the formation of intercalation complexes within layer-structured crystals, and subsequent heating which explodes the layers apart, to form a uniform substrate of large area. Furthermore, surface oxidation of carbon does not arise.

To study the role of positrons at physisorbed two-dimensional structures on Grafoil,[15] we have measured the annihilation photon spectrum with a germanium detector as a function of sample temperature. A conventional sandwich containing 100 μCi ^{22}NaCl was prepared. Because of the low density (0.94 g cm^{-3}) of Grafoil, the source was deposited directly at the center of a stack of 12 pieces of Grafoil, each $1\times1\times0.04$ cm^3, the number needed to stop all the positrons. After preparation the sample was transferred to a cryostat capable of maintaining controlled temperatures in the range 77—460 K.

The specimen chamber was made of brass which lay in a Dewar of liquid nitrogen. The oxygen and argon gases were introduced in sufficient amounts to ensure they condensed into liquid pools at the bottom of the chamber: hence their equilibrium pressures at 77 K prevailed for all measurements; i.e., 156 and 190 Torr, respectively. The suspended Grafoil sample was maintained at a range of temperatures and the gases were physisorbed on the carbon substrate under equilibrium conditions at the prevailing pressure. In the case of nitrogen four sets of measurements were taken at different pressures.

We have analyzed the spectra in several ways. Specifically, to seek the formation of orthopositronium, which entails 3γ decays, we have recorded the contents of the whole 511-keV photopeak (A) and also of a band of channels (B) in the Compton region corresponding to an energy band at 190—200 keV. Both A and Y ($=A/B$) will be indicators of the strength of 3γ events, i.e., orthopositronium decay.[16] The Doppler broadening is illustrated with the line-height parameter F, defined as the ratio of the contents of the central 15 channels in the 511-keV photopeak to A; and in the analysis of the peaks into parabolic and Gaussian components[17] by convoluting the intrinsic resolution (r) of the system determined with the ^{85}Sr line at 514 keV and fitting the expression:

$$f(x)=a\int_{-\infty}^{+\infty}\exp[-(x'-\bar{x})^2/2\sigma_G^2]r(x-x')dx'$$

$$+b\int_{-\sigma_P\sqrt{2}}^{\sigma_P\sqrt{2}}[1-(x'-\bar{x})^2/2\sigma_P^2]r(x-x')dx' ,$$

from which the widths (σ_G,σ_P) and the relative intensity of the parabolic component (if >2–3%) can be obtained. It has also been valuable on occasion to analyze instead for two Gaussian components.

Prior to the physisorption measurements we studied the positron-annihilation characteristics of Grafoil in vacuum. Figure 1, which shows the gentle trends of the parameters as a function of temperature, is presented to provide contrast with the physisorption experiments. The only comparable work on such a system has been on positron lifetimes,[18] which found essentially three components, 200, 410, and 1800 ps, interpreted as annihilations in the bulk, in surface-trapped states or quasi-Ps states bound on the surface, and as orthopositronium. We can note that in Fig. 1(b), a declining Y indicates a slow increase in the formation of positronium as the temperature rises above 200 K.

Figure 2(a) shows the results with argon in the chamber; the Y parameter shows a very distinctive minimum at 120 K indicating a maximum of orthopositronium. Figures 2(b), 2(c), 2(d), and 2(e) show the results for nitrogen at equilibrium pressures of 30, 130, 290, 790 Torr, respectively. Sharp minima are again observed, implying maximum o-Ps at 105, 119, 127, and 140 K. For both argon and nitrogen only slight variations were observed in the other parameters.

Oxygen is a different case. In Fig. 3(b) the dip in A (Ref. 19) indicates only a modest increase in o-Ps at low temperatures. However, the corresponding values of F rise sharply as the temperature declines below 140 K,

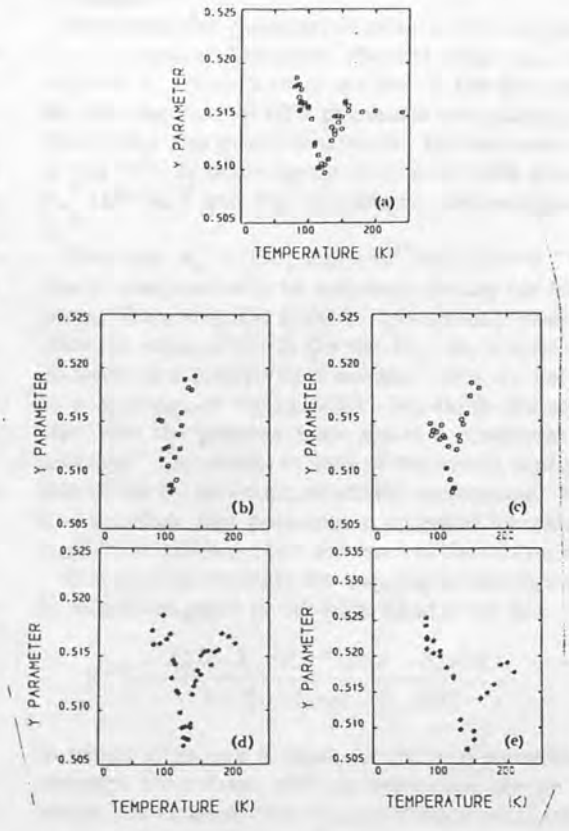

FIG. 2. Formation of orthopositronium: The Y parameter as a function of temperature for (a) Grafoil in argon at 190 Torr; and (b), (c), (d), and (e) Grafoil in nitrogen at 30, 130, 290, and 790 Torr, respectively, showing the displacement of the peak in Ps formation with pressure.

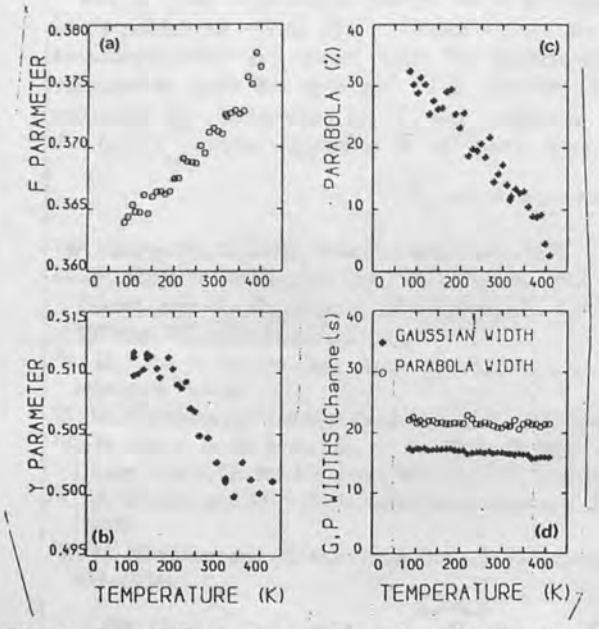

FIG. 1. Grafoil in vacuum: analysis of annihilation photon spectrum as a function of temperature with parameters

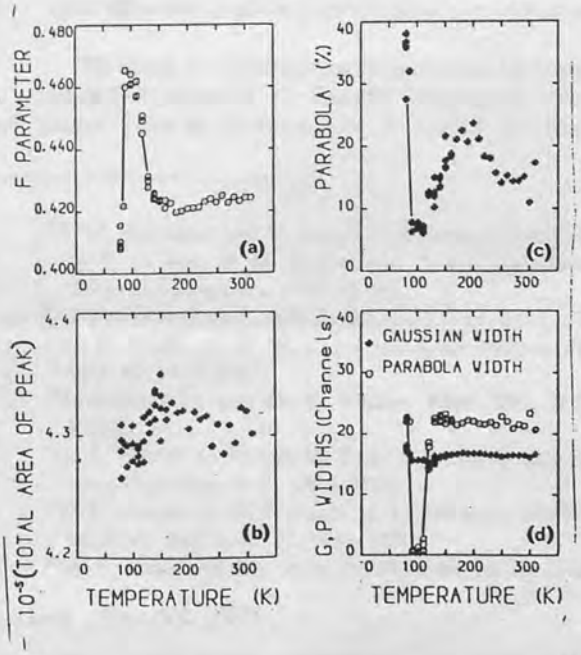

reaching a maximum at 100 K, only to drop again at 90 K. The origin of this rise is seen in Fig. 3(d), where a sharp spike of width of only about two channels appears in the Doppler spectrum. This must be parapositronium decaying via 2γ, implying a strong quenching of o-Ps by the oxygen, either in a condensed layer or in the gas. We attribute the disappearance of the 2γ spike at 90 K to the suppression of Ps formation by multiple overlayers of oxygen. The 2γ spike is reminiscent of the finding[16] of a reduction in the 3γ fraction for overlayers of chemisorbed oxygen on aluminium and a spin-exchange process leading to *p*-Ps.

The results must be mainly associated with the condensation of gas; it is inconceivable that the temperature alone could affect so discretely the interactions of positrons or the formation of positronium. Although an extensive literature exists on monolayers, the vast majority concerns layers laid down at very low temperatures with low pressures; very little appears comparable with our measurements in a context of high equilibrium pressures.

In the case of graphite in vacuum, the decline in Y at high temperatures suggests positrons in relatively deep traps on the carbon surface emerging as Ps. Assuming Ps emission is a thermal process,[2,3] fitting Fig. 1(b) with $Y=C\exp(-E_a/kT)$ yields a value for the activation energy E_a of 0.07 eV, which is lower than the 0.23 eV proposed in Ref. 18. If $E_a=E_b+\phi_- -6.8$ eV, where $\phi_-=5.0$ eV is the electron work function for carbon,[20] then the positron binding energy E_b is 1.87 eV which is lower than for most metals.[2]

For argon the simplest explanation is that the decline in Y for temperatures 160→120 K corresponds to enhanced Ps formation as a condensed monolayer develops, and that the rise for 120→80 K coincides with further condensation inhibiting Ps creation. Nitrogen is similar. With oxygen, however, rather than a sharp maximum in Ps production, a plateau appears in the F-parameter curve [Fig. 3(a)] which disappears only at 90 K, suggesting that multilayers fill the spaces within the Grafoil and stop all Ps formation at this temperature.

For a fluid monolayer, bound to a substrate and in equilibrium with the adjacent gas, the ideal two-dimensional gas model with the Boltzmann approximation may be applied.[9] The relation between coverage (n molecules m^{-2}) and pressure (P) is $P=(nkT/\lambda)\exp(-\varepsilon_0/kT)$, if $n\lambda^2\ll 1$ and where $\lambda=h/(2\pi mkT)^{1/2}$ and ε_0 is the binding energy of the molecule to the substrate. The equation can be applied to nitrogen which is fluid above 85 K for near-monolayer coverages.[10,12]

Assuming the Y-parameter minima for nitrogen in Fig. 2 correspond to the same physical state, i.e., the same value of n_m, in each case, one can fit the four minima to the two-dimensional (2D) gas equation to yield ε_0 and n_m. The fitting was most satisfactory: the optimum value of ε_0 was 1170 K which agrees reasonably with theory, 1070 K,[21] 1159 K,[22] and for calorimetric measurements, 1177 K.[23]

The best $n_m=(7.1\pm1.2)\times10^{18}$ molecules m^{-2}, which can be compared with an estimated density for 100% coverage. Assuming the fluid is "triangularly packed," and taking a value of 4.1 Å for the N_2-N_2 nearest-neighbor distance on a structureless surface,[21] this n_m corresponds to a coverage of (103±17%). We think the alternative view that the positron traps are at a maximum at 50% coverage[24] is unlikely in view of the strong mutual repulsion of the N_2 molecules at smaller separations. We therefore conclude that positronium emission increases as the monolayer builds up, but decreases as the bilayer develops.

It is possible to apply the trapping model formula[2,3] to fit individual peaks on the right-hand slope, i.e.,

$$Y^{-1}=\frac{Y_0^{-1}-Y_\infty^{-1}Z\gamma^{-1}\exp(-E_a/kT)}{1-Z\gamma^{-1}\exp(-E_a/kT)},$$

in which allowance is made for thermal promotion of Ps emission from traps with an activation energy E_a, and where it is assumed that the rate Z is proportional to coverage n at temperatures above the minimum in Y. Fair fits were achieved; our values averaged at $E_a=0.035\pm0.015$ eV for nitrogen.

We conclude that Ps is emitted from trapped states determined by physisorbed monolayers of atoms or molecules on a regular substrate, and that the finding represents an advance in our prospects of characterizing surface traps for positrons. Furthermore, we show the positron method enables one to explore the creation of fluid monolayers at high temperatures and high pressures.

We thank the Science and Engineering Research Council and Professor Y. C. Jean for sending us a copy of his paper,[24] and M. Fardis and M. A. Husain for their advice.

[1]W. Cherry, Ph. D. thesis, Princeton University, 1958.
[2]A. P. Mills, Jr., in *Positron Solid State Physics*, edited by W. Brandt and A. Dupasquier (North-Holland, Amsterdam, 1983), p. 432 and references therein.
[3]K. G. Lynn in *Positron Solid State Physics*, Ref. 2, p. 609 and references therein.
[4]R. M. Nieminen and J. Oliva, Phys. Rev. B 22, 2226 (1980).
[5]K. G. Lynn, A. P. Mills, Jr., R. N. West, S. Berko, K. F. Canter, and L. O. Roellig, Phys. Rev. Lett. 54, 1702 (1985).
[6]C. H. Hodges and M. J. Stott, Solid State Commun. 12, 1153 (1985).
[7]R. M. Nieminen and M. Manninen, Solid State Commun. 15, 403 (1974).
[8]P. M. Platzman and N. Tzoar, in *Positron Annihilation* edited by P. C. Jain, R. M. Singru, and K. P. Gopinathan (World Scientific, Singapore, 1985), p. 941.
[9]AUTHOR'S NAME, JOURNAL TITLE *xx*, xxxx (19xx).
[10]K. D. Miner, M. H. W. Chan, and A. D. Migone, Phys. Rev. Lett. 51, 1465 (1983).
[11]J. Stolkenberg and O. E. Vilches, Phys. Rev. B 22, 2920 (1980).
[12]J. K. Kjems, L. Passell, H. Taub, J. G. Dash, and A. D. Novaco, Phys. Rev. B 13, 1446 (1976).
[13]B. P. Cowan, M. G. Richards, A. L. Thomson, and W. J. Mullin, Phys. Rev. Lett. 38, 165 (1977).
[14]M. F. Toney and S. C. Fain, Jr., Phys. Rev. B 30, 1115 (1984).

Solid
(9) J.G. Dash, Films on Surfaces, (Academic Press, New York, 1975)

[15]Grafoil is the commercially available form of exfoliated graphite produced by the Union Carbide Corp., New York.
[16]K. G. Lynn and H. Lutz, Phys. Rev. B 22, 4143 (1980).
[17]P. Rice-Evans, I. Chaglar, and F. A. R. El Khangi, Phys. Lett. 81A, 480 (1981).
[18]Y. C. Jean, K. Venkateswaran, E. Parsai, and K. L. Chang, Appl. Phys. A 35, 169 (1984).
[19]For technical reasons B was not recorded, but A and Y behave similarly.
[20]*Handbook of Chemistry and Physics*, 63rd ed. (CRC, Boca Raton, Florida, 1982–83).
[21]W. A. Steele, J. Phys. (Paris) Colloq. 38, C4-xx (1977).
[22]L. W. Bruch, J. Chem. Phys. 79, 3148 (1983).
[23]J. Rouquerol, value reported in Ref. 21.
[24]C. Yu, N. Zhou, and Y. C. Jean, in *Positron Annihilation* edited by P. C. Jain, R. M. Singru, and K. P. Gopinathan (World Scientific, Singapore, 1985), p. 669.

J. G. Dash

BIBLIOGRAPHY

Anisimov O. A. and Molin Yu N., *High Energy Chem.*, **9**, 493 (1976)

Aston J. G., in "The Solid-Gas Interface" (E. A. Flood, *ed.*), Vol. **1**, Dekker, New York, 1966

Avgul N. N. and Kiselev A. V., "Chemistry and Physics of Carbon", Vol. **VI**, Walker P. jr., *ed.*, (Dekker M., New York), 1970

Ban L. L. and Hess W. M., *Proc. Bicenten. Conf. Carbon*, **9th**, Boston 1969

Band W., "An Introduction to Quantum Statistics", pp. 165-173, Van Nostrand-Reinhold, Princeton, New Jersey, 1955

Berry A. A., PhD Thesis, Bedford College (Univ. of Lond.), 1982

Bienfait M., Seguin J. L., Suzanne J., Lerner E., Krim J., Dash J. G., *Phys. Rev.*, **B29**, No.2, 983 (1984)

Brandt W., Berko S., Walker W. W., *Phys. Rev.* **120**, 1289 (1960)

Bruch L. W., *J. Chem. Phys.*, **79(6)**, 3148 (1983)

Brunauer S., Emmett P. H., Teller E., *J. Amer. Chem. Soc.*, **60**, 309 (1938)

Caflisch R. G., Berker A. N. , Kardar M., *Phys. Rev.*, **B31**, No.7, 4527 (1985)

Canter K. F., Coleman P. G., Griffith T. C., Heyland G. R., *J. Phys. B, Atom.* and *Mol. Phys.*, **5**, L167 (1972)

Canter K. F., Mills A. P. jr., Berko S., *Phys. Rev. Lett.* **33**, 7 (1974)

Canter K. F., Mills A. P. jr., Berko S., *Phys. Rev. Lett.* **34**, 177 (1975); **34**, 1541 (1975)

Cassel H. M., *J. Phys. Chem.*, **38**, 195 (1944)

Chaglar I., PhD Thesis, Bedford College (Univ. of Lond.), 1978

Chaglar I., Rice-Evans P., El Khangi F. A. R., Berry A. A., *Nuclear Instruments and Methods*, **187**, 581 (1981)

Cherry W., PhD dissertation (Princeton University, 1958)

Chung T. T., *Surf. Sci.*, **87**, 348 (1979)

Cole G. D. and Walker W. W., *J. Chem. Phys.*, **42**, 1692 (1965)

Costello, D. G., Groce D. E., Herring D. F., McGowen J. W., *Phys. Rev. B* , **5**, 1433 (1972)

Cotterill R. M. J., MacKenzie I. K., Smedskjaer L., Trumpy G., *ibid.* , **239**, 99 (1972)

Dale J. M., Hulett L. D., Pendyala S., *Surface and Interface Analysis*, **2**, 199 (1980)

Dalgarno A. and Davison W. D., *Advan. At. Mol. Phys.*, **2**, 1 (1966)

Dash J. G., "Films on Solid Surfaces", Academic Press, New York, San Francisco and London, 1975

Davé N. K. and LeBlanc R. J., *Phys. Lett.* **A63**, No. 2, 115 (1977)

Dericbourg J., *Surface Sci.*, **59**, 554 (1976)

Diehl R. D. and Fain S. C. jr., *J. Chem. Phys.*, **77**, 5065 (1982)

Diehl R. D. and Fain S. C. jr., *Surface Sci.*, **125**, 116 (1983)

Dirac P. A. M., *Proc. Camb. Phil. Soc.* **26**, 361 (1930)

Drir M. and Hess G. B., *Phys. Rev.*, **B33**, No.7, 4758 (1986)

Drude P., *Ann. Phys.*, 272, 532, 865 (1889); 275, 481 (1890)

El Khangi F. A., PhD Thesis, Bedford College (Univ. of Lond.), 1980

Eldrup M., Shantarovich V. P., Mogensen O. E., *Chem. Phys.*, **11**, 129 (1975)

Farell H. H., Strongin M., Dickey J. M., *Phys. Rev.* **B6**, 4703 (1972)

Farnsworth H. E., "The Solid-Gas Interface", (Flood E. A., *ed.*), Dekker, New York, 1966

Fischer D. A., Lynn K. G., Frieze W. E., *Phys. Rev. Letts.*, **50**, 1149 (1983)

Fowler R. H. and Guggenheim E. A., "Statistical Thermodynamics", Chap.**X**, Cambridge Univ. Press, London and New York, 1939

Goldanskii V. I., Prokop'ev E. P., *Sov. Phys. Sol. Stat.* **6**, 2641 (1965)

Groce D. E., Costello D. G., McGowan J. W., Herring D. F., *Bull. Amer. Phys. Soc.*, **13**, 1397 (1968)

Gullikson E. M. and Mills A. P. jr., *Phys. Rev. Lett.*, **57**, 376 (1986)

Haas T. W., *Progr. Surf. Sci.*, **1**, 155 (1971)

Hamilton J. J. and Goodstein D. L., *Phys. Rev.*, **B28**, No.7, 3838 (1983)

Held A. and S. Kahana S., *Can. J. Phys.*, **42**, 1908 (1964)

Hess W. M. and Ban L. L., *Proc. Int. Congr. Electron Microsc.* , 6th, Kyoto, **1**, 569 (1966)

Hirschfelder J. O. (*ed.*), "Intermolecular Forces", Wiley, New York, 1967

Hirschfelder J. O., Curtiss C. F., Bird R. B., "Molecular Theory of Gases and Liquids", Wiley, New York, 1954

Hodges C. H. and Stott M. J., *Solid State Commun.*, **12**, 1153 (1973)

Hoja R. and Marx R., *Phys. Rev.*, **B34**, No.11, 7823 (1986)

Hotz H. P., Mathiesen J. M., Harley J. P., *Phys. Rev.*, **170**, 351 (1968)

Howell R. H., Alvarez R. A., Stanek M., *Appl. Phys. Lett.*, **40**, 75 (1982)

Howell R. H., Rosenberg I. J., Fluss M. J., Goldberg R. E., Laughlin R. B., *Phys. Rev.*, **B35**, 5303 (1987)

Inaba A., Koga Y., Morrison J. A., *J. Chem. Soc. Faraday Trans.*, No.2, **82**, 1635 (1986)

Ishii A., preprint, *Phys. Rev. B*, 1987

Jackman T. E., Schulte C. W., Campbell J. L., Lichtenberger P. C., MacKenzie I. K., Wormald M. R., *J. Phys.*, **F4**, 11 (1974)

Jean Y. C. and Ache H. J., *J. Amer. Chem. Soc.*, **100**, 984 (1978)

Jean Y. C., Venkateswaran K., Parsai E., Cheng K. L., *Appl. Phys.* **A35**, 169 (1984)

Jean Y. C., Yu C., Zhou D. M., *Phys. Rev.*, **B32**, No.7, 4313 (1985)

Jorch H. H., Campbell J. L., *Nucl. Instrum. Methods*, **143**, 551 (1977)

Kim H. K., Zhang Q. M., Chan M. H. W., *J. Chem. Soc. Faraday Trans.*, No.2, **82**, 1647 (1986)

Kirkegaard P., Eldrup M., *Computer Phys. Commun.*, **3** , 240 (1972); **7**, 401 (1974)

Kjems J. K., Passel L., Taub H., Dash J. G., Novaco A. D., *Phys. Rev.*, **B3**, No.4, 1446 (1976)

Kobrin B., Shantarovich V., Mikhailov M., Tukina E., *Physica Scripta* , **29**, 276 (1984)

Lander J. J., *Recent Progr. Solid State Chem.*, **2**, 26 (1965)

Langmuir I., *J. Amer. Chem. Soc.*, **40**, 1361 (1918)

Larher Y., *Surf. Sci.*, **134**, 469 (1983)

Larher Y., *J. Chem. Phys.*, **68**, 2257 (1978)

Larher Y., *Trans. Faraday Soc.*, **70**, 320 (1974)

Lichtenberger P. C., Schulte C. W., MacKenzie I. K., *Appl. Phys.* , **6**, 305 (1975)

Lowy D. N. and Jackson A. D., *Phys. Rev.*, **B12**, 1689 (1975)

Lynn K. G. and Lutz H., *Phys. Rev.*, **B22**, 4143 (1980)

Lynn K. G. and Welch D. O., *Phys. Rev.*, **B22**, 99 (1980)

Lynn K. G., *J. Phys.*, **C12**, L435 (1979); *Phys. Rev. Lett.*, **43**, 391, 803(E) (1979)

Lynn K. G., Mills A. P. jr, West R. N., Berko S., Canter K. F., Roellig L. O., *Phys. Rev. Letts.*, **54**, No.15, 1702 (1985)

MacKenzie I. K., Eady J. A., Gingerich R. R., *Phys. Lett.*, **A33**, 279 (1970)

MacKenzie I. K., *Phys. Lett.*, **A30**, 115 (1969)

Madanski L. and Rasetti F., *Phys. Rev.* **79**, 397 (1950)

McGetrick M. J., PhD Thesis, Bedford College (Univ. of Lond.), 1981

McTague J. P. and Nielsen M., *Phys. Rev. Letts.*, **37**, No.10, 596 (1976)

Migone A. D., Li Z. R., Chan M. H. W., *Phys. Rev. Letts.*, **53**, 810 (1984)

Mills A. P. jr and Welch D. O., *Phys. Rev.*, **B22**, 99 (1980)

Mills A. P. jr, *Appl. Phys. Lett.*, **35**, 427 (1979a)

Mills A. P. jr, *Solid State Commun.*, **31**, 623 (1979b)

Mills A. P. jr. and L. Pfeiffer, *Phys. Rev. Lett.*, **43**, 1961 (1979)

Mills A. P. jr., *Phys. Rev. Lett.* **41**, 1828 (1978)

Mills A. P. jr., Platzman P. M., Brown B. L., *Phys. Rev. Lett.*, **41**, 1076 (1978)

Miner K. D., Chan M. H. W., Migone A. D., *Phys. Rev. Letts.*, **51** , No.16, 1465 (1983)

Mogensen O., Petersen K., Cotterill R. M. J., Hudson B., *Nature*, **239**, 98 (1972)

Mokrushin A., Prokop'ev E., Minaev V., Kisekka B., Kupriyanova R., *Sov. Phys. Semicond.*, 14, 751 (1980)

Moussavi-Madani M., PhD Thesis, RHBNC (Univ. of Lond.), 1986

Nieminen R. M. and Oliva J., *Phys. Rev.*, **B22**, 2226 (1980)

Nieminen R. and Manninen M., *Solid State Commun.*, **15**, 403 (1974)

Ore A. and Powell J. L., *Phys. Rev.*, **75**, 1696 (1949)

Pan R. P., Etters R. D., Kobashi K., Chandrasekharan V., *J. Chem. Phys.*, **77**, 1035 (1982)

Patrykiejew A. and Jaroniec M., *Thin Solid Films*, **70**, 363 (1980)

Patrykiejew A., Jaroniec M., Marczewski A. W., *Chemica Scripta*, **22**, 136 (1983)

Petersen K., in "Positron Solid-State Physics", *eds.* Brandt W. and Dupasquier A., Fermi School Varenna, North Holland, Amsterdam, 1983

Piper J. and Morrison J. A., *Phys. Rev.*, **B30**, 6, 3486 (1984)

Platzman P. M. and Tzoar N., "Positron Annihilation", (Jain P. C., Singru R. M., Gopinathan K. P., *eds.*), World Scientific Publ. Co., Singapore, 1985

Polley M. H., Schaeffer W. D., Smith W. R., *J. Phys. Chem.*, **57**, 469 (1953) "Positron Solid-State Physics", Brandt W., Dupasquier A., *eds.*, North-Holland, Amsterdam (1982)

"Positrons in Solids", Hautojarvi P. *ed.*, Springer Publ., Berlin (1979)

Rama K. R., Carrigan R. A., *Nuovo Cim.*, **66B**, 105 (1970)

Rice-Evans P., Chaglar I., El Khangi F. A. R., *Phys. Lett.*, **A64** , 450 (1978)

Rice-Evans P., Chagler I., El Khangi F. A. R., *Phys. Letts.*, **A81** , No.8, 480 (1981)

Rice-Evans P., Moussavi-Madani M., Rao K. U., Britton D. T., Cowan B. P., *Phys. Rev.*, **B34**, No.9, 6117 (1986)

Rollefson R. J., *Phys. Rev. Lett.*, **29**, 410 (1972)

Rollefson R. J., in *Proc. Symp. Submonolayer He Films* (J. G. Daunt and E. Lerner, *eds.*), Plenum Press, New York, 1973

Rosenberg I. J., Weiss A. H., Canter K. F., *Phys. Rev. Letts.*, **44**, 1139 (1980)

Rouquerol J., Partyka S., Rouquerol F., *J. Chem. Soc. Faraday Trans.*, **I73**, 306 (1976)

Schaeffer W. D., Smith W. R., Polley M. H., *Ind. Eng. Chem.*, **45**, 172 (1953)

Schulte C. W., *Solid State Commun.*, **35**, 759 (1980)

Shinotomai M., Takahashi T., Fukushima H., Doyama M., *J. Phys. Soc. Japan* , **52**, 694 (1983)

Smedsjaer L. C., Manninen M., Fluss M. J., *J. Phys. F.* **10**, 2237 (1980)

Steele W. A., *J. Phys. (paris)*, **38**, C4-61 (1977)

Stein T. S., Kauppila W. E., Roellig, *Rev. Sci. Instrum.* **45**, 951 (1974)

Stott M. J., In abstracts of papers of the 3rd international Conf. on positron annihilation, Helsinki (1973)

Suzanne J. and Bienfait M., *Acta. Cryst. A. (Denmark)*, **A28**, 5150 (1972)

Thomy A. and Duval X., *J. Chim. Phys. Physicochim. Biol.*, **67**, 1101 (1970)

Toney F. T. and Fain S. C. jr, *Phys. Rev.*, **B30**, No.2, 1115 (1984)

Torrens I. A., "Interatomic Potentials", Academic Press, New York, 1972

Volmer M., Z. *Phys. Chem.* **115**, 253 (1925)

Wei M. S. and Bruch L. W., *J. Chem. Phys.*, **75(8)**, 4130 (1981)

Young D. M. and Crowell A. D., "Physical Adsorption of Gases", Butterworths, London and Washington D.C., 1962